TECHNISCHE
UNIVERSITÄT
DARMSTADT

ONLINE CONTENT GENERATION in MOBILE GAME APPLICATIONS

Adaptation and Personalization for Location-based Game Systems

Dem Fachbereich Elektrotechnik und Informationstechnik
der Technischen Universität Darmstadt
zur Erlangung des akademischen Grades eines
Doktor-Ingenieurs (Dr.-Ing.)
genehmigte Dissertation

von

THOMAS TREGEL, M.SC.

Geboren am 21. Januar 1988 in Darmstadt

Vorsitz: Prof. Dr.-Ing. Griepentrog
Referent: Prof. Dr.-Ing. Ralf Steinmetz
Korreferent: Prof. Dr.-Ing. Helmut Hlavacs
Korreferent: PD. Dr.-Ing. Stefan Göbel

Tag der Einreichung: 20. Oktober 2020
Tag der Disputation: 18. Dezember 2020

Hochschulkennziffer D17
Darmstadt 2020

Thomas Tregel, M.Sc.: *Online Content Generation in Mobile Applications,*
Adaptation and Personalization for Location-based Game Systems
Darmstadt, Technische Universität Darmstadt,

Jahr der Veröffentlichung der Dissertation auf TUprints: 2021
Tag der mündlichen Prüfung: 18. Dezember 2020

Dieses Dokument wird bereitgestellt von: This document is provided by:

tuprints, E-Publishing-Service der Technischen Universität Darmstadt.
http://tuprints.ulb.tu-darmstadt.de
tuprints@ulb.tu-darmstadt.de

Bitte zitieren Sie dieses Dokument als: Please cite this document as:

URN: urn:nbn:de:tuda-tuprints-174994
URL: https://tuprints.ulb.tu-darmstadt.de/id/eprint/17499

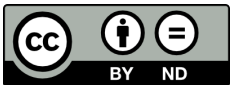

ABSTRACT

Location-aware mobile applications like navigation services or fitness trackers are inherently incorporated into our everyday life. The success of *Ingress* and *Pokémon GO* popularized the genre of location-based games, even indicating positive health effects for avid players that voluntarily cover large distances. However, the inconsistent and area-dependent supply of playable content, combined with superficial cooperation mechanisms, pose a considerable challenge for novel games in this genre. Furthermore, a suitable content generation based on real-world location data is complicated by the heterogeneity of populated areas. Continuously, in these movement-based games an inflexible mobility integration penalizes players deviating from the game's intended style of play.

Online procedural content generation, which creates content during run-time, is well suited for such scenarios. In numerous application domains, online content generation is utilized based on individual scenario parameters and contextual user data, providing personalized outcomes. But the optimization of content availability based on real-world location data, combined with a dynamic online generation, remains an open research challenge.

In this thesis, we design and implement automatic location-based content generation mechanisms as our *first contribution*, which address the aforementioned challenge. We develop an approach to identify suitable content locations and procedurally derive game areas. Consequently, we enable cooperation concepts by game area coupling, providing distinct game areas with similar urban characteristics, even in heterogeneous areas. Since movement is the main characteristic of such games, we propose a mobility personalization strategy as our *second contribution*. This incorporates a player routing approach in urban scenarios focusing on guided virtual reward optimization. On this basis, we develop a run-time mobility detection utilizing accumulated smartphone sensor data as our *third contribution*. To support this decision-making process, we employ a combination of accelerometer and location sensor readings to overcome the limitations of individual data sources for specific mobility types.

Finally, based on our developed GeoVis prototype, we conduct an extensive evaluation of our contributions. Therefore, we assess the effectiveness of our content approach under varying ambient conditions. We show that our location-based content generation leads to a reliable and flexible content selection in inhabited regions. Additionally, we demonstrate the utilization of route planning and automatic mobility detection as suitable mobility personalization strategies. In summary, we show that our contributions allow novel location-based game systems to create content worldwide and adapt to application-specific area and mobility characteristics by examining user mobility data during run-time.

KURZFASSUNG

Standortbezogene mobile Anwendungen wie Navigationsdienste oder Fitnesstracker sind fest in unser tägliches Leben integriert. Der Erfolg von *Ingress* und *Pokémon GO* hat dabei das verwandte Genre der Location-based Games populär gemacht, welches positive gesundheitliche Auswirkungen für begeisterte Spieler zeigt, die freiwillig große Entfernungen zurücklegen, um spielbezogene Belohnungen zu erhalten. Das inkonsistente Angebot an spielbaren Inhalten an verschiedenen Orten, kombiniert mit oberflächlichen Kooperationsmechanismen, stellt jedoch eine beträchtliche Herausforderung für neuartige Spiele in diesem Genre dar. Darüber hinaus wird eine praktikable Inhaltsgenerierung auf der Grundlage von Kartendaten durch die Heterogenität der besiedelten Gebiete erschwert. Bei diesen bewegungslastigen Spielen benachteiligt eine unflexible Mobilitätsintegration jene Spieler, die von der beabsichtigten Spielweise des Spiels abweichen.

Die *Online Procedural Content Generation*, bei der Inhalte automatisiert zur Laufzeit erstellt werden, ist für solche Szenarien besonders geeignet. In zahlreichen Anwendungsdomänen wird die Online-Generierung auf Basis individueller Szenarioparameter und kontextbezogener Nutzerdaten eingesetzt und liefert dabei personalisierte Ergebnisse. Die Gewährleistung einer flächendeckenden Verfügbarkeit der generierten Inhalte in Augmented Reality, kombiniert mit einer dynamischen Online-Generierung, wurden bislang nicht erforscht.

In dieser Dissertation erforschen wir ortsbasierte Mechanismen zur automatisierten Generierung von Inhalten. Im *ersten Beitrag*, der sich mit der flächendeckenden Verfügbarkeit beschäftigt, entwickeln wir einen Ansatz zur Identifikation geeigneter Standorte und der prozeduralen Konvertierung in bespielbare Gebiete. Anschließend, ermöglichen wir den Einsatz von Kooperationskonzepten durch Kopplung dieser Gebiete. Daraus resultieren gekoppelte Spielareale, die trotz Heterogenität der realen Umgebung, Orte mit äquivalenten urbanen Charakteristika auswählen.

Da die Bewegung der Nutzer das zentrale Merkmal solcher Spiele ist, schlagen wir als *zweiten Beitrag* eine Strategie zur Personalisierung der Spielermobilität vor. Diese beinhaltet einen Ansatz zur Routenplanung in urbanen Szenarien um Spieler bei der Optimierung der virtuellen Belohnungen zu unterstützen. Darauf aufbauend stellen wir als *dritten Beitrag* eine automatische Mobilitätserkennung zur Laufzeit vor. Diese setzt hierfür eine Kombination aus Beschleunigungs- und Standortssensoren ein, um die Einschränkungen einzelner Datenquellen für bestimmte Mobilitätsarten zu kompensieren.

Auf der Grundlage unseres entwickelten GeoVis-Prototypen führen wir eine umfassende Evaluierung dieser Beiträge durch. Dazu bewerten wir die Anwendbarkeit unserer Inhaltsgenerierung unter verschiedenen Umgebungsbedingungen. Unsere Evaluation belegt, dass unsere Mechanismen zu einer zuverlässigen und flexiblen Inhaltsgenerierung in bewohnten Regionen führen. Darüber hinaus belegen wir, dass eine

Routenplanung und automatische Mobilitätserkennung flexibel einsetzbare Strategien zur Personalisierung der Mobilität sind. Die Beiträge dieser Dissertation ermöglichen die Erstellung von weltweiten Inhalten für neue *Location-based Games*, sowie die flexible anwendungsspezifische Anpassung an aktuelle Gebiets- und Mobilitätsmerkmale der Nutzer, indem deren Mobilitätsverhalten zur Laufzeit analysiert wird.

ACKNOWLEDGMENTS

To my parents and my friends.

PREVIOUSLY PUBLISHED MATERIAL

This thesis includes material previously published in scientific journals and conferences. Table 1 summarizes the considered publications for the content of this thesis. No text in this thesis is directly copied out of these publications. Figures, particularly those illustrating core concepts or showcasing individual results, have been replicated. Similarly, tables containing conceptual overviews or evaluation data have been restructured, but their contents have been adopted.

Table 1: Previously published material

Section	[242]	[237]	[239]	[240]	[238]	[241]
Chapter 2: BACKGROUND AND RELATED WORK						
Location-based Games	✓		✓	✓		✓
Geographic Modeling Systems	✓		✓	✓		✓
Procedural Content Generation	✓		✓	✓		✓
Mobile Activity Detection		✓			✓	
Chapter 3: ONLINE CONTENT GENERATION FOR LOCATION-BASED GAMES						
Game Area Construction	✓					
Area Generation & Quality Assessment	✓					✓
Game Area Coupling						✓
Route Calculation			✓	✓		
Chapter 4: RUN-TIME MOBILITY DETECTION						
RUN-TIME MOBILITY DETECTION		✓			✓	
Chapter 5: GEOVIS: SYSTEM FOR ADAPTIVE LOCATION-BASED GAMES						
Overview of the GeoVis system	✓					✓
Chapter 6: EVALUATION						
Game Area Quality	✓					
Coupling Quality						✓
Route Quality			✓	✓		
Mobility Detection Quality		✓			✓	

Scientific work is usually the result of a joint team effort. For this thesis's context, we address a research area tackling computer science and information technology in the urban context. Hence, all contributions are the collaborative result of computer scientists, urban planners, and mobility researchers. Therefore, we will disclose all contributions of co-authors and contributors, including their affiliations. Whenever no dedicated affiliation is provided with the first mention, the respective person is or has been, a colleague at the Technical University of Darmstadt (TU Darmstadt) in the Multimedia Communications Lab. For the remainder of this thesis, the "we" is used, referring to each contribution's collaborative effort.

Following, I detail the chapters that include verbatim and rephrased fragments from publications or collaborative work. The complete list of my publications, including those out of this thesis's scope, is presented in Appendix B.

In general, for each contribution PD Dr.-Ing. Stefan Göbel supervised the whole process and provided valuable feedback regarding methodology, approach, and final development. Thus, he is not mentioned for each contribution repeatedly.

Chapter 3, ONLINE CONTENT GENERATION FOR LOCATION-BASED GAMES, presents the design of a Procedural Content Generation (PCG) approach to create game areas utilized for Location-based Games (LBGs).

I developed the game area construction in collaboration with Lukas Raymann. The identification of suitable locations in urban areas was initiated within the Urban Health Games interdisciplinary lecture series and driven by the continuing cooperation with Prof. Dr.-Ing. Martin Knöll (Faculty of Architecture, Research Group Urban Health Games, TU Darmstadt) and Marianne Halblaub Miranda (Faculty of Architecture, Research Group Urban Health Games, TU Darmstadt). I conducted a study with Lukas Raymann for the resulting content generation approach, which was published in [242], with all co-authors contributing to the manuscript's writing.

Following, I elaborated on coupling those generated game areas for multiplayer purposes in cooperation with Lukas Raymann. Concerning the location-based applicability and location-aware applications, Dr.-Ing Björn Richerzhagen provided valuable feedback to improve on, in terms of user movement dynamics and adaptation flexibility. The approach, evaluated for select game areas, was submitted for publication [241].

I worked together with Philipp Niklas Müller on the heuristic route-finding and data integration approach for the route-based movement personalization. We published those results, focusing on the algorithmic modeling in [239], with a follow-up publication in [240] with a focus on a thorough parameter-dependent evaluation. For both manuscripts, all co-authors contributed to the writing process. Following, I investigated different distance heuristics based on road networks in collaboration with Aurel Kilian, which I integrated into the aforementioned system with Philipp Niklas Müller.

Chapter 4, RUN-TIME MOBILITY DETECTION, presents the design of an automatic mobility detection applicable to smartphone devices. The original idea, with its integration into mobile game applications, emerged from discussions with Dr.-Ing. Tim Dutz and was substantially integrated into the LOEWE IDG ("project mo.de") research

project [245]. In collaboration with Maja Nöll, I designed an early acceleration-based mobility detection, which we published in [237]. After exploring possible boundaries of acceleration-based features, I elaborated purely location-based mobility detection in the lab course of [146], followed by cooperating with its members Yannik Klein and Maximilian Ratzke. Concurrently I investigated the possible effect of time tables in location-based mobility detection with Felix Leber, which we published in [238].

In collaboration with Sanja Tatjana Huhle, I developed a mobility detection approach incorporating acceleration and location data based on all my previous findings. Therein, Augusto Garcia-Agundez assisted me with sensor processing insights. Tim Steuer and Philipp Niklas Müller helped me verify the validity of our machine learning approach. To identify suitable application setups and sharpen our understanding of mobility scenarios, I closely worked with the members of "project mo.de" [245], namely in particular with Prof. Dr.-Ing. Petra K. Schäfer (New Mobility specialist group, Frankfurt University of Applied Sciences), Andreas Gilbert (New Mobility specialist group, Frankfurt University of Applied Sciences), Prof. Peter Eckart (Design Institute for Mobility and Logistics, University of Art and Design Offenbach am Main), Julian Schwarze (Design Institute for Mobility and Logistics, University of Art and Design Offenbach am Main), and Marianne Halblaub Miranda. In this project, many of the methods and application areas of our mobility concept have been elaborated and reviewed for real-world applicability.

Chapter 5, GEOVIS: SYSTEM FOR ADAPTIVE LOCATION-BASED GAMES, describes the important aspects of our developed prototypical framework. Therein, the backend components (Section 5.1.2) were realized with Lukas Raymann, providing requested OpenStreetMap data on an area-basis. For the mobility recording application presented in Section 5.2, I reiterated on the application design and the way of data recording, processing, and storage. In accordance with our currently investigated detection approach, the application needed to be adapted. Since mobility data of different subjects is required for our machine learning process, the application needed to function on as many mobile devices as possible (the subjects' private mobile device) and needed to be usable by subjects without constant supervision. With Maja Nöll, I developed the acceleration-based prototype, with further design inputs by Prof. Dr.-Ing. Petra K. Schäfer, Andreas Gilbert, Prof. Andrea Krajewski (Interactive Media Design, Darmstadt University of Applied Sciences) assisting in screen design and screen navigation design. With Sanja Tatjana Huhle, closely built upon these results, we developed the presented prototypical mobility data recording application. The application was then applied in the "Serious Games" lecture of the summer term 2020, given by PD Dr.-Ing. Stefan Göbel, accumulating our evaluation dataset.

Chapter 6, EVALUATION, presents the evaluation of our proposed approaches. For the game area location identification, Marianne Halblaub Miranda assisted me in the methodology of urban categorization to select opportune areas with different urban characteristics. An earlier evaluation was published with Lukas Raymann in [242].

Built upon the collaboration with Lukas Raymann and visualization assistance by Theo Kastner-Guhl, I evaluated the game area quality (Section 6.2.1) and the coupling quality (Section 6.2.2). Following, for the route personalization evaluation (Sec-

tion 6.2.3), I collaborated with Philipp Niklas Müller. We expanded on our earlier evaluation published in [239, 240] and further investigated the impact of route-based distance heuristics. In this part, the idea of comparing different distance heuristic accuracies arose from my cooperation with Aurel Killian.

For the evaluation of our automatic mobility detection, based on the insights of our previous work with Maja Nöll, Yannik Klein, Maximilian Ratzke, and Felix Leber published in [237, 238], I collaborated with Sanja Tatjana Huhle. We developed our evaluation approach utilizing a combination of different-sized time windows. Philipp Achenbach, Philipp Niklas Müller, and Augusto Garcia-Agundez assisted me in the evaluation methodology. I then performed the presented evaluation in collaboration with Sanja Tatjana Huhle, with valuable feedback by Tim Steuer.

CONTENTS

1 INTRODUCTION

Mobile entertainment applications are ubiquitous nowadays, enabled by the availability of mobile smart devices. Alongside streaming services and social media applications, mobile games are a continually growing area [40, 63] and an essential part of the entire games market [259].

Mobile pervasive games, which augment the game with the player's surroundings, are part of this mobile gaming culture. Multiple perspectives on pervasive games are considered in the research community [190], grouped into pervasive technologies enabling the personalized augmentation of a player's game world, and cultural implications corresponding to the players' interaction with the real world, their game worlds, and one another.

General mobile technical advancement, usually with the support of smart devices, impacts the area of visualization, like augmented reality applications, and in the area of constant sensor-based measurements [41], e. g., health parameters or fitness tracking. For pervasive games, similar technical advancements can be observed, such as augmented reality-based games [151, 199, 236] or adaptive exergames [57, 103, 210, 276], games adapting based on, e. g., a player's physical performance or their measured biosignals [78].

Technical advances

Cultural implications of pervasive games are broadly reported and researched concerning the impact on the individual and society. Especially Location-based Games (LBGs), a typical representative of pervasive games [154], have been extensively researched with their rise in popularity induced by *Pokémon GO*'s [199] release.

Cultural implications

Among many other authors, the World Health Organization draws a significant connection between physical activity and positive health effects [57, 260]. In a large cohort study using *Pokémon GO*, Althoff et al. [5] identified a game-induced increase of 25% in daily step count over 30 days, leading to positive health effects. This effect has been independent of gender, age, weight status, and prior activity level. Unlike leading mobile health applications [5], a lasting long-term effect could not be confirmed, partially due to missing long-term motivation [263]. Despite physical activity's high relevance for a healthy lifestyle, in Germany over 42% of all adults and over 83% of children must be treated as insufficiently physically active [261], with similar trends in other regions [5, 42, 57, 261].

Game impact on individual health

Another prominent effect on society is caused by the players' change in behavior, aiming to find the best location to play in, leading to clustered gatherings and highly dynamic movement [132, 207, 208, 228]. Implications were diverse, including the closure of traffic bottlenecks for player safety [218] and sudden player-induced traffic jams [202]. Besides these local effects, real-world game exhibitions and recurring weekly or monthly virtual game events have an ongoing impact on infrastructure, be it cellular network strain or region-wide booked-out accommodations [69].

Game impact on society

Implications of unbalanced content

An LBG's main characteristic goal has been reported to be getting people to walk around outside [114], which is hindered by two factors: Clustered content locations, which evolved to popular hotspots, promote only stationary gameplay. Additionally, the imbalance or even lack of available content in non-urban areas, outside of those hotspots, reduces retention rates, as players cannot play wherever they want.

Utilization of PCG to handle content imbalance

In this thesis, we tackle these content imbalances by first proposing a Procedural Content Generation (PCG) system capable of automatically generating LBG content in desired regions, with the objective of both availability and movement promotion. Consecutively, we enrich our approach in terms of personalization and adaptation options. On the one hand, this includes cooperative content options, emphasizing the social aspect of pervasive games. On the other hand, we propose mechanisms for route and movement type adaptation based on automatic mobility detection, since movement is the main characteristic and primary input of LBGs.

1.1 MOTIVATION FOR PROCEDURAL CONTENT GENERATION AND GAME ADAPTATION

PCG is particularly well suited to apply different content generation approaches to LBGs: Current day LBGs already utilize those approaches to select automatically generated content elements, whilst other content creation approaches are based on manual creation. Current automatic approaches are mostly randomized [54, 150], while manual approaches require tremendous efforts to cover whole countries, so games using those are usually limited to distinct places [264]. Utilizing crowd-sourced databases [20, 36, 38] is an effective methodology for nationwide content creation. The high availability leads to players' freedom of choice to play wherever desired. This approach is currently limited by the discrepancy in content quality, measured by the number of available locations in rural or suburban areas compared to urban areas [132].

PCG for nationwide content generation

Content variety

An effect of nationwide availability is the potential variety of content, fostering long-term motivation as new areas can be explored. The facilitation of online generation [235], which is the generation during run-time, further enriches options for variety and dynamic content adaptation in truly pervasive games.

Cooperation in spatial separate places

Further aspects of pervasiveness include the component of social interaction, which is an integral part of cooperative gameplay. Due to spatial restrictions, multiplayer options that are commonly observed in entertainment games are either superficial or force local gameplay [23]. Playing LBGs together in spatially separate places has been explored in individual prototypes [144, 217], removing the need for interaction locality. Incorporating such mechanisms into an online PCG approach increases availability, introduces novel cooperative formats [23], and integrates the social experience into a game's core loop [70, 99, 248].

Virtual reward optimization

Apart from occasional distance-based games [58, 276], whose concept is more prominent in gamified fitness applications [49, 163], LBGs outline the idea of travel between distinct content locations. To optimize their virtual reward, players employ route optimization approaches, increasing the number of visited locations [6, 270]. This is a generalization of common routing problems [9, 11, 86, 180, 182] and covers an integral aspect of LBGs: the coordinated travel between locations. Personalization options are

diverse and depend on player goals [107], ranging from time constraints over different mobility types to gameplay preferences, requiring a flexible routing approach to establish a player assistance system in a virtual game area [140].

When it comes to further personalized game adaptation, the user's mobility plays a pivotal role, as movement is the primary input for such games [57]. While current games employ a rudimentary mobility examination based on the player's current speed, the research area of automatic mobility detection is diverse. Non-motorized activities such as walking or cycling are already distinguishable [249] and integrated into commercial activity or fitness trackers. Distinguishing motorized activities is more challenging. Two main approaches are trip-based solutions [28, 32, 47, 153, 183, 250, 272], classifying entire trips in hindsight, and sliding window approaches [13, 68, 96, 108, 126, 168, 229, 252], allowing a classification during run-time.

Mobility personalization

While sliding window approaches fit a personalized game adaptation, the examined approaches are either limited to particular urban areas [126, 168], require area-specific data like timetables [229], or cannot be utilized on modern smartphones [13]. Thus, the underlying mobility detection needs to be geographically independent and function on generally available data.

To generate personalized LBG content, location-based generation systems require *i)* an automatic game area creation, and *ii)* individual personalization methods based on each user's surroundings. Our system addresses the emerging challenges with the utilization of PCG, which we explain in the following.

1.2 RESEARCH CHALLENGES

Global location-based game systems pose challenges for the automatic content generation and further the area-based adaptation and user personalization. We identified the following research challenges influencing the realization of an online location-based content generation.

Challenge: *Providing comprehensive generation availability*

Content availability is a determining factor for LBG quality. Modeling determining factors for appropriate game locations, including their automatic provision and integration, will be required to support a general content generation for LBGs. In contrast to current games, this should not be limited to urban areas, but emphasize a uniform distribution across game areas, and provide comparable generation outcomes across regions. The heterogeneous data needs to be adequately aggregated into high-level structures to support a flexible selection of content locations. Each selection needs to be quantifiable according to quality metrics that also allow for comparing different selection results.

Challenge: *Dynamic online generation with personalization*

A comprehensive personalization requires dynamic approaches that can be applied during run-time on a mobile device. Such approaches need to combine large quantities of geographic data entries with individual scenario parameters in a dynamic manner.

Those parameters are either determined by the game scenario or based on contextual user data [51], which needs to be analyzed. In contrast to static data pre-processing, a dynamic selection process considers the determined parameters to identify suitable content or eligible routing objectives. This reduces the number of permutations which need to be assessed in the process. Consequently, a dynamic online generation is required to apply on-demand personalization on mobile devices.

Challenge: *Differentiation of user mobility in heterogeneous areas*

In LBGs, player mobility is pivotal, with different types of mobility being common. For mobility-based adaptation to be feasible, a contemporary detection of the user's current mobility is required. Compared to established trip-based detection approaches, this requires the feature analysis to operate during run-time, working on time series data. Here, e. g., the sensor fusion of acceleration and location data, needs to be measured, processed, and interpreted. While machine learning methods have already been used for this problem, an area-independent approach with limitations on exclusive regional data is needed.

1.3 RESEARCH GOALS AND CONTRIBUTIONS

The main goal of this work is to model, design, and evaluate automatic location-based content generation providing adaptive georeferenced game content, including mobility personalization. This objective is divided into the following two research goals.

Research Goal 1: *Automatic content generation approaches across geographic regions.*

To develop promising content generation approaches for LBGs, game areas need to be modeled, and promising geographic data sources need to be examined. This goal focuses on three aspects: *i)* identifying game area content, *ii)* procedurally deriving generated areas, and *iii)* enabling cooperation by game area coupling. The former is required to derive a suitable content location scheme, allowing the identification of geographically or culturally relevant locations. Our contributions include an adaptable game area generation for different game scenarios [242]. The findings are extended by coupling multiple game areas based on their content locations, aiming for areas with similar urban characteristics [241].

Research Goal 2: *Run-time mobility detection and player mobility guidance.*

To realize mobility-dependent personalization, we require an approach to infer the user's current mobility type automatically. Our focus lies on detecting the mobility type utilizing a mobile device during run-time. Since content locations are reached through movement, planned routes allow for personalized gameplay. Consequently, for personalized mobility guidance, the user's current mobility is utilized to determine an optimized route according to player preferences. Within our contributions, the goal is approached in two ways: *i)* automatic mobility detection [237, 238], and *ii)* creation

of optimized routes with respect to game parameters [239, 240].

This thesis focuses on concepts for the automated generation of location-based game areas and essential components for adaptation and personalization, like mobility detection. Since we strive to support the creation of LBGs, we do not design an extensive game in any form, i. e., we neither design individual game mechanics nor investigate their practical integration into a game's flow. While we implemented numerous prototypical games in individual research projects [26, 83, 241], we neither perform extensive user experience studies nor present a game utilizing an individual technological concept in the course of this thesis. Since no individual game mechanics are designed, we refrain from individual adaptation mechanics based on, e. g., the day-night cycle, seasons, or the local weather. We gauge such adaptation mechanics vital for immersion and variety, but see no need for further research, as they are already commonly utilized.

Content generation focus

Scenario-based adaptation mechanics

To this end, based on our related work review, we include generation parameters to allow for customized game area generations. Additional limitations relate to the utilized geographic data source since we do not propose novel geographic data systems nor the systematic inclusion of potentially intriguing socio-cultural aspects.

While we design our concept for global application, this cannot be thoroughly evaluated worldwide for every functional aspect. Due to cultural differences or potentially diverging infrastructure, divergences may negatively impact the result quality of an individual approach.

Based on open map data

1.4 STRUCTURE OF THE THESIS

Extending this brief introduction to our primary research goals, we provide the background and previous work regarding the location-based content generation and mobility detection in Chapter 2. Based on our findings, we propose a location-based content generation in Chapter 3, addressing game area creation and the coupling of different game areas to each other. We further describe a routing approach to plan routes within game area-based LBG scenarios efficiently. In Chapter 4, we develop our mobility detection, discussing the findings of the respective research area, and realizing an approach for mobile detection during run-time. We then present our GeoVis framework in Chapter 5, discussing application components for geodata dissemination and mobility data acquisition. In Chapter 6, we conduct an in-depth evaluation of our prototype and its mechanisms for game area generation, personalization, and mobility detection. Therein, we specifically focus on each component's quality in extensive evaluation scenarios, exploring the individual boundaries of applicability. The thesis is concluded in Chapter 7 with a brief summary of the core contributions. Finally, we provide an outlook on potential future work.

2

BACKGROUND AND RELATED WORK

This chapter provides background information about Location-based Games (LBGs) and their underlying systems and discusses the current state-of-the-art regarding optimization methods in Procedural Content Generation (PCG) and mobile activity detection. First, we discuss the characteristics of current LBGs in Section 2.1. Afterward, we provide an insight into the underlying geographic systems in Section 2.2. In Section 2.3, we investigate the area of PCG, including commonly utilized optimization methods. This includes an analysis of current approaches to solve the traveling salesman problem and the related orienteering problem. Section 2.4 then covers the research area of automatic mobility detection, including employed data sources and utilized machine learning approaches. Finally, we conclude this chapter in Section 2.5 with the identified research gap.

2.1 LOCATION-BASED GAMES

LBGs are a typical representative of pervasive games, popularized by the physical realization of Geocaching [223]. Their main component is the real-world movement towards pre-defined game locations on a nowadays virtual map, followed by a game-specific interaction to obtain a virtual reward. They are played outdoors on mobile devices, with movement being measured by the device's location sensor. Before the smartphone era, pervasive games with external location sensors were utilized, laying the groundwork for today's LBGs [7, 22, 84, 219].

Building upon outdoor realizations of common board games [219], Kiefer et al. [144] presented an approach to competitively play those games in two distanced locations comparing game areas to achieve similar distances for each player. The authors stated the requirement for more sophisticated methods for larger datasets. Further on, spatial configuration is important when manually created content needs to be relocated to another location [106, 217], as not only suitable locations need to be identified, but also opportune paths between locations are required.

2.1.1 *Content and Gameplay*

In LBGs content is located at set locations, the Points of Interest (PoIs). Those PoIs usually relate to real-world locations that are, e. g., culturally relevant, particularly noteworthy, or specifically selected for the respective game [147]. In general there are three different game types [178]: Structured LBGs contain content, where all game locations are pre-determined at those PoIs [219]. Unstructured LBGs on the other hand, contain no pre-defined PoIs [7, 22], or are merely based on distances [276]. Semi-

Different game types

structured LBGs combine both aspects and are the common approach for current LBGs.

The data sources for a game's pre-determined locations vary from game to game depending on its content focus [150]. A pseudo random content generation selects PoI locations independent of any real-world association, offering content even in rural areas, but risking to generate content in unsafe or inaccessible locations [54]. Many research prototypes, and geographically restricted games, e. g., for tourism [18], utilize a manual PoI creation in which content designers manually select all suitable locations and provide respective content. User-generated or crowd-sourced content [223] are a popular choice for current commercial LBGs. This concerns purely user-generated content as found in Geocaching [223], and crowd-sourced platforms for users to submit candidate PoIs to. The latter are then rated by developers or the community[1]. For games based on the largest platform by Niantic [104, 121, 199], a strong discrepancy in content amount between rural and urban areas has been reported [45], restricting the opportunities to play for rural areas.

Different content types

Eligible content locations vary from game to game depending on its specific focus area, e. g., tourism, advertisement, or awareness. Niantic's portal network [189] aims to cover places of cultural relevance in general. Other commercial applications are based on Foursquare data[2] or Google Maps services [165].

Content data

Content at these locations is typically twofold. Static locations, like PokéStops and Gyms[3] in *Pokémon GO*, provide the players with the necessary resources required for the collection of game content on a cooldown. Those collectibles, which represent a core motivation [99], are located at spawn points, which are usually distributed around PoIs, but do not require a real object reference. These spawn points are also static and spawn content in recurring intervals.

Content types

Long-term motivational components, similar to classical entertainment games, depend on the player type [99, 258, 267]. They include the availability of content, social aspects (cooperative and competitive), the exploration of an area, and the drive to further improve or complete the virtual collection [99, 226]. Social aspects are approached differently for each game. Whereas most games offer cooperative [104, 134, 199] or competitive [121, 199] content at PoIs, social gameplay interaction independent from the players' position is limited [134, 199, 232], but offers unique multiplayer options.

LBG long-term motivation

The cultural impact of LBGs are diverse and have been researched especially for *Pokémon GO* due to its high popularity. Since its reported main characterizing goal is to get people outside walking [114], positive health effects have been thoroughly researched [5, 110, 149, 254]. The main findings reported a mild increase in physical activity, measured by an increase in step count over all age groups [149]. However, a lasting long-term effect could not be confirmed, as motivation started to decrease after six weeks [149, 263]. Especially personalization aspects play an essential role in health-related behavior change [107, 140].

Game impact on health

1 `https://wayfarer.nianticlabs.com/` (last accessed: October 02, 2020)

2 `https://developer.foursquare.com/places` (last accessed: October 02, 2020)

3 PokéStops and Gyms are virtual representations of interactable PoIs when players are within the interaction radius of 40m. There, Gyms have the additional functionality of promoting optional asynchronous player versus player combat.

Induced by the change in player behavior, their movement behavior becomes more dynamic [132, 208, 228] with diverse occurring implications. Urban areas becoming gaming hotspots can lead to safety issues [2, 14], traffic jams [202], and trespassing [184]. With the dependence on open cartographic data, users contribute to those platforms [178], but geographic data vandalism[4] can also be encountered [133]. Global game events, on the other hand, have a strong impact on event locations and the surrounding hospitality industry, similar to conventions and exhibitions [69].

Game impact on society

2.2 GEOGRAPHIC MODELING SYSTEMS

Geographic information (short: geodata) is any "information concerning phenomena implicitly or explicitly associated with a location relative to the Earth" [125]. The explicit location association is present, when a location is referenced by coordinates in a coordinate reference system [123], whereas implicit association relates to locations referenced by geographic identifiers [124]. Each geographic object has geographic features modeling its shape, consisting of a combination of the basic forms being points, curves, surfaces, and solids [122].

Geographic Information Systems (GISs) are used to access, collect, share, and analyze geographic information [90]. For the global position detection Global Navigation Satellite Systems, like GPS or Galileo, are used, with signal receivers commonly built into modern smartphones. To gain access to geodata multiple different sources like Open Government Data exists, unlike private geodata used by individual companies, e. g., for navigation. Besides the raw data provided by governments, many online map services exist, providing detailed data about landscape features, urban structures, or transport systems. OSM differs from other online maps, like Google Maps[5], Bing Maps[6], or Apple Maps[7], as they utilize Volunteered Geographic Information, a form of user-generated content, to collect and update their data.

GIS for geodata access

To collect, process and analyze geodata in a GIS an efficient form of data storage and retrieval is important. Allowing this functionality and employing efficient data structures, discrete global grids perform a division of the Earth's surface area into grid cells, often called tessellation [89]. Goodchild [89] identifies three key applications: georeferencing, spatial indexing, and discretization. Georeferencing within a discrete global grid has a distinct allocation of geographic identifiers like a city name, which otherwise requires additional domain information like a country name. In a linearized discrete global grid, arbitrary positions can be represented by a single string, encoding its cell size by the string's length [89, 91]. The string itself allows for efficient spatial indexing with its length, the whole string, or parts of it. The discretization maps the infinite number of geographic locations to a finite amount of grid cells. This also allows for hierarchical structures to index different cell sizes introducing multiple granularity levels [89]. Such hierarchical structures are called a discrete global grid system, which

Geodata storage

4 Players are manipulating OpenStreetMap (OSM) data to gain an advantage in the game based on their knowledge of how certain tags are processed to game content.

5 `https://www.google.com/maps` (last accessed: April 18, 2020)

6 `https://www.bing.com/maps` (last accessed: April 18, 2020)

7 `https://www.apple.com/ios/maps` (last accessed: April 18, 2020)

is congruent when a region of cell level k is a union of regions with cell level $k+1$ [215]. The geographic coordinates are then represented by the smallest cell, the coordinates are located in [215].

Map projections

Map projections, applied to geographic coordinate systems, like the commonly used WGS84, or the UTM system, transform geographic coordinates in a way to project the Earth's surface onto a flat map [173]. This inevitably leads to distortions in shape and size, commonly depending on the vicinity to the equator. The tessellation or so-called tiling divides the Earth into a grid of geometric shapes and is affected by the underlying projection, resulting in distorted cells. Common geometric shapes are triangles, parallelograms [215], and hexagons [172]. For spatial indexing of each cell, hierarchy-based, curve-based, or coordinate-based indexing schemes are utilized [171]. Depending on the origin point, especially curve-based schemes may result in rotated cells.

Geographic distance measurement

Different approaches can be used to measure geographic distances between geodata locations, depending on the required accuracy. Linear distance models, e. g., utilizing the Euclidian distance, or the Manhattan distance, measure the distances on a plain, neglecting the Earth's curvature. City-wide distances can be calculated with high accuracies for linear distance models [176]. More accurate, spherical distance calculations, are accomplished utilizing the great circle distance [138, 141], like the Haversine distance [213]. Since the Earth's surface is not perfectly round, it can be modeled as an oblate spheroid, taking into account its flattening at the poles. One common formula for this approach is the iterative Vincenty formula [138, 141].

2.3 PROCEDURAL CONTENT GENERATION

PCG offers an automatic creation of content with the use of algorithms in different areas of a game or an application [234], optimizing the content according to an objective function. The application areas are manifold and can be categorized into six groups, with the most common area being game area generation [109]. For the generation process, approaches are categorized according to a taxonomy developed by Togelius et al. [235]. Therein, a content generation is distinguished between online and offline generation. Online generation happens during run-time and requires no further manual input. It has the requirement to work in a predictable, reasonable time, and its results have a predictable level of quality [235]. Offline generation happens during a game's development and offers developers options to automate individual content creation processes with the option to lastly edit and polish the respective results [235].

PCG online generation

Online content generation is suitable for content personalization. This personalization commonly impacts a game's difficulty, as individual game parameters are adjusted according to the player's current performance, leading to a different perceived game experience [221]. According to player experience models this effect can be further emphasized, depending on the utilized data sources, even including biosignals into the generation process [266].

Since game area generation became popular for, e. g., role-playing games, the integration of real area data became intriguing. To introduce variety and recognition value

a concept to generate game boards based on open map data was proposed [77]. Further development translates this approach to different game genres like racing games and strategy games [95].

Applying PCG to LBGs

Utilizing PCG for LBGs has been proposed based on open map platforms, identifying relevant data and translating it to individual game elements [20, 36]. Resulting games are inspired by common board games, introducing the factor of real movement into the game [38]. To support the development of LBGs and reducing the necessary effort to identify suitable locations, Google recently introduced a service to obtain playable locations based on their map data [165].

2.3.1 *Optimization Methods*

An optimization problem aims to find an ideally optimal solution for a problem in a given time, which is commonly applied in PCG. Its solution quality is assessed by a target function, also known as objective function or fitness function [72, 145]. Its search area, containing all valid solutions, is constrained, with each element having a neighborhood with other solution candidates. A neighborhood's solution with the highest objective function value is the local optimum, while the overall highest value refers to the global optimum.

Local search [167] is a first heuristic optimization method that searches for a strictly better solution traversing its neighborhood, which when applied without modifications optimizes into local optima.

Simulated annealing

Simulated annealing [1, 145] is a heuristic neighborhood-based approach inspired by the heart treatment process in material science, hence the temperature parameter name as controlling parameter. It utilizes probabilistic acceptance criteria for worse generated neighbors depending on the temperature value, allowing it to escape large local optima in the early iteration process.

Evolutionary algorithms

Another heuristic neighborhood approach are evolutionary algorithms [72], inspired by biological evolution, with solutions represented by individuals and their fitness. They usually contain the following optimization steps [256]: initial population, evaluation, selection, reproduction, mutation, and repetition.

Traveling Salesman Problem & Orienteering Problem Solution Approaches

Common route finding problems

The Traveling Salesman Problem is a well-known optimization problem for finding the shortest route, visiting all locations in a given location set before returning to the start location [10, 113, 179, 182]. A common generalization is the Traveling Salesman Problem with Time Windows, which requires the locations to be visited during an active time window. The Orienteering Problem, is a combination between the Knapsack Problem and the Traveling Salesman Problem [247]. Its intention is to visit as many locations as possible or to maximize a score in a given amount of time, which, in addition can be incorporated with time windows. These problems are in the class of NP-hard problems and furthermore in NP-complete, meaning it currently cannot be solved in polynomial time [74, 86, 139, 156].

Exact solution approaches

For the Traveling Salesman Problem, exact algorithms are nowadays rarely used due to their comparatively long execution time. The previously employed exact branch and bound algorithms [17] are mostly replaced by branch and cut algorithms [11, 12], with the Concorde solver currently performing best [115].

Approximate solution approaches

For larger problem instances, approximative algorithms are necessary to keep computation costs low. Early constructive heuristics iteratively add locations [79, 135], with more recent approaches utilizing local search heuristics [130] like Tabu search [81, 82] or k-Opt [216] to find an optimum in a neighborhood of valid routes. Both simulated annealing [1, 97, 117, 119, 145] and evolutionary algorithms [72, 243] are among the best-performing algorithms, utilizing neighborhood structures. Further, more complex, neighborhood-based approaches, like Variable Neighbourhood Search utilize multiple different neighborhoods for optimization [180].

Alternative heuristic approaches

With the category of ant colony optimization algorithms [53] like BEAM-ACO [166] and Ant-Q [52] ant behavior is simulated in search for routes to food sources. Other heuristic approaches have shown to be applicable to the problem [44, 131], e. g., the Monte-Carlo search [60], but lack in either scalability or solution quality.

Orienteering problem solutions

For the lesser-known Orienteering Problem with Time Windows, significantly less tailored solution approaches exist. A similar problem, with a different name is the Steiner Traveling Salesman Problem [46, 186], which in fact has a similar goal, with the addition of incorporating traffic effects. The employed approaches are similar to the ones utilized for the Traveling Salesman Problem, using exact algorithms [209], constructive heuristics [137], or variable neighborhood search [175].

LBG Orienteering problem application

In the context of LBGs the Orienteering Problem has been used for exact optimized route determination using branch and cut, and branch and bound algorithms [6]. The approach makes use of the clustered nature of locations to reduce the problem size, for scalability reasons, resulting into the Clustered Orienteering Problem [9]

Vehicle Routing problem

A related problem is the Vehicle Routing Problem, which generalized the problem in the direction of having multiple vehicles minimizing the time for each location being visited once, as relevant for delivery vehicles [50, 198].

2.4 MOBILE ACTIVITY DETECTION

The idea of using mobile phones to distinguish user activities has been around for more than a decade, which is why the work in this area is diverse. We base our recap on existing reviews covering the research area [24, 191, 249] to identify relevant publications, with individual reviews specifying on distinct aspects, like GPS-based activity detection [262, 265]. Additionally, we included more recent publications, not yet covered in existing reviews.

Basic sensors

The two commonly utilized sensors are the accelerometer and the location sensor. Acceleration data is measured on three orthogonal axes. Since the sensor is affected by the Earth's gravity, its values are usually adjusted for further data processing. Location data is based on a Global Navigation Satellite System. Alongside the device's position in latitude and longitude, it contains information about altitude, speed, heading, and accuracy. The latter describes the measurement's expected deviation in meters [201].

2.4.1 *Automatic Mobility Detection*

Early approaches in this field have already shown that the fine granular distinction of human non-motorized activities such as *standing*, *walking*, *jogging* and *cycling* is possible. These approaches utilized mobile radio cells[8] [8, 185, 227] or separate GPS devices [159]. Today's approaches [249] are based mainly on smartphones' acceleration and location data. Existing commercial products, based on smartphones or fitness trackers, offer an automatic activity recognition, based on the non-motorized activities, e. g., Google Fit[9], Fitbit[10], or Garmin[11].

Non-motorized mobility detection

Distinguishing between non-motorized activities and motorized transport in general has also been investigated in detail [174, 193, 205]. Results, utilizing location and acceleration data, purely on mobile phones distinguish between the previously mentioned non-motorized activities and *motorized transport* with an accuracy of 93.6% [205]. Commercial solutions for this use-case already exist, detecting motorized transport during run-time, e. g., Google Activity Recognition API[12], or PathSense[13].

Motorized transport detection

The differentiation of motorized transport modes has also been the subject of scientific investigation for several years, with early works in 2003 [196]. Due to changes in technical options since then, we will focus on related works from the past decade, where two distinct approaches arose. First, trip-based approaches that classify entire trips in retrospect [28, 32, 47, 153, 183, 250, 272], e. g., for a travel diary. The approach focuses on the segmentation of trips and the assignment of segments to different modes of transport. Second, sliding window approaches [13, 68, 96, 108, 126, 168, 229, 252] allow for a transport mode detection during run-time depending on the window size, and whether processing and classification can be done within the given time frames.

Distinguishing motorized transport modes

Trip-based approaches are not suitable for detection during run-time, because trips finish after the data recording is stopped. Nevertheless, the publications are still considered, as they may incorporate valuable feature that can help to detect the respective transport mode. Commercial products for transport mode detection exist that assign specific sections of a route to a mode of transport retroactively, e. g., the Google Maps Timeline[14]. This presumably trip-based approach however is not documented.

Trip-based unsuitability

We provide an extensive overview over the identified, relevant publications in the area of mobility detection with at least two motorized transport modes, in Table 21. Here, we discuss prominent characteristics of the analyzed works.

A large number of possible sensors and information sources have been investigated for the detection of the mode of transport. Thus, there are the classical approaches,

8 Global System for Mobile Communications (GSM)
9 Google Fit for Wear OS - `https://wearos.google.com/#stay-healthy` (last accessed: July 16, 2020)
10 Fitbit SmartTrack - Auto exercise recognition - `https://www.fitbit.com/nl/smarttrack` (last accessed: July 16, 2020)
11 Garmin Fitness-Tracker: vivofit Auto Activity Detection Feature - `https://support.garmin.com/en-US/?faq=bMgN7dg30YAifXASdZjLN9` (last accessed: July 16, 2020)
12 Google Activity Recognition API - `https://developers.google.com/location-context/activity-recognition` (last accessed: July 16, 2020)
13 PathSense - `https://pathsense.com/` (last accessed: July 16, 2020)
14 Google Maps Timeline - `https://support.google.com/maps/answer/6258979?co=GENIE.Platform%3DDesktop&hl=en` (last accessed: July 16, 2020)

Employed data sources

which, as in the case of the differentiation of non-motorized transport modes, rely on mobile radio cell data, accelerometers, or location data. Additionally, some works add further information sources like georeferenced public transport data [183, 229], surrounding audio analysis [101, 155, 251], nearby device data of Bluetooth and Wi-Fi [47, 183] or socioeconomic characteristics, e. g., whether the user owns a car or a public transport ticket [250].

Detected mobility types

Standing and *walking* are recognized with higher accuracies than other mobility types [28, 32, 96, 126, 229, 250], which is also supported by reviews [191]. The distinction between motorized modes of transport such as *car*, *bus*, and *train* is far more challenging [191]. Only few authors [47, 108, 183] included *trams* in their distinction, which can be due to the scarcity of tram lines in the geographic area their data comes from. Frequent confusions are reported between *tram* and *bus* [47], *car* and *bus* [13, 68, 275], as well as *car* and *train* [32]. It is noticeable that often not all motorized mobility types are recognized equally well, where one mobility type reports high accuracies, other detection results are noticeably worse, e. g., *car* [229], *bus* [47], *tram* [183], and *train* [32].

Temporary stops

Dealing with temporary stops, e. g., stopping at a traffic light or a bus stop, provides a basis for discussion, whether such stops should be classified as *standing*. Detailed information about temporary stops are relevant to distinguish between *driving* and *standing* either inside or outside a vehicle [61]. In the research area of *Transportation Mode Detection*, only few approaches tackle this problem. Trip-based approaches in general and sliding window approaches with window sizes of several minutes suggest that temporary stops are ignored to obtain a continuous trip result. For sliding window approaches with small window sizes [13, 68, 108, 126, 168, 252], this becomes more relevant, where in some papers [126, 168] *standing* is not explicitly classified, thereby bypassing the differentiation between *standing* in person, and temporary vehicular stops. Hemminki et al. [108] explicitly describes their handling of stationary segments within an activity, assigning it to the original activity.

Employed datasets

The findings of many existing works are difficult to apply to European conditions where cities are usually smaller [32]. Related studies often used data collected in large cities such as Chicago [229], London [28], Tehran [153], Paris [183], Kōbe [220], Istanbul [96] or Shanghai [250, 275]. By contrast, Brunauer et al. [32], collected 322 hours of data in both European urban and rural areas. Dataset sizes differ largely, with work, containing only six [229] or twelve [252] hours of data. This leads to less data variance and less generalizable results [250]. Additionally, unbalanced data sets were frequently used for training and testing [108, 153, 220, 252, 272, 273], with *walking* being disproportionally overrepresented and means of public transportation being underrepresented.

Classification Approaches

Ensemble learners

In the area of transportation mode detection, machine learning approaches are commonly utilized, especially ensemble algorithms. These approaches train multiple classifiers and aggregate their results, aiming to reduce classification variance. Decision tree approaches are frequently used for this. Different methods are utilized to com-

bine the individual classifiers in an ensemble learner: Boosting performs a sequential training by re-weighting training instances each iteration, focusing on false classifications by increasing their weights [76, 160]. Bagging, for which Random Forests are a prominent example, construct multiple decision trees independently and report their results based on a majority vote [160].

Time series classification

Time series classification is a specific classification problem, where a sequence of time-ordered data needs to be assigned with a class label. A time series is usually separated into smaller series of constant length with a sliding window approach for processing [255].

Classification approaches

With regard to the classification algorithms, particularly decision tree approaches, notably Random Forest, were frequently used [47, 220, 229, 275]. Many studies, comparing different classification concluded Random Forests [96, 126, 168, 250] and decision tree learners [252] respectively provide the best results for their application. In one prominent study [108] Boosting was superior to all other approaches. In more recent studies also deep learning is evaluated [13], but usually without stating training and classification times.

Feature selection

Recent studies increasingly ignored the concept of feature selection [47, 153, 183, 220, 275]. In its absence, the resulting model may contain features that are irrelevant to the detection of the transport mode. Since features may contain redundant or correlating information, e. g., standard deviation and variance [108], this may impact the final model. For large sets of features, or even different sensor groups [183], e. g., Bluetooth and Wi-Fi [47], neither the influence of different sensor, nor the usefulness of individual features was examined.

Employed Features

Frequency-domain

Features based on the frequency-domain have been rarely used in previous works. The accelerometer was often sampled at 25 Hz or more [96, 108, 126, 168, 252], but either no [96] or only few [108, 126, 252] frequency-domain features are utilized. Even during high sampling rates of 35 Hz, oftentimes only features with low frequencies were used, e. g., between 0 Hz and 4 Hz [252], or below 5 Hz [108]. Aşçı and Güvensan [13] suggest that the inclusion of higher frequency features may lead to a better transport mode recognition.

External geo-referenced features

External geo-referenced information in conjunction with the user's location can improve the detection of *running*, *cycling*, and motorized transport modes [191]. Thiagarajan et al. utilizes features comparing spatio-temporal user data with timetables and geodata of bus and subway stops plus their routes [233], in addition to accelerometer-based features. Stenneth et al. [229] solely rely on location data, integrating live information about bus locations and information about train tracks and bus stops to differentiate between *bus*, *car*, and *train*. They showed an increase in detection accuracy based on the use of those external features. Montoya et al. [183] utilize the user's GPS trajectory to compare them with OSM public transport information, to differentiate between motorized mobility types, after detecting a vehicle mode based on accelerometer data.

Audio

Han et al. [101] use audio-based features to differentiate between different motorized vehicles, as soon as the movement type is narrowed down to those. Lee et al. [155] also utilize the microphone to perform run-time classification. In their dataset of South Korean cities they take advantage of unique vibrations and noise patterns of local public transport engines to train their model. Other approaches use a more in-depth audio analysis [251], including deep learning approaches (convolutional neural networks), leading to high training and classification times making run-time classification infeasible.

2.4.2 *Detection Quality Assessment*

Reported detection quality for selected works

The work of Shafique and Hato [220] shows that an accurate differentiation of different motorized transport modes is feasible with an accuracy $\geqslant 95\%$ with large window sizes (10 min). However, trip-based approaches and approaches with such large window sizes are not suitable for live detection during run-time. For the examined approaches, we specify their respective macro-averaged prediction accuracy. Compared to the micro-averaged accuracy, macro-averaging weighs all classes equally, instead of based on the number of instances [246]. Thus, for an unbalanced dataset, worse macro-averaged accuracies are likely due to overfitting more represented classes.

Live-detection results

To the best of our knowledge Stenneth et al. [229] and Güvensan et al. [96] provide the only recent works with an implemented and evaluated live detection. The former approach achieves an accuracy of 91% on a dataset from the city of Chicago with six different mobility types on 8 features. The latter approach utilized a significantly larger dataset with with eight mobility types on 348 different features without feature selection. However, only a macro-averaged accuracy of 79% could be achieved in live detection. To achieve the specified accuracy of 94%, a post-processing algorithm based on larger segments is required, which therefore classifies as a trip-based approach again. For Google's Application Programming Interface (API), a study shows a macro-average accuracy of 67% [274], which may change during its active development.

Sliding window approach quality

Other works that employ sliding window approaches [47, 68, 108, 126, 168, 252] are also relevant for this purpose. Particularly promising are those of Jahangiri and Rakha [126], Lu et al. [168], and Aşçı and Güvensan [13], which all achieve a macro-averaged accuracy of $\geqslant 95\%$ while only using inertial sensors. However, for the first two listed approaches, the number of distinguishable mobility types is small with two and three respectively.

Individual notable employed features

Jahangiri and Rakha [126] utilize a one second sliding window on time- and frequency-domain features, and report the spectral entropy as one of the most important features in their feature selection. Lu et al. [168] also extract features in the time- and frequency-domain based on each accelerometer axis in five and six second windows. Thereby they extract, among other things, the so-called Hjorth parameters [111] from time series analysis. However, they are reported to worsen the detection performance, since the parameters correlate with other employed features. Spectral energy features at 1, 2, and 3 Hz achieved a slight accuracy improvement. Aşçı and Güvensan [13] also use sensor values of each of the three axes, including the resulting

magnitude. Overall they utilize ten features in the time-domain and six features in the frequency-domain.

2.5 SUMMARY AND IDENTIFIED RESEARCH GAP

In this thesis, we investigate the concept of online content generation for the application area of LBGs. These games face considerable challenges regarding its content creation process due to the heterogeneous data in geographic areas. We examine potential types of content locations and propose a method enabling comprehensive generation availability. For this purpose, we develop an online generation approach, procedurally selecting suitable PoIs based on developed quality metrics. While approaches in the literature commonly utilize randomly [54, 150], manually [18], or user-created [189, 223] content, they have insufficient area coverage or fluctuating content quality. Both aspects limit the creation of new LBGs. The varying area quality further restricts the comparison of areas, which impedes novel multiplayer options [144, 217].

Online content generation for LBGs

Beyond that, dynamic online generation utilization allows for methods incorporating the current game scenario or contextual user data. While static contextual content adaptation has seen frequent use in current games [104, 134, 199, 232], player-based adaptation does not occur. With large quantities of suitable game locations to visit in these games, we propose a personalized mobility guidance to identify optimized routes offering promising virtual rewards. Since player mobility is pivotal, a contemporary user mobility detection is required, with each possible mobility type having its unique restrictions. In contrast to established trip-based mobility detection [47, 153, 183, 275], the current mobility needs to be determined during travel and not in retrospect. While sliding window approaches [13, 68, 96, 168, 229] conceptually offer a run-time detection, it is rarely realized. Thus, we model a run-time mobility detection distinguishing between different mobility types, including distinct public transport vehicles, to allow for a smart mobility-based adaptation during play for content adjustment and player safety.

Mobility personalization

3

ONLINE CONTENT GENERATION FOR LOCATION-BASED GAMES

Based on our findings in the related work in Chapter 2 and the resulting identified gap, we introduce an approach utilizing Procedural Content Generation (PCG) to provide automatically generated game area. We propose a system to automatically determine appropriate game locations suitable for a Location-based Game (LBG), including creating structured game areas. Thus, each game area consists of a collection of content locations, its Points of Interest (PoIs). By developing quality metrics, these areas become directly comparable, allowing an optimization approach to generate optimized game areas. At the same time, this allows us to couple game areas together according to their respective PoI characteristics. A flexible game area coupling enables the direct comparison of game areas, the transfer and re-localization of content, and allows for novel multiplayer game concepts. Since PoIs in LBGs offer virtual rewards, players aim to optimize their pathing through a game area. Consequently, we develop an approach to determine an optimized route in large game areas to assist players during gameplay.

In the following, we start with the construction of game areas and the geodata acquisition in Section 3.1. In Section 3.2, we describe our procedural game area generation approach to identify suitable PoIs according to proposed quality metrics. In Section 3.3, we focus on the comparison and coupling of game areas to break the colocation requirement of current multiplayer LBG systems. In Section 3.4, we propose a method to find optimized game routes, offering personalized guidance. These generalized concepts are integrated into our GeoVis platform described in Chapter 5 and systematically evaluated in Chapter 6.

3.1 GAME AREA CONSTRUCTION

A game area is a part of the game world with which players can interact directly or with contained objects. Each game area is associated with the real world, is specified by its geographic coordinates, and contains a distinct set of PoIs. For a given player position, a game area is required to retrieve geodata, and game content is generated. Each PoI is assigned a numerical value representing its quality, which we will further define in Section 3.2, with higher quality PoIs being selected over lower ones until a certain number (p_n) of selected PoIs is reached.

Game area definition

A first, intuitive, creation approach is to construct the game area as a circle, around the player's position. During player movement, it is not modified as long as the current player position remains within the given area. Because the area's content always depends on the available geographic data, it would change when an area was moved, as visualized in Figure 1. Using a discrete global grid system approach, as described

in Section 2.2, has multiple advantages over the repeating creation after movement updates:

Location handling

First, the content generation process can be costly in terms of required computation time, or the manual input of a content creator can even be required. By using a discrete global grid, positions close to each other are assigned to the same grid cell. Thereby, a small position input change does not change the resulting content, except for positions crossing cell borders. This allows us to use an identical game area for similar locations, which leads to higher generation consistency, comparability, and the option to pre-compute individual aspects of the generation process. Second, as illustrated in Figure 1, a changing game area can lead to disappearing content when a player approaches it.

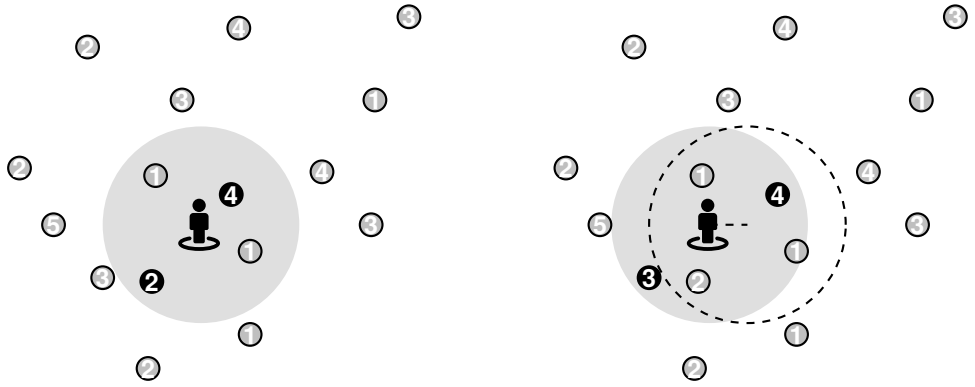

Figure 1: An example of PoI selection during movement. The number in each PoI indicates its quality, with the two highest quality PoIs being selected within the players circular game area. Left: the selection of two nearby PoIs with values of 2 and 4. Right: newly selected PoIs when moving left, leading to the previously selected PoI with value 2, no longer getting selected. Adapted from [242]

This approach works under the assumption that the player will always be within the game area. When a player leaves it, a new game area must be loaded to find game content outside the first area. For that demand, a circle is unsuitable due to its geometrical shape. Either a new game area would be created with no overlap, which would result in uncovered areas, or a new game area would be created despite the overlap, as illustrated in Figure 2. In the latter case, the previous inconsistency problem could reappear, as real-world areas would be part of multiple distinct game areas. Areas already covered by another game area would need to take parts of their generation result into account to keep already generated elements unmodified. With an increasing number of overlapping areas, the difficulty in generating appropriate content for the remaining areas rises. A new area would be required to use partial solutions not optimized for the new area.

Game area shapes

If game areas are shaped to be joinable together without gaps, the problem of loading new game areas can be solved. Good options for this uniform tiling problem [94], according to Sahr et al. [215], are hexagons, squares, and triangles, as shown in Figure 3. Unlike hexagons, parallelograms and triangular shapes can be subdivided into four smaller parallelograms and triangles of similar shape and size. Since, as explained

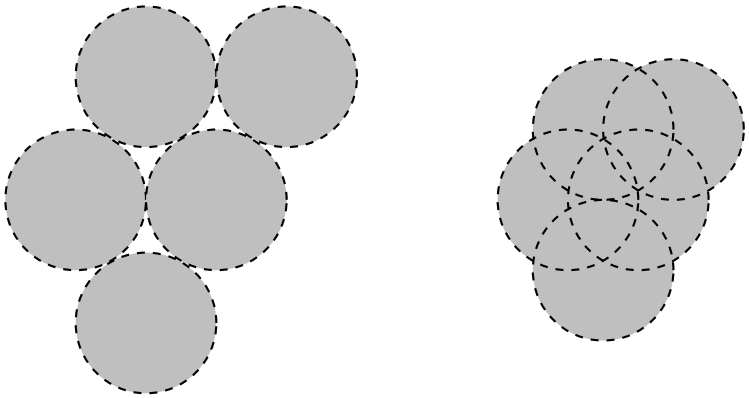

Figure 2: An illustration of tiling challenges for circular game areas. Left: uncovered areas, for non-overlapping game areas. Right: overlapping game areas, leading to consistency problems for overlapping game area regions. Adapted from [203]

later, the subdivision into smaller areas is necessary, hexagons are therefore unsuitable for modeling game areas. This also applies to circles, further preventing them from being used. Both triangles and parallelograms can be stretched or distorted, which is necessary to fit onto a sphere. Subsequently, we will use quadrangular shapes since it is also commonly used in related work, although triangles would also be applicable.

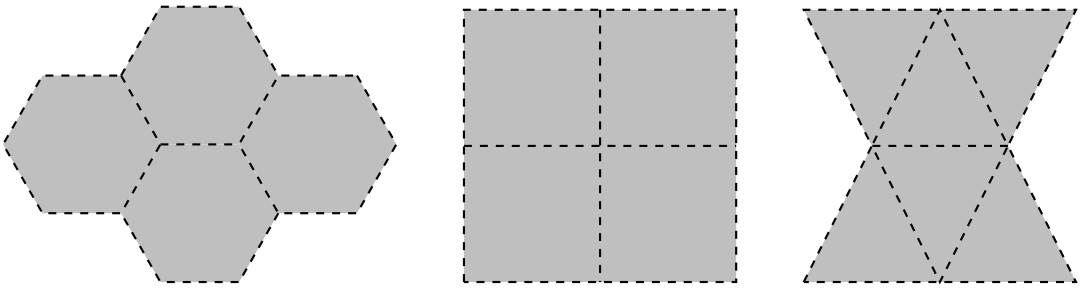

Figure 3: Valid uniform tiling options for game areas: hexagons (left), squares (center) and triangles (right). Adapted from [203]

Additional game areas can then be generated adjacent to already created ones whenever a player enters a new game area with no previously generated content, or in advance when a player approaches the boundary of the current game area, as shown in Figure 4. By using the adjacency relations and the option to subdivide areas hierarchically, the Earth can be efficiently covered through georeferencing and spatial indexing approaches. This ensures that game areas of different players match when they start in the same cell of the discrete global grid. Whenever a player leaves an area, the newly entered, adjacent game area becomes active, which should be pre-computed to avoid gameplay disruptions. The later introduced subdivision of game areas, among other aspects, leads to a partly local optimization with respect to the geographic distribution.

Therefore, we will assume that a procedure based on a quadrangular discrete global grid is used which maps a position uniquely to a game area. The specific choice of

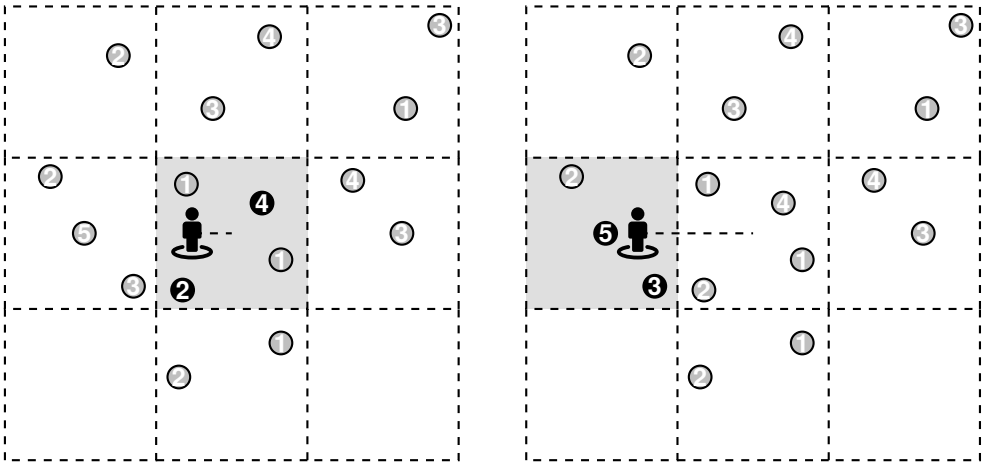

Figure 4: The example of Figure 1 selecting PoIs during movement utilizing a square discrete global grid for separation. Adapted from [242]

size and exact shape can be customized for the respective game scenario. For these game areas, a reasonable size should be chosen based on the game scenario. Smaller areas are then only locally optimized, likely resulting into bad generation results. This is especially problematic when the number of potential PoIs is not sufficient to create a good result, according to the chosen quality metrics. If game areas are too large, the online game area generation might need too much time to be used in practice as it needs to process all available geodata in the area. By subdividing these areas in question, we can use a flexible approach that recursively divides areas with too much geodata into smaller areas that are processed separately from each other. Afterward, these areas are merged again, resulting in a solution of combined local optima. The maximum number of recursive subdivisions thereby poses a trade-off between local and global optimization, whereby the more subdivisions are performed, the more locally optimized the resulting game area becomes.

Cell merging approach

In LBGs, movement is required to change a player's position. Depending on the player's speed, different locations are reachable within a given time. Thereby, we choose to link the grid cell size to the player's current mode of movement for two reasons: If we were to use a static size for different modes of movement, content would be accessible faster for players on a bicycle or a motorized vehicle. Alternatively, keeping the cell size constant and adjusting the location selection tied to the p_n parameter accordingly, would negatively influence the location selection approach. By adapting the number of content locations, the expected time required under a given mode of transportation to reach the locations would remain similar. A more suitable approach is to adjust the cell size accordingly and to take that adjusted cell size into account during content generation. This allows for a personalized online generation outcome. However, a constant adjustment during gameplay should not be applied since this affects the underlying grid, leading to possible aforementioned PoI inconsistencies.

Cell size adaptation

3.1.1 *Data Acquisition*

Based on the player's current game area, geodata is required to determine content locations players can interact with within the game. For this purpose, a Geographic Information System (GIS), which contains the required geospatial data, can be used. In conjunction with Volunteered Geographic Information, OpenStreetMap (OSM) is a suitable choice, as it can provide data for all locations worldwide, but may have fluctuating quality [73]. Geodata of many different types can thus be determined for any position on Earth using OSM alone. Other online map services such as Google Maps or Bing Maps specialize in providing maps without making the underlying geodata freely available. Since geodata available on OSM is freely usable according to Open Data Commons Open Database License, using a system based on OSM geodata is opportune and appropriate. Besides, OSM is one of the most researched systems in geographical science [73] regarding data completeness [31, 67, 112, 188] and both positional and thematic correctness [31, 73]. Heterogeneous data distribution has been a problem for all map providers with less available data for rural areas [187].

Data availability

For individual queries, OSM offers an openly available Application Programming Interface (API), which allows for a selection of specific tags and tag combinations in a given target area specified by a bounding box. However, the underlying data is also freely available, allowing the usage of a custom map server where data can be pre-processed according to the application requirements.

Access methods

Each data entry consists of positional information, representing a single geographic coordinate, or an ordered list of coordinates. For each entry, a list of tags is stated as key-value pairs that specify, e. g., the entry's name or a geographic attribute. Notably, these geographic attributes can be used to identify specific locations like sidewalks, town halls, or river banks by filtering for the respective tag combination.

Data format

3.1.2 *Geodata Filter*

Identifying and selecting suitable locations is the core challenge for the content generation of LBGs. As discussed in Section 2.1.1, each game has a different approach to select suitable locations and what geographic or cultural attributes make a location relevant. Our goal is to create a PCG-based approach, allowing the selection of relevant PoIs. In such an approach, it is essential to add customizability regarding the content selection, to allow the usage in different application scenarios. An appealing approach existing games that are not limited to a single geographic area have, is that they regularly distinguish content according to the PoI's cultural representation like historical monuments.

In a short analysis, we exemplarily examined different OSM tag groups that have been deemed relevant by most authors regarding their global data availability. This is important to allow our approach not to be limited to specific countries or cities. Tags that represent historically relevant locations or places of worship are particularly suitable for their global and frequent occurrence. Tags representing historic places and buildings could be found at 1,201,715 locations with a distribution illustrated in

Place of worship analysis

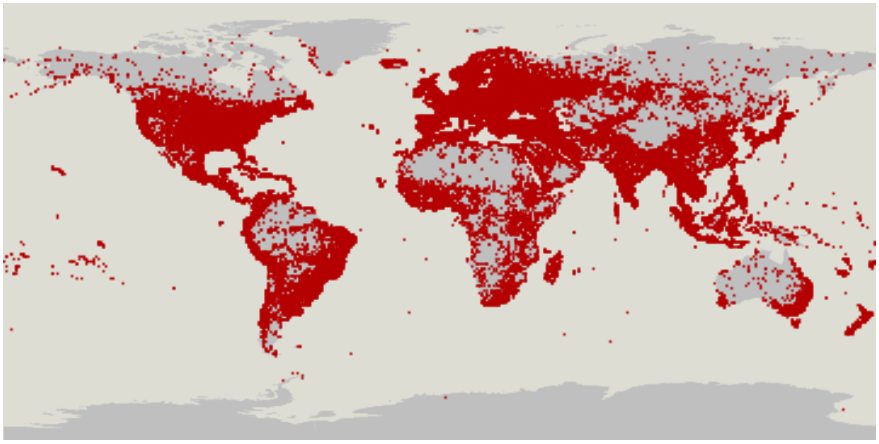

Figure 5: Data distribution of OSM tags for historic places and buildings extracted from taginfo[1].

Figure 5. These locations meet many criteria for good PoI candidates, as they often represent cultural and architecturally interesting buildings and exist in most countries.

Geodata filter definition

To apply and group available geodata according to its cultural representation, we define geodata filters. Each geodata filter contains a set of unique tags required to identify the particular map features. For the example of places of worship, both large cathedrals and small chapels are covered by the same category. To distinguish between different elements within a filter, priority values can be assigned to individual tags, indicating an assumed relevance based on the tag's frequency and cultural meaning [169]. Thereby, cathedrals are assigned a higher priority value than chapels in this filter.

Creating geodata filters

As described in Section 2.1.1, the difference in content quantity and quality in rural, suburban, and urban areas in current LBGs is measurable [132] and can negatively influence player experience and retention [194]. Our goal is to create a set of geodata filters that represents suitable game locations and is available in rural, suburban, and urban areas, i. e., is not limited to large cities. We subsequently analyze the available OSM tags and their respective frequency and distribution for suitability in a geodata filter. Following, we assign a priority value to each filter itself, to introduce an estimated relevance or representativeness for the area. This is led by the previous work of Lynch [169], identifying prominent locations in an urban landscape, and the assumption that, e. g., a town hall might be more expected to be shown as a PoI within a game, than the public benches in front of it.

Increase coverage

Our analysis focuses on tags and locations, likely to be found in all types of areas like town halls. Because the frequency of suitable locations in a city center is relatively high compared to less populated areas, we primarily aim to increase the coverage in those rural areas. This includes covering corner cases like parks, which have a distinctive characteristic in urban areas. Additional relevant categories are identified based on Niantic's guideline for high-quality content in their games [189] and locations

1 `https://taginfo.openstreetmap.org/keys/historic` (last accessed: August 25, 2020)

Table 2: Developed geodata filter and associated OSM tags. Prioritiy values are only noted on a category basis instead of on a tag basis.

priority	category
1	street and footway crossings
2	trees, stones and springs
3	wells, towers and survey points
4	waste disposal and toilets
5	public communication
6	benches
7	pedestrian walkways
8	parks
9	stations and stops for means of transport
10	product shops and services
11	healthcare and social facilities
12	places for food or drinks
13	places for doing sport
14	educational establishments
15	playgrounds
16	mountain peaks
17	huts and other shelters
18	places for picnic or barbecue
19	libraries and public bookcases
20	town halls
21	places of entertainment, arts, culture and tourism
22	places of worship
23	historic places

identified to be of high relevance for players [224]. For matters of direct comparability, each geodata filter is assigned a unique priority value resulting in a linear order.

Exclusion criteria for player safety

Along with the rise in popularity of LBGs with *Pokémon GO*, reports of trespassing and play in dangerous areas were reported in the media [184]. In a PCG system that can generate content worldwide, security and safety restrictions cannot be enforced manually. We thereby introduce a set of exclusion criteria, where geodata filters are not applied, leading to no content being generated in these areas. The exclusion criteria are also integrated with the use of OSM tags, e. g., *private* access to exclude locations on private property, company grounds, or military areas. Unsafe locations with *no foot* access like highways, or locations in front of police stations, hospitals, or fire brigade buildings are also excluded.

Prototypical list of filters

In Table 2, the resulting geodata filters are shown, without any claim to completeness. The filters can be extended and modified to cover additional missing areas and corner cases, not integrated yet. Further details about the developed filters are displayed in Table 19. Assigning similar priority values to multiple geodata filter categories would be an option to model an equal relevance of those categories in a scenario.

3.2 AREA GENERATION & QUALITY ASSESSMENT

PCG approaches use an objective function to assess generation quality, which assigns a numerical value to a given generation result. These functions usually consist of a combination of multiple parameters and metrics.

Metric categories: geographic & cultural

For our case of location-based content generation, we identify two categories of relevant metrics. First, the geographic location of a selected location can be assessed. It may include the quality of the location itself, or, when related to other selected locations, the geographic location quality of a set of locations. Second, the cultural meaning of a selected location can be assessed. This again may include a location's unique cultural quality or the cultural quality of a set of locations.

Absolute and relative metrics

Additionally, we differentiate between absolute and relative metrics. Absolute metrics are used to assess the quality of an outcome itself. A relative metric, on the other hand, cannot be used on a singular outcome but relates multiple outcomes to each other. It becomes useful when comparing different candidate outcomes for a subsequent generation, or when comparing final generation results to one another.

We identified the following metrics covering the previously presented metric categories:

Distribution

Distribution metric

To allow for gameplay in many places of a game area, a proper PoI distribution is required. Because the number of selected PoIs is limited to p_n, each location should be meaningful. If PoIs are clustered in a few areas, players have less available game content in areas outside of those clusters. Besides, they are tempted to stay in the clustered areas and only move to another area when the current area no longer suffices. An optimal situation would thereby be a uniform distribution within the game area, independent from the geodata availability. Especially in rural areas or areas verging on city borders, a uniform distribution is essential to avoid the content problem, which has become known from *Ingress* and *Pokémon GO*. Players have significantly less game content in remote locations than in cities [45, 132], which also translates to other LBGs [150].

$$
\begin{aligned}
\mathrm{NNI} &= \frac{\bar{d}_{obs}}{\bar{d}_{exp}} \\
\bar{d}_{obs} &= \frac{1}{n}\sum_{i=1}^{n} \min(d_i) \\
\bar{d}_{exp} &= 0.5 \cdot \sqrt{\frac{a}{n}}
\end{aligned}
\tag{1}
$$

For the calculation of distribution, we identify three applicable metrics. The Nearest Neighbor Index (NNI) introduced by Clark and Evans [43], shown in Equation 1, is an algorithm from spatial statistics, with d_i representing the nearest neighbor distance of a location i [158]. It compares the observed mean nearest neighbor distance of each location ($\bar{d}_{obs}$) to the expected mean distance for randomly distributed points ($\bar{d}_{exp}$)

in a given area with surface area a. Thereby $min(d_i)$ is the nearest neighbor distance of location i. A resulting index of 1 represents a random distribution. When the nearest neighbor distance is smaller than expected on a chance basis, with an index below 1, it is an indication for clustering. If the index becomes larger than 1, it indicates our targeted uniform distribution. For a sufficiently large location sample size of $n \geqslant 30$[2], the maximum index value is 2.1491 [43, 93], describing a uniformly distributed set of points. The theoretical maximum index value in a squared area is 4 for $n = 2$, where both points are located in diagonally opposite corners, which is no strong assertion as the sample size is too small. In practice, the index's empirical value is likely to range between 0.33 and 1.67 [93].

Nearest Neighbor Index

In a street network environment, the linear NNI is a modification mainly applied to street networks utilizing the Manhattan distance, also called the city block distance, instead of the Euclidian distance [157, 158].

A different approach to express the distribution of points in an area is motivated by the idea of each location having an area of influence around its position. The Voronoi diagram partitions a set of points into regions, where for each location in a region, the original point is the closest point of the original set. That way, each point's area of influence can be modeled. For clustered points, each Voronoi region is small. Points outside of clusters, by contrast, have a larger Voronoi region.

Voronoi area variation

Ripley's K statistic [16, 211] is another alternative clustering index. Rather than utilizing the single nearest neighbor distance, it is based on the number of PoIs within a circle with a given radius r around it. This can be compared to an expected number of PoIs within each circle, which is $\frac{n}{area}\pi r^2$. Varying r then allows the identification of clusterings and dispersion at different radii [136].

Ripley's K function

For our distribution metric we choose the general NNI, since the linear NNI mostly measures the distribution along, e. g., a street. Thereby, it is not directly applicable for game areas. As an alternative point distribution measurement, we can utilize the variance of Voronoi regions' surface areas with respect to the original area's size. Compared to the general NNI it can be applied for smaller PoI amounts, but in return requires attention for locations near a game area's border, which we address in Section 5.1.1. Integrating Ripley's K into PCG requires a fine-grained understanding of the expected dispersion characteristics, as dispersion at some radius leads to clustering at another radius. Additionally, it is particularly affected by area constraints, like excluded areas or the game area borders. For that reason, we do not employ Ripley's K for game area clustering analysis.

Distribution metric choice

Distance

To compare different outcomes based on their PoI distance, we establish a relative geographic metric, which compares a PoI's relative position to that of one in another area. It is another spatial metric, but focuses on the pairwise distance comparison of locations within distinct game areas. Exemplary game areas, visualizing the difference between both metrics, are shown in Figure 6. We assume a set of pairwise locations,

2 according to the central limit theorem

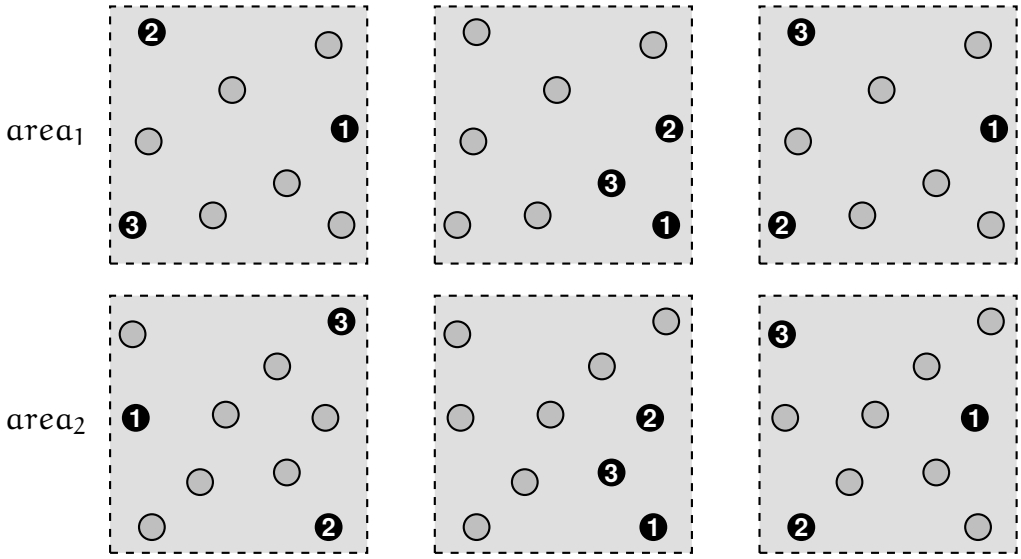

Figure 6: Three PoI selection examples combining distribution and distance metrics for two game areas with $p_n = 3$. PoIs with equal numbers are utilized in pairs for the distance calculation. Good distribution & bad distance (left), bad distribution & good distance (center), good distribution & good distance (right).

where each location belongs to a different game area. Depending on the individual game concept, it can be important in an LBG to have players require about the same time to travel from one PoI to the next one. For each pair, a location mean can be calculated, where areas are similar, when each PoI is as close as possible to their pair's location mean. A pair's distance is calculated using each PoI's relative position within a game area and calculating the distance between those relative coordinates. Different distance metrics can be used depending on the application scenario, e. g., Euclidian distance, Manhattan distance, or the individual street network distance using individual accessibility information. The latter is further investigated in Section 3.4.2.

Distance metric

A pair's or set's distance value is calculated with its PoI centroid $\mathbf{C_p}$ (Equation 2), which is relative to the respective game area g's center.

$$\mathbf{C_p} = \frac{1}{|pois|} \cdot \sum_{\mathbf{P_g} \in pois} \frac{2}{f_{maxDist}(g)} \cdot \mathbf{P_g} \tag{2}$$

To allow for different-sized game areas, each value is normalized with the term $\frac{2}{f_{maxDist}(g)}$, where $f_{maxDist}(g)$ returns the maximum possible distance between two PoIs for game area g. In a quadratic game area, this would be its diagonal length. Because distances are calculated relative to the area's center, the normalization quotient multiplies by two. Thereby, $\mathbf{C_p}$ is the location centroid of $pois$ normalized by each game area's size.

$$Dist(areas, pois) = \frac{1}{|pois|} \cdot \sum_{\mathbf{P_g} \in pois} \frac{2}{f_{maxDist}(areas_g)} \cdot \|\overrightarrow{\mathbf{P_g C_p}}\| \tag{3}$$

After calculating the normalized centroid $\mathbf{C_p}$, each PoI's ($\mathbf{P_g}$) average distance to the centroid is calculated and again normalized according to the game area's size. An example is shown in Figure 40 using the Euclidian distance.

Relevance

To point out the cultural relevance of a PoI, we use the geodata filter values introduced in Section 3.1.2. An intuitive approach is to sum up each selected PoI's priority value and divide it by the maximum possible priority value. That way, game areas with many selected historic places and places of worship have a high relevance metric. Selecting a PoI representing a culturally important monument over a park bench results in a higher relevance value. The monument is potentially more relevant and prominent for the game area.

Relevance metric

However, the metric can be specified in more detail, depending on the application scenario. In addition to the different priorization of utilized geodata filters, the aspect of content diversity may be integrated, where the number of different PoI categories is integrated into the metric. Additionally, focusing solely on individual categories of, e. g., shop locations would be possible for advertisement or customer acquisition, similar to approaches in *Ingress* [15] and *Pokémon GO* [64]. This focus is freely adjustable where aspects of tourism, health promotion, or education could be prioritized.

Similarity

The cultural similarity can be used to compare different game areas regarding their PoI composition. It can be used to compare the similarity or difference between two game areas regarding their data availability and between selected PoI pairs. Like the distance metric, we assume a set of pair-wise locations, where one location belongs to one game area, and the other location belongs to another game area. It is calculated as the ratio between the number pairs with equivalent priority values and all pairs. Thus, a high similarity refers to pairs having a similar PoI category, thereby representing a similar object in the real world. This is important as soon as cultural goals are integrated into the game concept, e. g., where a player is tasked to visit a certain number of monuments. In that scenario, game areas with a low similarity would pose widely different challenges for the players due to the different PoI selection. We define the similarity as the proportion of PoI tuples with identical relevance. Similar to the relevance metric, this value comparison can be adjusted to incorporate groups of categories or focus on individual aspects like tourism.

Similarity metric

3.2.1 *Area Generation*

To distinguish a generation outcome's quality, an objective function f_{score} is required, which assigns a numerical value to it, e. g., for a set of selected PoIs. We construct the function as a weighted sum of the proposed metrics, with adaptable weights depending on the application scenario. This corresponds to one consolidated metric. Each function relates to its respective metric: $\mathtt{Dist}(A, P)$ to the distance metric, $\mathtt{NNI}(A, P)$

to the distribution metric utilizing the NNI, $\mathrm{Sim}(P)$ to the similarity metric, and $\mathrm{Rel}(P)$ to the relevance metric:

$$f_{score}(A, P) = \omega_{Dist} \cdot \mathrm{Dist}(A, P) + \omega_{NNI} \cdot \mathrm{NNI}(A, P) + \omega_{Sim} \cdot \mathrm{Sim}(P) + \omega_{Rel} \cdot \mathrm{Rel}(P) \quad (4)$$

with $\omega_{Dist} + \omega_{NNI} + \omega_{Sim} + \omega_{Rel} = 1$.

Objective function

Each function calculates the arithmetic mean for its values and normalizes it to $[0, 1]$. For the NNI this corresponds to the mapping of values in $[0.33, 1.67]$ to $[0, 1]$, as we limit the metric to its empirical probable values. In our studies, values below 0.33 and above 1.67 were never encountered, but in case of such a scenario, we set the metric to 0 or 1, respectively. The distance metric value space is inverted, as we want to assign high values to small relative distances and vice versa.

The inputs utilized in Equation 4 are a set of game areas A and the selected PoIs P, which are a set of tuple-wise PoIs if multiple game areas are to be optimized.

Obtaining a set of selected PoIs is a typical optimization problem found similarly in PCG systems. Hereby, different solution approaches, according to Section 2.3.1, are feasible. In this case, an optimal solution often cannot be obtained due to the problem size. Thus, we do not use exact solution approaches, but rely on heuristics.

Both simulated annealing and evolutionary algorithms are metaheuristics used for neighborhood-based global optimization and have shown to be well-performing, particularly for large problem sizes [119, 243]. Due to their adaptability, they can be tailored towards a given problem by freely adjusting optimization parameters, neighborhood functions, and the objective function. Alternatives like tabu search are reported to scale poorly and are more likely to be stuck in local optima, requiring new approaches to compensate. A variable neighborhood search then again allows for multiple different neighborhood types, which may provide feasible generation candidates, when properly configured. We expect such a configuration to be harder to find and more inflexible regarding application scenario changes than simulated annealing or evolutionary algorithms. Additionally, both approaches can utilize the same objective function and the same neighborhood type, making them interchangeable. In the following, we describe the approach utilizing an evolutionary algorithm, while a simulated annealing approach would be similarly applicable.

Utilizing evolutionary algorithms

Area Separation

We can express the number of possible selection outcomes, with the binomial coefficient. In an exemplary scenario of 1,000 candidate locations in an area, we want to select the $p_n = 32$ best PoIs according to our objective function, resulting in $\binom{1000}{32} \approx 2.30 \cdot 10^{60}$ unique options. By subdividing the areas as mentioned in Section 3.1, e. g., into four equal areas and only optimizing within the subarea, the problem size can be reduced. Assuming a uniform distribution of candidate locations, this

Problem size

results in $\binom{250}{8} \approx 3.38 \cdot 10^{14}$ unique options for each subarea. The general formula for the total number of possible combinations would be

$$\underbrace{\binom{\binom{p}{s}^g}{\frac{p_n}{s}}}_{\substack{\text{combinations}\\ \text{in subarea 1}}} \cdot \underbrace{\binom{\binom{p}{s}^g}{\frac{p_n}{s}}}_{\substack{\text{combinations}\\ \text{in subarea 2}}} \cdot \ldots \cdot \underbrace{\binom{\binom{p}{s}^g}{\frac{p_n}{s}}}_{\substack{\text{combinations}\\ \text{in subarea } s}} = \binom{\binom{p}{s}^g}{\frac{p_n}{s}}^s$$

with p being the number of candidate PoIs, s being the number of subareas, g being the number of game areas (for the case of multiplayer areas), and p_n being the selection goal. While the total number of combinations only decreases slightly, the approach has one significant side effect: the initial distribution of PoIs is improved, as an equal number of candidate locations is selected for each equal-sized subarea.

Area separation trade-off

Utilizing an area separation presents an interesting trade-off. By separating a game area into more subareas the optimization in each subarea becomes increasingly more manageable. Only a small number of PoIs are selected, strongly reducing the number of unique options. However, this leads to a more locally optimized result. On the other hand, utilizing less area separation retains the chances to achieve results at or close to the global optimum at the cost of a larger number of unique options to consider.

Evolutionary Approach

Initial population

Generating the initial population is the first step in an evolutionary algorithm. In a recursive approach, we use the hierarchical structure of game areas to subdivide the area into four equal parts, similar to a quadtree. When the number of possible combinations within a subarea is smaller than a chosen threshold of maximum combinations, it is not split any further. Thereby, subareas with less available data are not split anymore, and dense subareas are divided further. Alternatively, a criterion based solely on the number of remaining candidate PoIs could be used to omit the binomial calculation. When the area is divided, a random initial population is chosen for each subarea.

Evolution algorithm for area generation

Algorithm 1 shows a code fragment for an evolutionary algorithm with the input of a set of given game areas and their divisions. Rows 2 to 9 show the previously described generation of an individual population. For the initial randomized selection, we use a *stochastic acceptance* approach. The goal is to integrate metrics based solely on the PoI's individual properties into the process, like the relevance metric. By weighting the selection process, we can address two potential problems. First, we developed multiple geodata filters that aim to increase data coverage in rural areas to both increase availability and diversity. However, objects like trees or park benches are far more common than highly suitable locations like monuments. Thereby, a random selection on the available data would category-wise be strongly biased towards more ordinary objects. Second, with a weighted approach, higher relevance categories can be further emphasized, addressing the relevance metric goals.

Selection

A weighted random selection can be made by a "fitness proportionate selection" (also known as roulette-wheel selection) or stochastic acceptance [162], with either usually used in the recombination step of an evolutionary algorithm. The latter ap-

Algorithm 1 : EVOLUTION

Input : • $A = \{area_1, \ldots, area_n\}$
• $A_{split} = \{(\{area_{1,1}, \ldots, area_{n,1}\}, p_{n,1}), \ldots, (\{area_{1,h}, \ldots, area_{n,h}\}, p_{n,h})\}$
A is a set of n different game areas. A_{split} is the subdivision of areas into a set of pairs. Each pair $(A_z, p_{n,z}) \in A_{split}$ represents a subarea of the original area in A. $p_{n,z}$ is the number of PoIs that are to be selected.

Output : A set of PoIs $\{(POI_{1,1}, \ldots, POI_{n,1}), (POI_{1,2}, \ldots, POI_{n,2}), \ldots\}$.

```
1  I ← ∅
2  while |I| < p_ind do
3      i_new ← ∅
4      forall (A_z, p_{n,z}) ∈ A_split do
5          M_z ← ∅
6          while |M_z| < p_{n,z} do
7              M_z ← M_z ∪ {StochasticAcceptance(A_z, M_z)}
8          i_new ← i_new ∪ {(A_z, p_{n,z}, M_z)}
9      I ← I ∪ {i_new}
10 forall j ∈ {1, ..., p_gen} do
11     I_new ← Reproduction(I) ∪ I
12     forall i ∈ I_new do
13         I_new ← (I_new \ {i}) ∪ {Mutation(A, i)}
14     I ← ∅
15     while |I| < p_ind do
16         M_bestUnsel ← ∅
17         i_bestUnsel ← ∅
18         forall i ∈ I_new do
19             M ← ∪_{(A_z, p_{n,z}, M_z) ∈ i} M_z
20             if M_bestUnsel = ∅ or f_score(A, M_bestUnsel) < f_score(A, M) then
21                 M_bestUnsel ← M
22                 i_bestUnsel ← i
23         I_new ← I_new \ {i_bestUnsel}
24         I ← I ∪ {i_bestUnsel}
25 M_best ← ∅
26 forall i ∈ I do
27     M ← ∪_{(A_z, p_{n,z}, M_z) ∈ i} M_z
28     if M_best = ∅ or f_score(A, M_best) < f_score(A, M) then
29         M_best ← M
30 return M_best
```

proach chooses a random individual and accepts its choice based on the individual's fitness value compared to the highest available fitness value, repeating the choice process when rejecting the previous choice.

The reproduction step in row 11 uses the current individuals and creates a number of p_{rep} new individuals. For each subarea, the individuals are evaluated based on the objective function f_{score}. The best p_{rep} sets for the current subarea are then reproduced and input randomly into one of the new individuals. After all subareas have been processed, the new individuals contain a combination of the best scoring subarea selections.

Reproduction

The mutation step, also frequently called neighborhood generation, in row 12 to 13 modifies the current individuals to include PoIs, aiming to increase the overall score. Each subarea in this step compares its result to the local subarea score and the score of the whole game area. In an iterative process, we perform a *replace* operation on the current selection, and evaluate it afterward, until no new global best score could be reached for a number of iterations p_{maxIt}. To allow for temporal f_{score} deteriorations within the mutation process, mutated selections only worse by a margin of p_{maxDec} are kept and further mutated, to possibly escape small local optima.

Mutation

The *replace* operation, as our sole neighborhood operation, is the core modification in a mutation process. Metaheuristic optimization approaches like evolutionary algorithms use these neighborhood operations to generate a new solution candidate, from a previous one. By replacing one PoI in the current individual, we can reach all valid solution candidates over a sequence of replace operations. Because the individual impact on the total f_{score} cannot be directly extracted, we choose to replace a random PoI instead of using a weighted selection. The newly inserted PoI, however, is again selected based on *stochastic acceptance*.

Replace as sole neighborhood operation

Repetition is the last essential part, included in row 10. The whole evolutionary approach repeats multiple (p_{gen}) times, independently. Finally, the best generation outcome is retrieved (row 25 to 29) and returned as result.

Repetition

The resulting best individual now contains a selection of p_n PoIs with an optimized f_{score} value.

3.3 GAME AREA COUPLING

Multiplayer options in current location-based games have shown to be either superficial or force players to play together only locally. One reason for this is the expected challenge when comparing each player's surroundings. Two players in distinct areas will find a different PoI representation, as well as different paths to reach them via road networks. Competitive multiplayer approaches would have problems establishing a fair and level playing field. Cooperative approaches could become biased towards singular players having far better circumstances for a given task and would be expected to fulfill most of the group's work.

Multiplayer balancing challenge

Our concept of generated game areas allows us to compare them to each other directly. When integrated into the selection process, PoIs in one game area can be selected according to criteria or circumstances present in another one. We introduce

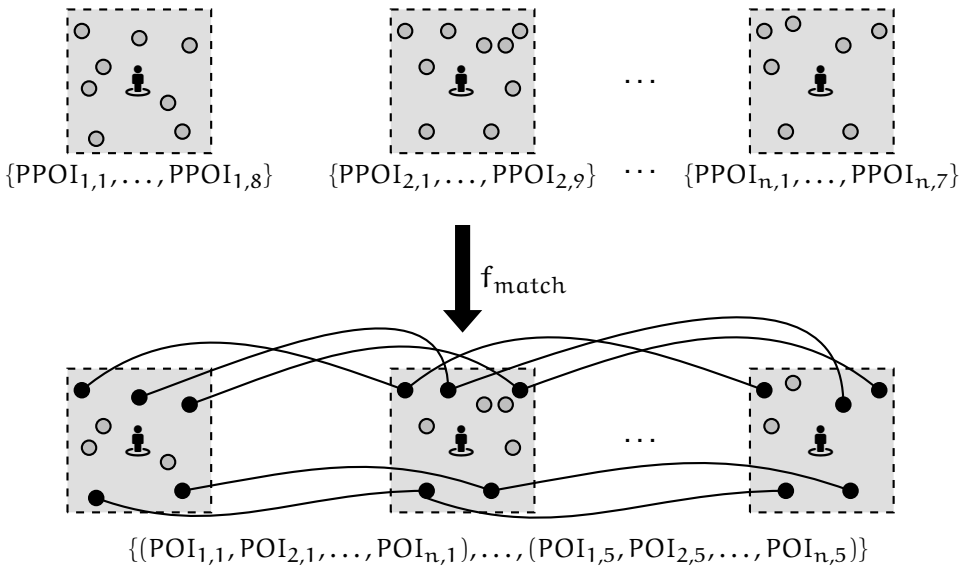

Figure 7: The individual step for the creation of coupled game areas using the example of three (but potentially n) players. Here, five PoIs are matched with each other, according to their relative position within each game area. Taken from [241]

Comparison allows for coupling

the aspect of coupling multiple game areas together. If two or more game areas are coupled, each selected PoI of one area is mapped to one PoI of every other game area. Coupled PoIs can be directly compared to each other according to all presented metrics in Section 3.2. We illustrate the approach in Figure 7, solely based on each PoI's relative position within its game area and the resulting selection process. Therefore, we assume $n \geqslant 2$ players, each in a distinct game area. We aim to find a match (f_{match}) of their potential PoIs onto those of the other game areas resulting in coupled game areas with similar PoI characteristics, according to f_{score}. f_{match} is thereby the call of our evolution algorithm, shown in Algorithm 1, with the input of multiple game areas and a similar subarea partitioning.

Game applicability

From a game perspective, this approach can be applied in various situations. In a competitive environment, game areas of players in different locations can be coupled automatically to provide a balanced, time-limited challenge. Otherwise, in a cooperative environment, players might need to overcome challenges against non-player characters, with each player contributing to the team's progress. This enables the integration of true simultaneous multiplayer concepts for LBGs.

Coupling goal

The main objective of this coupling approach is to provide each player with a game area similar to other players' game areas, to maintain equal opportunities in a respective game. In contrast to games with static content, our approach is integrated into the content selection process, likely resulting in different selected PoIs for one game area when coupled with different other game areas. The implications are varied.

When generating content for a single game area, the results can be stored and reused when other players enter the game area, as long as no player-specific parameters are integrated into the generation process. When areas are coupled with each other, they become interdependent, resulting in an at least quadratic growth of possi-

ble generation requests. The more areas are allowed to be coupled, the more possible game area permutations exist. Singular non-coupled game areas, however, can still be pre-computed. Because the generation outcomes have the absolute metrics (distribution and relevance) in common, these results, if available, can be used for the initial population setup in the coupling evolution process.

Pre-computation

Content variety can positively influence user motivation [206], which is one central reason PCG approaches are used in current AAA games[3]. By accepting slight reductions in content quality, compared to game content designed by professionals, a PCG approach provides diverse and unpredictable content, like levels or virtual items, within the game's rules. In an LBG, players quickly try to find optimal locations or routes [132] that allow them to play the game as effectively as possible, even though the optimal gameplay might require highly repetitive actions. We will go into detail regarding this aspect in Section 3.4.

Content variety

When coupling game areas, we achieve this variety due to the number of possible coupling permutations. In the case of fixed social groups or individual coupling that have already been computed before, the generation result can be reused or recalculated based on the application scenario. That depends on whether great variety or generation consistency is deemed to be more important. For our previous singleplayer generation, variety is only introduced by the algorithm's variance or when intentionally accepting slightly unoptimized results.

3.3.1 *Game Area Modification and Adaptation*

Especially in rural areas, geodata availability and spatial distribution can become a challenge [150]. Due to fewer potential PoIs, the number of possible selection outcomes drastically shrinks, up to a point where no good result can be obtained. In our coupling process, the only geospatial metric explicitly integrating a PoI's position is the distance metric, which, however, uses the relative position. Thereby, we can use area rotations or area reflections to increase the available possible outcomes. In an example of two coupled areas, a rotation of one game area might, e. g., overlap residential areas, where cultural aspects are similar or provide fitting distance-based locations, where previously none was available.

Area rotation and mirroring

We illustrate the process of a possible coupling outcome in Figure 8, with numbers indicating coupled pairings, in their original orientation. Exploring the example from the origin of $area_1$, it is coupled with $area_2$ with the latter being rotated 90° counterclockwise. Furthermore, $area_3$'s coupling is the result of mirroring along its horizontal axis. Because all game areas are interconnected, the coupling between $area_2$ and $area_3$ is reflected by both the rotation and the mirroring. As elaborated in Section 2.2, individual cells in a discrete global grid can already have different orientations due to the cells' projection on the Earth's surface. Because of the usage of quadrangular game areas instead of circular ones, valid rotations are limited to the four 90° steps. The mirroring is only done on either the horizontal or the vertical axis, as a mirroring along both axes is similar to a rotation by 180°.

Modification example

3 entertainment video games produced by the current major game developers and publishers

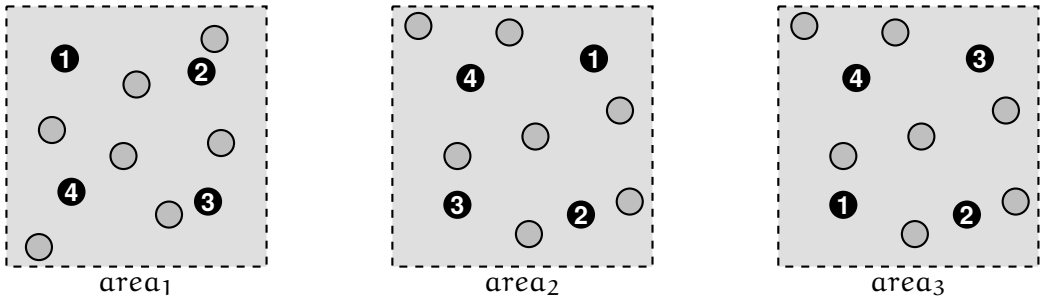

Figure 8: Illustration how rotation and mirroring of a game area $area_1$ allows for new possible solutions for game area coupling with another area. Black circles represent coupled PoIs with equal numbers belonging to the same match. $area_2$ contains 90° counter-clockwise rotated matches and $area_3$ was mirrored along the horizontal axis for the coupling process. Adapted from [203]

Game area resizing

Previously, we assumed a constant game area size. For adaptation purposes, it is useful to modify the size while retaining all previous characteristics as an opportunity to equalize the scenario for each player. First, similar to the previous aspect, each cell's projection in a discrete global grid may vary in size depending on the cell's absolute latitude. The closer it is towards the equator, the larger it becomes, depending on the employed map projection. Second, a core challenge in the context of LBGs is each player's movement speed. Because movement in the real world is required and is the primary player input, the estimated time needed to reach a location changes depending on the player's speed. This becomes evident when comparing one walking player with another player riding a bike. Therefore, we choose to link the player's current type of movement to their game area's size, as shown in Figure 9. Thus, we accommodate the difference in expected travel time from one PoI to another, based on the player's current or chosen movement type.

Mobility-based game area sizes

Because game areas are created during a game's or session's start, a speed value needs to be set, resulting in a scaling factor. For this, we use a default pedestrian speed of 5km/h [181] and an estimated cycling speed of 20km/h. This is coherent with our later evaluation data (Section 6.3) with an average of $\bar{x} = 5.004\text{km/h}$ with standard deviation $s = 1.116\text{km/h}$ for walking, and cycling speeds of $\bar{x} = 20.88\text{km/h}$ and $s = 4.248\text{km/h}$.

Vehicular game area sizes

In an application scenario, these values can be personalized and adjusted to the individual player. Apart from that, a more complex mobility detection can be utilized to accommodate for players in a car (when not actively driving), or players using public transport. The latter group poses an additional challenge for content selection because the players' movement flexibility is limited to public transport stops and their fixed routes.

3.4 ROUTE CALCULATION

In an LBG, the location-based accumulation of provided content presents the continuing challenge for players expanding their collection. The optimization process to find

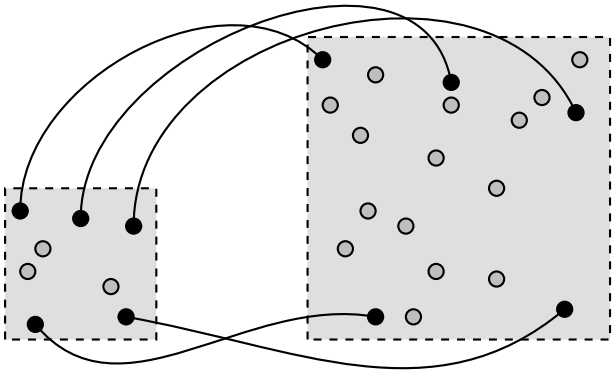

Figure 9: An example how two game areas of different sizes can be coupled, fokussing on the geospatial parameters. The coupled PoIs have a similar distribution and relative distance compared to their area size. Adapted from [241]

content clusters and effectively travel between them is an ongoing process in the player community. As content locations are usually static, optimized routes, maximizing the likelihood of sought-after content is in high demand. However, creating a personalized route is challenging due to the number of available locations, their intermediate distance, the associated real-world travel time, and the limited time at the player's disposal. Thereby a player has to select which locations to visit, rather than to go everywhere.

Route relevance for LBGs

These calculated routes have multiple application scenarios. For newer or inexperienced players, they can teach basic game mechanics, where more experienced players may use them to customize and improve their gameplay performance, maximizing their progress. In a tourism environment, users in a foreign city may plan and perform their trip according to personalized criteria.

Application areas

The problem of route-finding in LBGs is a combination of typical player requirements and system restrictions. Player requirements are expectations players would have towards a desirable route. Then again, system restrictions are imposed on a route depending on the underlying game mechanics of content locations.

Problem definition

A player would want to start a route at a specific location and time, e. g., directly at the current location, or pre-planned for a future trip. The time at the player's disposal is typically limited, requiring the route to finish before a given point in time at a target location. This target location can either be equal to the start location, implying a round walk, or an entirely different location. To optimize the game's progress, a player aims to maximize the visits of viable content locations. The viability or expected value of a content location changes depending on the game. In *Pokémon GO*, for example, a viable location is an active spawn point (a static location, where a Pokémon spawns in recurring intervals) capable of spawning a sought-after Pokémon. Depending on

Player requirements

the player's goals, this could be any Pokémon, especially rare ones, or the ones not yet encountered.

One distinctive game aspect in LBGs is the system of interaction cooldowns or time-based availability. A cooldown is applied to a PoI after interaction, requiring the player to wait for a fixed time, until the PoI can be interacted with again. This motivates constant movement around the area rather than repetitive interaction at a single location. Time-based availability means that content can be accessed once every given time frame, e. g., once for the first 30 minutes of each hour for a location with a spawn time at minute 0, a spawn time window size of 30 minutes, and a period length of 60 minutes. This periodicity forces players to go on a round walk to visit PoIs during their active period. In the context of tourism, this aspect is represented by a PoI's opening hours.

System requirements

Two significant aspects directly dependent on the player determine whether a route is feasible in practice. First, the estimated retention time for each PoI is required. In *Pokémon GO*, the expected time would be how long a player needs to catch a Pokémon at a given location, which could be either a constant value or be determined based on statistical player data, if available. Second, the player's travel speed directly impacts the estimated travel time between locations. Again, this can be set to a constant value based on the desired movement type. A more sophisticated approach can incorporate advanced route data and traffic conditions such as provided by navigation systems.

Travel behavior

Using an infinite period length for a spawn point's active period and no retention time when arriving at a location, we generalize to the Orienteering Problem with Time Windows. Any solution capable of solving our described problem would also be able to solve any instance of the Orienteering Problem with Time Windows [139], which is an NP-hard problem [86]. Thus, similar to our game area generation process in Section 3.2.1, a metaheuristic approach will be applied in large scenarios.

Computational complexity

3.4.1 *Route Candidate Pruning*

Before a route can be generated, we apply multiple pre-processing steps to our problem instance. Frequently used values can be pre-calculated, and the number of considered locations can be reduced to improve performance. Depending on the application scenarios, the precise specification and the impact of this pre-processing may vary. In the following, S represents the set of content locations, with S' being the pruned set.

The expected value of a content location depends on the player's preferences, like the chance of spawning a sought-after Pokémon. Filtering all content locations with an expected value of zero leads to a reduction in problem size. Alternatively, particularly low values that are not expected to be included in an optimized route can also be filtered according to a given threshold th. If a threshold is used, it needs to be chosen carefully depending on the value calculation, as a significant fraction of available spawn locations might be filtered out when said threshold is too high. Dynamically setting the threshold based on, e. g., the median value or another percentile is advised.

Value-based pruning

$$S' = \{s \in S | v(s) > th\} \tag{5}$$

The value $v(s)$ of a spawn point s includes two parameters: the location's relevance r and the probability p to encounter a desired content element at this location. The relevance can be, e. g., the cultural relevance of a location in the context of tourism, or the personalized relevance of the content element like a sought-after Pokémon. The latter can be either manually specified by the player or automatically derived based on the player's collection. In LBGs, the forthcoming content cannot be anticipated due to its randomness. However, the spawn point's content behavior can be represented by probabilities for each possible outcome. When exact probabilities are unknown, LBG communities established systems to analyze spawn points [200], based on individual sightings for each spawn period, to deduce spawn probabilities P.

Value calculation

$$v(s) = \sum_{i=1}^{P} (p_i(s) \cdot r_i) \tag{6}$$

Other LBGs may adjust the value calculation according to its unique properties. Additionally, external factors could be taken into account, as well. Including location properties such as noise level or air pollution could skew the route generation towards more relaxing and healthy routes.

Alternative value effects

Based on the start location s_s, the target location s_t, the targeted route duration t, the retention time for each spawn location $t_r(s)$ and travel time function $d(s_1, s_2)$ between two locations (see Section 3.4.2), all the spawn points not reachable by any viable route can be filtered out. This is done by calculating the path between s_s, a single chosen point, and s_t, including the retention time at the spawn point. Thereby we model the accessibility of a location within the route, filtering out all locations that cannot be part of any route due to the time constraint t.

Distance-based pruning

$$S' = \{s \in S | d(s_s, s) + t_r(s) + d(s, s_t) \leqslant t\} \tag{7}$$

This filter can be further extended by, e. g., including time windows, or using additional heuristics to determine spawn locations that are unlikely to be on a good route based on their distance to other spawn locations. However, the impact of these additions would need to be studied whether the route quality is not negatively affected, and the reduced problem size justifies the additional pre-processing time. For our scenario, we choose to use the distance filter shown in Equation 7, because users set route parameters during run-time, leading to the distance pre-processing also being done during run-time.

Possible distance filter extensions

3.4.2 *Distance Calculation with possible Road Networks*

To estimate travel times between locations, a distance metric is required allowing us to estimate distances. Ideally, a route service would be used to obtain exact distances on the road network. Depending on the number of locations and the respective distances to obtain, this may be not feasible due to the high amount of different routes examined

in a metaheuristic approach. When monitoring citywide traffic or mobile phone data estimated travel times can be calculated based on the underlying road network [128, 253]. However, this information is not commonly available in LBG scenarios.

Linear distance

A first distance calculation method is to estimate the linear distance between two spawn locations. For this method, the spherical distance (or great circle distance) needs to be calculated. Alternatively, the geographical coordinates can be converted into metric coordinates first, and an approximate distance obtained using the linear distance. For exact spherical distance calculation, the Haversine formula can be used. However, for small city-wide distances, the difference between the great circle distance and the linear distance is marginal, with a difference of 0.11% [176]. Even for distances above 2.000km, the linear distance is only off by 0.8%. Thereby we can use a linear distance metric like the Euclidian distance to approximate distances with less computational costs using the latitude lat and longitude lng of each coordinate.

$$d(s_1, s_2) = \sqrt{(\mathrm{lng}(s_2) - \mathrm{lng}(s_1))^2 + (\mathrm{lat}(s_2) - \mathrm{lat}(s_1))^2} \tag{8}$$

Grid generation

Our distance-based pruning filters out spawn points that are not reachable for any route given the time constraint. Because our goal is to find a route that visits a high number of valuable points, additional pruning would be required after each step. As this would evoke additional distance calculations, we employ a grid-based approach to approximate distances within our pruned set of spawn points. By separating the remaining area into equal-sized cells according to a discrete global grid, we can assign each spawn point to a cell. For each cell, its contained spawn locations are stored as well as its center coordinate. The distances between those grid centers can now be stored in a grid distance matrix, calculated once after distance-based pruning, and utilized for a simple lookup to estimate the approximate distance between two points.

Distance matrix

A concept that can be used to decrease route calculation times is to use a distance matrix to lookup distances instead of calculating them. It can be fully calculated during pre-processing, i. e., all distances of spawn points after pruning are calculated and stored. Another option is to use it as a cache, where already calculated distances during run-time are stored for faster retrieval when required again. This distance matrix could be incorporated into the dataset instead of being calculated during run-time, which would allow for more refined distance metrics, possibly including routing services. A different aspect is that a complete distance matrix has a quadratic growth with the number of locations, even though a possible symmetry of distances can be used for time-distance estimations based on pedestrians or cyclists. One possible run-time improvement is the usage of efficient Many-to-Many [214] route calculation approaches, to speed up the matrix creation.

Distance grid

Instead of storing distances for all spawn point pairs, we can use our grid distance matrix to access approximate distances quickly. In a metaheuristic optimization approach, the neighborhood function generates solution candidates, which, in our case, are candidates for routes, evaluated based on an objective function. This function, which we define in Equation 9, can now use the approximate distances to filter far-

distanced grid cells in each iteration. The calculated distances between spawn locations are then used to determine the total travel time and the resulting objective value.

Whereas the use of a routing service for exact distance would be beneficial, in a live environment, this is not feasible because the current distance matrix APIs are commonly limited in terms of matrix size[4], in addition to limited free query rates[5,6,7], or a total free query quota[8]. For a pre-defined dataset, this information can be acquired over time, which is infeasible in a live environment. Because locations close to each other most likely have limited required travel times but increase our matrix size in a naive querying approach, exploiting this proximity can reduce query amounts. However, the resulting approach is still required to calculate distance beforehand.

Direct distance calculation: Location to Location

Another conceivable approach would be to calculate road network distances only when presenting the final route. However, a route, calculated with a realistic travel speed, would rarely fit in the scenario. Reducing the travel speed by a constant factor to accommodate for longer routes, e. g., by $\sqrt{2} \cdot d(s_1, s_2)$ for the Manhattan distance, can compensate for this shortcoming. A scenario-specific solution would be able to determine an average detour factor for a given road network, comparing road network distances to linear distances. By applying this factor to the travel speed, delays caused by road network-induced detours could be compensated, allowing the route generation to work on linear distances with reduced travel speeds, bypassing the query limit problems of routing services.

Region-specific linear distance conversion

The following approaches assume that each spawn location can be reached by traversing the street network. LBGs, in general, employ a so-called interaction distance, allowing players to interact with game objects in a given radius around them. This both compensates for both location sensor inaccuracies, as well as content location errors, i. e., content placed within buildings instead of in front, where it would be accessible.

Interaction distance

A first approach to reduce our location set size, as illustrated in Figure 10a, is to map each spawn location to its nearest street crossing. When the content density is high, multiple spawn locations are mapped onto one street crossing, reducing the problem size. This assumes that street crossings are plentiful. The distance between the spawn location and the street crossing location can be approximated, resulting in road network distances being required on a crossing to crossing basis.

Mapping locations to crossings: Crossing to Crossing

The nearest street crossing can be calculated by linear distance. Assuming a straight road, we can determine the closest location on the street by a scalar projection of the spawn location onto the street vector. That allows us to determine the distance from the crossing using the Manhattan distance, representing a player traveling along the street until being as close as possible to the spawn location.

Finding the closest street crossing distance

4 `https://developer.tomtom.com/routing-api/routing-api-documentation/matrix-routing` Limit: 50x50

5 `https://developers.google.com/maps/documentation/distance-matrix` Limit: 25x75

6 `https://docs.graphhopper.com/#tag/Matrix-API` Limit: 50x50

7 `https://developer.mapquest.com/documentation/directions-api/route-matrix/post` Limit: 25x25

8 `https://www.microsoft.com/en-us/maps/distance-matrix` Total Limit

(a) PoIs mapped onto their nearest crossing with two visualized path projections.

(b) PoIs mapped onto their closest street segment.

(c) PoIs clustered according to a given interaction radius illustrated in a dashed circle.

Figure 10: Three different distance heuristics mapping spawn locations to their closest crossing, closest street segment, or clustering nearby spawn locations.

Because only the distances towards the crossings are saved, these routes include unnecessary detours. The player is expected to return to the crossing after visiting a spawn location before advancing any further.

Mapping locations to street segments: Street to Street

In a refined approach, we use the projected location of each spawn point as our mapped location, as illustrated in Figure 10b. While still assuming a straight road, we can determine the street segment of our location and store it as a fraction of total street length. By accessing this parameter, the route distance calculation can determine a user's progress on the street and better calculate real distances. While each spawn location retains a unique position, only real road network distances are required on a crossing to crossing basis.

According to the crossing link displacement problem presented by Roth [214], in this scenario, we need to retrieve the shortest route of four candidates. Since each spawn point is connected to two crossings, there are four possible paths with different distances when searching for the distance between two spawn points.

Clustering spawn locations

A third approach, illustrated in Figure 10c, is independent of the underlying street network and utilizes the spatial proximity of spawn locations to group them up into cluster locations. The cluster location is calculated using the coordinate centroid, a fitting approximation to the geographic midpoint calculation [176]. The clustering takes advantage of the interaction radius concept, where players can interact with a location from several meters away. The more content clusters exist, the more this reduces our problem size. We can combine the clustering with one of the previous

two approaches to further decrease the problem size. This may be useful when a small clustering radius is used, or streets contain many clusters, e. g., in rural areas with long streets without intersections. Since the interaction radius is already common in LBGs, we decide to utilize a clustering approach and evaluate the impact of the other two heuristics in terms of distance accuracy and problem size reduction.

3.4.3 *Route Generation*

Based on our related work analysis, we consider exact solution algorithms to be currently infeasible for large scenarios. The best-performing exact algorithms for the Traveling Salesmen Problem, like the Concorde solver, have run-times of more than three hours per problem instance for instances with 8,000 locations [19, 115]. Among the high number of different approximation approaches presented in Section 2.3.1, we decide to use the two metaheuristic optimization approaches simulated annealing and evolutionary algorithms. They apply to our problem, similar in nature, which allows us to compare their solution quality directly. Other popular approaches like Ant Colony optimization [53] or machine learning approaches [52] require distinct models optimized to the respective approach. The difference in solution quality could not be directly attributed to the solution approach, but dependent on the employed model.

Optimization algorithms

Our selected metaheuristic optimization approaches can utilize the same route representation, objective function, and neighborhood function. This allows us to compare the solution quality based on the selected approach.

Simulated annealing operates with a so-called cooling schedule T at time t, which influences its convergence properties, with faster cooling leading to faster convergence. Based on the related work, we choose $T_t = \frac{C}{\log(t)}$ [97] with the value C set to the maximum value $v(s_i)$ for all spawn locations. This approach directly influences the behavior to not get stuck in a local optimum, as it resembles the maximum value a route can change within one iteration step. Additional algorithm-specfic parameters include the number of restarts, the number of temperatures per restart, and the number of runs per temperature.

Simulate annealing model

Similar to our evolutionary algorithm approach in Algorithm 1, we utilize a roulette wheel selection for a weighted selection of individuals. Instead of having a constant number of reproductions, only individuals that died are replaced by new ones. The death rate again depends on a roulette wheel selection with higher death probabilities for lower objective values, i. e., bad routes are more likely to get replaced in the next iteration. Similarly, good routes are chosen with a higher probability of being parents in the reproduction step.

Evolutionary algorithm model

Similar to the general Traveling Salesmen Problem and the Orienteering Problem, we can fully represent a solution to our problem as a sequence of locations to visit. Thereby, an optimized arrival time t_i for each location l_i can be determined as follows: The expected arrival time $t_{i_{exp}} = t_{i-1} + t_r(l_{i-1}) + d(l_{i-1}, l_i)$ is the optimized arrival time if it is within an active time window, and l_i has not been visited yet within that window. Otherwise, t_i is equal to the next spawn event, i. e., the earliest time

Route representation

a time window becomes active again after the expected arrival time $t_{i_{exp}}$. In our scenario, the latter represents a player waiting for a given time for a spawn point to become active again, before moving further along the route. The advantage of this representation is that every represented route is automatically viable regarding time window constraints. Our neighborhood function can use simple operations such as swapping or location removal within the sequence without checking for the adherence of time window constraints.

Travel time calculation

To calculate route arrival and departure times, we need to go through all locations in order of the route sequence. For each location, we calculate the earliest time it can be accessed by a player depending on the travel time from the previous location, the location's active time window, and whether the player already accessed the location within the currently active time window. The player-chosen start and end location are arbitrary and can thereby not be mapped to a spawn location. To respect this within our model, start and target location are integrated into the route sequence at the start and the end, respectively, without an associated retention time. As a result, the last location's expected arrival time represents the route's total travel time.

Objective function goals

To determine the quality of a generation, an objective function f_{route} is required, which assigns a numerical value to the generated route. For this function, we want to achieve the following properties:

- We want to maximize the total expected route value v_{route}, which is the combined sum of its expected location values $v(s)$ (Equation 6).
- To enforce a maximum total travel time, the objective value needs to decrease significantly, the more the maximum travel time is exceeded.
- To minimize total travel time for routes below the maximum total travel time, a higher total travel time should lead to a slightly lower objective value for equal expected route values v_{route}.
- If the maximum travel time is not exceeded, a higher objective value should be prioritized over lower total travel time.

Travel time constraint

The maximum total travel time constraint could be enforced by setting the objective value to zero when breaking the constraint. However, a slight modification of a route by the neighborhood function, e. g., removing a single location, can result in substantial travel time changes. Additionally, we expect an optimized route to have a total travel time close to the maximum travel time to reach as many spawn locations as possible when each spawn point has a similar expected value. Thereby, the neighborhood function is likely to produce candidates close to the constraint value. By setting the objective value to zero for any candidate route exceeding the constraint, we would remove the option to find an optimal route by removing a location in the sequence or swapping locations, limiting how an optimized route can be achieved in the metaheuristic process. Instead, we decide to penalize routes that exceed the total travel time.

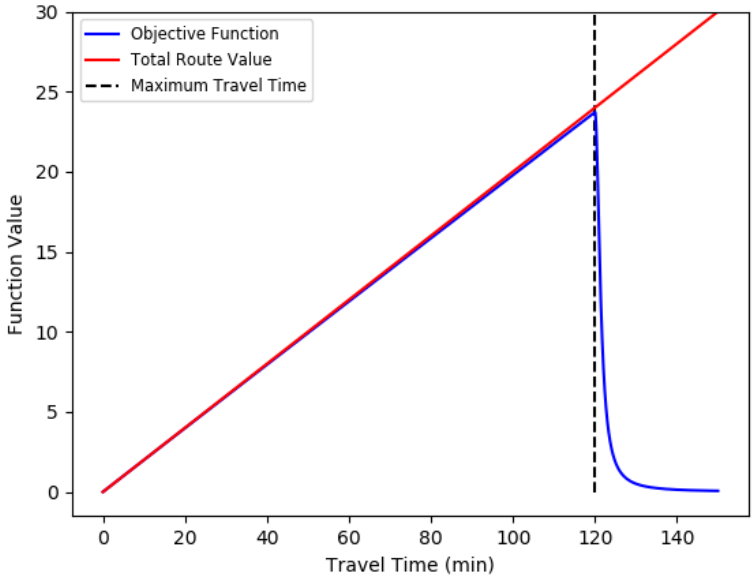

Figure 11: Route objective function value compared to total route value for routes with varying total travel time. The maximum total travel time $t_{r_{max}}$ has been set to two hours. Taken from [240]

We model our objective function as follows:

$$f_{route} = \frac{v_{route}}{1 + \frac{\sqrt{\min\{t_{route}, t_{r_{max}}\}} + c \cdot \max\{0, t_{route} - t_{r_{max}}\}^2}{t_{r_{max}}}} \tag{9}$$

Objective function

The objective value scales proportionally with the expected route value v_{route} in the nominator. The divisor is at least one and increases with increasing travel time, resulting in a lower objective value. Any travel time exceeding the maximum total travel time is squared ($\max\{0, t_{route} - t_{r_{max}}\}^2$), which heavily reduces objective values for routes exceeding the time constraint. Any time spent before the desired maximum travel time is only taken into account as a square root ($\sqrt{\min\{t_{route}, t_{r_{max}}\}}$) to adhere to our third desired objective function property. Both properties in the denominator are normalized by the maximum total travel time $t_{r_{max}}$. Figure 11 exemplarily shows the behavior of this function for a desired maximum travel time $t_{r_{max}}$ of 120 minutes. This assumes that the value of v_{route} increases proportionally to its travel time t_{route}, caused by visited spawn locations on the respective route.

Alternative remaining time model

The remaining travel time could alternatively be integrated into the nominator by instead subtracting $v_{min} \cdot \frac{\min\{t_{route}, t_{r_{max}}\}}{t_{r_{max}}}$ from the expected route value, with v_{min} being the smallest available spawn location value. In contrast to Equation 9, this function would guarantee an increased objective value, when adding additional locations even for small location values. While this property may be promising, we decide against it in our scenario. As stated during the modeling of our value calculation, exact spawn probabilities are typically unknown. Therefore, the individual sighting

reports may contain erroneous data leading to marginal probability for distinct spawn events. In this alternative objective function, these locations would be included at any travel time costs, if available. In practice, this route is unlikely to perform better, be it because of truly erroneous data or our algorithm being more likely to invest iterations on routes that only add marginal value at best.

Penalization factor

To adjust the severity of penalization for exceeding the maximum total travel time, we add a factor c to the penalty term. When utilizing c-value close to zero, exceeding the maximum travel time is punished far less, resulting in more of a rough guideline.

Neighborhood function

Metaheuristic optimization approaches use neighborhood functions to generate new solution candidates, i. e., new routes. Since all considered solutions are created as neighbors of previous solution candidates, an optimized solution must be reachable from the initial solution candidate over neighborhood relations. Like an objective function, the choice of a neighborhood function can have a substantial effect on the optimization performance. Problem-specific neighborhood functions have been shown to accelerate the optimization process or even significantly increase the solution quality when limiting numbers of iterations [180].

To achieve a complete function space, we design four operations for our neighborhood function:

- Add: A random spawn location $s \in S$ is added to the route at a random position.
- Remove: A random spawn location $l \in L$ is removed from the route.
- Swap: Two consecutive spawn locations $l_1, l_2 \in L$ from the route are selected, and their position on the route is swapped.
- Replace: A random spawn location $l \in L$ from the route is replaced by a random spawn location $s \in S$ from all spawn locations.

Neighborhood operations

The *replace* and *swap* operations are not necessary for our neighborhood function to reach all viable solution candidates, as they are similar to a series of *add* and *remove* operations. Nevertheless, including them allows for a change in solution candidates in fewer iterations. We expect these operations to be valuable in the context of local optima. If a solution candidate represents a route close to the maximum travel time, an *add* operation would violate the constraint, while a *remove* operation would lower the route value. A *swap* or a *replace* operation can address this problem by potentially allowing routes that are better within one iteration step, e. g., by replacing a low-value spawn location with a high-value spawn location without a significant increase in travel time. Limiting our *swap* operation to consecutive spawn locations has shown no significant differences in initial tests compared to swapping two arbitrary route locations. Additionally, adding the *replace* operation showed no significant gain in solution quality. We assume that the reason for this is the behavior of our metaheuristics that are already getting out of local optima by occasionally accepting locally worse neighboring solutions.

A first simple approach would be to choose one neighborhood operation at random in an iteration step to generate a respective route candidate. However, by weighting the operations, we can prioritize operations that are more likely to increase the route's

Heuristically determined neighbor

overall quality. Our intention behind this weighting process is to prioritize adding locations to the route, whist the maximum route time has not been exceeded yet, to increase the route's value. When the time constraint is violated, the operation becomes unavailable. We assign initial weights of $\omega_{\mathrm{Add}} = \frac{4}{7}$, $\omega_{\mathrm{Swap}} = \frac{2}{7}$, and $\omega_{\mathrm{Remove}} = \frac{1}{7}$ to represent our design of a higher likelihood of certain operations. The *swap* operation is unavailable for routes of one element.

Heuristic add operation

As described for our distance grid, instead of a full random selection of an added spawn location, we utilize our grid to filter out spawn locations that would exceed the time threshold. Because the grid distances are approximations based on the grid cells' center, the values can be directly accessed. However, on rare occasions, this may lead to valid routes becoming unavailable through neighborhood operations. We consider this acceptable for two reasons. First, filtered out locations are part of a different cell, where it is unlikely that adding a detour into that cell for a single spawn location is part of an optimal solution. Second, when most cells are filtered out by this approach, the current route candidate is close to the maximum travel time. Thereby local optimization with same-cell distances is still available for use to include minor modifications.

Subroute calculation

When calculating route times, information about previously visited spawn locations is determined to check whether an active spawn window has already been visited. This information can be used in multiple scenarios. For particularly long routes, the route calculation process could be split into subroutes and optimized individually. This would require us to determine good intermediate locations that are likely to be on an optimal route at determinable times. While certainly interesting, in practice, it is not likely to be required to plan a multi-hour-long route with an accuracy of seconds.

Context-aware recalculation

A much more likely application scenario is the requirement for route recalculation during run-time. Delays or quicker advancements, while routing are likely to happen, due to traffic, road network structure, diverging movement behavior, or different retention times. In a live environment, the information of previously visited locations can be used to generate a follow-up route, based on the current time and location. A system that detects deviations from the initially calculated route above a certain threshold can trigger a recalculation and provide the user with a new valid route.

4 RUN-TIME MOBILITY DETECTION

With mobility being the central aspect in Location-based Games (LBGs), different mobility types need to be distinguished. A player's current mobility type is relevant for multiple aspects like the accessibility of content, the permitted game interaction, and game area creation. As discussed in Chapter 2, especially motorized vehicles and public transport lines are challenging to distinguish. Thus, we propose a machine learning-based approach to distinguish different mobility types, focusing on motorized vehicles and different public transport types, utilizing common smartphone sensors. By combining acceleration, location, and public map data, we aim to build a robust model for general mobility detection. In Table 3, we present an overview of all classified mobility types. Since sufficient labeled data is required for a machine learning approach, some mobility types could not be included[1]. One requirement to enable a mobility-based adaptation for mobile game systems is that the classification results need to be obtainable during run-time.

In the following, we assess suitable data sources in Section 4.1. Following, we develop our classification model, focusing on different mobility type characteristics in Section 4.2. Based on each identified data source and our extensive related work review, we compose a collection of features for our classification problem.

Table 3: Overview of the classified mobility types.

label	description
`stand`	standstill and halts at traffic lights or station stops in a vehicle
`walk`	different walking speeds including running
`bike`	biking on a conventional bike or an e-bike
`car`	driving in a car during common traffic situations (e. g., urban areas, highway, in traffic jams), including taxis and e-cars
`bus`	buses in the public transport excluding coaches
`tram`	tram
`train`	suburban railway, regional trains, and long-distance trains

4.1 DATA SOURCE SELECTION

For the purpose of run-time mobility detection, it is necessary to analyze the sensors provided by a smartphone and select those that draw conclusions about the mode of transportation. We do not consider those cases where two modes of transportation

Generalizable model

1 Not enough data could be collected for e-scooters and subways, as they were not available for evaluation participants in their area at the time of data recording.

overlap, such as walking in a moving tram for our model. Additionally, we refrain from considering data favoring personalization, e. g., weekday, time of day, or the used start or destination stop, because this would hurt our approach's generalized applicability. Furthermore, this could establish strong privacy concerns.

Public transport data

As noted in Section 2.4.1, the inclusion of external georeferenced information has been reported to increase the detection accuracy for the motorized transport modes *car*, *bus* and *train*. By adding *tram* information we intend to extend the classification to further fixed-route transportation modes.

No audio signal integration

Both audio recording and Bluetooth nearby device data were considered as possible data sources but turned out to be unsuitable. Audio recordings are too dependent on a concrete application or public transport operator, e. g., announcements in public transport or car radio. Supplementary noise by music or radio announcements is unrelated to the chosen vehicle and further complicates the distinction. Additionally, distinctive noises of each mode of transport are hard to generalize [155], and high accuracy audio analysis might not be processable during run-time on a smartphone [251].

Bluetooth nearby devices

Bluetooth has already been used in previous works [47, 183] to detect changes in the mode of transport. The detection is based on a change of nearby devices, e. g., smartphones, fitness trackers, or wireless headphones, which assumes that the devices are visible or detectable over a longer period of time. The visibility of a Bluetooth device, usually induced by the pairing mode's activiation, needs to be manually activated by the user for most devices, making it unsuitable for our scenario.

Acceleration-based sensor data

The accelerometer for conventional mobile devices distinguishes between hardware and software sensors. Since the gravitational direction does not influence the mode of transportation, we include software sensor acceleration data, which is corrected by gravitational influence. Furthermore, to provide orientation independence, we utilize the acceleration vector magnitude $|a|$ of all three axes as the acceleration direction depends on the device orientation, shown in Equation 10.

$$|a| = \sqrt{a_x^2 + a_y^2 + a_z^2} \tag{10}$$

Location-based sensor data

For location-based sensor data, the position itself cannot be directly used for non-personalized models. The W3C Geolocation Application Programming Interface (API) standard [201], however, contains additional parameters we include: accuracy, speed, and heading. We deemed altitude data to not be applicable due to their area dependent data. While map data in general provides valuable information, altitude data is available over individual APIs[2], which poses additional challenges regarding query limits or data accuracy.

Location-based external data

In terms of additional location-based data, OpenStreetMap (OSM) provides information about the following public transport-related locations: *i)* the location of bus and tram stops and train stations including train platforms, *ii)* the routes of buses, trams, and trains, and *iii)* the position of traffic lights.

Information about railway crossings is also available but is similarly tagged like tram crossings, which does not allow further distinctions. Under the assumption that public

2 `https://open-elevation.com` (last accessed: September 22, 2020)

transport vehicles adhere to these routes and do not take detours due to, e. g., traffic or diversions, this can be used to improve the differentiation process. Cars driving along those public transport routes provide an additional challenge, as they might be mistaken for public transport vehicles given their location trace.

OSM relation tags for public transport

Similar to the extraction of geodata for Points of Interest (PoIs) in Section 3.1.1, we extract all public transport-related data in a grid-based approach. The assignment of objects or path segments to a public transport line are stored in OSM relations, which we can obtain: *route=train*, *route=bus*, *route=subway*, *route=tram*. This relation-based method also includes traffic signals affecting the ride.

4.2 MODEL ARCHITECTURE

To determine the type of transport, we use a model trained by supervised machine learning since our problem is a classification problem. To train and test the model, we need labeled data, i. e., data consisting of sensor values with the corresponding transport mode. Since training a model, including data pre-processing and data persistence, is expensive in computation time and storage capacity, we decide to train a generalized model on a server. The final model, however, needs to be feasible on a mobile device for run-time classification.

Generalized model architecture

For time series classification, frames are usually used, each representing a specific time series interval. Each frame thereby represents an instance, labeled with a class for classifier training. These instances are generated during pre-processing and contain features, which we will discuss in Section 4.3.

Time series classification

Our main idea here is to create synthetic instances for training that are later described as frame instances. An instance is a data segment with a fixed length on which we want to classify the mobility type. No temporal coherence is modeled in these instances other than the ordering of data entries for, e. g., determination of movement direction. Thus, the features are computed on the whole instance, without distinguishing individual time segments. Therefore, we treat our problem as a classification problem.

(Frame) instance definition

We expect that different features may be relevant, and different frame lengths may be advantageous for different activities depending on the frame length. Related work has shown that *standing* and *walking* can already be recognized with high accuracy [28, 32, 96, 126, 229, 250], where in contrast, other types of transport are more difficult to detect. Especially for the differentiation of motorized vehicles among themselves, we expect that longer observed time intervals improve the detection. We assume that short intervals are advantageous for the differentiation between *standing* and *walking* since these can react quickly to short-term changes. On the other hand, motorized vehicle usage is unlikely to change on a short-term basis, which is why longer intervals should be advantageous to detect motorized movement in, e. g., a *car*, *bus*, *tram*, or *train*.

Different frame lengths

During run-time on a smartphone, we choose to perform a classification in short time intervals to ensure a timely system response for activity changes. A classification every $T_C = 5s$ is a suitable interval, providing the user or the mobile system with an updated mobility type prediction. However, the parameter choice entirely depends on

Run-time mobility detection

Figure 12: Overview over the applied mobility model building steps.

the application scenario. A classification every second or every minute is also feasible, introducing a trade-off between strain on the system and responsiveness.

An overview of the entire process developed in the following is shown in Figure 12.

4.2.1 *Frame Classifier*

Combination of frame classifiers

To detect short-term changes in the movement type and at the same time still be able to distinguish motorized transport modes, we base our concept on intervals of three different sizes: `short` (with the interval length T_S), `medium` (T_M) and `long` (T_L). For each interval size, we train a classifier, which we call frame classifier. To obtain an overall prediction result based on these three frame classifiers, we employ a meta-classifier that combines the three classifiers' outputs into an overall prediction.

Short-term standing

We assign different goals to each frame classifier. The `short` classifier should be particularly good at distinguishing between *standing*, *walking*, and the remaining mobility types, so that it can react to short-term changes in movement. The other two frame classifiers, on the other hand, should be able to distinguish primarily between motorized modes of transport. To achieve our goal of recognizing short-term *standing* and differentiate between extended intentional *standing*, both `short` and `medium` classifiers should recognize *standing*. For the example of a pedestrian or vehicle waiting at a traffic light, or a bus stopping at a bus stop, the `long` classifier should continue to predict the overall, longer-lasting movement type.

Temporary standing label

This goal requires two labels during the data acquisition process: The main movement type label recorded during data acquisition and, if necessary, in some places, a secondary, more precise *standing* label. The latter is only used for special cases such as stopping at a traffic light or bus stop and is manually assigned to the training data, based on the route speed and acceleration data, described in detail in Section 4.2.4. It is important to note that each instance only contains one class label, with the exception of temporary *standing*. Thus, the frame length must not be exceedingly long, as this would introduce possible misclassifications when switching mobility types. Because the switchover usually requires intermediate *standing* or *walking*, those frame instances will most likely not contain two distinct vehicular mobility types.

Possible reduction of short classifier

If the `short` classifier cannot reliably differentiate between movement types, based on their short frame length, it would be possible to reduce its classification spaces to the three labels of *standing*, *walking*, and *other means of transportation*. However, in the course of this thesis, it has been valuable to integrate all available classes for `short`.

4.2.2 *Classification Approach*

Employed machine learning approaches

Among the classical classification algorithms, especially random forests, have led to the best results in related work [96, 168, 220, 229, 275]. For our described multi-class problem, we focus our work on decision tree learners, e. g., Random Tree, Reduced Error Pruning Tree, or J48, as well as ensemble approaches, e. g., Adaptive Boosting, or Random Forest.

Approach to under- and overfitting

Under- and overfitting is a severe problem in machine learning. To counteract underfitting, we will identify as many fitting features as possible, for which we suspect them being relevant for the current transport mode, or features reported in related work. Thereby, we accept that individual features may overlap or correlate with each other. Subsequently, to counteract overfitting, we perform a feature selection, reducing the features that are ultimately used to those with the greatest relevance. We utilize a stratified 10-fold cross-validation for the final evaluation, which reduces the variance between distinct folds as each fold aims to have a similar class distribution. It is important to note that the raw data itself contains inaccuracies and noise. Additionally, due to the manual labeling process, inaccuracies in the transition between *standing* and a specific transport type cannot be ruled out, especially if certain sensor values such as speed are missing in the recording.

4.2.3 *Data Cleansing*

Data acquisition application

To collect the required raw data, an application is required that records the acceleration sensor and location data of a smartphone and labels this data with the corresponding label, based on user input. We will present this application in Section 5.2.

Activity separation

In our scenario, an activity represents a continuous course of movement of a smartphone for a certain type of transport. During data acquisition, the labeled sensor data is recorded in a continuous data stream. With data coming from different users and thereby different smartphones, the data stream is separated according to the user device ID and split into activities. We separate activities, whenever the transport mode changes according to its label, or two data points are separated by more than a certain amount of time $\mathtt{maxGap}$, indicating an interruption of data recording.

Manual re-labeling

The manual assignment of the additional *standing* label is shown in Figure 13. Due to latency between the acceleration and velocity data, a precise assignment was not always possible in all datasets. Whenever velocity data was inaccurate, the manual labels were applied according to acceleration data. If manual labeling was not possible due to ambiguous or missing data, we excluded the activity from the training set.

Ambiguous location data

The ambiguity or low quality of location data may also be an indicator for, e. g., routes through tunnels. Thus, the respective data is not discarded. For scenarios where location data is unavailable or the retrieval is not authorized, features based on acceleration data can still be used for classification.

Speed data cleansing

According to the Geolocation API, no speed is returned unless it can be determined [201]. Missing data, however, is reported as having a velocity of $0\mathrm{m/s}$, being indistinguishable from a true standstill. Thus, we decide to fill in missing speed values

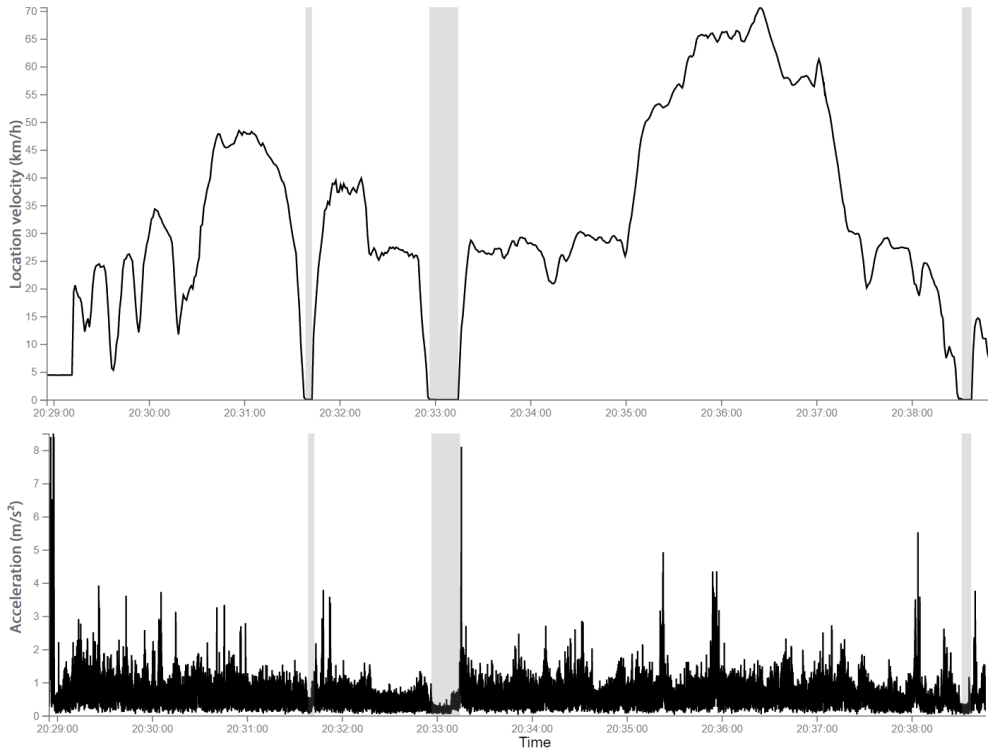

Figure 13: Setting the additional *standing* label in the marked areas using the velocity data (top) and the acceleration data (bottom) in an exemplary *car* dataset entry.

for singular cases based on linear interpolation when both previous and next speed values are available. This is not applied for the special cases of, e. g., tunnels or when the location sensor has not yet initialized, as we only want to fill up single missing values and not replace the whole time series.

Acceleration data compensation

To compensate for missing speed data, it would also be possible to calculate the current speed from the accelerometer values using a Kalman Filter [129]. For a Kalman Filter to work reliably, additional parameters like the initial speed would be required, which is not obtainable from previous speed data when facing the scenario of location sensor initialization. As a result, we decide against using additional approaches to compensate for missing speed data.

Delay and bad accuracy for location data

It is common knowledge that GPS-based location data is prone to errors [27, 126, 177, 229, 233, 275]. In addition to that, there is a latency between the velocity and acceleration data, which is induced by technical conditions: The acceleration data are determined directly by a smartphone's sensor, whereas a sufficiently good GPS signal from several satellites is necessary for the exact position determination. Furthermore, inaccuracies of the GPS signal can be observed frequently in the following situations: *i)* signal isolation in a building or tunnel, *ii)* signal distortion by the environment, e. g., close to tall buildings, reflecting signals [48], and *iii)* attenuation of signals through metal coatings [34, 143] of multi-pane insulating glass inside buildings or trains. The metal coating attenuates radio waves (including GPS signals) by up to 33 dB, which

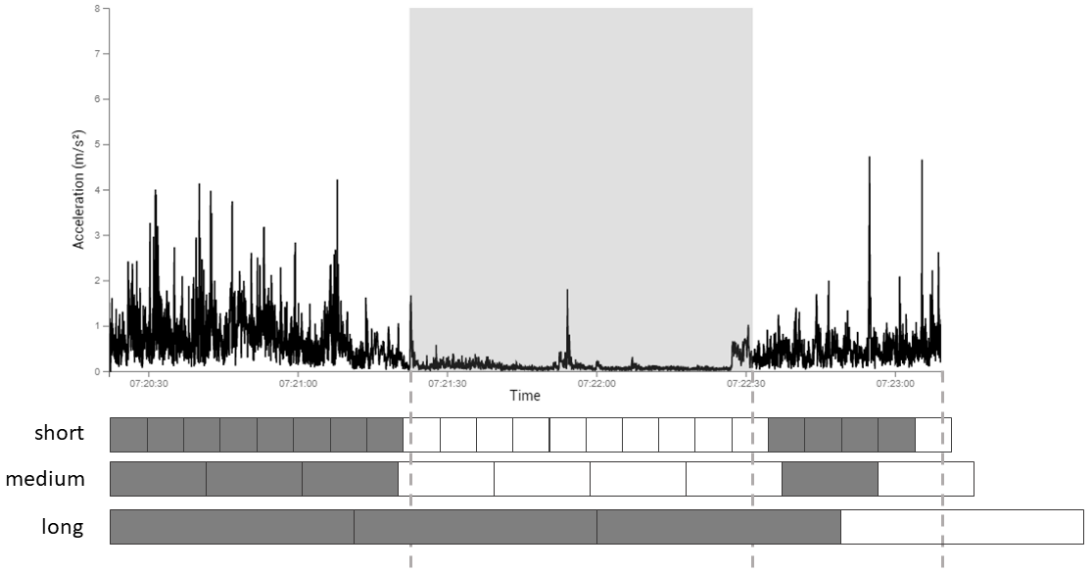

Figure 14: Windowing to generate frames for `short`, `medium` and `long` for an example without overlap. For `short` and `medium` those frames are removed that are overlapped by a secondary label (highlighted). In addition, at the end of an activity, the last frame is removed if it does not reach the specified frame length. Adapted from [116]

corresponds to an almost complete shielding. Such insulating glass is increasingly used in glass facades, trains, and cars.

During data analysis, we observed these effects, especially during train rides and in dense urban areas, where location data was less accurate than in open air. In situations with metal-coated windows in trains, such inaccuracies occur systematically. Instead of removing these scenarios as reported for other works [183], we retain this data and expect the location sensor accuracy to be an important feature in these scenarios.

No speed-related data removal

We refrain from threshold-based filtering of acceleration and speed data for multiple reasons, which is regularly reported in related work, e. g., speeds $\geqslant$ 125 km/h [153], or speeds $\geqslant$ 150 km/h [177]. Most of the data has been collected in Germany, which has no generally valid speed limit, and high-speed trains can also easily exceed the reported thresholds. In general, we could observe from our data that outliers are rare. In this scenario an outlier would be a strong deviation from the expected speed or acceleration values for a given mobility type, e. g., 70 km/h for bikes induced by incorrect location data. For this reason, we decide to focus on attributes that are more robust against outliers, e. g., different quantiles, instead of removing them.

4.2.4 *Pre-processing & Training*

Frame instance creation

Since instances are needed to train the frame classifiers, we generate frames of the duration T_S, T_M, and T_L from the time series of the respective activity during pre-processing, independent from each other. Thereby, a sliding window iterates over the time series with a certain shift of $\texttt{shift}_i$. Instead of utilizing an overlap solely based

on the percentage length of a frame, we include an absolute value of shift_{max} into the calculation, which provides higher overlap for longer frames. To achieve an overlap of at least 50% for shorter frames, we use the following shift for frames with length T_i:

$$\text{shift}_i = \min(0.5 \cdot T_i, \text{shift}_{max}) \tag{11}$$

Frame windowing

Since we want to correctly classify short-term *standing*, we remove all `short` and `medium` frames that overlap with such an additional label. Those frames are then utilized to train *standing* classification. For `long`, we only remove frames that overlap more than 70% with a secondary label, which is rare, as it requires either very long stops or training data where users forgot to stop the recording. Following, we remove intervals that are shorter than 95% of the specified frame length, which only happens for very short activities or the last instance of an activity, as shown in Figure 14.

Pseudo activities for temporary standing

To train our model for frames containing a temporary *standing* label, we extract the intervals to pseudo activities with a *standing* label. Thus, we can frame them with the same procedure and use them for classifier training, ensuring that our classifiers are trained to detect temporary *standing*. The `long` classifier should be able to identify the means of transport independent of temporary stops, which is why those frames containing a temporary stop (if not $> 70\%$) are not removed.

Pre-processing & Training for Frame Classifiers

Accelerometer data resampling

After separating the data stream into individual frame instances, the previously described speed data cleansing is performed, i. e., single missing velocity values are interpolated. However, we sample acceleration data during data collection at the device's maximum possible sampling rate. Thereby, the achieved sampling rate depends on the particular smartphone and its current workload. Thus, the raw data sampling rates range from 6.5 Hz in rare cases to 62.5 Hz in normal cases. Therefore, our model needs to be able to handle diverging sampling rates. For some of the features developed in Section 4.3, e. g., statistical or frequency spectrum features, it is required that the data within a frame is equispaced. This can be achieved by evenly sampling the respective signal in the time domain. For this purpose, a suitable sampling frequency $f = 1/T$ must be determined for each frame. To determine a suitable sampling frequency, we analyzed our recorded data in terms of time difference between data measurements using the minimum, average, median, and first quartile.

Accelerometer data distance analysis

We could deduce right off that utilizing the minimum time difference, i. e., the maximum sampling frequency, would not be representative of the data, as it ranged between 1ms and 7ms. It would have an impact on pre- and live processing performance, due to a significant increase in data, without providing much added value in terms of accuracy as most data would be interpolated. The mean value is also unsuitable, with values between 17ms and 29ms, as it is influenced by outliers. This could be avoided by using the median, which, however, also has a high range between 17ms and 27ms. The first quartile had by far the lowest variance in time difference between 14ms and 18ms for our data. Thereby we choose to utilize the first quartile of the time

difference between data points as our sampling frequency for the respective frame. During resampling in equidistance intervals, we utilize the closest sensor value of the original sample for each new sampling time value.

Unbalanced dataset

Due to the nature of the data collection process being split up to multiple users recording their movement activities of varying durations, the data records are unbalanced. This holds true for the number of intervals for each frame classifier. Training a classifier on an unbalanced set may lead to a biased classifier. Two data sampling options to avoid biasing a classifier during training are reweighting and resampling.

Reweighting and resampling

Reweighting of instances, assigns a weight to each training instance, to compensate for varying class amounts. However, not all algorithms for classifier training and hardly any algorithms for feature selection can handle weighted instances. Resampling, in contrast, achieves an even class distribution by adding or removing instances. We choose to use oversampling for each individual frame classifier by multiplying instances for a balanced dataset. Applying the oversampling process only to the raw data stream or one selected frame classifier would still lead to unbalanced datasets for the other frame classifiers because of the individual frame windowing approach, as shown in Table 4. Undersampling, i. e., leaving out instances to achieve a balanced class distribution, would impact our approach, as our dataset would be reduced according to the least represented mobility type.

Table 4: Distribution of instances for each class for the utilized training data for $T_S = 5s$, $T_M = 15s$, and $T_L = 90s$. The meta-classifier utilizes $stepSize = 5s$. The exact number of instances depends on the respective frame length, and the window shift.

frame classifier	stand	walk	bike	car	bus	tram	train
short	6,207	10,618	5,185	14,829	5,115	1,793	3,936
medium	2,266	5,082	2,514	7,070	2,199	739	1,826
long	1,135	3,884	2,255	6,704	2,457	1,042	1,578
meta	3,708	5,395	2,650	7,578	2,736	974	2,029

Feature selection

The resampling process is an integral part of machine learning, especially when there are many initial features. For performance reasons, we have chosen a filtering approach, and because the alternative wrapper approaches can be prone to overfitting. In Section 4.2.2, we stated that we accept features correlating with each other. In feature selection, we use correlation-based feature selection [98] that preferably selects features that correlate strongly with the class and as little as possible with other features. This reduces redundancies between features. There are several approaches to finding feature subsets, for which we identified four applicable search methods:

- Exhaustive Search [127] checks all possible feature subsets. This leads to a computationally intensive and impractical selection process, which is why we decided against this approach.
- Best First search [197] selects features based on their performance and selected the fewest features in our initial tests.

- Evolutionary Search [148], in contrast, selected the most features, and is based on an evolutionary algorithm employing a heuristic selection.
- Genetic Search [85] uses a random selection algorithm allowing the search in large search spaces.

Because each of our frame classifiers can contain different features, or at least has a different task, the employed feature selection search can be different for each classifier.

Meta-pre-processing & Training for the Meta-Classifier

Our meta-classifier is designed to combine the predictions of the three frame classifiers, which is called stacking. For this reason, we perform a meta pre-processing simulating the activities that determine the frame classifiers' predictions at the respective points in time and provide them with the actual label. Thereby, we generate meta instances with which we train the meta-classifier.

In the meta pre-processing, we iterate over the activities in a certain step size $\mathtt{stepSize}$, determining the respective three frame classifiers for each step. When choosing the step size, we can relate to the T_C parameter, i. e., the time interval, after which a classification update should be shown to the user. In systems with infrequent updates, the step size should not be an order of magnitude larger than the length of the `short` frame T_S, as valuable training opportunities might then be wasted. Similar to the general pre-processing, frames that have not yet reached at least 90% of their intended frame length are not used because some features depend on its frame length. Thus, at the beginning of an activity or recording, there is a phase, where first only `short` frames are used, being later supplemented by `medium` and `long` frames. This results in an initialization duration of $0.90 \cdot T_L$ until all frames are used. This also means that the first classification can be done only after the first `short` frame, i. e., after T_S.

Meta instance creation

In the case of transitions between different movement types, we introduce the $\mathtt{transitionDuration}$, which represents a certain amount of time that may pass until enough data is available to recognize the new movement type. We thereby aim for a transition duration that is less than a `short` frame length T_S to allow for a responsive classification result. In our meta-classification, for the time of the transition, the previous label will be treated as the expected classification result. Thus, each frame is labeled with the movement type that was active during $t' = t - \mathtt{transitionDuration}$.

Transition duration

Those transitions also happen in situations where the temporary *standing* label was set, like halting at a traffic signal. We choose to design our meta-classifier to detect these temporary stops. Thereby, each meta-instance is assigned with this temporary label as the expected prediction class, otherwise the primary label is expected.

Meta-classification for temporary standing

Just like the instances for the frame classifiers, the meta instances are unbalanced, as shown in Table 4. Accordingly, we resample the meta instances before training the meta-classifier.

Meta-instance feature selection

The prediction of our meta-classifier solely depends on the output of the three frame classifiers. This results in a limited amount of features. For feature selection, this allows for more exhaustive approaches, which we will need to evaluate.

Table 5: Overview over the employed feature categories for mobility detection. A detailed insight over all features is provided in Tables 22-26.

feature type	description of utilized sensors or sources
Statistical features	statistical features for acceleration, location sensor speed, and location accuracy
Measures of dispersion	measures of dispersion for acceleration, location sensor speed, and location accuracy
Time-domain features	gravity-adjusted acceleration in time-domain
Frequency-domain features	Fourier-transformed gravity-adjusted acceleration
Location sensor information	covered distance, heading, and speed features
External map data features	OSM map data for public transport stations
Meta-features	classification results for each frame classifier

4.3 FEATURE ENGINEERING

Feature engineering

Feature engineering is the process of developing the most relevant features for the problem based on the given data [271]. We define features for the three frame lengths with the intention to map relevant data features to singular values that are usable in a classification process.

Features from related work

We intend to add features that have either shown a promising impact in related work or have been used without feature selection, meaning that their individual impact is unknown to us. In individual cases, we have modified, expanded, or added features, which we state accordingly. The features have been constructed based on the data sources selected in Section 4.1: acceleration data, location sensor data, and external location information.

Feature name abbreviations

To allow for a better intuitive representation of each feature, we try to only introduce abbreviations when necessary or when related work commonly uses the given abbreviation, e. g., FFT for fast Fourier transform. We choose feature names to allow for a sensor-based grouping after alphabetic sorting. Two consistently used abbreviations from here are `accu` for the location sensor `accuracy`, and `acce` for the accelerometer acceleration vector magnitude (Equation 10). All employed features are shown in detail in Section A.5.2 with a category overview provided in Table 5.

Basic statistical features

We start by including basic statistical features commonly used in the related work for the three data sources of `acceleration`, geolocation `speed`, and its `accuracy`. As noted before, we accept features correlating with each other at this stage. We present the developed features in detail in Table 22, which include common individual statistical values, e. g., mean or commonly used quantiles, and measures of dispersion, e. g., variance, and interquartile range. In the recorded sensor data outliers are found with particularly high values. For that reason, we include the 95% quantile and also utilize

an alternative range measurement between the minimum value and the 95% quantile (`RangeTo95`).

4.3.1 *Acceleration Data Features*

Acceleration data separation

Apart from basic statistical features, acceleration data is rich in information, which is why many authors solely rely on acceleration data [24, 191, 249]. We divide the identified features into two groups: features in the time-domain, and features in the frequency-domain, e. g., following a Fourier transformation. Acceleration data has the advantage to be readily available in smartphones, as no external signal is required, and accelerometers are part of the built-in inertial measurement unit. The detailed resulting features are shown in Table 23.

Acceleration data features in the time-domain

Root mean square

The root mean square (RMS), also known as the quadratic mean, is a simple feature based on the mean values, with the goal of emphasizing higher values.

$$\text{acceRMS} = \sqrt{\frac{1}{n} \cdot \sum_{i=1}^{n} {a_i}^2} \tag{12}$$

Inspired by the normalized spectral energy, which we will develop later in the frequency domain in Equation 17, we propose the normalized acceleration energy, which in this case is the is the square of the root mean square, and is thereby directly correlated.

$$\text{acceNormEnergy} = \frac{1}{n} \cdot \sum_{i=1}^{n} {a_i}^2 = \text{acceRMS}^2 \tag{13}$$

Zero-crossing rate

The zero-crossing rate (ZCR) is the rate at which a signal changes its sign. Since we use the acceleration vector's magnitude, its value is never negative. For this reason, we count how often the signal touches the value 0, normalizing it with the number of signal data points for the given frame. This does not correspond to a true zero-crossing rate for each individual axis, as all axes need to be zero to result in a magnitude of zero.

Mean-crossing rate

The mean-crossing rate (MCR) works similarly to the zero-crossing rate, except that it counts the crossings through the mean, again normalizing it by the number of signal data points.

Skewness

The skewness describes the asymmetry of a frequency distribution and is commonly used for probability distributions. It is the third central moment in a frequency distribution, where the variance is the second central moment. It characterizes the asymmetry of the tapering sides of the distribution, with negative values representing a left-sided skew and positive values a right-sided skew. We calculate the skewness [4,

92] based on the standard deviation SD and the mean value $\overline{a}$ of data series a with length n.

$$\text{acceSkewness} = \frac{1}{n \cdot SD^3} \cdot \sum_{i=1}^{n} (a_i - \overline{a})^3 \tag{14}$$

The kurtosis is a measure of the steepness of a frequency distribution and is the fourth central moment. The higher the value of the kurtosis, the steeper the distribution. The lower the value, the more convex the distribution. We, similarly to the skewness, calculate the kurtosis [4, 92] based on the standard deviation SD and the mean value $\overline{a}$ of a data series a with length n.

Kurtosis

$$\text{acceKurtosis} = \frac{1}{n \cdot SD^4} \cdot \sum_{i=1}^{n} (a_i - \overline{a})^4 \tag{15}$$

The slope sign change rate was used by Aşçı and Güvensan [13] without specifying a formula. We comprehend the feature as the zero-crossing rate of the derivation of a time series. For this reason, we calculate it based on the difference between every consecutive acceleration value.

Slope sign change rate

Other features we have considered in the time-domain include a peak detection, which showed no added value over the features used in the evaluation process.

No peak detection

Acceleration data features in the frequency-domain

A representation in the frequency-domain is a common way to describe a signal or the course of sensor values. For our discrete data, we use the discrete Fourier transform to calculate the frequency spectrum [225]. A commonly used algorithm for fast discrete Fourier transform calculation is the Fast Fourier Transform (FFT), which is applicable since we earlier resampled the sensor values into equispaced segments.

Discrete Fourier transform application

An alternative to resampling the data into equispaced segments would be to use the FFT for non-equispaced data. The non-equispaced FFT [55, 56] is a generalization of the FFT with existing reference implementations by Keiner et al. [142]. This approach best works for periodic signals, which does not necessarily apply for our data, which is why we decided to resample our data.

Non-equispaced FFT

The common FFT implementation expects the number of data points corresponding to 2^n, which does not hold true for our data, which is why the FFT algorithm of Bluestein [25, 105] is used. According to the Nyquist theorem, the sampling rate must be at least twice the maximum frequency to be detected [3]. During initial data collection, reported in Section 4.2.4 identified an average first quartile signal time difference of 16ms. This corresponds to a sampling rate of 62.5 Hz, leading to frequencies up to 31.25 Hz being measurable.

Maximum measured frequency

To receive the amplitude for a given frequency, we determine the magnitude of each Fourier coefficient, combining its real-valued component $\text{Re}(X(f_i))$ with its imaginary component $\text{Im}(X(f_i))$.

Fourier amplitude

$$|X(f_i)| = \sqrt{\text{Re}(X(f_i))^2 + \text{Im}(X(f_i))^2} \tag{16}$$

High-pass filter for noise

The DC term in Fourier transformation is the 0 Hz term, i. e., a constant amplitude wave with zero frequency, with low-frequency noise being close-by. After an initial analysis, we chose a high-pass filter with a cutoff frequency of 0.03 Hz to eliminate these frequency components. For a signal without any noise, a cutoff frequency of 0 Hz would be sufficient to remove the term.

Frequency bins

Since the discrete Fourier transform is calculated in-place, more data points are obtained for the frequency spectrum, the longer the time series is. Grouping them up into frequency bins is a common method to retain performance. For each frequency bin, the maximum frequency component $|X(f_i)|$ from the frequency band is selected. We choose a width of 0.2 Hz for the frequency bins, significantly increasing performance while retaining as much information as possible.

Frequency bands

To calculate meaningful features, the frequency bins are too small. Therefore, we use frequency bands, which are intervals of the frequency spectrum, each limited by a lower frequency of f_l and an upper frequency of f_u. The frequency band is then defined as the sum of the Fourier coefficients of the frequency bins between f_l and f_u. While arbitrary numbers and band lengths would be possible to use as features, we determined our resulting frequency band features by inspecting our recorded data and identifying promising bands. Our list is by no means exhaustive but covers all frequency bins between 1 Hz and 30 Hz.

In addition to frequency bands, features based on a frequency component's amplitude $|X(f_i)|$ are commonly used. We will use the prefix `spectral` for these features.

Normalized spectral energy

The energy of a coefficient can be calculated by squaring its amplitude. Thereby, we define the normalized spectral energy as the normalized sum of energy coefficients with N frequency bins. The normalization is required because signals contain different amounts of frequency bins due to their sample rate.

$$\text{spectralNormEnergy} = \frac{1}{N} \cdot \sum_i |X(f_i)|^2 \tag{17}$$

Spectral centroid

The spectral centroid was originally introduced as a feature for speech recognition [195], where each frequency bin is weighted by its amplitude. It is therefore defined as the frequencies' weighted average.

$$\text{spectralCentroid} = f_{SC} = \frac{\sum_i |X(f_i)| \cdot f_i}{\sum_i |X(f_i)|} \tag{18}$$

Spectral flatness

The spectral flatness is a measure of a spectrum's noisiness [62]. It is calculated by normalizing the geometric mean of the FFT coefficients by its arithmetic mean [170] for N frequency bins.

$$\text{spectralFlatness} = \frac{\sqrt[N]{\prod_i |X(f_i)|}}{\frac{1}{N}\sum_i |X(f_i)|} \tag{19}$$

Spectral crest

The spectral crest factor is strongly related to the spectral flatness [62]. It is the ratio of the maximum amplitude coefficient to the root mean square of the amplitude coefficients [29].

$$\text{spectralCrest} = \frac{\max(|X(f_i)|)}{\sqrt{\frac{1}{N} \cdot \sum_i |X(f_i)|^2}} \tag{20}$$

Spectral roll-off

The spectral roll-off has a cut-off frequency that divides the total spectral energy into a high- and low-frequency band. We choose a ratio of 0.85 between the energy of the low-frequency band and the total spectral energy [62]. This feature can sometimes correlate with the spectral centroid.

Spectral spread

The spectral spread indicates the current effective bandwidth and assesses the shape's spectrum in terms of the width distribution around the spectral centroid f_{SC} [62].

$$\text{spectralSpread} = \sqrt{\frac{\sum_i (f_i - f_{SC})^2 \cdot |X(f_i)|^2}{\sum_i |X(f_i)|^2}} \tag{21}$$

Spectral skewness & kurtosis

Similar to the features in the time-domain, we include the `skewness` and `kurtosis` in the frequency-domain.

4.3.2 *Location Sensor Data Features*

Travel distance calculation

Features based on the distance traveled were often utilized in related work when complete trips based on location data were classified [88, 275]. In contrast to the authors, we apply distance measurements on a frame-basis. In doing so, we normalize the distance in terms of time. For distance measurement, we use Vincenty's inverse problem formula [138], which models the Earth as an oblate spheroid, presenting a higher accuracy than models calculating the great circle distance.

Travel distance features

Feature-wise we decide to use the traveled distance within the frame, i. e., the distance between the first and the last location, to utilize the covered distance. For a more comprehensive distance estimation, we use the accumulated distance, which is the sum of distances between consecutive locations. Unlike Zhou et al. [275], we do not use the maximum distance of the most distant positions for the maximum distance, but the maximum distance of two consecutive positions. The latter feature is expected to correlate with the maximum speed feature presented before.

Travel speed features

In their work, they also introduce features based on the location sensor's speed parameter [275]. They model the ratio of speed measurements that are below a given threshold. We adopt their features and supplement additional thresholds for higher speeds, but again apply them to our frames instead of the whole route.

Heading variation

The heading variation is a measure of the frequency of directional changes. Similar features have already been used in [229, 272, 275]. Using the absolute difference in heading between consecutive `heading` data entries, with each entry in $[0°, 180°]$, we can calculate the accumulated change in heading.

Stopping behavior

Previous publications have shown that enriching vehicle discrimination with features for vehicle-specific stopping behavior can be promising [183, 229, 233]. Looking at the reported stopping behavior differences in related work [233] and when analyzing our recorded data, we identify multiple key aspects.

- Cars stop mainly at traffic lights or level crossings. The stops at traffic lights are relatively short.
- Trams stop regularly, but primarily at tram stops. Between two tram stops, in most cases, we observed a maximum of 90s, with durations between 5s and 30s. This is comparatively short because tram drivers usually do not sell tickets themselves. In some cities, public transport is given priority at traffic lights. For this reason, trams in these cities stop at traffic lights less frequently or for shorter periods than cars.
- Buses can be either city buses or intercity (regional) buses. City buses, like trams in the corresponding cities, also benefit from public transport priority. In contrast to trams, a stop can last much longer if the driver sells tickets on the bus. Differences between city and intercity buses exist in terms of shorter, more equidistant stop intervals in a city, and higher maximum speeds for intercity buses due to regional transfer.
- Trains stop less often than trams or city buses, with stops usually taking much longer than 60s.

Based on this information, we create features based on the number and duration of recognized stops. Recognizing these stops is independent of the *standing* classification, meaning that segments identified as stops are not automatically classified as *standing*.

Stop amount and frequency features

We define a stop as a sequence of `speed` data that does not exceed a threshold of `maxStopSpeed` for more than 2s. A threshold-based approach is chosen, to offset for a potential location sensor drift during a real stop. The duration was chosen, as we want to avoid treating slow-moving traffic as a sequence of stops. In terms of stop duration, we choose to group up durations into differently sized bins, with one open-ended bin containing stops above a duration of `minDurationLongStop`, representing the presumable train stops. Because the stop durations are rather long and frames with a temporary *standing* label are not used in `short` and `medium` training, we apply these stop features only in the `long` frame classifier.

4.3.3 *External Data Features*

Not only the frequency and length of stops may allow conclusions about current mobility type, but also the positions of these stops. While classifiers without any station information may result in false *car* classifications, the vicinity towards a nearby public transport line or a station may increase public transport detection confidence. For this purpose, we extracted OSM relations for public transport lines, which include the individual stations.

Public transport spot detection

We define a radius `stopRadius`, specifying the radius around an OSM node, in whose radius we assign the stop to the public transport stop or the traffic signal. The definition of a radius is necessary because of location sensor inaccuracies. Additionally, the locations are represented as single coordinate, whereas a stop in a public transport vehicle or in a line in front of a traffic light, might deviate in its distance due to the length of the vehicle or the waiting line. It must be noted

that an OSM node can have several tags, e. g., a location can represent both a bus and a tram stop at the same time. The information about the exclusiveness of a stop, i. e., it only being served by this one means of transport, can be helpful if encoded into a feature.

For all public transport features included, we make an assumption on the operating principles in the respective area. We assume that public transport vehicles stop at pre-defined stations to load or unload passengers, whereby individual stops can be skipped. During each trip, they follow a fixed route.

Public transport route retrieval

In addition to station data, OSM provides detailed route data, which we can use to compare a user's movement trajectory to a particular public transport line. Public transport routes are represented by an ordered list of positions, annotated with the public transport type and in many cases the specific line identifier, e. g., the bus or train number.

Trajectory comparison

Our goal is to compare the smartphone's position data with the various routes of the public transport network. Both routes are continuous in space and time and can be represented as a trajectory, generally described as a time-sampled and ordered sequence of data points [87, 118, 230, 231].

Public transport timetable availability

To the best of our knowledge, neither live public transport data nor country-wide public transport timetables are openly available at the time of writing. For individual transport organizations in Germany, timetable APIs are available[3,4,5]. They are, however, presented in different formats and only cover the country to some degree. Thereby, we can only compare our route trajectories in the spatial dimension.

Hausdorff distance

Shao et al. [222] describe a trajectory as a discrete image of a continuous polygon course, which can be generalized to the comparison of two geographic trajectories. An often used similarity measure of two trajectories in geographical scenarios is the Hausdorff distance [21, 102, 152, 222], which is a metric for the distance $H_{A\leftrightarrow B}$ of two non-empty point sets A and B on a plain. It is based on the one-sided Hausdorff distance $h_{A\to B}$, which describes the maximum deviation of a point set A from a second point set B:

$$h_{A\to B} = \max_{a\in A}(d(a, B)) \tag{22}$$

$$d(a, B) = \min_{b\in B}|a - b| \tag{23}$$

$d(a, B)$ describes the minimum distance between a single point a and a point set B, according to a given distance metric. Thus, each $a \in A$ is at most $h_{A\to B}$ away from B. Because the Hausdorff distance is not symmetric [21], the distance of $h_{B\to A}$ (defined equivalently) is required, to define $H_{A\leftrightarrow B}$. The two-sided Hausdorff distance $H_{A\leftrightarrow B}$ is then defined as the maximum of both one-sided distance measurements.

3 https://www.delfi.de/de/strategie-technik/mitglieder/
4 https://www.opendata-oepnv.de
5 https://opendata.rmv.de/site/start.html

Hausdorff distance application

In our scenario, we want to compare a frame of a whole movement trajectory to a full public transport route. As a result, only the one-sided Hausdorff distance $h_{A \to B}$ contains the relevant information, as we want to know how much our position data A diverges from a public transport route B. The inverse case of $h_{B \to A}$ is usually not relevant, because the route is unlikely to be traversed in the given time frame, and it would expect the user to use the vehicle from the departure stop until the terminal station. Because $h_{B \to A}$ is most likely greater than $h_{A \to B}$, the two-sided Hausdorff distance $H_{A \leftrightarrow B}$ has a worse distance estimation than $h_{A \to B}$.

Direction of travel

The Hausdorff distance only calculates the maximum distance between two routes independent of their direction. For this reason, before applying it, we have to check whether both trajectories have a similar direction. Two congruent trajectories with opposite directions would have a very small Hausdorff distance, but would not correspond to the public transport route it is compared to.

Hausdorff features

To derive concrete features from the information described above, we calculate the smallest trajectory distance per transport type. We consider only routes not excluded by travel direction filtering and with a Hausdorff distance below a given `cutoffDistance`. If the `cutoffDistance` is exceeded, the distance calculation is terminated early, and the public transport route is discarded.

Consequently, we employ a feature for each type of public transport station related to the smallest Hausdorff distance.

4.3.4 *Delta Features*

In order to model the temporal course of activities in features, we introduce delta features for each previously described feature. A delta feature sets a feature value of the current frame in relation to the feature's value of the previous frame. If no previous value exists, the delta feature remains empty. Thereby, we double the number of available features, where the previous value does not need to be recalculated as their value has already been determined for the previous frame due to the calculation happening in sequence.

Since we want to use the `short` frames to be able to react to short-term activity changes, and the idea of time dependency opposes this, we do not use delta features for the `short` frame classifier.

4.3.5 *Meta-Classifier Features*

As stated before, we use the results of the three frame classifiers `short`, `medium`, and `long` to determine the overall prediction results in the form of the meta-classifier result. Feature-wise we include the individual predictions and each classifier's prediction for the previous frame. In ensemble approaches like the Random Forest, the frame classifiers prediction is determined by a majority voting approach over the individual Random Tree predictions.

Furthermore, we want to include the outcome of this voting process into our prediction because the uniformity or diversity of the trees' predictions can be promising.

Meta-classifier score features

To provide a measure of prediction reliability, we utilize the proportion between weights of the trees' prediction, the overall prediction, and all tree weights. In a non-weighted Random Forest approach, this corresponds to the ratio of individual trees predicting the given class. In an Adaptive Boosting approach, individual trees can be weighted, requiring the weights to be included in the calculation. We name the resulting measure of reliability `score`, which must not be mistaken for a measurement of confidence [269]. The higher this score, the more reliable the respective frame classifier is with its prediction resulting in the features. Additionally, we use the scores of the previous classification per frame classifier.

This results in twelve features per Meta-instance, which are shown in detail in Table 26.

5

GEOVIS: SYSTEM FOR ADAPTIVE LOCATION-BASED GAMES

To assess the performance of our content generation approach and its adaptation components, we need to implement the respective components for the utilization with mobile devices. For this purpose, we introduce the GeoVis platform. It combines a mobile app component operating on each player's smartphone device with a server component responsible for game data provision and information processing. Further, the mobile component incorporates a prototypical visualization to present the processed results as a foundation for a fully developed game presentation.

In the following section we provide an overview of the platform, before presenting details about the mobile application components in Section 5.1.1, and the server components in Section 5.1.2. Finally, we discuss the development of a mobile application utilized to collect mobility data for model building in Section 5.2. In these sections, we focus on select implementory details for each component to provide additional insights into the architecture and highlight its design choices.

5.1 OVERVIEW OF THE GEOVIS SYSTEM

In Figure 15, we provide an overview on all system components.

Android-based mobile app

The Android-based mobile application deployed on each player's smartphone is the core component of our system. It accumulates local sensor data and processes it for *i)* game area creation base on the location sensor utilizing a Global Navigation Satellite System (GNSS), *ii)* a repeating mobility detection, and *iii)* on-demand route calculation within the game area. The processed data is then fed into the respective game's runtime and applied for visualization accordingly.

Server instances for data processing

Our server instance is responsible for request processing, which mainly concerns the content generation of game areas. To obtain the requested number of suitable Points of Interest (PoIs) it manages its own OpenStreetMap (OSM) database. For mobility detection, the applied model is created on the server utilizing mobility data recorded in our user study described in Section 6.3. This incorporates a web application we utilize for mobility data visualization, data cleansing steps, and model management.

Privacy concerns for personalization and adaptation

Especially for personalization and run-time adaptation aspects, privacy is a highly relevant concern. For that reason, we do not communicate personal data to our server. The only data sent to the server are the game area generation requests. However, these requests only contain the game area identifiers relating to the geographic area the player is located in. Since these areas are sufficiently large[1], the player's accurate position is not communicated. For the route personalization component, the optional PoIs distances can be downloaded from the server, processing the route on the player's mo-

1 The commonly used game area size correspond to the sizes utilized in our later evaluation scenario of at least $0.32 km^2$.

bile device. For the mobility detection component, the pre-built model is downloaded from the server once and contains no player-specific data.

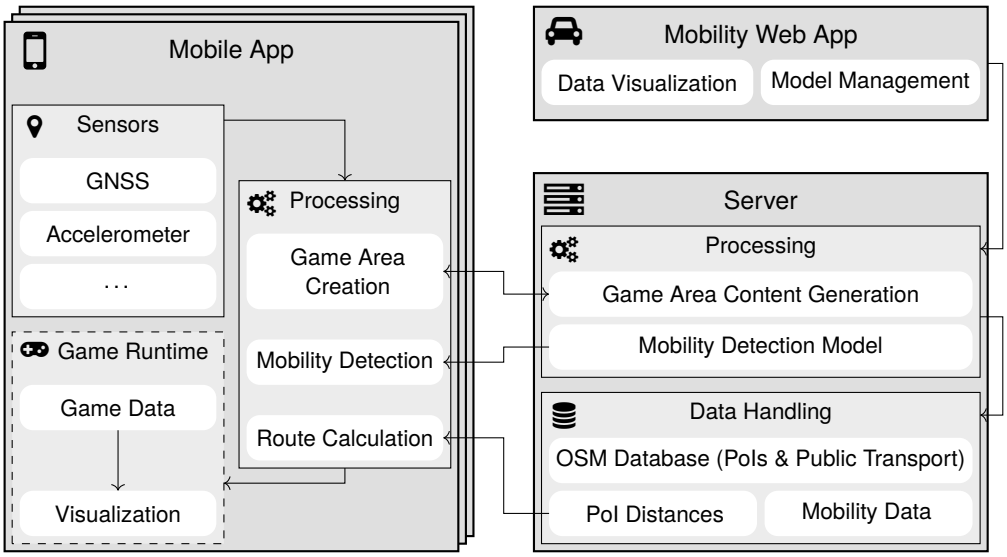

Figure 15: Components in the GeoVis platform.

5.1.1 *Mobile Application Components*

S2 Library

For our rectangular discrete global grid implementation, we utilize the *S2 Geometry Library*[2], as it offers the functionality of hierarchical cells with uniform tiling, neighbor determination, and cell vertex information in an efficient manner. Furthermore, current Location-based Games (LBGs) [104, 199] utilize this library for game area provision, allowing us to compare respective game areas directly. Each cell has a numeric cell level up to 31, where an increase in cell level by one corresponds to a division into a cell's four children. The largest cells with a level of zero cover the whole globe and consist of six cells arranged as a cube. Within our evaluation scenario, we will be exclusively using level 12, 13, and 14 cells, as they have appropriate sizes to cover inhabited areas matching suitable game areas. Level 14 S2 cells have an average area of 0.32km^2, which is approximately the size of a common park area in cities, and therefore a suitable size for a LBG game area. Level 13 S2 cells combine their four level 14 children into an area fourfold the size. Then again, level 12 S2 cells combine their four level 13 children in an area of $16 \cdot 0.32\text{km}^2 = 5.12\text{km}^2$, which corresponds to the approximate area of a suburban area. Although possible, utilizing smaller or larger cell levels would limit our options to either apply the approach to villages when game areas become too large or select meaningful PoIs when game areas become too small. The latter example results in areas with hardly any locations to select from.

Due to the nature of geographic projections (see Section 2.2), a cell's size slightly varies for similar cell levels depending on its latitude. Cells might be rotated, as cell

2 `http://s2geometry.io` (last accessed October 10, 2020)

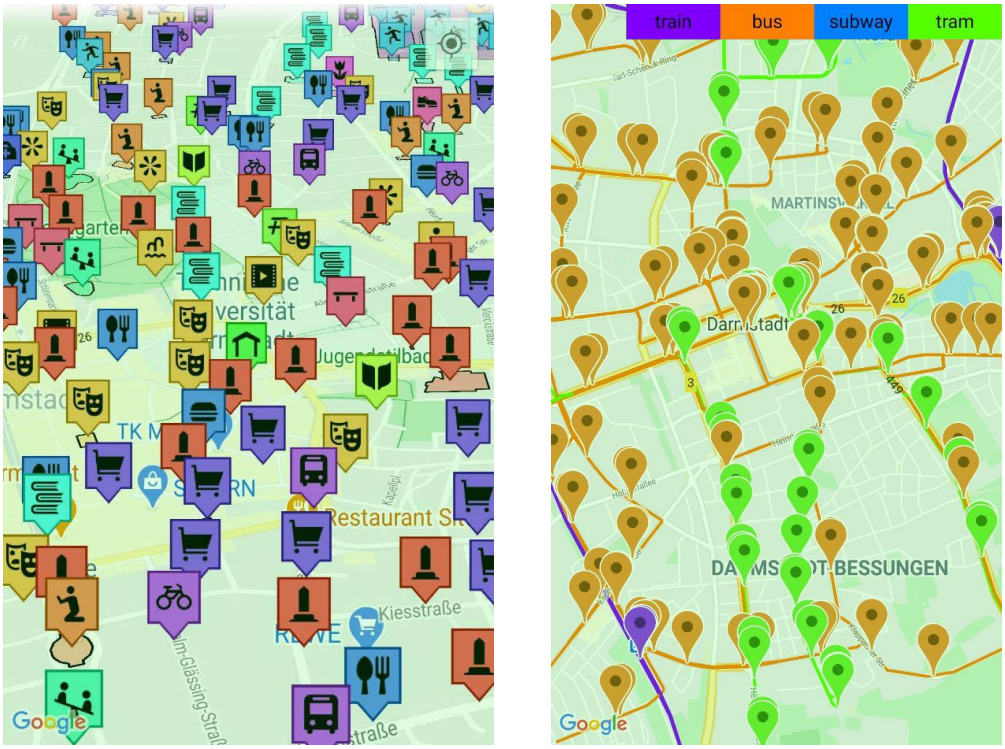

(a) PoI view. (b) Route view.

Figure 16: PoI and public transport route visualization for the city center of Darmstadt. The PoI view utilizes a p_n value of 16. For the route view, all public transport lines with their respective stations are shown.

identifiers are created based on a space-filling curve, in that case, a Hilbert Curve, and projected onto the Earth's surface similar to six faces of a dice. These identifiers allow for an efficient examination and calculation of parent relations between two cells of different S2 levels[3]. We utilize this characteristic to split an area into its subcells of similar sizes during the content generation process described in Section 3.2.1.

Cell parent relation

For data visualization, we developed a game-like component showing the selected PoIs with their respective geofilter category on a geographic map. In Figure 16a, an exemplary view of this component is visualized for the city center of Darmstadt. This component builds the foundation for a fully developed game presentation and was utilized in numerous game prototypes [26, 241], which are not within the scope of this thesis. Since public transport data is separately retrieved for automatic mobility detection, we show a corresponding data view for Darmstadt in Figure 16b, which has been utilized for location-based mobility detection [146].

Data visualization

3 `https://s2geometry.io/devguide/s2cell_hierarchy.html` (last accessed October 10, 2020)

5.1.2 *Server Components*

To reduce our reliance on the uptime and query limits of OSM Application Programming Interfaces (APIs)[4], as well as establish caching approaches, we create a data provision service for all necessary OSM data on a self-hosted server.

Global OSM data is available as *.osm.pbf* files and updated daily[5]. This data usually covers the whole continent but is also individually available for countries. Since country borders are irrelevant for area separation, we split[6] the data according to level 6 S2 cells. The chosen cell level shows good filtering times for the further processing steps.

Data provision

Subsequently, we filter[7] all restricted areas (see Section 3.1.2). The remaining data is then filtered into two files, with one containing an area's relevant PoIs covered by our OSM geodata filters, and one containing all available public transport information including stations and affected traffic signals. Finally, each resulting file is converted[8] into an *.o5m* file designed for fast processing and data merging.

The resulting data is available with an API requiring the type of content (PoI or route data), the area of interest specified by a list of S2 cell ids, and for a PoI request a list of included geodata filter identifier, and the number of requested PoIs p_n. Due to this request's customizability, allowing any desired combination of geodata filters, the game areas are not pre-calculated. In a game scenario with static parameters, i. e., designated geodata filters and PoI amounts, game areas can be calculated for solo gameplay. Then again, for our coupling approach, areas need to be generated dynamically due to the number of possible area combinations for coupling.

Data API

Public transport API

Furthermore, we establish an option to retrieve all OSM public transport data (see Section 4.3.3) for a given S2 cell.

Data processing

Both the game area generation (Section 3.2.1) and the game area coupling (Section 3.3) is written in *javascript*, allowing for deployment as a web service for server-based calculation and local calculation on a mobile device.

Game Area Distribution Determination

To determine the PoI distribution in a game area, we developed two possible metrics, with one being the geographic area of each PoI's Voronoi cell. We calculate an area's Voronoi diagram using the Delaunay triangulation due to their duality [75]. Voronoi border cells are known to be open, having edges of infinite length, leading to incalculable geographic areas. We approach this challenge with two distinct approaches.

Voronoi duality and open border limit

Integrating the game area's geographic borders allows us to limit each Voronoi cell to them. By examining intersection points between game area borders and Voronoi cell edges, all open cells can be closed to match the respective borders. An example for the resulting Voronoi cells adhering to the game areas' outer borders is shown in Figure 17.

Voronoi area border integration

4 `https://overpass-api.de` (last accessed October 10, 2020)
5 `https://download.geofabrik.de/` (last accessed October 10, 2020)
6 `https://wiki.openstreetmap.org/wiki/Osmosis` (last accessed October 10, 2020)
7 `https://wiki.openstreetmap.org/wiki/Osmfilter` (last accessed October 10, 2020)
8 `https://wiki.openstreetmap.org/wiki/Osmconvert` (last accessed October 10, 2020)

(a) Open Voronoi diagram. (b) Closed Voronoi diagram.

Figure 17: Open and closed Voronoi diagrams for four game areas in London with dots representing the individual PoIs. The inner borders exceed each area's individual borders as neighboring areas exist.

While the former approach works reliably, the resulting Voronoi cell size for all previously open cells is problematic. PoIs close to the border are restricted, resulting in significantly smaller area size values. When integrated into an optimization process, those content candidates would be more likely to be neglected due to the false causation between small Voronoi area to likely clustering. In our game area generation process, the problem is divided into subcells, which allows us to integrate neighboring cells' Voronoi calculations. For border subcells, the neighboring subcells outside the original game area are also determined to close the Voronoi areas. PoIs close to the game area border can now calculate their representative cell areas. This results in the sum of all Voronoi cell areas most likely slightly differing from the game area's geographic area, which we deem to not be an issue.

Voronoi neighbor integration

If not otherwise stated, the latter method for Voronoi area calculation is used, if neighboring data is available.

For the Nearest Neighbor Index (NNI) metric calculation for uniform distribution, we require nearest neighbor information for all PoIs, which corresponds to a k-Nearest-Neighbor with $k = 1$. In three-dimensional space, usually, a *k-d tree* data structure is used, which returns inaccurate results for geographic measurements. Thereby we use a *balltree* [192], allowing for a spherical representation including the Haversine distance for distance measurements.

Ball tree

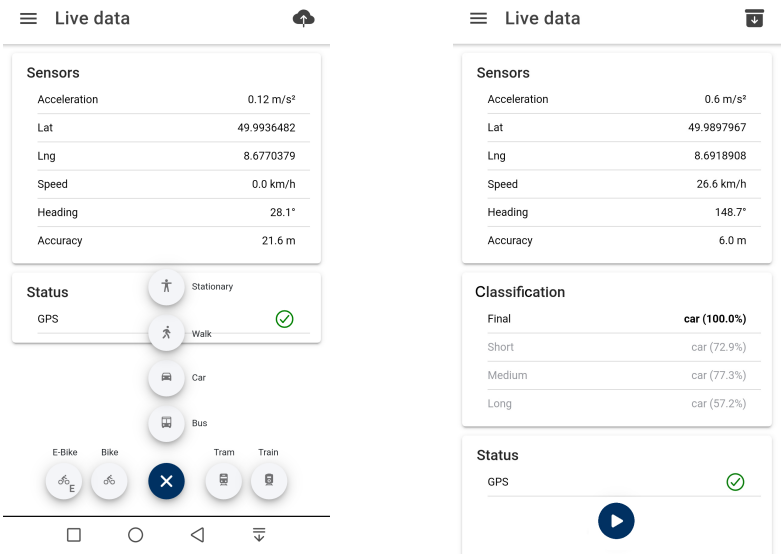

(a) Data collection view with mobility type selection.

(b) Live classification view with frame classifier results.

Figure 18: Mobile application for mobility data collection of accelerometer and location data. Adapted from [116]

5.2 PROTOTYPICAL REALIZATION OF MOBILE MOBILITY DETECTION

Mobility data collection

To record labeled data for mobility detection, we developed a mobile application depicted in Figure 18a that continuously records the sensor data of the acceleration and location sensors and stores them with a label chosen by the user. The data is stored within a database, which is also responsible for the storing of pre-processing runs, preliminary classification results, and all trained models.

Live detection

The live mobility detection, utilizing the final trained model, is integrated into the same application, shown in Figure 18b.

Data source combination

Apart from the recorded acceleration and location sensor data, the external geographic information is retrieved. For this purpose, we incorporate our OSM data provision into our processing pipeline, and cache recently retrieved data to reduce the number of queries. This is particularly useful, as much recorded data originate from the same geographic region. Finally, we cleanse all data from unused information, like unused OSM relation data or tags.

Data analysis and additional labeling

To analyze the recorded data we set up a *Node.js*-based platform, depicted in Figure 19. This allows us to visualize the data of, e. g., acceleration, speed, and route position and compare individual aspects for each recording. Built-on this analysis, we identify the temporary stops within each dataset and manually add the temporary *standing* label, as shown for the highlighted area.

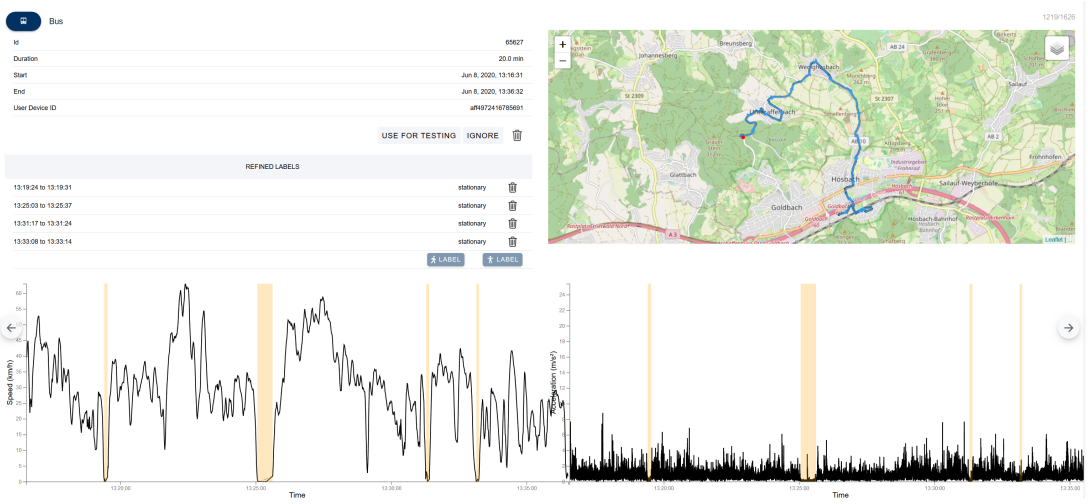

Figure 19: Prototypical data analysis view, showing the location sensor's speed, and the accelerometer vector magnitude with the route on a map. It is utilized during development to visualize each recorded dataset, allowing the identification of special scenarios.

Weka integration

For resampling of instances, classifier training, and feature selection, we integrated Weka[9] in our workflow. It provides a multitude of machine learning and data mining approaches. By using Weka's command line interface, we automatize and schedule the training process. This requires us to convert all data into *.arff* files, which can be processed by Weka. The Weka training process is then multi-threaded, which allowed us to test more processing-heavy approaches like adaptive boosting.

9 WEKA - The workbench for machine learning `https://www.cs.waikato.ac.nz/ml/weka/` (last accessed: August 04, 2020)

6 EVALUATION

Based on our GeoVis prototype, we conduct an extensive evaluation of game area generation, personalization, and mobility detection approaches presented in this thesis. In Section 6.1, we detail our evaluation methodology and how evaluation data was gathered and selected. This includes the specification of evaluated locations and the acquisition of *Pokémon GO* data for comparison.

Next, we address the availability and the corresponding online generation quality for the specified locations in Section 6.2.1. This includes all GeoVis components designed in Chapter 3 and concludes with our route-based personalization approach's quality assessment. Consequently, we evaluate the performance of our automatic mobility detection approach described in Chapter 4.

This evaluation aims to show the applicability of online content generation for Location-based Games (LBGs) across geographic regions. For quality measurement, we apply geographic and cultural metrics, as proposed in Chapter 3. Given our research goal, we explore the boundaries of applicability induced by the fluctuating OpenStreetMap (OSM) data quality and the game areas' heterogeneity. Furthermore, we assess the quality of route-based player mobility guidance in a metropolitan game area to explore virtual reward optimization. Here, we explore the impact of different distance heuristics and the quality of created routes regarding its expected virtual reward. Since mobility in LBG game areas is pivotal and different mobility types are common, we utilize recorded mobility data to evaluate our run-time mobility detection. Therein, we focus on evaluating detection accuracy and comparing the impact of employed features and algorithms on our detection model.

Each evaluated component has scenario-specific characteristics and evaluation scenario parameters, which are described in the corresponding section.

6.1 GAME AREA EVALUATION SETUP AND METHODOLOGY

In this thesis, we utilized box plots, line plots and scatter plot grids to present our evaluation results. Other kinds of data and result presentation are of tabellaric nature.

We utilize box plots as a method to visualize statistical data and its corresponding distribution. Figure 20a demonstrated each individual part of a box plot. The box represents the range between upper (75%) and lower (25%) percentile with the median in between. The two whiskers show the 1.5-times interquartile range (IQR) as a measurement of dispersion. There, the interquartile range is the range between the upper and lower percentile. Values outside of this range are statistical outliers and presented as pluses. When the statistical data consists of multiple subclasses with possible varying distributions, we provide additional markers with error bars on the box's right side.

Box plot

Line plot

The line plot, shown in Figure 20b, aims to visualize the development for the variation of one parameter according to a given metric. We apply the parameter on the x-axis and its respective metric on the y-axis. Different evaluation aspects are shown in one line plot visualizing their development according to their mean value. For the main evaluation aspect, the standard deviation is shown accordingly.

Scatter plot grid

As shown in Figure 20c, a scatter plot grid shows scatter plots partitioned according to one or two parameters on a nominal scale. Thus, each row or column is assigned to one distinct parameter value. Each scatter plot then shows its respective data as a collection of points, according to two chosen continuous metrics, aiming to investigate their correlation. The grid aims to identify parameter-based dependencies in terms of quantity or metric correlation.

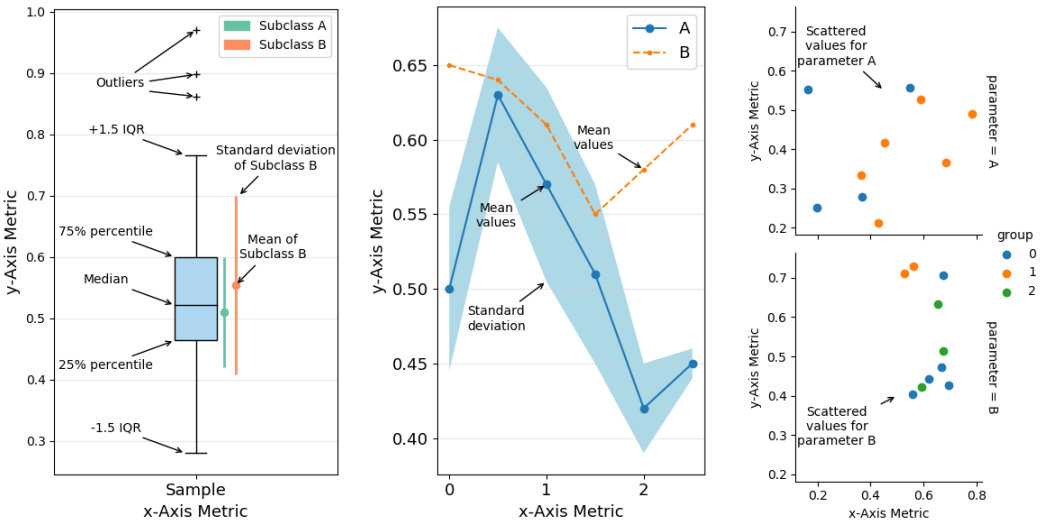

(a) Box plot. (b) Line plot. (c) Scatter plot grid.

Figure 20: Example of utilized plots in this evaluation.

6.1.1 *Location Identification*

Our goal is to evaluate both the global applicability of our system as well as the area dependent generation quality. Differentiating between land use characteristics is important to obtain results about our generation quality for rural and urban areas. However, an area's urban category or its land use is not clearly defined.

Population-based land use characterization

The National Center for Health Statistics presents an area classification scheme to differentiate between rural, suburban, and different sizes of metropolitan areas [120] based on their population size. Comparable classifications can be found for European countries as well [33, 80]. In OSM data, administrative boundaries[1] distinguish be-

1 `https://wiki.openstreetmap.org/wiki/Tag:boundary%3Dadministrative` (last accessed: September 09, 2020)

Table 6: Different categories of urban areas based on their population size according to government classification [120].

Urban category	Population size
Medium & Large Metropolitan	> 250,000
Urban / Small Metropolitan	50,000 - 250,000
Suburban / Micropoliton	10,000 - 50,000
Rural	< 10,000

tween different urban areas, which, however, is inconsistent across and also within countries.

Alternative land use characterization

Urban planners further describe the land use in terms of density, diversity, and design [39], later followed by destination accessibility and distance to transit [66]. In census data, population density is occasionally used to differentiate between urban and rural areas [244], but the definition of metropolitan or urban areas is not consistent across countries, which would lead to uneven comparisons when integrating the reported density. Therefore we utilize a population-based approach to differentiate between populated areas, as shown in Table 6.

Systematic location selection

We choose an evaluation approach, where we systematically select distinct areas around the globe to evaluate. For each continent, excluding Antarctica due to its low population size, we select five metropolises belonging to distinct countries or at least to distinct regions to achieve a proficient coverage for the continent. For each of the remaining three population categories and for each metropolis, we select one location with the appropriate population size according to accumulated census data [30] in the metropolis's broad vicinity. Alternate data sources provided by the European Commission's Global Human Settlement Layer [65, 71] have a detailed focus on urban areas, but lack information about rural areas. We manually select locations instead of a truly random selection to reduce storage strain for our backend service (Section 5.1.2) and because OSM data is reported to be more accurate around populated areas [31, 73]. A complete list of evaluated regions can be found in Table 20, with a description of region-based parameters in Table 7.

6.1.2 *Pokémon GO Locations*

Pokémon GO scanning approach

Pokémon GO provides no open Application Programming Interface (API) for data acquisition. Early on, libraries[2,3] were created by the community. These allow for multiple accounts to extract relevant game information about the position of Pokémon, PokéStops, and Gyms from the communication between their smartphone application and the game servers. Systematically walking around an area allows the programmatic scanning of its content and learning about the different content locations. Due to the

2 `https://github.com/tejado/pgoapi` (last accessed: August 14, 2020)

3 `https://rocketmap.readthedocs.io/en/develop` (last accessed: August 14, 2020)

Table 7: Different regional parameters employed to described the characteristics of a selected location.

parameter name	parameter description
`continent`	the name of the continent being one of the followng: *Africa*, *Asia*, *Australia*, *Europe*, *North America*, *South America*
`area`	the metropolitan area's name the respective selected location is based on
`town`	the selected area's name
`category`	the urban category being one of the following: *Metropolitan*, *Urban*, *Suburban*, *Rural*
`s2cells`	a list of S2 cells representing the given town

temporary (typically 30 minutes) availability of spawn points each hour, this process needs to be repeated continuously to extract the exact time a spawn point becomes active.

Impact of scanning on the players

Due to the developers' large efforts to prevent the automatic scanning of areas, the scan results, as well as community sites making them available, have not been perfectly reliable. The scanned information provides an unfair advantage to players, knowing the exact location of a sought-after Pokémon, which led to a playing style of rushing to those locations by other means of transportation than walking, conflicting with the idea of the game [114].

Possible informative value of scanned areas

The data, however, is highly interesting to analyze, as it provides an opportunity to discover the underlying game mechanics, optimize gameplay for different game areas, and understand more about the regional content quality of the game. Other options we will not cover are the impact of the day-night cycle, the game's weather[4], or different spawn behaviors, e. g., nearby water bodies or different geographic habitats [200].

Two datasets acquired of Berlin and Rhine-Main area

For our analysis, we obtained two datasets. The first dataset obtained for Berlin[5] contains data from 32,148 unique spawn points, which we employ for our route-finding approach described in Section 3.4. The dataset contains no data about Gyms and PokéStops and is limited to a metropolitan area, which both required us to obtain a second dataset. Over the course of six months (July 18, 2017 to Jan 22, 2018), we collected all scanned data in the Rhine-Main area, utilizing a community site unavailable afterward[6]. During this time, the actively scanned areas changed regularly, allowing us to accumulate a total of 12,913 Gym and PokéStop locations and 210,769 unique spawn points. The scanned areas primarily consist of inhabited areas, while some rural areas are still included, leaving many unscanned areas between cities or towns without an organized player base.

Because the latter dataset contains only verified content locations and has no data about scanned areas that contain no content, we cannot know whether an empty cell

4 The game's weather directly depends on the real-world weather and gets updated at every full hour.

5 `https://www.reddit.com/r/pokemongodev/comments/4vckgh/5_million_logged_spawns_over_multiple_days_for/` (last accessed: August 14, 2020)

6 `https://gomap.at` (last accessed: March 22, 2018)

Dataset processing

is empty because no content is available, or because it was not scanned. This becomes an issue when processing the data to calculate Voronoi areas, as the full neighborhood integration is required. Otherwise, the Voronoi area would be primarily dependent on the cell size rather than its area of influence. Therefore, we filter the dataset, including only areas with a full neighborhood, shown in Table 8. This consequently leads to an overestimation on mean content locations per cell, as corner areas or scattered cells, which characteristically have less content, are filtered out. The dataset's area coverage is shown in Figure 43.

Table 8: *Pokémon GO* filtered dataset split by S2 level, including only cells with a fully occupied neighborhood. Cell counts are reported based on three cell sizes (see Section 5.1.1). Thereby, each decrease in level corresponds to a fourfold increase in game area. Thus, the mean number of content locations within a cell increases accordingly.

S2 level	Gyms and PokéStops			Spawn points		
	cell count	Mean	Std	cell count	Mean	Std
14 (small cells)	463	9.68	9.22	3366	44.80	28.34
13	411	17.64	21.63	1335	128.05	98.59
12 (large cells)	278	36.43	49.33	383	451.87	323.03

6.2 ONLINE GENERATION QUALITY

This section will investigate our online generation approaches' quality and relate them to the game data obtained for *Pokémon GO*. Since the obtained dataset is limited to particular game areas in Germany, a worldwide quality comparison is not feasible. Hence, we create individual evaluation scenarios employing the given dataset for comparison. Additionally, we evaluate generation quality and its parameters independent from the dataset in detail.

6.2.1 *Game Area Quality*

Game area data construction

To build a dataset for game area quality evaluation, we need to determine a game area for each selected location. For each location, we select 16 game areas arranged in a four times four grid, with an S2 level of 14 to cover a quadratic section. On average, these cells have an area of 0.32km^2, depending on their latitude, with each decreasing level increasing its size by a factor of four. This results in a total selected area of about $16 \cdot 0.32\text{km}^2 = 5.12\text{km}^2$, which we deemed appropriate to still be able to cover rural areas and small towns, without the majority of the area being purely environmental. Since we also want to evaluate our approach for larger cell levels up to level 12, our grid approach allows us to construct a level 12 game area out of the collective level 14 cells. Because we are not familiar with all selected locations, we select the game areas

based on our perception while inspecting each area on OSM, especially looking for prominent indicators like town halls or city centers.

Game area data acquisition

After identifying the game areas, we generate our content for each game area, based on the pair-wise variation of two game area parameters: the target amount of Points of Interest (PoIs) p_n, and a list of geodata filters. For p_n, we vary between $4, 8, 16$ and 32. For comparison, we include the result containing all available PoIs without any optimization. For our 23 geodata filters (see Table 2), a large amount of filter combinations is possible, which is why we construct three groups. The first group includes all filters between 13 and 23, which mostly correspond to Niantic's guidelines for high-quality content in their games [189]. The second group additionally includes the filters from 7 to 12, representing locations with shops, relevant societal buildings, or leisure areas. The final, third group now also incorporates filters 2 to 6 intended for better coverage in suburban and rural areas. We thereby ignore the street and footway crossing filter as it turned out to provide too much data for practical use, with over 80% of total potential PoI being attributed to it. While it is always an option to include this data, the results in terms of PoI distribution lose in explanatory power, since it is usually possible to select an appropriate location for distribution optimization when fully ignoring the priority metric.

Count-to-target ratio p_{c2t}

As a measure of generation completeness, we introduce the metric of p_{c2t} being the ratio between the number of PoIs in a result and the total target amount p_n. However, this is not a direct measure of generation quality, as it is directly dependent on underlying potential PoIs. Reasons for an unmet PoI amount goal in some subareas are manifold, e. g., excluded company grounds, water bodies, outskirts, insufficiently tagged OSM areas, or even just the absence of notable locations for the given selected geodata filters. Henceforth, we utilize p_{c2t} as a criterion for acceptable results, relating to the number of required PoIs and, in return, the number that can be omitted in some subareas.

Data availability

Before analyzing the different aspects of generation quality itself, we evaluate the applicability of our approach to the different `continents` and urban `categories`. Figure 21 shows the number of areas that contain any data according to our filters, indicating an increase in applicability from 60.42% to 70.52% by utilizing the third geofilter group. Five full areas[7] (all 16 cells) led to no PoI, indicating that no OSM data is available for that region.

World state analysis

In Figures 44-46 we show the impact of problem parameter variation for the p_n values of 8, 16, and 32, with p_{c2t} thresholds of 0.5 and 0.9, split by `continent` and `category`. This is still no measure of generation quality, but about the applicability to different regions. Intuitively, for the laxest criteria of $p_n = 8$ and $p_{c2t} \geqslant 0.5$, the approach is applicable to most regions. By comparing different parameter sets we identified pairs with an equal coverage, e. g., ($p_{c2t} \geqslant 0.5$; $p_n = 32$) and ($p_{c2t} \geqslant 0.9$; $p_n = 8$). This implies that relaxing the p_{c2t} criterion can allow for a strong increase in target PoI amount p_n when allowing for a more clustered result. This is a feasible

7 Simão Pereira (Rural, Rio de Janeiro), Damalliij (Rural, Kairo), Lemode (Rural, Lagos), Igbo Ora (Suburban, Lagos), Zhangyan Zhen (Suburban, Shanghai)

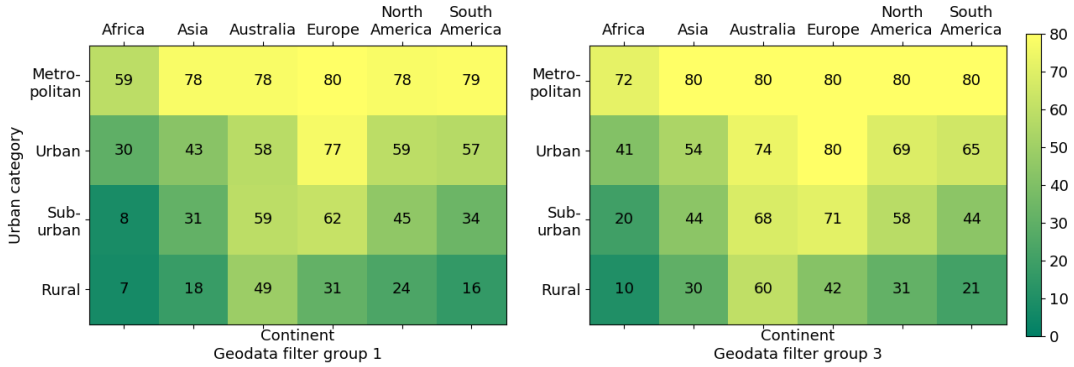

Figure 21: Data availability for all examined locations for geodata filter groups 1 and 3. For each combination of `continent` and `urban category`, the number of game areas containing data of a given filter group is shown with a maximum of 80 ($16 \cdot 5$). The resulting availabilities are $\frac{1160}{1920} = 60.42\%$ (group 1) and $\frac{1354}{1920} = 70.52\%$ (group 3).

option when a slight loss in expected content quality is accepted in favor of a much higher generation availability.

In the following, we will investigate the value of our proposed distribution metrics. Since the Nearest Neighbor Index (NNI) is on a continuous scale with an intermediate value of 1, it is not transparent whether a value represents more of a uniform or more of a random distribution. Thus, its explanatory power is not intuitively clear. For that reason, a Z-test was proposed [43, 100, 157, 212] to compare the present area distribution to a random one. The test relates the differences between the mean nearest neighbor distances for both distributions ($\overline{d}_{obs} - \overline{d}_{exp}$) to the standard error of the mean random distance. It is defined as shown in Equation 24 [157, 158]. Here, n corresponds to the number of PoIs and a to the game area's surface area.

Z-test for uniform distribution

$$
\begin{aligned}
Z &= \frac{\overline{d}_{obs} - \overline{d}_{exp}}{SE_{\overline{d}_{exp}}} \\
SE_{\overline{d}_{exp}} &= \sqrt{\frac{(4-\pi)\cdot a}{4\pi \cdot n^2}} \approx \frac{0.26136}{\sqrt{\frac{n^2}{a}}}
\end{aligned}
\tag{24}
$$

With this Z-test we can quantify the confidence of a spatial distribution actually being uniformly distributed, rather than randomly. The resulting Z-value represents the number of standard deviations differing from the mean according to the cumulative distribution function. Thereby, values above a given threshold apply to the respective confidence level. Because NNI values below 1, representing a clustered distribution, are still possible, we employ a two-tailed test[8]. Before applying the Z-test, we have to check each set of nearest neighbor distances for normal distribution, which is usually done using a Shapiro Wilk Test. When its p-value is > 0.05, the distances are normally distributed.

Translating Z values to p values

8 The respective two-sided confidence level thresholds are defined as follows: $|Z| \geqslant 1.645 : 90\%$, $|Z| \geqslant 1.96 : 95\%$, $|Z| \geqslant 2.576 : 99\%$, $|Z| \geqslant 3.291 : 99.9\%$.

Since a game area is constructed utilizing an area subdivision, the NNI can barely be optimized for scenarios with many empty or partially filled subareas. Thus, we evaluate the metric's explanatory power under the assumption of a close to fully filled area with $p_{c2t} \geqslant 0.9$. As shown in Table 9, a high number of game areas that suffice the p_{c2t} requirement achieve NNI values with high confidence levels for not randomly dispersed. Since all NNI values in this dataset are above one it shows their uniform distribution. For the example of $p_n = 16$, this shows that our approach can optimize game areas for uniform PoI distributions, even though individual subareas could be filtered out, or inversely contain clusters along streets or at public spaces. In this data, the decreasing confidence ratios with an increasing p_n stand out. We identify two reasons for this behavior. First, selecting 64 PoIs in a game area of the given size limits the selection options, since it is unlikely that an area contains many more PoI candidates. Second, the clustering along streets or public spaces plays a role for large PoI numbers, leading to small local clusters.

Z-test results

Table 9: NNI significance test against a random distribution for the distribution of game areas with $p_{c2t} \geqslant 0.9$. All game areas have been generated with equal metric weights ($\omega_{NNI} = 0.5$, $\omega_{Rel} = 0.5$) at S2 level 14. The confidence levels show the accumulated ratio of areas with at least the respective confidence for a uniform distribution.

p_n	$p_{c2t} \geqslant 0.9$	not normal distributed	confidence level			
			99.9%	99%	95%	90%
Geodata filter group 3						
16	31.83%	5.57%	44.08%	60.32%	72.39%	77.03%
32	25.92%	7.12%	27.35%	41.31%	53.56%	59.26%
64	18.46%	9.60%	21.60%	33.60%	44.80%	53.20%
Geodata filter group 1						
16	10.17%	6.78%	32.20%	52.54%	63.56%	70.34%
32	4.48%	0.00%	19.23%	36.54%	46.16%	61.54%

To check for a correlation between the Voronoi area and NNI, we calculate its Spearman's rank correlation. In correlation measures the resulting p-values lead to the respective confidence levels, e. g., $p < 0.05 : 95\%$. Because we want to find a correlation between those parameters in general, a game area-specific correlation measure cannot be used. For the Voronoi's area measure, we choose its standard deviation, as we expect the standard deviation to be small for uniformly distributed PoIs.

Correlation between NNI and Voronoi area

A Pearson correlation was not applicable for two reasons. First, we could only confirm the NNI's normal distribution visually, utilizing a Q-Q plot (quantile-quantile plot), as the Shapiro Wilk Test is prone to individual outliers on large datasets [59, 204]. For the Voronoi areas this could not be confirmed. Second, the homoscedasticity constraint is not satisfied, i. e., the variable's variance is not homogeneous, which we confirmed in a scatter plot.

Grouping the game areas based on the parameters of `category` and `continent` each exposed no further insights as the results were close to each other and similar in nature. We obtained a Spearman's rank correlation of -0.696 with $p = 4 \cdot 10^{-52}$, which represents a monotonic decrease of Voronoi standard deviation with increasing NNI. Thus, we can utilize the Voronoi standard deviation to compare game areas where the NNI is not applicable due to the low amount of locations.

Spearman's r=-0.696

Parameter Dependent Area Generation Quality

To assess the overall area generation quality, we investigate the game areas based on their two utilized metrics, distribution and relevance. Therefore, we employ the NNI and the mean priority value of the selected PoIs, with higher values indicating a better generation result. As a measure of generation success, all results with $p_{c2t} < 0.5$ are filtered out, showing only game areas that provided an acceptable number of PoIs. All game areas are generated with an equal weighting of distribution and relevance metric ($\omega_{NNI} = 0.5$, $\omega_{Rel} = 0.5$), examining the potential trade-off between both metrics. Further analysis without filtering and for the strictest acceptance criterion of $p_{c2t} \geqslant 0.9$ can be found in Section A.2. We conclude that p_{c2t} acceptance criteria should be utilized to avoid low-quality game areas and the effect of a strict criterion.

Game area quality scenario: $p_{c2t} \geqslant 0.5$

To analyze differences between different geographical areas, we split up our data based on continents and urban categories, as shown in Figure 22. Each individual plot contains a scatterplot to visualize the relation between our two metrics and the utilized geofilter group. For the presented scenario, we choose $p_n = 32$ on the level 14 S2 cells, which is intended to be a challenging target for most game areas.

$p_n = 32$ in level 14 S2 cells

For geofilter group 1, containing highly relevant locations, we achieve a mean priority value of 19.5 for metropolitan areas, which is more than 50% higher than that of the other groups. The difference between groups 2 and 3, however, is remarkably small, with the difference in means being between 1.0 and 1.9. Additionally, the amount of game areas meeting the constraint is only 4.6% higher for group 3 compared to group 2. Thereby, we deduce that the geofilters included in group 3 accomplish their goal of providing backup data for sparse areas without having a noticeable negative impact on generation quality. For the NNI, only a marginal difference can be measured between these groups. This also confirms that the resulting game areas are not filled with less meaningful PoIs, but include as many meaningful locations as possible.

No meaningful difference between groups 2 and 3

The characteristics for geofilter group 1 confirm our previous observations that they are mostly applicable to metropolitan areas. It has to be noted that this does not exclude meaningful locations, but that game areas exclusively containing these PoIs are only feasible for metropolitan areas. For urban areas, the generation is successful in 88% of cases in Europe, dropping to 46% in suburban areas, which is still high given the requirement of having at least 16 PoIs in an area of about 0.32km^2.

Generation success rate for group 1 and Europe

As observed before, the generation quality of individual small (level 14) cells may vary due to excluded areas or a general scarcity of PoIs. Utilizing larger game areas can bypass these local problems, but may lead to a more clustered solution. Another problem with a naive approach is the static position of larger cells, i. e., a level 12 cell may not cover a small town, as their borders do not align with each other. Therefore,

Cell merging for larger custom cells

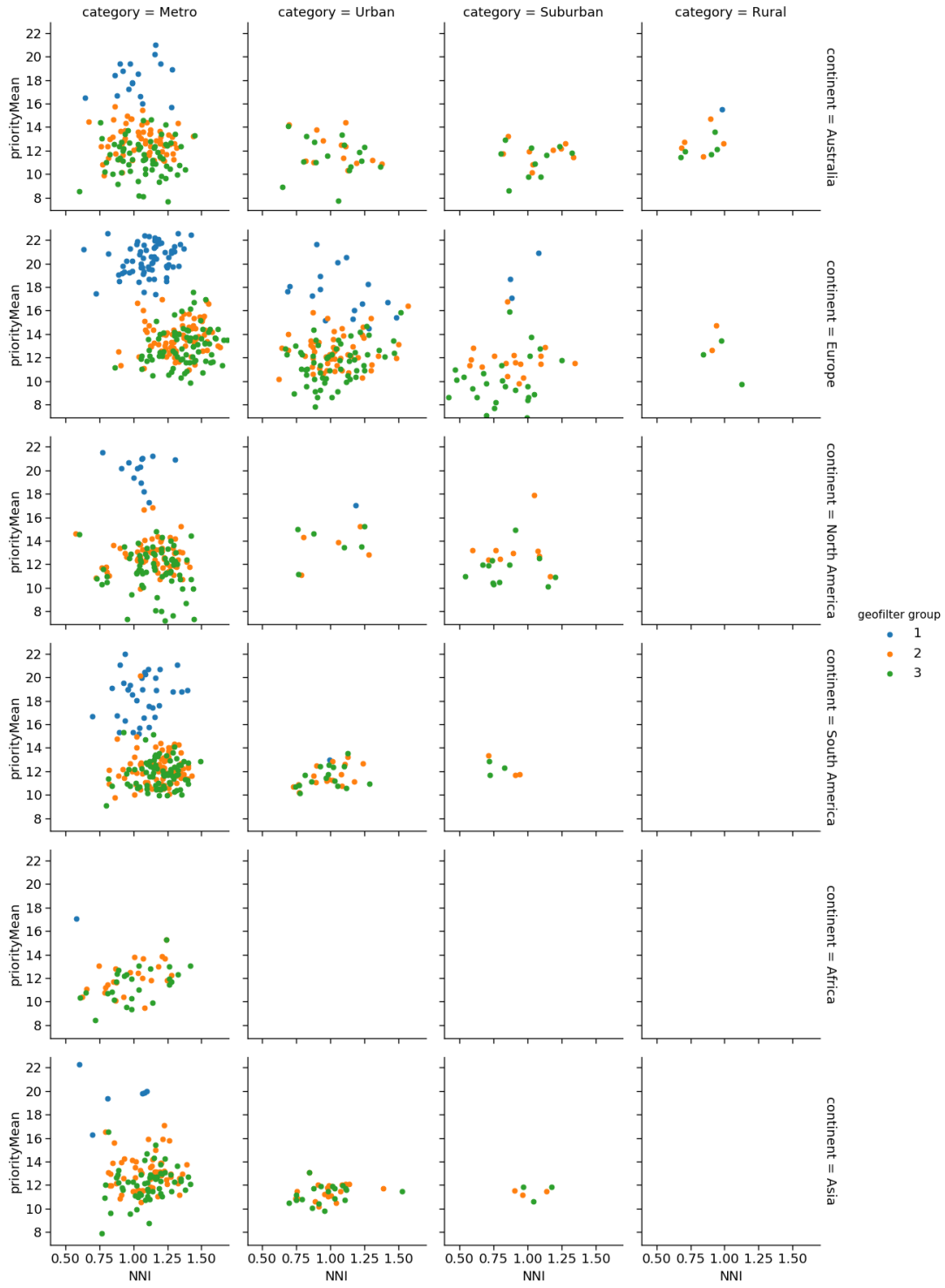

Figure 22: Game area generation quality, split by continent and urban category. Each plot shows the results for all three geofilter groups, relating the mean priority value to the Nearest Neighbor Index (NNI). Parameters: $p_n = 32$, $p_{c2t} \geqslant 0.5$.

we evaluate our cell merging approach that merges the content of four quadratically arranged level 14 cells into one custom level 13 cell and combining four of those custom level 13 cells into one custom level 12. Thereby, borders can be better aligned with towns or city center areas. In Figure 23, we show the Voronoi area standard deviation and the NNI for all three game area sizes. By merging the areas, both metrics become more stable, with a small decrease in NNI value at the top end, after each merge.

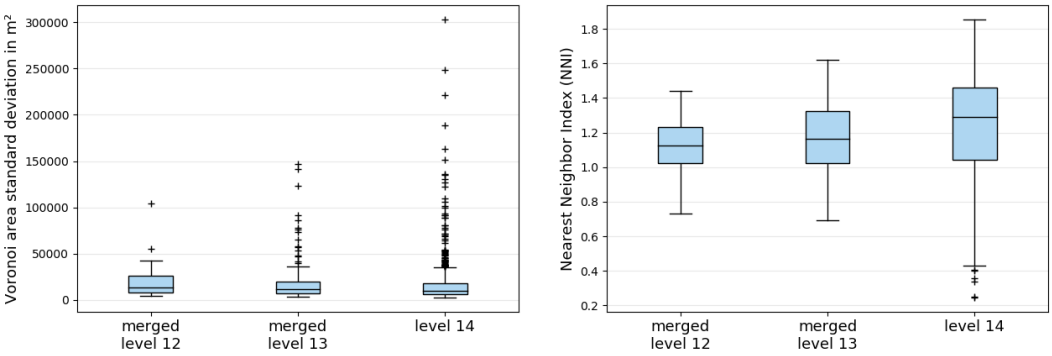

Figure 23: Comparison of different cell sizes for Voronoi area standard deviation and NNI. The cells are merged for geofilter group 3, $p_n = 16$, $p_{c2t} \geqslant 0.5$.

With similar average mean Voronoi area sizes between $23,600m^2$ and $25,400m^2$, the merging process has no major impact on this area metric and shows the effect of integrating neighbor cells during the calculation. In the example of merging four level 14 cells into one level 13 cell for $p_n = 16$, seven PoIs of each uniformly distributed child cell are affected by the merging process, as they are located at a cell's inner border. This would lead to a significant change in NNI and Voronoi area variance when ignoring neighboring cells during generation.

Merged level 13 cells

Regarding the quality of the merged cells, similar observations for merged level 13 cells can be made as before, shown in Figure 24. In this scenario we want to get at least 32 PoIs, resulting in $p_n = 16$ for $p_{c2t} \geqslant 0.5$, since four cells are merged. Geofilter groups 2 and 3 each have an average NNI of 1.16 with higher values for metropolitan areas and mean priority values of 13.2 and 12.5, respectively, having a smaller difference than the level 14 cells. Similar to before, only 4.8% more group 3 areas are generated than group 2 ones. The merging process can compensate for lower-performing subareas up to the p_n value, which we can see in a rate of 92.6% of game areas with a merge, meeting the constraint of $p_{c2t} \geqslant 0.5$ for equal parameters.

Merged level 12 cells

For the merged level 12 cells, all 16 level 14 cells are merged in one virtual cell. For a similar goal of getting at least 32 PoIs, this results into $p_n = 4$ for $p_{c2t} \geqslant 0.5$, which are laxer criteria for each individual level 14 cell. This results in a constantly high mean NNI of at least 1.33 for all geofilter groups, with mean priority values of 15.8 and 15.3 for groups 2 and 3, as shown in Figure 25. For the merged areas, 82.6% of all game areas meet the constraint of $p_{c2t} \geqslant 0.5$ for equal parameters. Compared to the merged level 13 cells, 53.5% more game areas are generated with at least 32 PoIs when utilizing these four times larger cells while having a significant increase in generation quality.

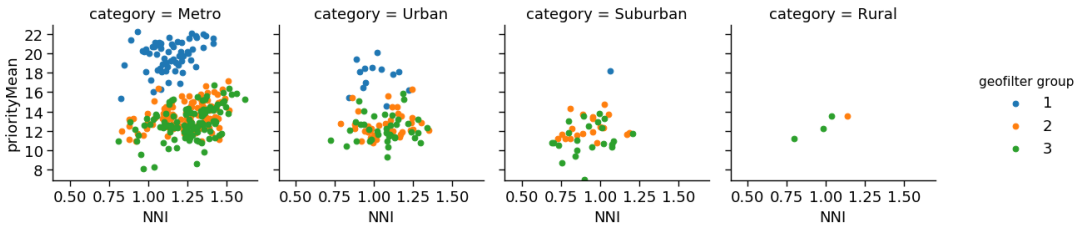

Figure 24: Game area generation quality for merged cells by urban category. Parameters: $p_n = 16$ for 4 cells, $p_{c2t} \geqslant 0.5$, $level = 13$.

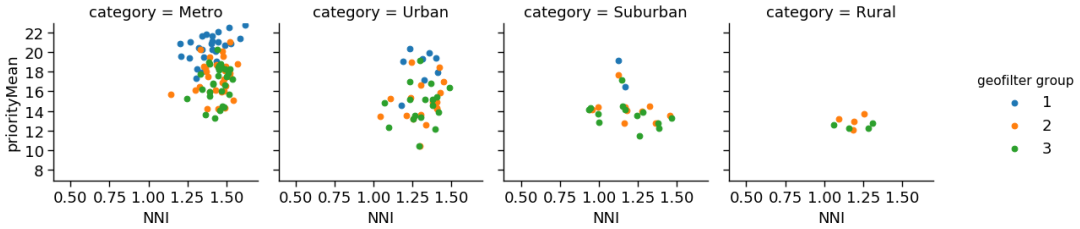

Figure 25: Game area generation quality for merged cells by urban category. Parameters: $p_n = 4$ for 16 cells, $p_{c2t} \geqslant 0.5$, $level = 12$.

We thereby highlight the importance of thoughtful parametrization for the given game scenario since an increase in game area size drastically increases generation quality at the cost of content density, which at the end is a design choice to be made for each individual application scenario.

Exemplary generation result

In Figure 26, we show an exemplary generation result for the metropolitan area of London, compared with its nearby rural area of Towcester, to visualize the limitations but also the contributions of our approach. While the London area has a uniform distribution of high-quality PoIs, due to its 26 times larger data availability, the Towcester area still allows for a successful content generation in the inhabited area. Every game area in London meets the generation requirement and selects well distributed PoIs of high relevance. Towcester, on the other hand, cannot select sufficiently enough PoIs in the outer regions, since these areas no longer belong to the town. However, for its populated area good results are achieved, resulting into an average NNI of 1.18. We observe similar patterns for less populated areas in other evaluated countries, where outer regions cannot provide enough PoIs, but game areas around the cultivated area provide good results. Thus, our approach only provides scattered PoIs in areas of varying quality for non-populated areas or countryside between towns. This is expected since we did not create geodata filters focusing on, e. g., highways, fields, or forests. Additional geodata filters could be designed covering such areas. However, location-based gameplay in such areas needs to adhere to safety regulations and might not be generally advisable.

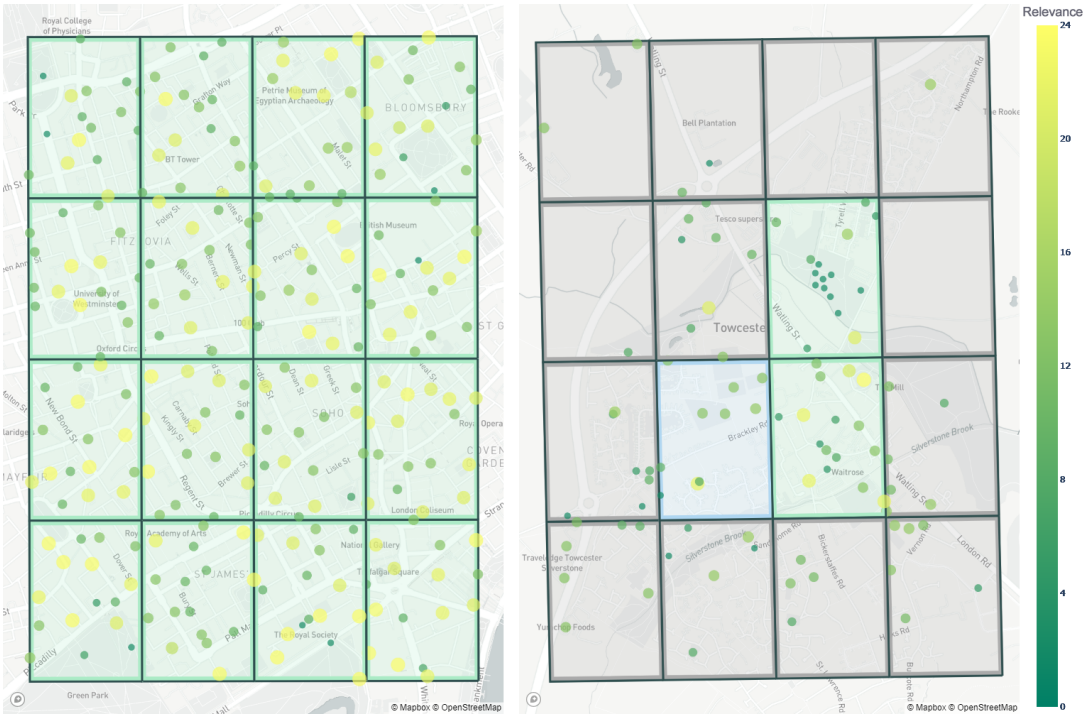

(a) Metropolitan game area London.

(b) Rural game area Towcester.

Figure 26: Comparing the game areas of London and nearby rural Towcester. Selected PoIs for $p_n = 16$ are shown within each of their game areas. Each game area is colored according to their p_{c2t} values. Green areas indicate $p_{c2t} \geqslant 0.9$, blue areas $p_{c2t} \geqslant 0.5$, and grey areas $p_{c2t} < 0.5$.

State of the Art Area Quality

Comparison to Pokémon GO dataset

In the following, we want to compare our results to retrieved data from *Pokémon GO* described in Section 6.1.2. Since we determined the direct relation between Voronoi area and NNI, we will utilize the Voronoi areas here because many areas contain only few content locations, in which case the NNI would not be meaningful. A clear identification, to which urban category a game dataset cell belongs to, is hardly feasible. For that reason, we compare against our generated dataset without rural areas, as those were not included for the game dataset.

Difference between spawn points and Gyms & PokéStops

For the whole dataset, more than 16 times as many spawn points as Gyms and PokéStops exist. Even for the densest Gym and PokéStop areas in the dataset, Darmstadt, Frankfurt, and Wiesbaden, there still exist at least three times as many spawn points as Gyms and PokéStops. This is mostly because every Gym and PokéStop has at least one, typically more, spawn points nearby, with additional spawn points seemingly randomly distributed on the road network.

Comparing the mean number of Gyms and PokéStops in the scanned dataset to our approach, we achieve an increase from 9.6 to 14.0 for $p_n = 16$, and to 28.0 for $p_n = 32$ for geofilter group 3. The generated area data for geofilter group 1, on the continent of Europe, and $p_n = 32$ can be compared to the dataset due to the similar area and

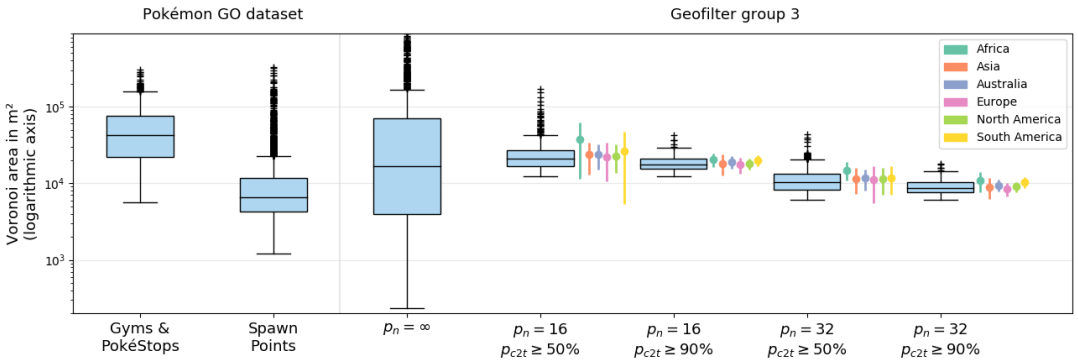

Figure 27: Related work comparison for the Voronoi area of each PoI between *Pokémon GO* data and generation results for geofilter group 3. Values for $p_n = \infty$ are shown to display the variance without any content selection steps.

Increase in PoIs of 31% for similar parameters

PoI characteristics. When comparing this data with the dataset, we achieve a mean PoI number of 12.6, which is an increase of 31%. This indicates that, by directly embedding OSM data, *Pokémon GO* could increase their number of PoIs without changing their content criteria. The mean number of spawn points of 44.8 cannot be directly compared, since they are not directly associated with PoIs. By scattering virtual locations around our PoIs, this could be simulated, which, however, does neither guarantee the locations' accessibility nor their safety.

Voronoi area comparison to Pokémon GO

The Voronoi area comparison in Figure 27 shows a particularly high variance for the *Pokémon GO* related data. The high number of outliers for spawn points indicates a tendency of many isolated locations with no other content nearby. For our generated game areas, Africa's data again confirms that most of its analyzed areas have significantly fewer PoIs, leading to less content that is also strongly scattered.

Generation availability for Pokémon GO dataset

To directly assess our approach's applicability compared to the *Pokémon GO* dataset, we generated game areas for each cell with existing corresponding game data in the dataset. In total, there are 2249 game areas, with 1539 areas containing Gym or PokéStop data. Since Gyms and PokéStop have similar location demands to our geofilter group 1 [189], we can confirm a 98.83% coverage of these game areas for our generation approach. Investigating the areas where the *Pokémon GO* dataset contains only spawn points, i. e., no content related to PoIs represented by Gyms or PokéStop exists, we achieve an area coverage of 87.61%. Those results corresponds to an increase in game areas with suitable PoIs from 68.43% for the *Pokémon GO* dataset to 95.29% with our generation approach.

6.2.2 *Coupling Quality*

To evaluate our game area coupling approach, we limit our scenario that we analyze in detail to game areas in Europe. For game areas outside Europe, the matching is applied but only discussed on a case-by-case basis. Based on our previous results, we decide to utilize level 13 S2 cells with $p_n = 16$ and two coupled game areas for our evaluation

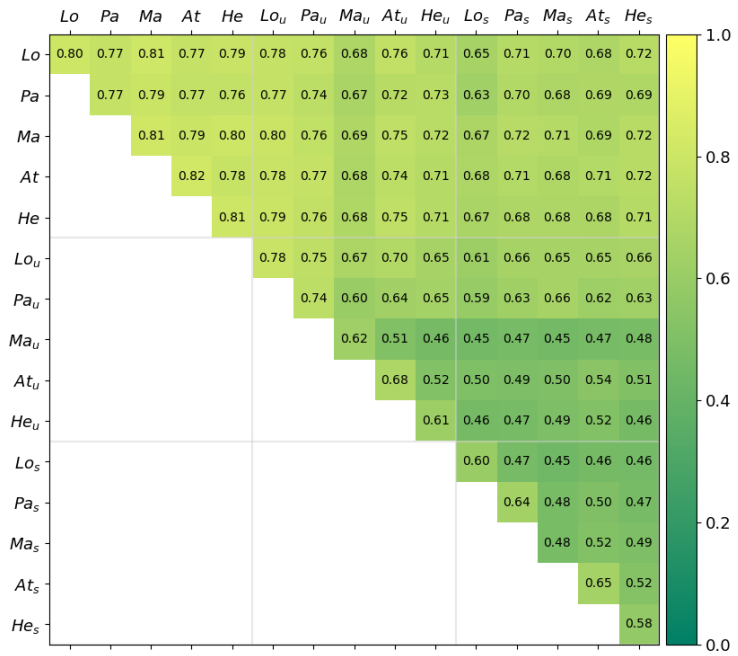

Figure 28: Total f_{score} values for coupled European game areas with our chosen default weighting ($\omega_{Dist} = 0.35$, $\omega_{NNI} = 0.25$, $\omega_{Sim} = 0.05$, $\omega_{Rel} = 0.35$).

scenario. Since multiple game areas are present for each match, we can employ both absolute and relative metrics, namely distance, distribution, similarity, and relevance. Our primary goal is to achieve a geographically well-distributed matching. Due to the different availability of distinct geofilters in different cultural regions, we choose to weight the similarity metric lower. The default values for the evaluation are selected as follows: $\omega_{Dist} = 0.35$, $\omega_{NNI} = 0.25$, $\omega_{Sim} = 0.05$, $\omega_{Rel} = 0.35$, having a larger focus on geographical metrics.

We utilize the geofilter group 3 to incorporate all categories except street and footway crossings since its inclusion led to increased scores, but with game areas mainly consisting of those crossings. The reason for that is the almost universal availability of crossings, which allows for an optimization of all but one metric, the relevance metric. We decide against using these crossings because we do not deem a matching mainly consisting of crossings to be appropriate for LBGs.

Individual Metric Impact

The target function f_{score} indicates the overall quality of selected matches, according to our four metrics. Figure 28 shows the f_{score} values for all game areas in our evaluation scenario, with the exception of rural areas, because individual areas could not provide sufficient PoIs. For all other areas, the respective values are reported, with the location being abbreviated by the metropolitan area's first two letters and the urban category as an index, e. g., Lo_u for the urban area near London, which is Oxford (see Table 20). Since every matching is symmetrical, only the triangular matrix is shown.

Overall coupling results

As expected, the highest scores are achieved for game areas that are coupled to themselves, which can occur when players are within the same game area. The higher values are explained by high expected values in both distance and similarity metric because, in that scenario, one PoI can be matched to itself, resulting in a value of 1 for both metrics since position and priority are identical.

Similar to our game area generation, coupled game areas in the metropolitan areas achieve the highest values due to their significantly higher amount of potential PoIs. In addition to the impact on the absolute metrics of distribution and relevance, the wider variety of PoIs allows for shorter relative distances for coupled PoIs and better options to match PoIs of the same geodata filter.

Despite this advantage, the coupled areas for the other urban categories result in matching scores with small variations. This shows that the coupling, in general, is applicable to any area, and still achieves sufficiently high evaluation scores in most cases. It should be noted that values close to 0.5 do not necessarily represent a mediocre qualityİn comparison, the relative metrics of distance and similarity are in practice optimizable to values above 0.9 for all game areas. These values are often unattainable for the absolute metrics of distribution and relevance since they depend on the underlying geodata.

Data dependence of metrics

For a perfect relevance score, each PoI would need to fit into the category of historical places, which is unlikely due to the game areas' heterogeneity. A good coupling distribution score is, however, already achieved when reaching values well above 0.5, since we normalized the empirical NNI interval of $[0.33, 1.67]$ to $[0, 1]$, thereby representing values with an NNI above 1. Since distribution and relevance metrics are both heavily weighted, the resulting f_{score} values are already satisfactory.

Comparing the different urban categories shows a steady decrease in objective value with decreasing population sizes. However, matching game areas of different urban categories shows interesting results: coupling with one metropolitan area can be enough to achieve consistent high values, as it offers lower populated areas more options to match its PoIs to. To better understand the impact and range of each metric, we will now examine them in detail. The detailed visualized data is provided in Section A.3.

Distance impact

A low distance for matched PoIs is necessary so that all players need about the same time to get from one PoI to the next one. For that reason, we chose ω_{Dist} accordingly high. As shown in Figure 53, all urban categories achieve similarly high values, with suburban areas being slightly lower. Exploring the empirical lower boundary of this metric by setting $\omega_{Dist} = 0$ in Figure 54, and weighting all other metrics equally, values above 0.4 are still common in more popularized areas. The main reason for this behavior is the game area subdivision limiting the maximum relative distance that two matched PoIs can have to the diagonal of that subarea. To explore the empirical upper boundary, we only optimize for distance, setting $\omega_{Dist} = 1$, with all other weights to zero. In that scenario, only values above 0.9 are present when at least one metropolitan area is in the match. Even in suburban area matchings, enough potential PoIs are present to optimize this value, showing that very low relative distances can be achieved for all areas when prioritizing it accordingly.

The difference between the optimized distribution metric ($\omega_{\mathrm{NNI}} = 1$) and the ignored metric ($\omega_{\mathrm{NNI}} = 0$) in Figure 56 shows the range it can achieve in our scenario. An optimized distribution reaches NNI values of up to 1.55, while individual lesser populated areas indicate a clearly clustered result with values below 0.5. According to the previously utilized Z-test, all urban and metropolitan matchings have a high likelihood of being uniformly distributed. For the default parameterization, in Figure 55, we observe strictly worse values in suburban areas.

Distribution impact

Since our default similarity weight $\omega_{\mathtt{Sim}}$ is small, its values vary in many cases, as shown in Figure 57. However, compared to ignoring the metric altogether, occasional improvements can still be observed. Especially areas that are coupled with themselves reach high similarity values, which is plausible since priority values are identical when distance values are maximized. When the metric is optimized ($\omega_{\mathtt{Sim}} = 1$), a maximum value of 1 can be achieved in many areas, especially in metropolitan areas. It has to be noted that optimizing this metric is, in many cases, achieved by choosing the most frequently occurring PoI categories in all game areas. Since these are usually objects of low relevance, like trees or stones, the respective relevance values are correspondingly poor. In this example, the mean relevance value is only 0.43.

Similarity impact

Together with the distance metric, we assigned the highest weight to the relevance metric. Nevertheless, only low values can be achieved for many game areas. As shown in Figure 59, high relevance values mainly occur when metropolitan areas are coupled with one another. This is expected since PoIs with the highest assigned relevance, historical places, places of worship, and entertainment and tourism places, are far more common in larger cities. The differences between an optimized relevance metric ($\omega_{\mathtt{Rel}} = 1$) and an ignored metric ($\omega_{\mathtt{Rel}} = 0$), shown in Figure 60 illustrate the weight's notable influence on the resulting quality since the similarity metric occasionally counteracts high relevance values.

Relevance impact

Different Sizes

Game areas of different sizes can be coupled, representing different travel speeds, e. g., as part of personalization options. To evaluate this approach's feasibility and generation quality, we coupled all game areas in our evaluation scenario with fourfold larger game areas at the same location. Thereby, one-fourth of that area corresponds to the original area.

The $\mathtt{f}_{\mathtt{score}}$ values, shown in Figure 29, show a similar tendency as found for the default scenario. Couplings which include metropolitan areas result in consistently high scores, with a maximum value of 0.83 and a mean value of 0.73. Compared to the default scenario, the scores are impacted by two factors. First, game areas of level 12 are four times as large as game areas of level 13 and therefore have about four times as many potential PoIs, assuming consistent PoI availability. Accordingly, it is more likely that potential PoIs of high relevance exist, and better distribution and relative normalized distance values can be obtained. Second, coupling a game area with itself no longer happens in this scenario, as the game areas have different sizes. The effect can be observed at the matrix's main diagonal, which no longer has comparatively high values. In general, the coupling of game areas of different sizes shows to be

Similar $\mathtt{f}_{\mathtt{score}}$ values

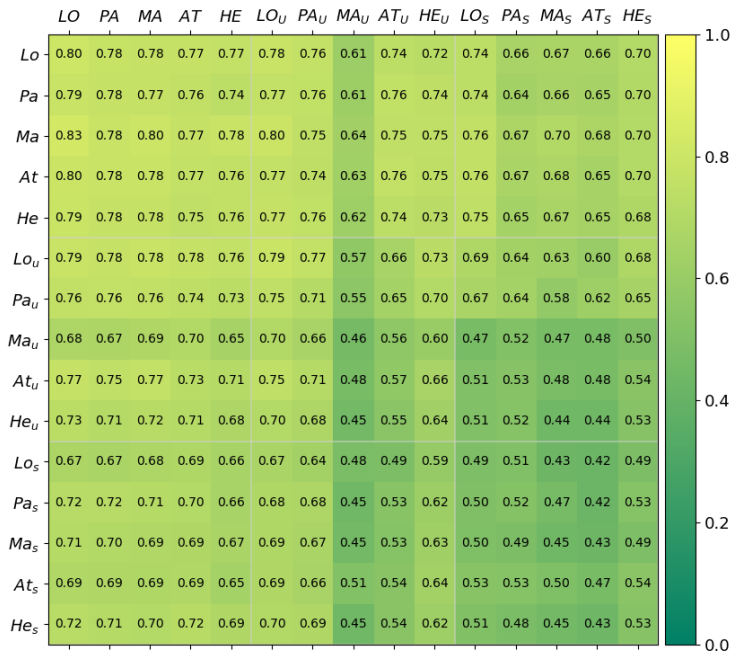

Figure 29: Total f_{score} values for coupled European game areas of different sizes. Game areas in uppercase letters on the x-axis represent game areas with a fourfold larger size than the areas on the y-axis. Thus, x-axis areas utilize level 12 S2 cells.

feasible. It does not lead to a loss of quality, allowing for a flexible selection of game area sizes.

Matching more than Two Areas

Our approach is not limited in regard to the amount of coupled game areas. This allows us to create PoI matches for multiple game areas at once, enabling the realization of larger multiplayer settings. Since increasing the number of coupled game areas drastically increases the problem size, we investigate its effects on the coupling quality. To this end, we gradually increased the number of areas, coupling them in descending order with respect to population size, according to Table 20, with results shown in Figure 30.

Reduced scores for more areas

An expected trend that can be observed is the decrease in overall coupling quality represented by f_{score}. For comparison, we also show the resulting values adding areas in order of their population size, starting with the highest. With an increasing number of game areas, the values converge to the total result of 0.42, whereas the coupling scores are significantly higher when only coupling metropolitan areas with each other for the sorted approach.

Analyzing the metric impact shows that the distance metric is mainly responsible for the drop in coupling quality. One reason for that behavior is the lack of PoIs in certain regions due to either filtered out areas or just the absence of any tagged OSM locations. The similarity values are notably low, which is explained by their low weighting in

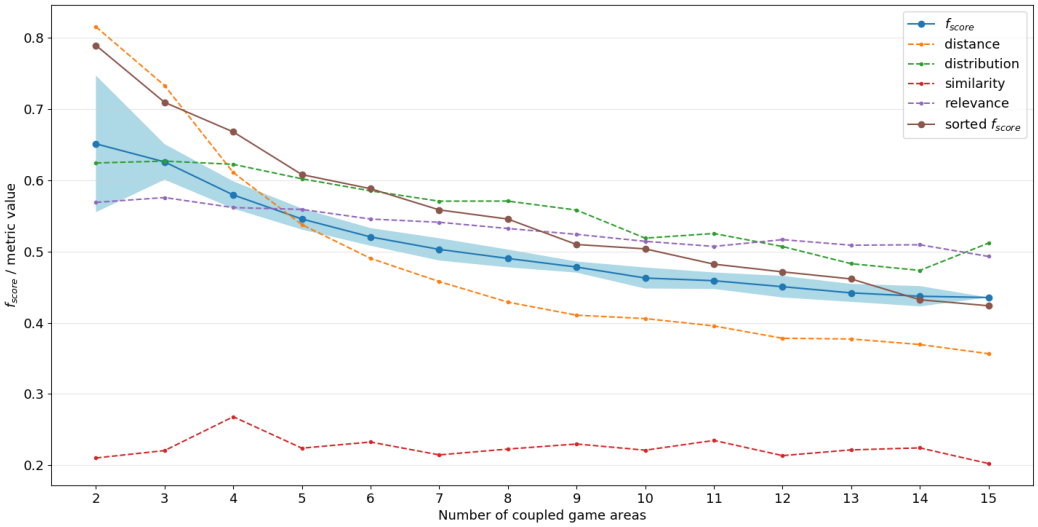

Figure 30: Resulting mean f_{score} and metric values for an increasing number of coupled game areas, combined in Table 20's order. The f_{score} values as "sorted" for comparison, when combined in descending order with respect to population size, starting with the highest.

the optimization process. However, the relevance metric is relatively stable, while the distance metric quickly declines in value. Thus, each PoI matching's distance has the highest impact on the f_{score} when utilizing more than two game areas.

Exemplary Coupling Analysis

In the following, we analyze the coupling of two separate game areas on an exemplary basis. As shown in Figure 31, we compare the game areas of Madrid and Tokyo. The distorted shapes result from map projections, which have no impact on our approach since we normalize each game area's coordinates. Because both cities have a similar latitudinal coordinate, the game area sizes only differ slightly (0.97km^2 and 0.94km^2 respectively). Accordingly, this can be equalized by scaling up Tokyo's area when it is essential for the game scenario.

The coupling with $p_n = 16$ achieves a high f_{score} of 0.78, with an NNI of 1.38, a high distance score of 0.88, and a mean priority value of 19.4. It is generated without rotating or mirroring a game area to make them better visually comparable. Additionally, the visualization shows the separation of each game area into its four subareas. For the coupled PoIs with the identifier of 4, the difference in relative position and the resulting larger distance to one another is notable. While Tokyo's PoI is close to the northwestern subarea border, its counterpart in Madrid is displaced southward.

Exceptionally high metric values

Furthermore, the same PoI in Tokyo negatively influences the NNI since it has a small nearest neighbor distance to the PoI with the identifier of 12. While both PoIs represent a restaurant, leading to a good similarity, the associated geofilter priority value is only 12, not contributing to a high relevance value. We deduce that this

(a) Coupled PoIs for Madrid.

(b) Coupled PoIs for Tokyo.

Figure 31: Coupling the game areas of Madrid and Tokyo with $p_n = 16$. Coupled PoIs are indicated with the similar number. Both game areas have an equal size, where the Tokyo game area has a distorted visualization due to the nature of map projections.

individual coupling is subject to a local optimization, where a higher number of iterations or multiple reruns would potentially yield a better result.

Content accessibility difference

Another important aspect is the accessibility of each location. For the PoIs with identifiers 13 and 14 in Tokyo, both locations have a river nearby, which is visually covered by a highway on top of it. While highway PoIs are not selected, the movement close to a river is restricted, as it is only crossable at bridges. Both PoIs are located at bridges, representing monuments, but the movement is still affected, as players would need to plan their trip around these PoIs carefully.

6.2.3 *Route Quality*

Berlin dataset with large problem size

To assess the generated route quality and the scalability of our approach, we utilize our *Pokémon GO* dataset containing over 5 million automatically registered spawn events at 32,148 unique spawn locations, spanning over a large area of Berlin with an urban area of 309km^2.

Generation run time & Route quality

Due to the large problem size, exact solvers like the Concorde solver [115] are not feasible, which is why no optimal route is calculated for comparison. We instead analyze different parameter configurations for both employed metaheuristic approaches, simulated annealing, and evolutionary algorithms. For each approach, results from

100 generated routes are statistically evaluated regarding their run time performance and the resulting route quality, measured by its objective value.

To evaluate the different distance heuristics in terms of accuracy and computation load, we integrated the GraphHopper API[9], which allows the street network distance calculation on a local device, without query limits. Therefore, we pre-calculate all distances between spawn locations, depending on the selected approach, to provide them in a distance matrix. In doing so, we assume symmetric distances between two locations, cutting the number of required values in half. This assumption is applicable for pedestrians, but not for vehicular transportation due to, e. g., traffic management, or one-way streets.

GraphHopper API pre-calculation

The evaluation is performed on an Intel Core i7-8750h with 4.1 GHz and 16 GB of RAM.

Scenario Parameter Determination

For our evaluation, we specify the individual parameters of our approach according to the evaluated game scenario. In *Pokémon GO*, almost all spawn points are active for 30 minutes once every hour [200], which can be verified in our data. Thereby we select $windowsize = 30min$, and $periodlength = 60min$. We estimate the retention time, i. e., the time a player interacts with the game at a spawn location, to be 30 seconds on average.

We define one typical use case as our scenario: the player starts at the Brandenburger Tor at 16:00, with two hours to spare, until they arrive at the Potsdamer Platz, wanting to catch as many Pokémon as possible by foot. The player's travel mode and speed, and the maximum travel time are problem-specific parameters that can be varied. They depend on the player's choice, which is why we analyze their impact, instead of optimizing them.

Routing scenario

Figure 61 shows the route performance with four different travel speeds. Since they are applied for linear distance, a higher travel speed proportionally reduces the required travel time between spawn locations. We choose values approximately representing the activities of slow gait (3km/h), regular gait (5km/h), jogging (10km/h), and biking (20km/h). A higher travel speed also results in a higher objective value, which was expected, as more spawn points can be visited with less time spent traveling between spawn locations. Due to the retention time and a limited number of spawn locations available in a given area, the objective value does not increase by the same factor as the travel speed. Run times are far more affected by the parameter variation because many more spawn locations are reachable with higher travel speeds, especially for the case of 20kmh/h. This reduces the impact of our distance-based pruning during pre-processing, leading to larger effective problem sizes.

Impact of travel speed

Comparing both approaches, simulated annealing performs better for smaller problem instances, i. e., lower speeds, whereas the evolutionary algorithm is superior for larger problem instances. Simulated annealing generates 3% better routes with an

9 GraphHopper Routing Engine `https://github.com/graphhopper/graphhopper` (last accessed: August 08, 2020)

equal median run time for the case of 3km/h. By contrast, the evolutionary algorithm achieves 21% better results in 18% less median time for the case of 20km/h, indicating a better scalability.

Figure 62 shows the route performance with four different maximum travel times. Again as expected, routes with more time at their disposal achieve higher objective values. However, the increase in objective value is not linearly proportional to the increase in time. Between route durations of 30 and 60 minutes, the median objective value increases by 130%, indicating that clustered spawn points with low travel times are reached on the route. For two hours, the increase is only 60%, compared to the 100% increase in available time. We observe another increase of only 49% for four hour routes.

Impact of maximum travel time

The analyzed data suggests that generated routes with small travel times are likely closer to the optimal route than larger ones. Additionally, the behavior, again, shows the impact of larger problem sizes due to their effect on our distance-based pruning. Therefore, routes should either be limited in maximum travel time, or stronger heuristics need be employed, filtering out more spawn locations that are unlikely to be in an optimized route. A fitting alternative here is our suggested subroute approach, splitting the route generation into shorter, more optimized, subroutes.

Comparing both algorithms, the findings reinforce our previous observation that simulated annealing works slightly better for small problem instances, while the evolutionary algorithm scales better. For large problem instances, the evolutionary algorithm also takes less computation time.

Our pre-processing approach, especially including a distance-based pruning, aims to significantly decrease the problem instance size. For our default scenario, a decrease in relevant spawn points by 77% to 7,375 can be achieved, not yet including any distance heuristics like clustering. The impact of our value-based pruning heavily depends on the selection of the specific Pokémon. In our tests, even looking for the most common Pokémon led to a spawn point decrease by 99%, indicating that targeting one individual Pokémon might not be worthwhile in the evaluation scenario, due to the random spawn behavior.

Pre-processing impact

Heuristic Parameter Determination

We will now compare the different heuristic parameters to determine an optimized parameter value in our scenario. The algorithmic parameters depend on our evaluation scenario and especially the problem size, which might not be optimal in a different scenario. First, we will evaluate the respective impact of our four distance calculation heuristics.

In Figure 32, we compare the accuracy of our proposed distance calculation approaches. The goal here was to reduce the number of required routing calculations, by either utilizing the spawn locations' geographic relation to the street network or a proximity-based clustering. We show the absolute and proportionate error the approach introduces, compared to the actual routing information, i. e., the shortest direct route between two locations. Because routing information is particularly important for close spawn locations, we confine the analysis to distances within our grid cells. While

Distance heuristic comparison methodology

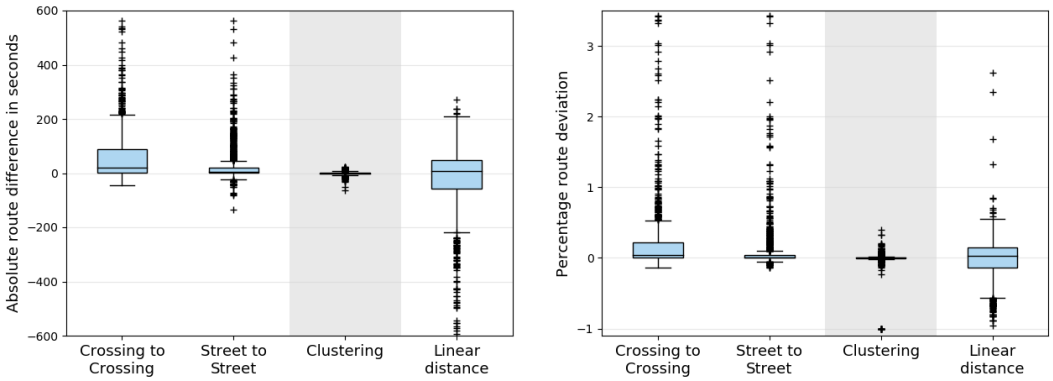

Figure 32: Different heuristic distance approaches with their absolute and percentage error compared to the true route between locations.

distances between far apart points are also relevant, the introduced error becomes more evident when comparing close spawn locations. Additionally, in an optimized route, it is far more likely that nearby active spawn points are visited in succession.

Distance heuristic: Clustering

The Crossing to Crossing approach resulted in 18,081 relevant locations, which is a reduction to 56.24% of the original locations. However, on average, its routes were 58.8s longer than the real shortest route between the actual locations, with a median increase of 20.4s and a high standard deviation of 88.7s. This corresponds to, on average, 35.14% longer routes. We can observe many strong outliers, which is because this heuristic requires going to a location's closest crossing first, which can be a major detour in the wrong direction.

The Street to Street approach resulted in 23,860 relevant locations (74.22%). On average, its routes were 25.2s longer than the real shortest routes with a median of 4.0s and still a high standard deviation of 60.7s, which corresponds to, on average, 23.7% longer routes.

The clustering approach, with a radius of 40m, resulted in 6,430 clusters containing 21,123 spawn points, leading to 17,455 relevant locations (54.30%). Its routes are, on average, 0.2s shorter than the real shortest route, with a median of 0s. This median was expected, as it represents the distance calculation for two spawn locations that have not been clustered, leading to an accurate distance value. The clustering approach also has a low standard deviation of 7.2s, corresponding to, on average, 0.7% shorter routes. Thereby the clustering heuristic is superior in both spawn location reduction and accuracy.

Travel speed = 4.24km/h

We calculate the proposed average detour factor for all spawn points, indicating how much longer the real route between two spawn locations is compared to its linear distance. We select the median value instead of the arithmetic mean, as we observe strong individual outliers, especially for some close-by spawn points that are nevertheless accessed from different streets. The resulting distance factor is 1.18, leading to an optimized median linear travel speed of $\frac{5\text{km/h}}{1.18} \approx 4.24\text{km/h}$ for the dataset and road network of Berlin. This signals that the Manhattan distance would be an overestimation of a detour factor, which would have been $\frac{5\text{km/h}}{\sqrt{2}} \approx 3.54\text{km/h}$.

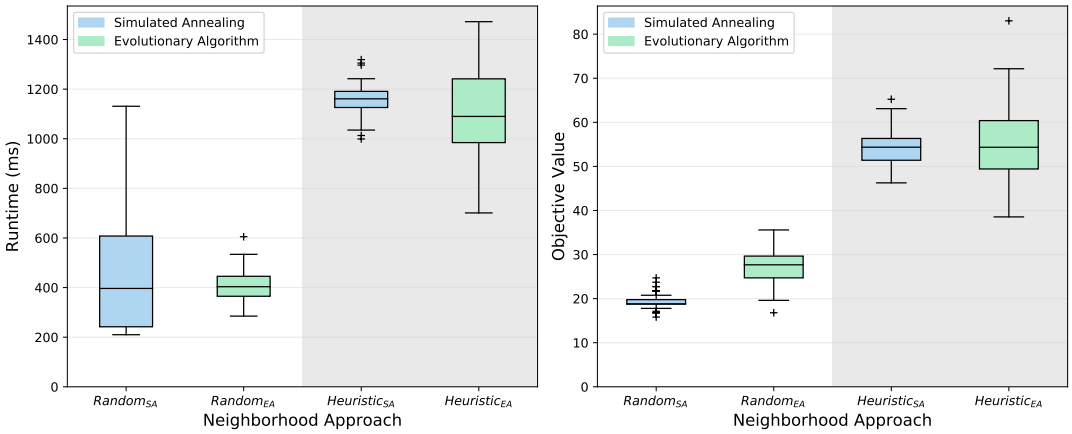

Figure 33: Route performance comparison between the utilization of a random neighborhood function and our heuristic neighborhood function.

Heuristic neighborhood function

Figure 33 shows the performance difference when using either our random neighborhood function or the developed heuristic neighborhood function, for which we will treat the random neighborhood approach as a baseline. Simulated annealing, here has the largest gain increasing its objective value by a factor of 2.9. The evolutionary algorithm also has a notable objective value gain, with both approaches reaching an identical median objective value of 54.3. In terms of run time, the simulated annealing profits from a significant decrease in run time variance. The evolutionary algorithm increases its run time variance, leading us to assume that the heuristic neighborhood grid could still be optimized to achieve high-quality outcomes consistently. The median run time values are equivalently increased for both algorithms. For the simulated annealing, we observe median run times longer by a factor of 2.9 and longer by a factor of 2.7 for the evolutionary algorithm, respectively. Since the heuristic neighborhood allows for vastly superior route results, we deem this trade-off acceptable and further utilize this approach.

Algorithm-specific parameters

Within our algorithm evaluation, provided in detail in Section A.4.1, we assess the effect of different algorithm-specific parameters on generated route quality and performance. Both algorithms are viable when applying them to the problem but perform differently depending on the given problem size. We select our default parameters based on the trade-off between route quality and required run time in our scenario. A clear better algorithm cannot be determined, as both showed overall comparative results, with weaknesses in individual scenarios.

For our distance matrix, we evaluated whether linearizing the matrix has an advantage in terms of computation time compared to a two-dimensional array. Because both approaches performed similarly well, we did not investigate any other storage optimization approaches. Linearizing the matrix has the primary advantage to utilized the distance symmetry more efficiently, thus saving memory.

Based on our collected data, in most scenarios, the simulated annealing approach achieves marginally better median results for smaller problem instances, and slightly

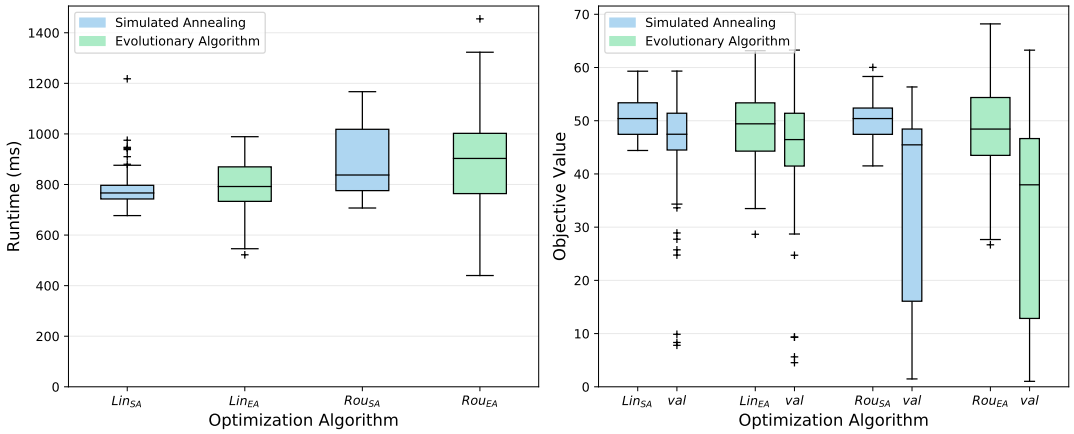

Figure 34: Route generation results and their validation, for our evaluation scenario with the determined default parameters. Linear routes (Lin) are validated based on our cluster distance matrix, while distance matrix-based routes (Rou) are validated using a full GraphHopper route.

worse median results for larger problem instances. One notable factor is the consistently higher variance in objective value of the evolutionary algorithm approach, which can lead to the preference of simulated annealing for its generation consistency. For simulated annealing, we observe that the number of restarts seems to significantly decrease its variance in objective value. Its slight scalability issues could be approached by employing stricter pre-processing filtering to keep the problem size in dimensions where the approach still performs well.

Route Quality Verification

After determining our default parameter set, we evaluate the approach's performance within our defined scenario. Since all approaches utilize some sort of heuristic to model the required travel time between two spawn locations, we employ two validation methods. After a successful route generation, the resulting route gets verified, either by using the heuristic distance matrix, which is only applicable for generated routes based on the linear distance or by utilizing it into a GraphHopper API call. For the latter approach, we expect routes, generated with our distance matrix to become invalid since the clustering radius, i. e., the interaction radius, is not utilized, leading to differing travel times. Since it is possible for a route to reach a spawn point before an active spawn window, small waiting times can be included in each route. Within our evaluation, we experimented with different wait time approaches for validation, allowing routes to wait at a spawn point for a maximum fixed time or to wait an additional amount of time on top of the time scheduled by the route initially. However, no promising findings were achieved here, with the best approach having no artificial waiting time alterations.

Route validation methods

In our validation process, we observed many routes, becoming slightly longer, leading to reduced objective values. To allow for a better comparison between generated

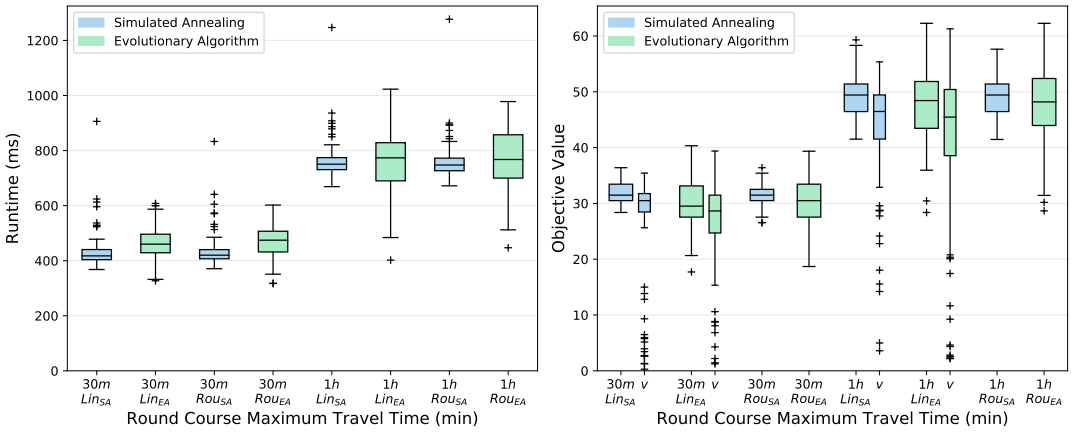

Figure 35: Modification of our evaluation scenario, simulating a round course for the duration of 30 minutes and 1 hour. Validated route results are marked with *v*.

Cutting rear spawn points to adhere to time constraints

and validated routes, we adjusted the validated routes, to match the maximum time constraint. Finding and removing those spawn points responsible for the longest detours while still adhering to the subsequent active spawn windows, is a separate optimization problem. We instead decided to remove the last spawn locations on the route until the target location can be reached in time, since removing later spawn locations does not influence earlier ones. The route results with their respective validation approach are shown in Figure 34.

Route validation effect

The results show consistent median objective values between 48 and 51, indicating that the included detour factor for linear distance calculation results appropriately compensates for detours. Investigating the validation results shows that the full GraphHopper route validation leads to worse objective value results with high variance. This is explained by the employed wait time methodology. Since the route is generated using the distance matrix based on clustered spawn locations, short detours are inevitable when trying to verify the route visiting each spawn location instead of only its cluster location. These detours add up until a spawn point has just become inactive when arriving, leading to an extensive wait time until it becomes active again about 30 minutes later. Judging from the median and variance in objective value, this occasionally affects routes, with most routes being close to the generated ones.

Round course scenario

A different application scenario we want to investigate is the route generation for a round course, i. e., start and target location being the same. The results, shown in Figure 35, display an interesting behavior compared to our basic scenario. Linear distance routes, those validated using our distance matrix, and distance matrix routes are close in median objective value. The variance in objective value does not increase to the same extent as our basic scenario, with an outlier rate between 10% and 15%. Since a threshold-based approach can easily detect an outlier, another route can be calculated instead.

Similar to our results regarding maximum travel time, in Figure 62, the increase in objective value is not linearly proportional to the gain in time. Beneath possible

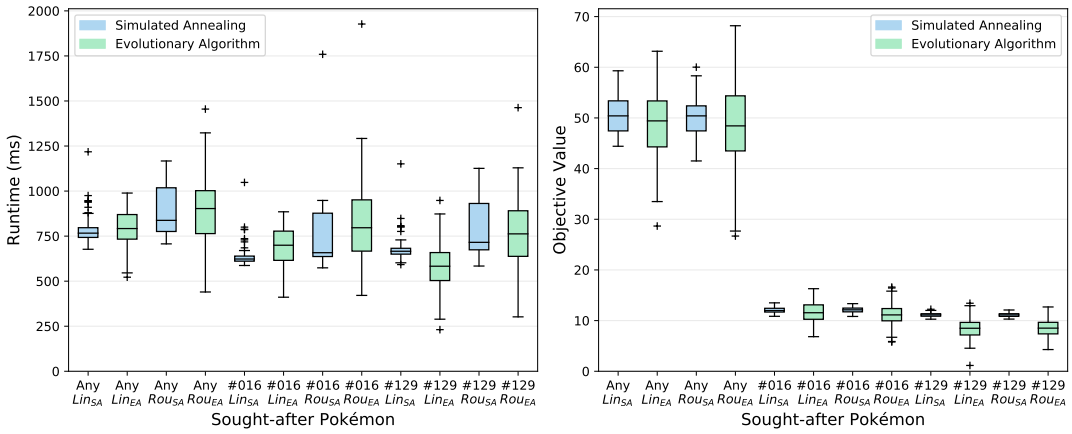

Figure 36: Route performance for routes when focusing on either every spawn point (Any), Pidgey (#016), or Magicarp (#129), showing the routes objective value, which does by no means equate the number of visited spawn points.

scalability issues, the lack of available spawn points could be another reason for this. Since the player returns to the starting location, individual spawn points on the way back may have already been visited when no perfect round course is generated.

No linearly proportional increase

A reduction of retention time to model experienced players and a variation of different start times is examined in Section A.4.2. Regarding the employed algorithm, no additional findings could be deduced. The reduction in retention time led to an expected increase in objective value, with no major side effects. Varying the start time showed that round courses starting at hh:45, i. e., any desired time 45 minutes into an hour, seems to be worse than starts at other quarter-hourly times. This is likely to be caused by the spawn points' time-limited availability, leading to worse routes, and shows that a start time analysis for optimized routes can be advantageous.

Modeling of experienced players

In Figure 36, we show the route performance when looking for specific Pokémon, compared with aiming to catch as many Pokémon of arbitrary species as possible, i. e., visiting the most spawn points. We look for the particularly common Pokémon Pidgey (#016), and the water Pokémon Magikarp (#129), whose spawn frequency is influenced by the vicinity of water bodies.

Sought-after Pokémon

As expected, we see a substantial decrease in objective value when looking for specific Pokémon because a spawn point's value is now resembled by its probability to spawn the respective sought-after Pokémon. Thereby, scores vary for each spawn location. Additionally, it leads to large numbers of spawn locations being filtered out during pre-processing, because, according to the dataset, they are unlikely to spawn the given Pokémon. Due to the random spawn mechanics, the spawned Pokémon cannot be anticipated, but only predicted based on historical data, always assuming that spawn mechanics remain unchanged.

Impact of value-based pruning

For both evaluated Pokémon, we achieve a comparable average objective value, with simulated annealing routes being very consistent, while the evolutionary algorithm introduces much more variance, with a higher run time. Since the objective value depends on the sum of spawn probabilities of each visited spawn point, the objective

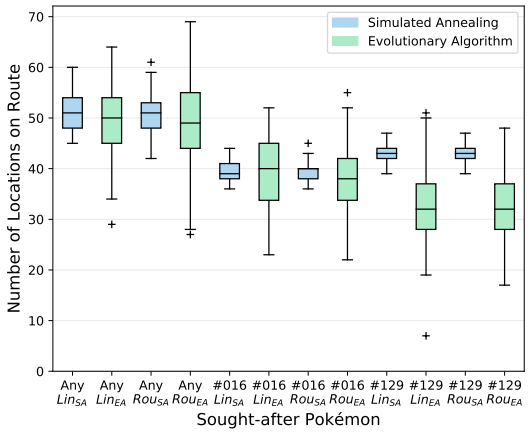

Figure 37: Number of visited spawn points on the route evaluated in Figure 36.

Consistent results for simulated annealing

value results are self-explanatory. In Figure 37, the number of locations on each route is shown, which is comparatively close to a default scenario route. The difference for Magikarp (#129) routes is noticeable, where simulated annealing appears to perform significantly better for this reduce problem size, with mostly tightly clustered locations along water bodies.

In an additional evaluation of the rarer Pokémon Bulbasaur (#001), an interesting phenomenon could be observed. Depending on the maximum travel time, the resulting objective value was either close to zero or well above that. A game mechanic called nests is responsible for this, where most spawn locations within a park have a high chance of spawning one specific Pokémon. This changes for each park and on a bi-weekly basis[10]. The resulting route identified a distanced Bulbasaur nest, traveled there, passed by its spawn points repeatedly, and returned to the target location, ignoring almost all spawn locations on its way. This is an expected and realistic behavior for players looking for a Pokémon with a nearby active nest.

Looking for a rare Pokémon species

6.3 MOBILITY DETECTION QUALITY

To evaluate our automatic mobility detection, we acquired a dataset utilizing our mobile application recording mobility data of study participants, described in Section 5.2.

For our data acquisition, 43 participants were asked to record data on their personal Android smartphones. This led to 65.8 hours of raw data collected in multiple European countries with a cluster point in the Rhine-Main area. The raw data distribution across the mobility types is not uniformly distributed as participants were asked to record their daily travels[11]. Data was collected in urban, suburban, and rural areas, as well as during transit between locations, and covers a variety of different situations such as traffic jams and heavy rush-hours. The smartphone position was not specified for the recording. It was worn at the body, in a bag, a backpack, smartphone holder in

Collected data

10 `https://thesilphroad.com/atlas` (last accessed: August 17, 2020)

11 Recorded data in total: 11.8h stand, 18.5h walk, 4.9h bike, 17.6h car, 5.0h bus, 2.4h tram, and 5.6h train

cars, or on bikes. Neither of those locations was compulsory, allowing users to change their smartphone's position during travel freely.

All participants were asked to record sessions of at least 10 minutes of length so that we can investigate our system's performance over time if it turns out to require a cold starting phase until prediction quality converges. Thereby we excluded all recordings shorter than 10 minutes from the dataset. Not all the recorded data was used for training, as specific datasets were reserved for testing purposes only so that our final model could be tested with yet unknown data. For the training, we used recordings of 38.6 hours of data by 23 participants[12].

Training data split

In our multi-class classification problem, we use two primary quality measurements. For each examined model, we calculate its macro-averaged prediction accuracy, which, compared to the micro-averaging approach, weights all classes equally [246]. Each class's performance is reported using the F_1 measure. We select the balanced F-score as we have no particular emphasis on precision[13] or recall[14], as it calculates their harmonic mean. When recall would require a higher emphasis, the F_2 measure would be chosen, and conversely, the $F_{0.5}$ measure for a higher focus on precision. All evaluation runs use a stratified 10-fold cross-validation[15], which provides a similar class distribution for each fold, as present in the dataset. Finally, an automatic feature selection for all three frame classifiers is employed to determine all relevant features and their respective information gain. The data itself is oversampled beforehand to construct a balanced dataset. Both individual class precision and recall values and evaluation run confusion matrices were obtained and are provided when relevant.

Employed quality metrics

The evaluation is performed on an Intel Xeon E5-2660 v3 with 2.60GHz and 32 GB of RAM. Weka is adjusted to use `num-decimal-places = 8` as it strongly increases individual feature accuracies, compared to its default value 2.

6.3.1 *Default Parameter Determination*

Simulation Setup

To evaluate the meta-classifier's performance and the overall system, the recorded activities are simulated and inserted into our classification system. For this simulation the recordings are processed in steps of $T_C = stepSize = 5s$. As noted in Table 4.2.4, we choose a $stepSize$ equal to the time interval T_C, after which a classification update is expected. For each step, the respective frames of the length `short`, `medium` and `long`, and their associated features are determined and classified. Finally, the meta-classifier determines the final prediction and is compared to the actual data label. We choose a $transitionDuration = 2s$, representing the transition delay after a change in mobility type. Thereby, we expect the system to predict the previous activity during the transition period since we assumed that the new activity cannot yet be detected.

Simulation setup

12 Training data in total: 5.7h stand, 7.7h walk, 3.9h bike, 11.3h car, 4.9h bus, 1.9h tram, and 3.2h train

13 Precision is the ratio between true positives and the sum of all positives.

14 Recall is the ratio between true positives and the sum of true positives and false negatives.

15 The k-fold cross-validation separates data into k folds and, in each case, trains on $k-1$ folds and tests on the remaining one.

shift$_{max}$ = 5s

The shift$_{max}$ parameter is relevant to create the frame classifiers during training, determining the overlap each frame has. Selecting this value is twofold. It concerns the frame classifiers' overlap, which is vital for sliding window approaches. Additionally, the resulting number of frame instances needs to be observed, as a too narrow overlap can strongly boost computation requirements to infeasible levels. We decide to use shift$_{max}$ = 5s, as it provides us with pre-processing times between one and two hours, which allowed us to gradually improve on parameter values and later on analyze further parameter combinations.

Default parameter determination methodology

For the other introduced parameters, good default values must be determined for an optimized mobility type distinguishment. To determine one parameter, we vary one at a time while keeping all other parameters constant. Subsequently, we select the value for which the meta-classifier obtains its maximum accuracy. In earlier experimental evaluation runs, we narrowed each parameter down to promising value ranges, for which we now determine its final value. After an optimized parameter has been determined, it is used in succession.

Early algorithm usage

Since random forests have proven to be promising approaches in related work and our early evaluation runs, we use it for default parameter determination for both the frame classifiers and the meta-classifier[16]. For similar reasons, we use *genetic search* for automatic feature selection. Since the number of meta-features is low, we do not use an automatic feature selection for the meta-classifier.

Early frame length methodology

The frame length variation is especially challenging since different combinations can have different effects on the overall system. For this reason, we first define all other parameters by using two parameter setups: We perform an evaluation with small frame lengths for `medium` and `long` ($T_M = 20s$ and $T_L = 90s$) and one with longer frames ($T_M = 30s$ and $T_L = 300s$), as we assume that different features are more relevant for different frame lengths, to better assess the effects of parameter selection. Since affected parameters mainly influence features of the `medium` and `long` frames, we use a fixed length for the `short` frame of $T_S = 5s$.

Parameter Determination

S2 level = 14

The S2 level, i. e., the area size for which OSM information is obtained for feature calculation, is utilized in `medium` and `long` frames. However, the S2 level choice had no substantial impact on the overall system accuracy, which is why we selected the smaller level of 14, as less data needs to be obtained and processed. A detailed S2 level evaluation can be found in Table 27.

cutoffDistance = 800m

The `cutoffDistance` serves as a threshold, from which point on public transport routes further away are not considered. The variation of this parameter, however, had little impact. For the shorter frame setup, a 600m threshold was sufficient, while for longer frames, 800m showed an improvement. For that reason, we choose to use `cutoffDistance = 800m`, with a more detailed evaluation shown in Table 28.

maxStopSpeed = 0.5m/s

Stop-based features are only calculated for `long` frames. The maximum stop speed serves as an upper threshold value, below which a segment is treated as halting.

16 hyperparameters: 20 iterations; at least 2 instances per leaf; maximum depth of 20

The evaluation for the two different scenarios shows small effects of the choice of `maxStopSpeed` on the overall system accuracy. Based on the results shown in Table 29, we select a value of $0.5\mathrm{m}/s$ as it achieved the best results for both scenarios.

The stop radius indicates up to which range nearby PoIs are considered. When a low value is chosen, relevant PoIs might be ignored due to the location inaccuracies. When the radius is set too large, stations not relevant for the stop can be included. In Table 30, we provide detailed results for this parameter, in which we select `stopRadius = 20m`.

stopRadius = 20m

The minimum duration for a long stop helps to identify meaningful stops instead of stops caused by dense traffic and stop-and-go. Similar to the previous radius parameter, the variation had no significant impact when varying between 6s, 8s, 10s, and 15s. For the shorter frame scenario, a `stopDurationLongStop` of 8s performed best, while for the longer frame lengths, a value of 15s achieved the best results, although the differences within the two setups were marginal ($\leqslant 0.1\%$). Since the shorter frame lengths seem to be more accurate than the longer frame lengths, we choose `minDurationLongStop = 8s`.

stopDuration-LongStop = 8s

Interval Lengths

After selecting the individual parameter, a preliminary evaluation showed that Adaptive Boosting with a J48 classifier[17] performed significantly better for the meta-classifier than the previous random forest. For that reason, we use this algorithm for frame length determination, with frame classifier algorithms remaining as previously defined.

We again decide on the optimized parameter based on the meta-classifiers performance. Alternatively, the performance of the individual frame classifier could have been used. However, this would only locally optimize the frame classifier, which we deemed problematic in individual evaluation runs, where the overall system accuracy declined when optimizing individual frame performance. Even though all frames are calculated independently from another, the choice of frame length influences the others because the overall system accuracy is a deciding factor. For that reason, we start with the `long` frames since we expect them to be more independent from the other two frames. Subsequently, we determine the `short` length and, finally, the `medium` frames, as the latter serves as a connection between both other frame lengths.

As shown in Table 10, the highest accuracy of the meta-classifier is achieved at 90s. Especially *car* and *bus* benefit from a this longer frame length compared to 60s. Although the frame classifier's accuracy increases for higher frame lengths, the meta-classifier does not increase simultaneously. We therefore choose $T_L = 90\mathrm{s}$.

`long` frame length = 90s

A similar pattern can be observed for the `short` frames, as shown in Table 11. While the frame classifier's accuracy increases with an increased frame length, the meta-classifier's accuracy reaches its maximum at $T_S = 5\mathrm{s}$ and decreases rapidly with longer frame length. One possible reason would be the detection of temporary stops becoming worse for longer `short` frames. Since the results for $T_S = 4s$ and $T_S = 5\mathrm{s}$ are

`short` frame length = 5s

17 hyperparameters: AdaBoostM1 with 20 iterations; J48 with at least 2 instances per leaf; pruning confidence c = 0.25

Table 10: Evaluation results for `long` interval length T_L highlighting the selected parameter value. Parameters: $T_S = 5s$, $T_M = 20s$, `s2Level = 14`, `cutoffDistance = 800m`, `maxStopSpeed = 0.5 m/s`, `stopRadius = 20m`, and `minDurationLongStop = 8s`.

T_L	accuracy		F1 scores of meta-classifier						
	meta	`long`	stand	walk	bike	car	bus	tram	train
60s	98.37%	99.49%	97.0%	99.5%	99.2%	97.4%	97.5%	99.2%	98.8%
90s	98.48%	99.71%	97.0%	99.5%	99.3%	97.8%	98.0%	99.1%	98.7%
120s	98.45%	99.80%	96.8%	99.4%	99.2%	97.6%	97.9%	99.2%	98.9%
150s	98.44%	99.93%	96.8%	99.5%	98.9%	97.8%	98.0%	99.3%	98.8%

similar, we will consider both frame lengths for `medium` frame length determination in the next step.

Table 11: Evaluation results for `short` interval length T_S highlighting the selected parameter value. Parameters: $T_M = 20s$, $T_L = 90s$, with remaining parameters identical to Table 10.

T_S	accuracy		F1 scores of meta-classifier						
	meta	`short`	stand	walk	bike	car	bus	tram	train
3s	98.38%	96.84%	97.2%	99.5%	99.2%	97.6%	97.8%	99.0%	98.3%
4s	98.44%	97.27%	96.9%	99.6%	99.2%	97.6%	98.0%	99.1%	98.7%
5s	98.48%	97.26%	97.0%	99.5%	99.3%	97.8%	98.0%	99.1%	98.7%
6s	96.83%	97.36%	93.9%	98.9%	98.7%	96.2%	95.8%	97.7%	96.6%

`medium` frame length = 15s

Based on the results in Table 12, we can identify a `short` frame length of $T_S = 5s$ performing better in each scenario. For the `medium` frame length, the meta-classifier reaches its best result for $T_M = 15s$, which is why we select it accordingly.

Algorithms and Feature Selection

Employed feature selection approach

To determine suitable search methods for feature selection, we use an AdaBoostM1 [76] with J48 and a Random Forest, selecting the smallest possible feature set with good detection accuracies. We use the correlation-based feature selection (`CfsSubsetEval` in Weka) as an evaluator and define the Random Forest baseline as a full run with all available features. We expect this baseline to have comparable accuracy to the selection strategies. Our goal is to reduce the number of features required to identify particularly important features for a mobility type's detection. For AdaBoostM1, we do not calculate a baseline because AdaBoost's training times are already slower by a factor of 10 to 20 with a reduced number of features. We show the summarized feature selection results in Table 13, with a more detailed one in Tables 31-33.

Table 12: Evaluation results for `medium` interval length T_M highlighting the selected parameter value. Parameters: T_S, and T_L defined in Table and remaining parameters identical to Table 10.

T_M	accuracy		F1 scores of meta-classifier						
	meta	`medium`	stand	walk	bike	car	bus	tram	train
$T_S = 4s$, $T_L = 90s$									
10s	98.39%	98.25%	97.0%	99.6%	99.2%	97.3%	97.7%	99.2%	98.7%
15s	98.48%	98.73%	96.9%	99.5%	99.3%	97.7%	98.1%	99.1%	98.7%
20s	98.44%	99.02%	96.9%	99.6%	99.2%	97.6%	98.0%	99.1%	98.7%
25s	98.35%	99.13%	96.8%	99.6%	99.3%	97.3%	97.8%	99.0%	98.6%
$T_S = 5s$, $T_L = 90s$									
10s	98.52%	98.25%	97.2%	99.4%	99.3%	97.8%	97.9%	99.2%	98.9%
15s	98.55%	98.73%	97.2%	99.5%	99.2%	97.8%	98.1%	99.1%	98.9%
20s	98.48%	99.02%	97.0%	99.5%	99.3%	97.8%	98.0%	99.1%	98.7%
25s	99.41%	99.13%	96.9%	99.4%	99.3%	97.6%	97.9%	99.3%	98.6%

Best First for `medium` and `long`

The Best First feature selection always results in the fewest selected features, leading to shorter training times. When analyzing the individual F1 scores, we identified the differentiation between *bus* and *car* being influenced the most by the feature selection. For both `medium` and `long` frames, a Best First selection was the most suitable, as it required far fewer features with an only slightly worse macro-averaged accuracy. This leads to a considerable decrease in training time by a factor of three compared to the baseline allowing for faster iteration during development.

Genetic Search for `short`

For the `short` frames, the Genetic Search achieves the best results, requiring only seven more features. We deliberately omitted delta features for the `short` classifier to react faster to short-term activity changes without being influenced by the previous frame. A brief evaluation confirms that approach, where although delta features' inclusion minimally increases the frame classifier's accuracy, the meta-classifier's accuracy decreases. For this reason, we retain the exclusion of delta features for the `short` frames.

Algorithm selection methodology

We test five classification algorithms for the frame classifiers, three based on singular decision trees: J48, REP-Tree, Random Tree, and two ensemble learners: Random Forest and AdaBoostM1 with J48. For each ensemble learning algorithm, we vary the number of iterations I. We specify both the required training time per fold on our system and the resulting classifier's size.

With the detailed results presented in Tables 34-36, we can conclude that ensemble learners perform significantly better compared to individual decision trees. Especially the distinction between motorized transport types improves. For the `short` classifier,

18 hyperparameters: 30 iterations; at least 2 instances per leaf; maximum depth of 30

Table 13: Evaluation results for feature selection in `short`, `medium`, and `long` frame classifiers, indicating selected feature counts and frame classifier accuracies. Detailed results containing individual F1 scores can be found in Tables 31-33.

feature selection	`short`		`medium`		`long`	
	feature count	accuracy	feature count	accuracy	feature count	accuracy
Random Forest with I = 30 [18]						
Baseline	65	97.60%	136	98.77%	180	99.79%
Evolutionary Search	32	97.43%	65	98.83%	84	99.76%
Genetic Search	32	97.59%	48	98.62%	53	99.67%
Best First	25	97.53%	29	98.77%	29	99.73%
AdaBoostM1 with I = 15 and J48						
Genetic Search	32	97.66%	48	98.89%	53	99.76%
Best First	25	97.55%	29	98.89%	29	99.81%

AdaBoostM1 for frame classifiers

the algorithm choice leads to an improvement in macro-averaged accuracy from 92.98% (REP tree) to 97.84% (AdaBoostM1 with J48 with 25 iterations). The differences are especially prominent for *bus*, where the F1 score improves from 86.6% to 95.5%. Similar trends can be observed for `medium` and `long` frames. Comparing both ensemble learners, Adaptive Boosting reaches a higher overall accuracy with the same number of trees, which are two to three times smaller due to J48's integrated pruning. Then again, the required training time is significantly longer compared to equally parametrized Random Forests. Since the training is only performed once on a server, we choose to use AdaBoostM1 and select the minimum iteration counts that achieve the highest accuracy. This is 35 iterations for `medium` and 30 iterations for `long`. For the `short` frame, we select a lower-than-optimal number of 15 iterations to allow for accelerated training time and a smaller classifier size.

Meta-classifier feature selection

For the feature selection of the meta-features, the same three search methods were examined, where each result selected the same five features[19], resulting in lower accuracies. To identify the least important features, we utilized a feature ranking based on each feature's information gain for its class. The feature with the least information gain `prevScoreS` resulted in no accuracy change and thereby appeared not to be required. However, we intend to analyze the impact of different feature types next, for which the removal may impact the feature selection options. For that reason, and because using all meta-features has no negative impact on the system's performance, we will use all meta-features for our classifier.

Meta-classifier algorithm

The selection of a suitable classifier for the frame classifiers has shown that the best results could be achieved using AdaBoost. We, therefore, use an AdaBoostM1 with J48 for the meta classifier as well. The best results were achieved with 20 maximum

19 `predS, predM, predL, prevPredM, scoreS`

iterations, where increasing the number of iterations further did not lead to higher accuracies.

6.3.2 *Feature Set Importance*

In the following, we examine the influence of different feature sets on the system, in which we want to identify those feature sets that are essential for the system or, if possible, identify dispensable components. In Table 14, we present a detailed analysis of the different sets that can be freely combined for each group. The δ indicator behaves slightly differently, as it corresponds to the inclusion of delta features for all utilized features. Each result provided uses the previously determined parameters, feature selection settings, and algorithm parameterizations in a stratified 10-fold cross-validation.

Table 14: Different feature sets that can be freely combined.

feature set	description
A	Features based on the accelerometer in the time-domain.
A_F	Features based on the accelerometer in both time- and frequency-domain.
L	Features based on the location sensor.
L_E	Features based on the location sensors and additional external information.
δ	For each feature in the feature set an additional delta feature is used.

Relevance of delta features

Negative δ feature effect

The delta features introduced in Section 4.3.4 are used for `medium` and `long` frames aim to represent the chronological sequence of feature changes. However, results in Figure 38 show that, in direct comparison, feature sets without delta features perform equally at best, with the only exception being the L_E feature set, i. e., the one without any acceleration data features.

Going into detail onto changes per movement type, shown in detail in Table 37. For the example of *car*, we can observe an interesting tendency comparing AL, AL_E, and L_E with and without delta features. By adding external information (AL_E, L_E), there is an accuracy gain provided by delta features, whereas the acceleration delta features alone seem to have a negative effect (A, A_F, $AL \leftrightarrow L_E$) on *car* classification. A similar pattern can be observed for *bus* classification.

Relevance of frequency-domain features

Features based on the frequency spectrum of the accelerometer have been rarely utilized in related work. Looking at our results, it is noticeable that in direct comparison these features always contribute to a notable detection improvement: $AL_E \leftrightarrow A_FL_E$

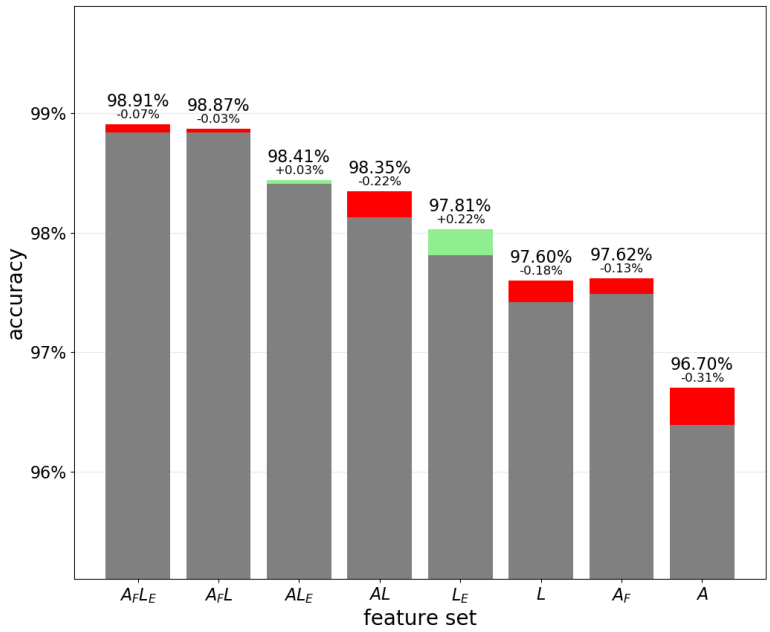

Figure 38: Meta-classifier macro-averaged accuracy with select combinations of feature sets, showing the accuracies without delta features. The secondary value represents the loss or gain in accuracy when including delta features in the respective feature set.

Performance increase attributed to frequency-domain features

(+0.50%), AL ↔ A_FL (+0.52%), A ↔ A_F (+0.92%). Especially the detection of *cars* and *buses* benefits from the features of the frequency domain, which have been reported to be particularly challenging in related work. In case location features are missing, the *train* detection is also increased by adding the frequency features: A ↔ A_F (+1.6%).

Selected frequency-domain features

When analyzing the selected features when frequency-domain features are included, we observe features based on frequency bands achieving a high information gain. Thereby the whole frequency spectrum up to 30 Hz appears to be relevant. One possible explanation we found is the vibration of combustion engines in vehicles is covered by a broad frequency spectrum, e. g., 1,800 rounds per minute corresponding to 30 Hz. Additionally notable is that all frames select the features spectral roll-off, spectral crest, and spectral spread. For the `short` frame, the spectral skewness is selected. For the feature set without location features A_F, the normalized spectral energy and the spectral centroid are selected. Thus, all frequency-domain features except the spectral spread have been utilized.

Relevance of location features

Performance increase attributed to location features

In the related work, location-based features have been frequently used, provided that these approaches rarely combined them with many acceleration-based features. When directly comparing feature sets including location features, we notice a detection improvement: A_F ↔ A_FL (+1.25%), A ↔ AL (+0.90%).

According to our results, *standing* classification benefits the most from location features, which is likely to be due to features based on speed and distance traveled.

Improved confusion of motorized mobility

Car, *bus*, and *train* confusion also improves, which we suspect to be due to heading and location accuracy features. The latter is especially prominent for metal-coated train windows, which lead to high location `accuracy` values, i. e., values indicating that a high location variance is expected. For the location accuracy in AL, the `accu95` feature is selected for `short`, and the feature `accu25` is selected for `medium`.

Relevance of external information features

Small external information features improvement

Our results are consistent with the findings of Stenneth et al. [229], who showed that the addition of external geo-referenced information could improve transport mode detection for location-based systems. When directly comparing features sets with external information, we notice only small detection improvements: $A_FL \leftrightarrow A_FL_E$ (+0.04%), $AL \leftrightarrow AL_E$ (+0.06%), $L \leftrightarrow L_E$ (+0.21%). Thus, when accelerometer-based features are already utilized, the gain in detection quality is minimal.

Possible limitation: local vibration patterns

It is possible that a model is more valid in general when including external features. However, we do not know to what extent public transport vehicles in the recorded datasets have specific vibration patterns and whether they differ from other transport vehicles in other regions. In this case, a model that supports detection via uniformly available, external information from OSM could be more generalizable.

Exemplary impact of public transport station distance

In Figure 39, we show an example from our dataset where information about public transport routes is beneficial. While the classifier without any route information results in a false *tram* classification, the external feature provides the information that there is no tram station or tram line nearby, increasing the confidence for *bus* detection. In contrast, the addition of public transport routes can also lead to a false prediction, e. g., where the proximity to a bus station while passing in a tram might lead to a false *bus* prediction.

Selected external information features

When analyzing the selected features when external information features are included, we observe that the same four features are always selected: `distanceTram`, `distanceTrain`, `stopsBusStop` and `stopsTramStop`. For the model without acceleration data L_E, the additional feature of `stopsExclTramStop` is selected.

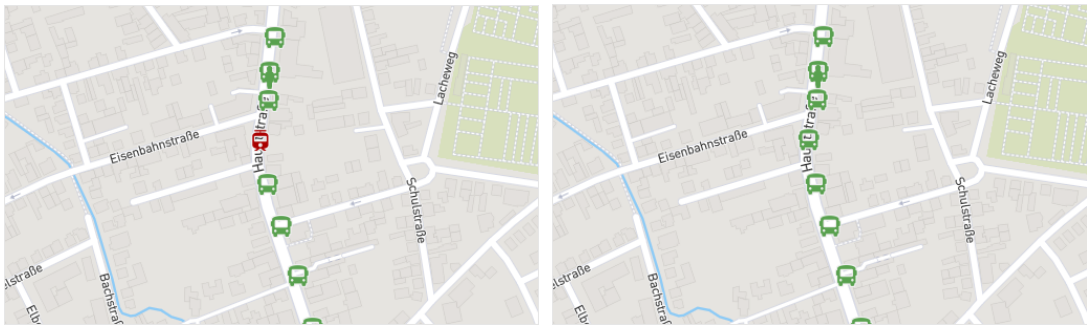

(a) Activity without external information (A_FL). (b) Activity with external information (A_FL_E).

Figure 39: Individual activity comparison without and with external information.

6.3.3 *Frame Classifier Importance*

To analyze the difference between using the meta concept as a whole and individual frames, we trained a meta-classifier solely based on one frame classifier feature (`predS`, `predM`, `predL`). As shown in Table 15, each feature's accuracy is drastically lower than the overall accuracy with all meta-features. Among the simple classifiers, the classifier `predM` performed best, likely because it can still detect short stops fairly well and contains relevant location features to distinguish different motorized mobility types. Since the feature `predL` does not receive information about temporary stops, it performs worse in the *standing* scenario. This factor becomes particularly clear in its recall value of 45.1% and in conjunction with the vehicles' precision values. The `predM` precision values, especially for *tram* and *train*, show the successful training on the special characteristics of public transport, despite its duration of only $T_M = 15s$. The contribution of `predL`, on the other hand, can be seen from its recall values, where it identifies motorized mobility types particularly well.

Combining these two frames can compensate for each other's worse precision for some mobility types and allow the `short` classifier's high recall to work for detecting *standing* and *walking*. Thus, the meta concept combines the advantages of short frames with those of long frames.

Table 15: Evaluation results of frame classifiers prediction features for $A_F L_E$ including precision and recall due to its variation. Precision and recall values are listed in brackets in that order.

`feature sets`	accuracy	F1 scores of meta-classifier + (precision, recall)						
	overall	stand	walk	bike	car	bus	tram	train
Meta	98.91% (98.9%, 98.9%)	97.7% (97.8%, 97.7%)	99.6% (99.7%, 99.5%)	99.4% (99.2%, 99.6%)	98.3% (98.6%, 98.0%)	98.5% (98.6%, 98.4%)	99.5% (99.2%, 99.7%)	99.3% (99.1%, 99.5%)
`predS`	91.67% (91.8%, 91.7%)	92.6% (89.4%, 96.1%)	99.6% (99.2%, 99.2%)	97.1% (97.6%, 96.6%)	87.3% (83.1%, 92.0%)	86.1% (88.5%, 86.1%)	87.7% (93.6%, 82.4%)	91.5% (91.5%, 91.5%)
`predM`	93.43% (93.5%, 93.4%)	83.7% (82.2%, 85.3%)	98.9% (98.6%, 99.3%)	97.8% (98.3%, 97.4%)	94.0% (93.6%, 94.5%)	90.5% (89.8%, 91.3%)	93.0% (97.2%, 89.2%)	96.1% (95.1%, 97.0%)
`predL`	90.99% (91.8%, 91.0%)	61.7% (97.7%, 45.1%)	97.8% (96.2%, 99.5%)	98.1% (96.2%, 100%)	91.9% (85.7%, 99.0%)	88.8% (81.9%, 97.0%)	95.5% (92.1%, 99.1%)	94.9% (92.7%, 97.2%)

To analyze the importance of each frame in detail, we trained meta-classifiers with a subset of meta-features. Each subset is grouped by frame classifier length and either contains one, two, e. g., `short` and `long`, or all three groups of meta-classifier features.

As shown in Table 16, a system based solely on the `long` frame would have a significant loss in accuracy compared to our final system. Especially the detection quality of *standing*, and to a degree, *car* and *bus* decreases and would have a long initialization time of $0.9 \cdot T_L = 81s$. The analysis shows only a marginal difference between systems based solely on `short` or `medium` frames, with the former performing slightly better. For the `medium` frame, especially the differentiation between *car* and *bus* improves. Similarly, the accuracy for the other two public transport modes improves, likely due to the external information features being included in this frame classifier.

Frame classifier importance

Classifiers based on two different frames performed best when including the `short` frame, reinforcing its importance for our system. The highest accuracy can only be achieved by combining all three frame lengths. Especially vehicular mobility types profit from the combination of all three frame lengths with a net gain of at least 0.3% accuracy. The overall high accuracy values show that the system does not inevitably require the longest frames but can accurately predict the current mobility type early on while the system is in a cold starting phase.

Reliable accuracy for system cold start

Table 16: Evaluation results of frame classifiers combinations.

`frame combination`	accuracy	F1 scores of meta-classifier						
	overall	stand	walk	bike	car	bus	tram	train
`short, medium & long`	98.91%	97.7%	99.6%	99.4%	98.3%	98.5%	99.5%	99.3%
`short & long`	98.63%	97.5%	99.6%	99.1%	97.8%	98.2%	99.2%	99.0%
`short & medium`	98.60%	97.4%	99.7%	99.2%	97.6%	97.9%	99.4%	99.0%
`medium & long`	97.97%	94.4%	99.4%	99.2%	97.3%	97.1%	99.3%	99.1%
`short`	97.57%	97.4%	99.4%	99.0%	95.3%	95.2%	98.2%	98.5%
`medium`	97.47%	94.1%	99.4%	99.0%	96.4%	96.4%	98.4%	98.7%
`long`	94.51%	80.3%	98.3%	98.6%	94.3%	94.4%	97.4%	97.1%

6.3.4 *Final Model and Comparison to Related Work*

The individual F1 scores of our final $A_F L_E$ model, the confusion matrix, and the selected features with their information gain are shown in Tables 37-40. Since all classes are weighted equally, the results are macro-averaged. We achieve a macro-averaged accuracy of 98.9% on a 10-fold cross-validation for the feature sets of $A_F L_E$ and $A_F L$, i. e., with and without external features, both excluding delta features. If the *standing* class is neglected, the macro-averaged accuracy increases to 99.1%.

Final accuracy of 98.9%

Analyzing the $A_F L_E$ model in detail shows that the lowest accuracy is achieved for *standing*. Although *standing* is fundamentally the easiest to identify, the reason for this result lies within the transitions to a temporary *stand*, which make up a large portion of our data used for the class. On the one hand, these transitions are difficult to detect

Temporary standing analysis

accurately, differing between intentional stops or stop-and-go. On the other hand, the detection is influenced by the quality of our manual labeling. Since these were set after data recording utilizing acceleration and velocity data, inaccuracies and errors are likely. Especially since there is a delay between the acceleration and velocity data, it makes accurate transition labeling more difficult. This can also be observed in the confusion matrix.

Vehicular mobility confusion

For vehicular transportation, we can detect *bus* and *car* with a macro-F1 score of 98.3% and 98.5%, respectively. *Tram* and *train* detection works best with a score of 99.5% and 99.3%, respectively. For the confusion matrix, it is noticeable that *cars* and *bikes* are confused for one another, which mostly occurs during start-up. One possible explanation for this is the frequent use of e-bikes within our training data, which allow for strong acceleration, and may contain frequency-domain signals on the motor. This might make the distinction between *cars* and *bikes* more difficult. One observation from related work is the frequent confusion of *buses* and *cars*, which we can still confirm for our data. Another observed confusion is *buses* being confused for *trams*. We deem the distinction between these two types of transport as particularly challenging since, in our recorded data, buses often travel on roads with integrated tram tracks.

Final employed feature characteristics

The developed model is rotation invariant since only the acceleration magnitude is used. Additionally, no personalized data is utilized, and data originates from different subjects reducing the possible impact of different walking styles. Since we use a `short` length of $T_S = 5s$, the system's first prediction is obtainable 5 seconds after its activation. Since only OSM features and no detailed timetables are used, external information is globally available, if tagged accordingly. Then again, the model without any additional external information has been verified to be of equal quality for our data, allowing us to neglect missing OSM data.

Run-time mobility detection

Finally, we have tested our final model's live detection on a smartphone to ensure its functionality on a mobile device itself. The resulting models take up an acceptable amount of storage (A_FL_E : 8.7MB, A_FL : 9.1MB), which depends on the number of employed features and their names' length. Compared to the reported models in related work, our model is considerably smaller than 150MB and suitable for mobile applications.

Table 17: Google Activity Recognition API mapping to mobility type and resulting detection accuracy.

class	Google API	accuracy	`Unknown`
stand	`Still`	52%	25%
walk	`On Foot`	87%	12%
bike	`On Bicycle`	31%	45%
car	`In Vehicle`	85%	13%
bus	`In Vehicle`	36%	58%
tram	`In Vehicle`	34%	58%
train	`In Vehicle`	43%	26%

We want to compare our final model to existing solutions and related works regarding detection accuracy in the following. With the Google Activity Recognition API [164], Google provides a way to recognize activities without differentiating between different motorized means of transport. We recorded the API's predicted activity for 12.7 hours of our dataset and expect the most similar mobility type to our label as a prediction result. In Table 17, we show this mapping and the respective prediction accuracies. It is noticeable that the API often returns `Unknown`, especially frequent for *bikes*, *buses*, and *trams*. The best results are achieved for *walking* with 87% accuracy and *car* with 85% accuracy.

Comparison to Google Activity Recognition API

A similar evaluation has been reported in 2018 [35], which stated that the API only predicted 3% of all cases, which does not hold true anymore, as either the API itself or its embedding into the Android framework, has been drastically improved. For our data, the API achieves a macro-averaged accuracy of 53%, which is largely comparable with other earlier studies [274]. We suspect the still large proportion of `Unknown` predictions being due to its wide range of users and likely focus on producing too many false positive predictions.

Google API improvement

Table 18: Comparison of our models with results of Stenneth et al. [229] including feature selection and Aşçı and Güvensan [13]. The F1 scores are calculated from the authors' reported precision and recall values. The macro-averaged accuracies are determined only for the compared classes and thereby differ from our other reports.

model	accuracy	F1 scores					
		walk	bike	car	bus	tram	train
Stenneth et al. [229]	90.70%	98.4%	89.2%	81.2%	90.4%	-	94.3%
our L_E model	97.63%	98.9%	98.6%	95.5%	96.9%	99.4%	98.3%
our $L_E\delta$ model	97.92%	99.0%	98.9%	96.1%	97.1%	99.4%	98.5%
Aşçı and Güvensan [13]	96.45%	97.0%	96.9%	97.1%	94.7%	-	96.6%
our A_F model	98.09%	99.4%	99.1%	97.6%	97.1%	98.7%	97.2%

Although a direct comparison with related studies is not feasible because the datasets have not been published in most cases, an accuracy-based comparison per mobility type is possible. For our comparison, we use the two works with the highest reported macro-averaged accuracy from related works, excluding *standing*, since it usually is not reported how temporary stops are handled. Our goal with this is not to compare the quality of the final model by numbers but to evaluate our meta-classification concept, so we choose the feature set closest to the work in question.

Related work comparison methodology

Stenneth et al. [229] uses a purely location-based approach, including external geographic information about the public transport network. It should be noted that the authors used real-time information about the positions of buses, which we cannot provide. Because they do not use the accelerometer, we decide to use both our L_E and $L_E\delta$ models for comparison, shown in Table 18. We can significantly increase the

Comparison of L_E and $L_E\delta$ to Stenneth et al.

detection quality of *bike*, *car*, *bus*, and *train* through our meta-concept. Additionally, the direct distinction between *car* and *bus* works well for our model, where Stenneth et al. has a strong bias towards *bus* detection. We deduce that real-time information on bus positions is unnecessary for our model to detect *buses* with high accuracy.

Comparison of A_F to Aşçı and Güvensan

Aşçı and Güvensan [13] use an orientation-dependent model based on the accelerometer, gyroscope, and magnetometer in both time- and frequency-domain in a recurrent neural network. Since we only use the accelerometer, a comparison with our A_F model is evident, which is orientation invariant. As shown in the results in Table 18, their accuracy for *cars* is slightly higher than ours, whereas we detect *buses* better. Overall, these results suggest that the gyroscope and magnetometer are not required for mobility detection, and an orientation-invariant model performs similarly well.

7 SUMMARY, CONCLUSIONS, AND OUTLOOK

Concluding our work, we summarize the previous chapters' content and state our main contributions in the following. We then draw conclusions based on our obtained results and discuss potential future work.

7.1 SUMMARY OF THE THESIS

In Chapter 1, we described the challenges for an online content generation system applicable to Location-based Game (LBG) applications. We motivated the advantages of online generation based on the customizability and personalization of content towards each individual player. In Chapter 2, we studied existing content creation approaches regarding their applicability for global content location identification. As a possible strategy for mobility-based adaptation, we analyzed heuristic route-finding and automatic mobility detection approaches utilized in different application domains. Based on our analysis of the state of the art, we presented the following contributions in our thesis.

7.1.1 *Contributions*

Chapter 3 contains our first two contributions, focusing on the online content generation for LBGs. As the first contribution, we propose a globally applicable content generation with scenario-specific customization options to *i)* identify and retrieve promising Points of Interest (PoIs) data for a given region, *ii)* select a number of PoIs according to four quality metrics to construct a game area, and *iii)* couple multiple game areas based on their available PoIs. The latter option enables the utilization of multiplayer gameplay across regions despite the players' different geographic locations, aiming for game areas with similar geographical and cultural characteristics. Furthermore, our approach considers the generation of multiple coupled game areas, resulting in regularly new game areas providing additional variety for the underlying game. To determine a suitable selection of PoIs, we solved an optimization problem, utilizing heuristic approaches, applicable to an online generation scenario.

Global content generation

In Section 3.4, we develop our second contribution, which covers the location-dependent determination of routes in a city-wide game area, obtaining a route optimizing the expected virtual reward during gameplay. Due to the large number and time-dependent variety of available content locations, we develop a heuristic route-finding approach to provide personalized mobility guidance for LBG players, aiming to optimize their gameplay according to their preferences.

Personalized route optimization

In our third contribution, found in Chapter 4, we propose our concept of automatic mobility detection. Therein, we include the impact of acceleration and location-based

Run-time mobility detection

mobile device sensor data to extract features allowing the differentiation between common types of mobility like walking or biking. Furthermore, we provide a detailed differentiation between different vehicular modes of transportation, particularly focusing on different public transport vehicles. Our concept includes features of different temporal lengths, specifically designed to detect everyday traffic situations like station or traffic light stops.

The resulting mobility detection is directly applicable for mobility-based adaptation in LBGs, allowing for a versatile adaptation during run-time. For our previous two contributions, suitable adaptation options are as follows: game area content and size can be selected based on accessibility and expected time to reach. Similarly, routes can be planned, monitored, and adapted according to the given mobility type.

Further, we developed our GeoVis system, described in Chapter 5, as the basis for our extensive evaluation. For this purpose, we constructed an evaluation scenario and compared our results to the current state of the art in Chapter 6.

7.1.2 *Conclusions*

In our extensive evaluation, we analyzed the effects of online location generation for a mobile game system. We showed that our approach enables the utilization of LBG content generation nationwide, optimizing the content selection concerning geographical and cultural quality characteristics. Its selection is freely adaptable for different application scenarios, providing a flexible foundation for game area generation. For its basic configuration, we could verify well-distributed game areas, containing culturally relevant PoIs, with viable results even in rural areas. By coupling those game areas together, we subsequently proved the applicability for an innovative multiplayer approach. Our proposed coupling approach achieves noteworthy generation results for our employed metrics and constructs comprehensive PoI matchings, even across continents. With flexible game area sizes and multi-area matching, we evaluated our approach's adaptability to players with different movement conditions and its scalability beyond a two-player setting.

Good generation results in all areas

Moreover, we showed the validity of route finding for virtual game reward optimization in an LBG. In a game area with thousands of valid PoIs, where it is yet infeasible to calculate an optimal solution, we applied heuristic approaches to reliably obtain high-quality routes. Since linear distances in an urban scenario are infeasible for accurate measurements, our proposed distance heuristics successfully utilize a clustering to reduce the problem size drastically. By verifying those routes using a routing service, we prove its suitability in the real-world environment. Our resulting route-finding strategy successfully utilizes the spatial density of locations to find customizable routes during gameplay. For those, we evaluated different common scenario parameters such as route duration, target location, movement behavior, and game objective as a generic way for LBG route customization.

Route-finding validity

Lastly, we showed the strong performance of our proposed automatic mobility detection concept for mobile adaptation purposes. By utilizing a combination of different time windows, meaningful features for different movement and vehicle types

have been identified and integrated into a classification pipeline. Our evaluation results demonstrated strong classification accuracies for all examined mobility types. The proposed meta-classification approach reached an overall 98.9% accuracy, emphasizing the successful combination of time windows with different lengths. We investigated the different effects of varying sensor sources and feature sets, which allows for area-specific detection approaches in scenarios where different mobility distinctions are necessary, or where sensor quality varies.

Mobility integration

7.2 OUTLOOK

Our presented results motivate the evaluation of location-based applications in different scenarios where specific PoIs are required. It is particularly intriguing to investigate long-term motivational effects in extensive cohort studies, based on the systematic utilization for, e. g., game-based health or culture promotion. Such applications would not only require an interdisciplinary team for realization. They would potentially also require new content assessment approaches [99] to generate other aspects than the map layout [109], further utilizing the PoI data for location-specific information processing.

Study long-term motivational effects

The presented personalization approaches build the foundation for further research in the area of mobility-based adaptation. While we proposed them for the application of LBGs, each contribution is applicable in its respective area. Applying our routing approach to, e. g., (data) delivery services [161], is expected to enable more efficient delivery schemes for dynamically shifting location properties. Regarding our mobility detection, we focused on the differentiation of vehicular transportation. A more human-centered activity or exercise detection, highlighting more precise movement and adapting accordingly, is an exciting research topic in the Internet of Things and the quantified-self area [41]. For that purpose, a detailed motion recording is required, favoring the utilization of multiple sensors for fine-granular motion differentiation [37, 257]. Thus, LBG content can be individually connected with exercises for movement and health promotion.

Routing with shifting location properties

Human-centered exercise detection

Our contributions to the development and systematic evaluation of online content generation in mobile game applications and its generalization and customization in the GeoVis platform fuel new and further research questions in the aforementioned directions.

ACKNOWLEDGMENTS

The research described in this thesis was co-funded by the LOEWE initiative (Hessen, Germany) within the IDG “Infrakstruktur - Design - Gesellschaft” project.

BIBLIOGRAPHY

[1] Emile Aarts, Jan Korst, and Wil Michiels. "Simulated Annealing." In: *Search Methodologies*. Ed. by Edmund K Burke and Graham Kendall. Boston, MA, USA: Springer, 2014. Chap. 10, pp. 265–285. DOI: 10.1007/978-1-4614-6940-7_10.

[2] Paula Alavesa, Minna Pakanen, Hannu Kukka, Matti Pouke, and Timo Ojala. "Anarchy or Order on the Streets: Review Based Characterization of Location Based Mobile Games." In: *Proc. Annual Symposium on Computer-Human Interaction in Play*. 2017, pp. 101–113. DOI: 10.1145/3116595.3116614.

[3] Jonathan B Allen. "Short Term Spectral Analysis, Synthesis, and Modification by Discrete Fourier Transform." In: *IEEE Transactions on Acoustics, Speech, and Signal Processing* 25.3 (1977), pp. 235–238.

[4] Noor Almaadeed, Muhammad Asim, Somaya Al-Maadeed, Ahmed Bouridane, and Azeddine Beghdadi. "Automatic Detection and Classification of Audio Events for Road Surveillance Applications." In: *Sensors* 18.6 (2018), pp. 1858–1875. DOI: 10.3390/s18061858.

[5] Tim Althoff, Ryen W. White, and Eric Horvitz. "Influence of Pokémon Go on Physical Activity: Study and Implications." In: *Journal of Medical Internet Research* 18.12 (2016), pp. 1–10. DOI: 10.2196/jmir.6759.

[6] Eduardo Álvarez-Miranda, Martin Luipersbeck, and Markus Sinnl. "Gotta (efficiently) catch them all: Pokémon GO meets Orienteering Problems." In: *European Journal of Operational Research* 265.2 (2018), pp. 779–794.

[7] Rob Anastasi, Nick Tandavanitj, Martin Flintham, Andy Crabtree, Matt Adams, Ju Row-Farr, Jamie Iddon, Steve Benford, Terry Hemmings, Shahram Izadi, and Ian Taylor. "Can You See Me Now? A Citywide Mixed-Reality Gaming Experience." In: *Proc. 4th Conference on Ubiquitous Computing (UbiComp)*. 2002, pp. 1–18.

[8] Ian Anderson and Henk Muller. "Practical Activity Recognition using GSM Data." In: *Proc. 5th International Semantic Web Conference (ISWC)*. Springer. 2006, pp. 1–8.

[9] Enrico Angelelli, Claudia Archetti, and Michele Vindigni. "The Clustered Orienteering Problem." In: *European Journal of Operational Research* 238.2 (2014), pp. 404–414.

[10] David L Applegate, Robert E Bixby, Vasek Chvatal, and William J Cook, eds. *The Traveling Salesman Problem: A Computational Study*. Princeton, NJ, USA: Princeton University Press, 2006.

[11] Anna Arigliano, Gianpaolo Ghiani, Antonio Grieco, Emanuela Guerriero, and Isaac Plana. "Time-dependent asymmetric traveling salesman problem with time windows: Properties and an exact algorithm." In: *Discrete Applied Mathematics* 261 (2019), pp. 28–39. DOI: 10.1016/j.dam.2018.09.017.

[12] Norbert Ascheuer, Matteo Fischetti, and Martin Grötschel. "Solving the Asymmetric Travelling Salesman Problem with time windows by branch-and-cut." In: *Mathematical Programming* 90.3 (2001), pp. 475–506. DOI: 10.1007/s101070100218.

[13] Güven Aşçı and M Amaç Güvensan. "A Novel Input Set for LSTM-based Transport Mode Detection." In: *Proc. 2019 IEEE International Conference on Pervasive Computing and Communications Workshops (PerCom Workshops)*. IEEE. 2019, pp. 107–112.

[14] John W Ayers, Eric C Leas, Mark Dredze, Jon-Patrick Allem, Jurek G Grabowski, and Linda Hill. "Pokémon GO – A New Distraction for Drivers and Pedestrians." In: *JAMA Internal Medicine* 176.12 (2016), pp. 1865–1866. DOI: 10.1001/jamainternmed.2016.6274.

[15] Sarwat Y Azeem. *The promotional potential of Pokemon Go*. Available: https://aurora.dawn.com/news/1141509. [Accessed Jul. 31, 2020]. July 2016.

[16] Trevor C Bailey and Anthony C Gatrell, eds. *Interactive Spatial Data Analysis*. Longman Scientific & Technical, 1995.

[17] Edward K Baker. "An exact algorithm for the time-constrained traveling salesman problem." In: *Operations Research* 31.5 (1983), pp. 938–945. DOI: 10.1287/opre.31.5.938.

[18] Rafael A Ballagas, Sven G Kratz, Jan Borchers, Eugen Yu, Steffen P Walz, Claudia O Fuhr, Ludger Hovestadt, and Martin Tann. "REXplorer: a mobile, pervasive spell-casting game for tourists." In: *Proc. Conference on Human Factors in Computing Systems (CHI)*. 2007, pp. 1929–1934.

[19] Pouya Baniasadi, Vladimir Ejov, Michael Haythorpe, and Serguei Rossomakhine. "A new benchmark set for Traveling salesman problem and Hamiltonian cycle problem." In: 2018, pp. 1–21. arXiv: 1806.09285.

[20] Gabriella A B Barros. "Data Games: Towards Generating Content using the Real World." In: *Proc. of Doctoral Symposium of the 9th International and Interdisciplinary Conference on Modeling and Using Context (CONTEXT 2015)*. 2015, pp. 15–22.

[21] Michael Bartoň, Iddo Hanniel, Gershon Elber, and Myung-Soo Kim. "Precise Hausdorff Distance Computation between Polygonal Meshes." In: *Computer Aided Geometric Design* 27.8 (2010), pp. 580–591.

[22] Steve Benford, Andy Crabtree, Martin Flintham, Adam Drozd, Rob Anastasi, Mark Paxton, Nick Tandavanitj, Matt Adams, and Ju Row-Farr. "Can You See Me Now?" In: *ACM Transactions on Computer-Human Interaction* 13.1 (2006), pp. 100–133.

[23] Arpita Bhattacharya, Travis W Windleharth, Rio Anthony Ishii, Ivy M Acevedo, Cecilia R Aragon, Julie A Kientz, Jason C Yip, and Jin H Lee. "Group Interactions in Location-Based Gaming: A Case Study of Raiding in Pokémon GO." In: *Proc. Conference on Human Factors in Computing Systems (CHI)*. 2019, pp. 1–12. DOI: 10.1145/3290605.3300817.

[24] Jacopo Biancat, Chiara Brighenti, and Attilio Brighenti. "Review of Transportation Mode Detection techniques." In: *EAI Endorsed Transactions on Ambient Systems* 1.4 (2014), pp. 1–10. DOI: 10.4108/amsys.1.4.e7.

[25] Leo I Bluestein. "A Linear Filtering Approach to the Computation of the Discrete Fourier Transform." In: *IEEE Transactions on Audio and Electroacoustics* 18.4 (1970), pp. 451–455. DOI: 10.1109/TAU.1970.1162132.

[26] Boehringer Ingelheim Accelerator Program. *Obesity Game – Lands of Bhur*. unpublished. 2018.

[27] Adel Bolbol and Tao Cheng. "GPS Data Collection Setting For Pedestrian Activity Modelling." In: *Proc. Geographical Information Science Research UK Conference 2010 (GISRUK)*. 2010, pp. 1–8.

[28] Adel Bolbol, Tao Cheng, Ioannis Tsapakis, and James Haworth. "Inferring hybrid transportation modes from sparse GPS data using a moving window SVM classification." In: *Computers, Environment and Urban Systems* 36.6 (2012), pp. 526–537. DOI: 10.1016/j.compenvurbsys.2012.06.001.

[29] Stephen Boyd. "Multitone Signals with Low Crest Factor." In: *IEEE Transactions on Circuits and Systems* 33.10 (1986), pp. 1018–1022.

[30] Thomas Brinkhoff. *City Population*. Available: https://www.citypopulation.de. [Accessed Jul. 03, 2020]. 2020.

[31] Maria A Brovelli and Giorgio Zamboni. "A New Method for the Assessment of Spatial Accuracy and Completeness of OpenStreetMap Building Footprints." In: *International Journal of Geo-Information* 7.8 (2018), pp. 289–314. DOI: 10.3390/ijgi7080289.

[32] Richard Brunauer, Michael Hufnagl, Karl Rehrl, and Andreas Wagner. "Motion Pattern Analysis Enabling Accurate Travel Mode Detection from GPS Data Only." In: *Proc. 16th International IEEE Conference on Intelligent Transportation Systems (ITSC 2013)*. IEEE. 2013, pp. 404–411.

[33] Bundesinstitut für Bau-, Stadt- und Raumforschung. *Raumabgrenzungen und Raumtypen des BBSR*. Available: https://www.bbsr.bund.de/BBSR/DE/veroeffentlichungen/analysen-bau-stadt-raum/ausgaben/Bd06.html. [Accessed Sep. 29, 2020]. 2012.

[34] Luc Burnier, Matteo Lanini, Olivia Bouvard, Damiano Scanferla, Abiraam Varathan, Carine Genoud, Arnaud Marguerit, Bernard Cuttat, Noémie Dury, Reiner Witte, Andrea Salvadè, and Andreas Schüler. "Energy saving glazing with a wide band-pass FSS allowing mobile communication: up-scaling and characterisation." In: *IET Microwaves, Antennas & Propagation* 11.10 (2017), pp. 1449–1455. DOI: 10.1049/iet-map.2016.0685.

[35] Claudia Carpineti, Vincenzo Lomonaco, Luca Bedogni, Marco Di Felice, and Luciano Bononi. "Custom Dual Transportation Mode Detection by Smartphone Devices Exploiting Sensor Diversity." In: *Proc. IEEE International Conference on Pervasive Computing and Communications Workshops (PerCom Workshops)*. 2018, pp. 367–372.

[36] Ana M C Carraca. "Procedural Content Generation for Location-based Games." PhD thesis. Porto, PT: University of Porto, 2014.

[37] Polona Caserman, Augusto Garcia-Agundez, Robert Konrad, Stefan Göbel, and Ralf Steinmetz. "Real-time body tracking in virtual reality using a Vive tracker." In: *Virtual Reality* 23.2 (2019), pp. 155–168. DOI: 10.1007/s10055-018-0374-z.

[38] Irene Celino, Dario Cerizza, Simone Contessa, Marta Corubolo, Daniele Dell'Aglio, Emanuele Della Valle, and Stefano Fumeo. "Urbanopoly – a Social and Location-based Game with a Purpose to Crowdsource your Urban Data." In: *Proc. International Conference on Privacy, Security, Risk and Trust and International Conference on Social Computing*. 2012, pp. 910–913.

[39] Robert Cervero and Kara Kockelman. "Travel demand and the 3Ds: Density, diversity, and design." In: *Transportation research. Part D, Transport and environment* 2.3 (1997), pp. 199–219.

[40] Stephanie Chan. *Global App Revenue Reached $50 Billion in the First Half of 2020, Up 23% Year-Over-Year*. Available: https://sensortower.com/blog/app-revenue-and-downloads-1h-2020. [Accessed August. 28, 2020]. June 2020.

[41] Eun K Choe, Nicole B Lee, Bongshin Lee, Wanda Pratt, and Julie A Kientz. "Understanding Quantified-Selfers' Practices in Collecting and Exploring Personal Data." In: *Proc. Conference on Human Factors in Computing Systems (CHI)*. 2014, pp. 1143–1152. DOI: 10.1145/2556288.2557372.

[42] Yvette Chong, Dean Krishen Sethi, Charmaine Hui Yun Loh, and Fatimah Lateef. "Going Forward with Pokemon Go." In: *Journal of Emergencies, Trauma, and Shock* 11.4 (2018), pp. 243–246. DOI: 10.4103/JETS.JETS_87_17.

[43] Philip J Clark and Francis C Evans. "Distance to Nearest Neighbor as a Measure of Spatial Relationships in Populations." In: *Ecology* 35.4 (1954), pp. 445–453.

[44] Kester D Clegg, Julian F Miller, Kieran Massey, and Mike Petty. "Travelling Salesman Problem Solved 'in materio' by Evolved Carbon Nanotube Device." In: *Proc. International Conference on Parallel Problem Solving from Nature*. 2014, pp. 692–701.

[45] Ashley Colley, Jacob Thebault-Spieker, Allen Y Lin, Donald Degraen, Benjamin Fischman, Jonna Häkkilä, Kate Kuehl, Valentina Nisi, Nuno J Nunes, Nina Wenig, Dirk Wenig, Brent Hecht, and Johannes Schöning. "The Geography of Pokémon GO: Beneficial and Problematic Effects on Places and Movement." In: *Proc. Conference on Human Factors in Computing Systems (CHI)*. 2017, pp. 1179–1192. DOI: 10.1145/3025453.3025495.

[46] Gérard Cornuéjols, Jean Fonlupt, and Denis Naddef. "The Travelling Salesman Problem on a Graph and some Related Integer Polyhedra." In: *Mathematical Programming* 33.1 (1985), pp. 1–27.

[47] Vlad C Coroamă, Can Türk, and Friedemann Mattern. "Poster: Exploring the Usefulness of Bluetooth and WiFi Proximity for Transportation Mode Recognition." In: *Proc. 2019 ACM International Joint Conference on Pervasive and Ubiquitous Computing and the 2019 International Symposium on Wearable Computers (UbiComp/ISWC 19 Adjunct)*. ACM. 2019, pp. 37–40. DOI: 10.1145/3341162.3343847.

[48] Emanoel Costa. "Simulation of the Effects of Different Urban Environments on GPS Performance Using Digital Elevation Models and Building Databases." In: *IEEE Transactions on Intelligent Transportation Systems* 12.3 (2011), pp. 819–829. DOI: 10.1109/TITS.2011.2122258.

[49] Victor Cotton and Mitesh S Patel. "Gamification use and design in popular health and fitness mobile applications." In: *American Journal of Health Promotion* 33.3 (2019), pp. 448–451. DOI: 10.1177/0890117118790394.

[50] George B Dantzig and John H Ramser. "The truck dispatching problem." In: *Management Science* 6.1 (1959), pp. 80–91.

[51] Anind K Dey. "Understanding and Using Context." In: *Personal and Ubiquitous Computing* 5.1 (2001), pp. 4–7.

[52] Marco Dorigo and Luca M Gambardella. "Ant-Q: A Reinforcement Learning approach to the traveling salesman problem." In: *Proc. 12th International Conference on Machine Learning (ICML)*. 1995, pp. 252–260.

[53] Marco Dorigo and Thomas Stützle. "Ant Colony Optimization: Overview and Recent Advances." In: *Handbook of Metaheuristics*. Ed. by Michel Gendreau and Jean-Yves Potvin. Vol. 272. Cham, CH: Springer, 2019, pp. 311–351. DOI: 10.1007/978-3-319-91086-4_10.

[54] *Draconius GO: Catch a Dragon!* Elyland LLC. Android, iOS. 2017.

[55] Alok Dutt and Vladimir Rokhlin. "Fast Fourier Transforms for Nonequispaced Data." In: *SIAM Journal on Scientific Computing* 14.6 (1993), pp. 1368–1393.

[56] Alok Dutt and Vladimir Rokhlin. "Fast Fourier Transforms for Nonequispaced Data, II." In: *Applied and Computational Harmonic Analysis* 2.1 (1995), pp. 85–100.

[57] Tim Dutz. "Pervasive Behavior Interventions - Using Mobile Devices for Overcoming Barriers for Physical Activity." PhD thesis. Darmstadt, DE: Technische Universität Darmstadt, 2017.

[58] Tim Dutz, Sandro Hardy, Martin Knöll, Stefan Göbel, and Ralf Steinmetz. "User Interfaces of Mobile Exergames." In: *Proc. International Conference on Human-Computer Interaction*. 2014, pp. 244–255.

[59] George S Easton and Robert E McCulloch. "A Multivariate Generalization of Quantile-Quantile Plots." In: *Journal of the American Statistical Association* 85.410 (1990), pp. 376–386.

[60] Stefan Edelkamp, Max Gath, Tristan Cazenave, and Fabien Teytaud. "Algorithm and knowledge engineering for the TSPTW problem." In: *Proc. IEEE Symposium on Computational Intelligence in Scheduling (SCIS)*. 2013, pp. 44–51. DOI: 10.1109/SCIS.2013.6613251.

[61] Hamid R Eftekhari and Mehdi Ghatee. "An inference engine for smartphones to preprocess data and detect stationary and transportation modes." In: *Transportation Research Part C: Emerging Technologies* 69 (2016), pp. 313–327. DOI: 10.1016/j.trc.2016.06.005.

[62] Gunnar Eisenberg, ed. *Identifikation und Klassifikation von Musikinstrumentenklängen in monophoner und polyphoner Musik*. Göttingen, DE: Cuvillier Verlag, 2008.

[63] Ericsson. *Ericsson Mobility Report June 2020*. Available: https://www.ericsson.com/en/mobility-report/reports/june-2020. [Accessed August. 28, 2020]. June 2020.

[64] Darrel Etherington. *Pokémon GO is officially teaming with Starbucks for 7,800 new Gyms and PokéStops*. Available: https://techcrunch.com/2016/12/08/pokemon-go-is-officially-teaming-with-starbucks-for-7800-new-gyms-and-pokestops/. [Accessed Jul. 31, 2020]. Dec. 2016.

[65] European Commission, Joint Research Centre. *Atlas of the Human Planet 2018*. Tech. rep. Publications Office of the European Union, Dec. 2018. DOI: 10.2760/124503.

[66] Reid Ewing and Robert Cervero. "Travel and the built environment: a meta-analysis." In: *Journal of the American planning association* 76.3 (2010), pp. 265–294. DOI: 10.1080/01944361003766766.

[67] Hongchao Fan, Alexander Zipf, Qing Fu, and Pascal Neis. "Quality assessment for building footprints data on OpenStreetMap." In: *International Journal of Geographical Information Science* 28.4 (2014), pp. 700–719. DOI: 10.1080/13658816.2013.867495.

[68] Shih-Hau Fang, Hao-Hsiang Liao, Yu-Xiang Fei, Kai-Hsiang Chen, Jen-Wei Huang, Yu-Ding Lu, and Yu Tsao. "Transportation Modes Classification Using Sensors on Smartphones." In: *Sensors* 16.8 (2016), pp. 1324–1336. DOI: 10.3390/s16081324.

[69] Megan Farokhmanesh. *I went to Pokémon Go Fest, and it was a disaster*. Available: https://www.theverge.com/2017/7/25/16019404/pokemon-go-fest-refunds-disaster-review. [Accessed Sep. 9, 2020]. July 2017.

[70] Ernst Fehr and Urs Fischbacher. "Why social preferences matter–the impact of non-selfish motives on competition, cooperation and incentives." In: *The Economic Journal* 112.478 (2002), pp. 1–33.

[71] Aneta J Florczyk, Christina Corbane, Daniele Ehrlich, Sergio Freire, Thomas Kemper, Luca Maffenini, Michele Melchiorri, Martino Pesaresi, Panagiotis Politis, Marcello Schiavina, Filip Sabo, and Luigi Zanchetta. *GHSL Data Package 2019*. Tech. rep. Publications Office of the European Union, Dec. 2019. DOI: 10.2760/290498.

[72] David B Fogel. "Evolutionary algorithms in theory and practice." In: *Complexity* 2.4 (1997), pp. 26–27.

[73] Cidália Costa Fonte, Vyron Antoniou, Lucy Bastin, Jacinto Estima, Jamal Jokar Arsanjani, Juan-Carlos Laso Bayas, Linda See, and Rumiana Vatseva. "Assessing VGI data quality." In: *Mapping and the Citizen Sensor*. Ed. by Linda See, Giles Foody, Steffen Fritz, Peter Mooney, Ana-Maria Olteanu-Raimond, Cidalia Maria Parreira da Costa Fonte, Vyron Antoniou, and Cidália Costa Fonte. London, GBR: Ubiquity Press, 2017. Chap. 7, pp. 137–163. DOI: 10.5334/bbf.g.

[74] Lance Fortnow. "The status of the P versus NP problem." In: *Communications of the ACM* 52.9 (2009), pp. 78–86.

[75] Steven Fortune. "Voronoi diagrams and Delaunay triangulations." In: *Computing in Euclidean Geometry*. Ed. by Ding-Zhu Du and Frank Hwang. World Scientific, 1995. Chap. 6, pp. 225–265. DOI: 10.1142/2463.

[76] Yoav Freund and Robert E Schapire. "Experiments with a New Boosting Algorithm." In: *Proc. 13th International Conference on Machine Learning (ICML)*. 1996, pp. 148–156.

[77] Marie Gustafsson Friberger and Julian Togelius. "Generating Interesting Monopoly Boards from Open Data." In: *Proc. IEEE Conference on Computational Intelligence and Games (CIG)*. 2012, pp. 288–295.

[78] Augusto Garcia-Agundez Garcia. "Clinical Decision Support Systems with Game-Based Environments: Monitoring Symptoms of Parkinson's Disease with Exergames." (Unpublished doctoral dissertation). PhD thesis. Darmstadt, DE: Technische Universität Darmstadt, 2020.

[79] Michel Gendreau, Alain Hertz, Gilbert Laporte, and Mihnea Stan. "A Generalized Insertion Heuristic for the Traveling Salesman Problem with Time Windows." In: *Operations Research* 46.3 (1998), pp. 330–335. DOI: 10.1287/opre.46.3.330.

[80] Geographic Information Science & Analysis Team Rural and Environment Science and Analytical Services Division. *Scottish Government Urban Rural Classification 2016*. Edinburgh, GBR, 2018.

[81] Fred Glover. "Tabu Search-Part I." In: *ORSA Journal on Computing* 1.3 (1989), pp. 190–206.

[82] Fred Glover. "Tabu Search-Part II." In: *ORSA Journal on Computing* 2.1 (1990), pp. 4–32.

[83] Stefan Göbel, Alvar Gámez-Zerban, Philipp Müller, Thomas Tregel, Andreas Gilbert, Jason Christian, and David Schmoldt. "SG4Mobility: Educational Game for Environment-Friendly Mobility Behaviour." In: *Proc. 13th European Conference on Games Based Learning (ECGBL)*. Academic Conferences International Limited. 2019, pp. 261–276. DOI: 10.34190/GBL.19.092.

[84] Stefan Göbel, Oliver Schneider, Daniel Holweg, and Ursula Kretschmer. "GEIST – Mobile Edutainment with GIS and Interactive Storytelling." In: *Proc. Ubiquitous GIS*. 2004, pp. 1–6.

[85] David E Goldberg, ed. *Genetic Algorithms in Search, Optimization and Machine Learning*. Boston, MA, USA: Addison-Wesley Longman Publishing Co., Inc., 1989.

[86] Bruce L Golden, Larry Levy, and Rakesh Vohra. "The Orienteering Problem." In: *Naval Research Logistics (NRL)* 34.3 (1987), pp. 307–318.

[87] Xuri Gong, Zhou Huang, Yaoli Wang, Lun Wu, and Yu Liu. "High-performance spatiotemporal trajectory matching across heterogeneous data sources." In: *Future Generation Computer Systems* 105 (Nov. 2019), pp. 148–161. DOI: 10.1016/j.future.2019.11.027.

[88] Paola A Gonzalez, Jeremy S Weinstein, Sean J Barbeau, Miguel A Labrador, Philip L Winters, Nevine L Georggi, and Roxana Perez. "Automating mode detection for travel behaviour analysis by using global positioning systems-enabled mobile phones and neural networks." In: *IET Intelligent Transport Systems* 4.1 (2010), pp. 37–49. DOI: 10.1049/iet-its.2009.0029.

[89] Michael F Goodchild. "Discrete Global Grids for Digital Earth." In: *Proc. 1st International Conference on Discrete Global Grids*. 2000, pp. 1–9.

[90] Michael F Goodchild. "Geographic information systems and science: today and tomorrow." In: *Annals of GIS* 15.1 (2009), pp. 3–9. DOI: 10.1080/19475680903250715.

[91] Michael F Goodchild and Shiren Yang. "A hierarchical spatial data structure for global geographic information systems." In: *Computer Vision, Graphics and Image Processing: Graphical Models and Image Processing (CVGIP)* 54.1 (1992), pp. 31–44.

[92] Richard A Groeneveld and Glen Meeden. "Measuring Skewness and Kurtosis." In: *Journal of the Royal Statistical Society. Series D (The Statistican)* 33.4 (1984), pp. 391–399.

[93] Sanford L Grossbart, Robert A Mittelstaedt, and Gene W Murdock. "Nearest Neighbor Analysis: Inferring Behavioral Processes From Spatial Patterns." In: *NA - Advances in Consumer Research* 5 (1978), pp. 114–118.

[94] Branko Grünbaum and Geoffrey Colin Shephard, eds. *Tilings and Patterns*. Mineola, NY, USA: Dover Publications, 1987.

[95] Marie Gustafsson Friberger, Julian Togelius, Andrew Borg Cardona, Michele Ermacora, Anders Mousten, Martin Møller Jensen, Virgil-Alexandu Tanase, and Ulrik Brøndsted. "Data Games." In: *Proc. Foundations of Digital Games (FDG)*. 2013, pp. 1–8.

[96] M Amaç Güvensan, Burak Dusun, Baris Can, and Hafiza Turkmen. "A Novel Segment-Based Approach for Improving Classification Performance of Transport Mode Detection." In: *Sensors* 18.1 (2018), pp. 87–105. DOI: 10.3390/s18010087.

[97] Bruce Hajek. "Cooling Schedules for Optimal Annealing." In: *Mathematics of Operations Research* 13.2 (1988), pp. 311–329.

[98] Mark A Hall. "Correlation-based Feature Subset Selection for Machine Learning." PhD thesis. Hamilton, New Zealand: University of Waikato, 1999.

[99] Juho Hamari, Aqdas Malik, Johannes Koski, and Aditya Johri. "Uses and gratifications of Pokémon Go: why do people play mobile location-based augmented reality games?" In: *International Journal of Human–Computer Interaction* 35.9 (2019), pp. 804–819. DOI: 10.1080/10447318.2018.1497115.

[100] Robert Hammond and Patrick S McCullagh, eds. *Quantitative Techniques in Geography: An Introduction*. Oxford University Press, 1978.

[101] Manhyung Han, La The Vinh, Young-Koo Lee, and Sungyoung Lee. "Comprehensive Context Recognizer Based on Multimodal Sensors in a Smartphone." In: *Sensors* 12.9 (2012), pp. 12588–12605. DOI: 10.3390/s120912588.

[102] Jean-Francois Hangouet. "Computation of the Hausdorff distance between plane vector polylines." In: *Proc. AutoCarto Conference*. 1995, pp. 1–10.

[103] Sandro Hardy, Stefan Göbel, Michael Gutjahr, Josef Wiemeyer, and Ralf Steinmetz. "Adaptation Model for Indoor Exergames." In: *International Journal of Computer Science in Sport* 11.1 (2012), pp. 73–85.

[104] *Harry Potter: Wizards Unite*. Niantic, Inc. Warner Bros. Games San Francisco. Android, iOS. 2019.

[105] Markus Hegland. "Block Algorithms for FFTs on Vector and Parallel Computers." In: *Proc. Parallel Computing: Trends and Applications (PARCO)*. 1993, pp. 129–136.

[106] Thomas Heinz and Christoph Schlieder. "Addressing Spatio-Temporal Geogame Relocation Issues Using Design Evaluation Heuristics and Agent-based Simulation." In: *Proc. 11th International Conference on Virtual Worlds and Games for Serious Applications (VS-Games)*. 2019, pp. 1–4.

[107] Christopher Helf and Helmut Hlavacs. "Apps for life change: Critical review and solution directions." In: *Entertainment Computing* 14 (2016), pp. 17–22. DOI: 10.1016/j.entcom.2015.07.001.

[108] Samuli Hemminki, Petteri Nurmi, and Sasu Tarkoma. "Accelerometer-Based Transportation Mode Detection on Smartphones." In: *Proc. 11th ACM Conference on Embedded Networked Sensor Systems (SenSys)*. ACM. 2013, pp. 1–14. DOI: 10.1145/2517351.2517367.

[109] Mark Hendrikx, Sebastiaan Meijer, Joeri Van Der Velden, and Alexandru Iosup. "Procedural Content Generation for Games: A Survey." In: *ACM Transactions on Multimedia Computing, Communications, and Applications (TOMM)* 9.1 (2013), pp. 1–22. DOI: 10.1145/2422956.2422957.

[110] Kimihiro Hino, Yasushi Asami, and Jung Su Lee. "Step Counts of Middle-Aged and Elderly Adults for 10 Months Before and After the Release of Pokémon GO in Yokohama, Japan." In: *Journal of Medical Internet Research* 21.2 (2019), pp. 1–9. DOI: 10.2196/10724.

[111] Bo Hjorth. "EEG analysis based on time domain properties." In: *Electroencephalography and Clinical Neurophysiology* 29.3 (1970), pp. 306–310.

[112] Hartwig H Hochmair, Dennis Zielstra, and Pascal Neis. "Assessing the Completeness of Bicycle Trail and Lane Features in OpenStreetMap for the United States." In: *Transactions in GIS* 19.1 (2015), pp. 63–81. DOI: 10.1111/tgis.12081.

[113] Karla L Hoffman, Manfred Padberg, and Giovanni Rinaldi. "Traveling salesman problem." In: *Encyclopedia of Operations Research and Management Science*. Ed. by Saul I Grass and Michael C Fu. Boston, MA, USA: Springer, 2013, pp. 1573–1578. DOI: 10.1007/978-1-4419-1153-7_1068.

[114] David Hollin. "Origins of Pokémon GO." Talk at the Animation on Display (AOD) conference by the technical artist & game designer at Niantic, Inc. Mar. 2017.

[115] Holger H Hoos and Thomas Stützle. "On the empirical scaling of run-time for finding optimal solutions to the travelling salesman problem." In: *European Journal of Operational Research* 238.1 (2014), pp. 87–94. DOI: 10.1016/j.ejor.2014.03.042.

[116] Sanja Huhle. "Live Modalitydetection with Smartphone Sensors using Machine Learning." Master Thesis. TU Darmstadt, 2020.

[117] Frederick John Humphreys and Max Hatherly, eds. *Recrystallization and related annealing phenomena*. Elsevier, 2012.

[118] Chih-Chieh Hung, Wen-Chih Peng, and Wang-Chien Lee. "Clustering and aggregating clues of trajectories for mining trajectory patterns and routes." In: *International Journal on Very Large Data Bases (VLDB)* 24.2 (2015), pp. 169–192. DOI: 10.1007/s00778-011-0262-6.

[119] Lester Ingber. "Simulated Annealing: Practice versus Theory." In: *Mathematical and Computer Modelling* 18.11 (1993), pp. 29–57.

[120] Deborah D Ingram and Sheila J Franco. "2013 NCHS Urban-Rural Classification Scheme for Counties." In: *Vital and Health Statistics. Series 2* 166 (2014), pp. 1–73.

[121] *Ingress*. Google Inc. Niantic Labs. Android, iOS. 2013.

[122] ISO Central Secretary. *Geographic information – Spatial schema*. Standard ISO 19107:2019. Geneva, CH: International Organization for Standardization, 2019.

[123] ISO Central Secretary. *Geographic information – Referencing by coordinates*. Standard ISO 19111:2019. Geneva, CH: International Organization for Standardization, 2019.

[124] ISO Central Secretary. *Geographic information – Spatial referencing by geographic identifiers*. Standard ISO 19112:2019. Geneva, CH: International Organization for Standardization, 2019.

[125] ISO/TC 211. *ISO/TC 211 Multi-Lingual Glossary of Terms*. 2020. URL: https://isotc211.geolexica.org/registers/.

[126] Arash Jahangiri and Hesham A Rakha. "Applying Machine Learning Techniques to Transportation Mode Recognition Using Mobile Phone Sensor Data." In: *IEEE Transactions on Intelligent Transportation Systems* 16.5 (2015), pp. 2406–2417. DOI: 10.1109/TITS.2015.2405759.

[127] Anil K Jain, Robert P W Duin, and Jianchang Mao. "Statistical Pattern Recognition: A Review." In: *IEEE Transactions on Pattern Analysis and Machine Intelligence* 22.1 (2000), pp. 4–37.

[128] Andreas Janecek, Danilo Valerio, Karin A Hummel, Fabio Ricciato, and Helmut Hlavacs. "The Cellular Network as a Sensor: From Mobile Phone Data to Real-Time Road Traffic Monitoring." In: *IEEE Transactions on Intelligent Transportation Systems* 16.5 (2015), pp. 2551–2572. DOI: 10.1109/TITS.2015.2413215.

[129] Soo Jeon and Masayoshi Tomizuka. "Benefits of acceleration measurement in velocity estimation and motion control." In: *Control Engineering Practice* 15.3 (2007), pp. 325–332. DOI: 10.1016/j.conengprac.2005.10.004.

[130] David S Johnson and Lyle A McGeoch. "The traveling salesman problem: a case study." In: *Local Search in Combinatorial Optimization*. Ed. by Emile Aarts and Jan Karel Lenstra. Hoboken, NJ, USA: John Wiley & Sons, 1997. Chap. 8, pp. 215–310.

[131] Jeff Jones and Andrew Adamatzky. "Computation of the travelling salesman problem by a shrinking blob." In: *Natural Computing* 13.1 (2014), pp. 1–16. DOI: 10.1007/s11047-013-9401-x.

[132] Levente Juhász and Hartwig H Hochmair. "Where to catch 'em all? – a geographic analysis of Pokémon Go locations." In: *Geo-spatial Information Science* 20.3 (2017), pp. 241–251. DOI: 10.1080/10095020.2017.1368200.

[133] Levente Juhász, Tessio Novack, Hartwig H Hochmair, and Sen Qiao. "Cartographic Vandalism in the Era of Location-Based Games—The Case of OpenStreetMap and Pokémon GO." In: *ISPRS International Journal of Geo-Information* 9.4 (2020), pp. 197–216. DOI: 10.3390/ijgi9040197.

[134] *Jurassic World: Alive*. Ludia Inc. Android, iOS. 2018.

[135] Andrew B Kahng and Sherief Reda. "Match twice and stitch: a new TSP tour construction heuristic." In: *Operations Research Letters* 32.6 (2004), pp. 499–509. DOI: 10.1016/j.orl.2004.04.001.

[136] Stephen P Kaluzny, Silvia C Vega, Tamre P Cardoso, and Alice A Shelly, eds. *S+ SpatialStats: user's manual for Windows and UNIX*. Springer, 1998.

[137] Marisa G Kantor and Moshe B Rosenwein. "The Orienteering Problem with Time Windows." In: *Journal of the Operational Research Society* 43.6 (1992), pp. 629–635. DOI: 10.1057/jors.1992.88.

[138] Charles F F Karney. "Algorithms for Geodesics." In: *Journal of Geodesy* 87.1 (2013), pp. 43–55. DOI: 10.1007/s00190-012-0578-z.

[139] Richard M Karp. "Reducibility among combinatorial problems." In: *50 Years of Integer Programming 1958-2008*. Springer, 2010, pp. 219–241.

[140] Stephen Karpinskyj, Fabio Zambetta, and Lawrence Cavedon. "Video game personalisation techniques: A comprehensive survey." In: *Entertainment Computing* 5.4 (2014), pp. 211–218. DOI: 10.1016/j.entcom.2014.09.002.

[141] Hannu Karttunen. "Spherical Astronomy." In: *Fundamental Astronomy*. Ed. by Hannu Karttunen, Pekka Kröger, Heikki Oja, Markku Poutanen, and Karl J Donner. Springer, 2016. Chap. 2, pp. 11–45. DOI: 10.1007/978-3-540-34144-4.

[142] Jens Keiner, Stefan Kunis, and Daniel Potts. "Using NFFT 3—A Software Library for Various Nonequispaced Fast Fourier Transforms." In: *ACM Transactions on Mathematical Software (TOMS)* 36.4 (2009), pp. 1–30. DOI: 10.1145/1555386.1555388.

[143] Ghaffer I Kiani, Lars G Olsson, Anders Karlsson, and Karu P Esselle. "Transmission of infrared and visible wavelengths through energy-saving glass due to etching of frequency-selective surfaces." In: *IET Microwaves, Antennas & Propagation* 4.7 (2010), pp. 955–961. DOI: 10.1049/iet-map.2009.0439.

[144] Peter Kiefer, Sebastian Matyas, and Christoph Schlieder. "Playing Location-based Games on Geographically Distributed Game Boards." In: *Proc. 4th International Symposium on Pervasive Gaming Applications (PerGames)*. 2007, pp. 63–71.

[145] Scott Kirkpatrick, C Daniel Gelatt, and Mario P Vecchi. "Optimization by Simulated Annealing." In: *Science* 220.4598 (1983), pp. 671–680. DOI: 10.1126/science.220.4598.671.

[146] Yannik Klein, Felix Klose, Sarah Lettmann, and Maximilian Ratzke. "TrainyMcTrainface: Wie heißt mein Zug?" Serious Games Lab Course Report. TU Darmstadt, 2018.

[147] Martin Knöll and Magnus Moar. "The Space of Digital Health Games." In: *International Journal of Computer Science in Sport* 11.1 (2012), pp. 1–13.

[148] Krzysztof Krawiec. "Evolutionary Feature Selection and Construction." In: *Encyclopedia of Machine Learning and Data Mining*. Ed. by Claude Sammut and Geoffrey I Webb. Boston, MA, USA: Springer, 2016, pp. 353–357. DOI: 10.1007/978-1-4899-7502-7_90-1.

[149] Samuli Laato, Sonja Hyrynsalmi, Sampsa Rauti, and Erkki Sutinen. "The Effects Playing Pokémon GO has on Physical Activity -A Systematic Literature Review." In: *Proc. 53rd Hawaii International Conference on System Sciences*. 2020, pp. 3407–3416.

[150] Samuli Laato, Tarja Pietarinen, Sampsa Rauti, and Teemu H Laine. "Analysis of the Quality of Points of Interest in the Most Popular Location-based Games." In: *Proc. 20th International Conference on Computer Systems and Technologies (CompSysTech)*. 2019, pp. 153–160. DOI: 10.1145/3345252.3345286.

[151] Teemu H Laine. "Mobile Educational Augmented Reality Games: A Systematic Literature Review and Two Case Studies." In: *Computers* 7.1 (2018), pp. 19–46. DOI: 10.3390/computers7010019.

[152] AS Lakhtin and VN Ushakov. "Minimization of the Hausdorff distance between convex polyhedrons." In: *Journal of Mathematical Sciences* 126.6 (2005), pp. 1553–1560.

[153] Zahra Ansari Lari and Amir Golroo. "Automated Transportation Mode Detection Using Smart Phone Applications via Machine Learning: Case Study Mega City of Tehran." In: *Proc. Transportation Research Board 94th Annual Meeting*. 2015, pp. 1–15.

[154] Lasse Juel Larsen and Gunver Majgaard. "The Concept of the Magic Circle and the Pokémon GO Phenomenon." In: *Augmented Reality Games I*. Ed. by Vladimir Geroimenko. Springer, 2019. Chap. 3, pp. 33–50. DOI: 10.1007/978-3-030-15616-9_3.

[155] Sungyong Lee, Jinsung Lee, and Kyunghan Lee. "VehicleSense: A Reliable Sound-based Transportation Mode Recognition System for Smartphones." In: *Proc. 18th International Symposium on a World of Wireless, Mobile and Multimedia Networks (WoWMoM)*. IEEE. 2017, pp. 1–9.

[156] Jan Karel Lenstra and Alexander H G Rinnooy Kan. "Complexity of vehicle routing and scheduling problems." In: *Networks* 11.2 (1981), pp. 221–227.

[157] Ned Levine. "Crime mapping and the Crimestat program." In: *Geographical Analysis* 38.1 (2006), pp. 41–56. DOI: 10.1111/j.0016-7363.2005.00673.x.

[158] Ned Levine. "CrimeStat III: Distance Analysis I and II." In: *CrimeStat III: A Spatial Statistics Program for the Analysis of Crime Incident Locations (v 3.3)*. Houstan, TX, USA, and National Institute of Justice, Washington DC, CO, USA: Ned Levine & Associates, 2010. Chap. 5, pp. 1–42.

[159] Lin Liao, Donald J Patterson, Dieter Fox, and Henry Kautz. "Learning and inferring transportation routines." In: *Artificial Intelligence* 171.5-6 (2007), pp. 311–331. DOI: 10.1016/j.artint.2007.01.006.

[160] Andy Liaw, Matthew Wiener, et al. "Classification and Regression by randomForest." In: *R News* 2.3 (2002), pp. 18–22.

[161] Patrick Lieser. "Decentralized Communication Services for Post-Disaster Scenarios: Resource Allocation, Prioritization, and Long-Range Communication Support." PhD thesis. Darmstadt, DE: Technische Universität Darmstadt, 2019.

[162] Adam Lipowski and Dorota Lipowska. "Roulette-wheel selection via stochastic acceptance." In: *Physica A: Statistical Mechanics and its Applications* 391.6 (2012), pp. 2193–2196. DOI: 10.1016/j.physa.2011.12.004.

[163] Cameron Lister, Joshua H West, Ben Cannon, Tyler Sax, and David Brodegard. "Just a Fad? Gamification in Health and Fitness Apps." In: *Journal of Medical Internet Research Serious Games* 2.2 (2014), pp. 1–12. DOI: 10.2196/games.3413.

[164] Google LLC. *Google Activity Recognition API*. Available: https://developers.google.com/location-context/activity-recognition. [Accessed Jul. 29, 2020]. 2020.

[165] Google LLC. *Google Maps Platform Gaming Services*. Available: https://developers.google.com/maps/documentation/gaming. [Accessed Sep. 10, 2020]. 2020.

[166] Manuel López-Ibáñez and Christian Blum. "Beam-ACO for the Travelling Salesman Problem with Time Windows." In: *Computers & Operations Research* 37.9 (2010), pp. 1570–1583.

[167] Helena R Lourenço, Olivier C Martin, and Thomas Stützle. "Iterated Local Search." In: *Handbook of Metaheuristics*. Ed. by Fred W Glover and Gary A Kochenberger. New York, NY, USA: Kluwer Academic Publishers, 2003. Chap. 11, pp. 320–353.

[168] Dang-Nhac Lu, Duc-Nhan Nguyen, Thi-Hau Nguyen, and Ha-Nam Nguyen. "Vehicle Mode and Driving Activity Detection Based on Analyzing Sensor Data of Smartphones." In: *Sensors* 18.4 (2018), pp. 1036–1060. DOI: 10.3390/s18041036.

[169] Kevin Lynch, ed. *The Image of the City*. Cambridge, MA, USA: MIT Press, 1960.

[170] Nilesh Madhu. "Note on measures for spectral flatness." In: *Electronics Letters* 45.23 (2009), pp. 1195–1196.

[171] Ali Mahdavi-Amiri, Troy Alderson, and Faramarz F Samavati. "A Survey of Digital Earth." In: *Computers & Graphics* 53 (2015), pp. 95–117. DOI: 10.1016/j.cag.2015.08.005.

[172] Ali Mahdavi-Amiri, Erika Harrison, and Faramarz F Samavati. "Hexagonal connectivity maps for Digital Earth." In: *International Journal of Digital Earth* 8.9 (2015), pp. 750–769. DOI: 10.1080/17538947.2014.927597.

[173] Derek Hylton Maling, ed. *Coordinate Systems and Map Projections*. Oxford, UK: Pergamon Press, 2013.

[174] Andrea Mannini and Angelo Maria Sabatini. "On-line Classification of Human Activity and Estimation of Walk-Run Speed from Acceleration Data using Support Vector Machines." In: *Proc. 2011 Annual International Conference of the IEEE Engineering in Medicine and Biology Society (EMBS)*. IEEE. 2011, pp. 3302–3305.

[175] Renata Mansini, M Pelizzari, and R Wolfer. *A granular variable neighbourhood search heuristic for the tour orienteering problem with time windows*. Tech. rep. University of Brescia, IT, 2006.

[176] Eny Maria, Edy Budiman, Haviluddin, and Medi Taruk. "Measure distance locating nearest public facilities using Haversine and Euclidean Methods." In: *Journal of Physics: Conference Series* 1450 (2020), pp. 1–7. DOI: 10.1088/1742-6596/1450/1/012080.

[177] Alessio D Marra, Henrik Becker, Kay W Axhausen, and Francesco Corman. "Multimodal passive tracking of passengers to analyse public transport use." In: *Proc. 18th Swiss Transport Research Conference (STRC)*. 2018, pp. 1–24. DOI: 10.3929/ethz-b-000264733.

[178] Sebastian Matyas. "Playful Geospatial Data Acquisition by Location-based Gaming Communities." In: *International Journal of Virtual Reality* 6.3 (2007), pp. 1–10.

[179] Karl Menger. "Untersuchungen über allgemeine Metrik." In: *Mathematische Annalen* 103.1 (1930), pp. 466–501.

[180] Nenad Mladenović, Raca Todosijević, and Dragan Urošević. "An efficient general variable neighborhood search for large travelling salesman problem with time windows." In: *Yugoslav Journal of Operations Research* 23.1 (2013), pp. 19–30. DOI: 10.2298/YJOR120530015M.

[181] Betty J Mohler, William B Thompson, Sarah H Creem-Regehr, Herbert L Pick, and William H Warren. "Visual flow influences gait transition speed and preferred walking speed." In: *Experimental Brain Research* 181.2 (2007), pp. 221–228. DOI: 10.1007/s00221-007-0917-0.

[182] Jérôme Monnot and Sophie Toulouse. "The Traveling Salesman Problem and its Variations." In: *Paradigms of Combinatorial Optimization: Problems and New Approaches*. Ed. by Vangelis T Paschos. Wiley Online Library, 2014. Chap. 7, pp. 173–214. DOI: 10.1002/9781119005353.ch7.

[183] David Montoya, Serge Abiteboul, and Pierre Senellart. "Hup-Me: Inferring and Reconciling a Timeline of User Activity from Rich Smartphone Data." In: *Proc. 23rd SIGSPATIAL International Conference on Advances in Geographic Information Systems*. ACM. 2015, pp. 1–4. DOI: 10.1145/2820783.2820852.

[184] Kate Motsinger. "Pokémon Go Away: Augmented Reality Games Pose Issues with Trespass and Nuisance." In: *Sand Diego Law Review* 54.3 (2017), pp. 649–703.

[185] Min Y Mun, Deborah Estrin, Jeff Burke, and Mark Hansen. "Parsimonious Mobility Classification using GSM and WiFi Traces." In: *Proc. 5th Workshop on Embedded Networked Sensors (HotEmNets)*. 2008, pp. 1–5.

[186] Saeideh Dehghan Nasiri. "Vehicle routing on real road networks." PhD thesis. Lancaster, UK: Lancaster University, 2014.

[187] Pascal Neis and Dennis Zielstra. "Recent Developments and Future Trends in Volunteered Geographic Information Research: The Case of OpenStreetMap." In: *Future Internet* 6.1 (2014), pp. 76–106. DOI: 10.3390/fi6010076.

[188] Pascal Neis, Dennis Zielstra, and Alexander Zipf. "The Street Network Evolution of Crowdsourced Maps: OpenStreetMap in Germany 2007–2011." In: *Future Internet* 4.1 (2012), pp. 1–21. DOI: 10.3390/fi4010001.

[189] Niantic, Inc. *What makes a High-Quality Portal?* Available: https://niantic.helpshift.com/a/ingress/?s=portal-network&f=what-makes-a-high-quality-portal. [Accessed September. 09, 2020]. 2020.

[190] Eva Nieuwdorp. "The Pervasive Discourse: An Analysis." In: *Computers in Entertainment (CIE)* 5.2 (2007), pp. 1–17. DOI: 10.1145/1279540.1279553.

[191] Marija Nikolić and Michel Bierlaire. "Review of transportation mode detection approaches based on smartphone data." In: *Proc. 17th Swiss Transport Research Conference*. 2017, pp. 1–18.

[192] Stephen M Omohundro. *Five Balltree Construction Algorithms*. Tech. rep. TR-89-063. International Computer Science Institute Berkeley, Nov. 1989.

[193] Melis Oner, Jeffry A Pulcifer-Stump, Patrick Seeling, and Tolga Kaya. "Towards the run and walk activity classification through step detection - an android application." In: *Proc. 2012 Annual International Conference of the IEEE Engineering in Medicine and Biology Society (EMBS)*. IEEE. 2012, pp. 1980–1983.

[194] Janne Paavilainen, Hannu Korhonen, Kati Alha, Jaakko Stenros, Elina Koskinen, and Frans Mayra. "The Pokémon GO experience: A location-based augmented reality mobile game goes mainstream." In: *Proc. Conference on Human Factors in Computing Systems (CHI)*. 2017, pp. 2493–2498. DOI: 10.1145/3025453.3025871.

[195] Kuldip K Paliwal. "Spectral subband centroid features for speech recognition." In: *Proc. IEEE International Conference on Acoustics, Speech and Signal Processing (ICASSP'98)*. 1998, pp. 617–620.

[196] Donald J Patterson, Lin Liao, Dieter Fox, and Henry Kautz. "Inferring High-Level Behavior from Low-Level Sensors." In: *Proc. 5th Conference on Ubiquitous Computing (UbiComp)*. Springer. 2003, pp. 73–89.

[197] Judea Pearl. "Informed, Best-First Search: A Way of Using Heuristic Information." In: *Heuristics: Intelligent Search Strategies for Computer Problem Solving*. Boston, MA, USA: Addison-Wesley Longman Publishing Co., Inc., 1984. Chap. Basic Heuristic-Search Procedures, pp. 46–55.

[198] Victor Pillac, Michel Gendreau, Christelle Guéret, and Andrés L Medaglia. "A Review of Dynamic Vehicle Routing Problems." In: *European Journal of Operational Research* 225.1 (2013), pp. 1–11. DOI: 10.1016/j.ejor.2012.08.015.

[199] *Pokémon GO*. The Pokémon Company, Nintendo. Niantic, Inc. Android, iOS. 2016.

[200] Pokémon GO Hub. *Researching Pokémon GO Spawn Mechanics*. Available: https://pokemongohub.net/generation-2/researching-pokemon-go-spawn-mechanics. [Accessed Aug. 5, 2020]. 2017.

[201] Andrei Popescu. *Geolocation API Specification*. Tech. rep. [Accessed Jul. 29, 2020]. World Wide Web Consortium (W3C), 2010.

[202] R. Darren Price. *Rare Pokemon Sparks Stampede in Central Park*. Available: https://www.nbcnewyork.com/news/local/pokemon-go-players-stampede-new-york-central-park/642115/. [Accessed Sep. 9, 2020]. July 2016.

[203] Lukas Raymann. "Concepts and Implementation for Cross-Location-based Games to enable simultaneous Multiplayer." Master Thesis. TU Darmstadt, 2019.

[204] Nornadiah Mohd Razali, Yap Bee Wah, et al. "Power comparisons of Shapiro-Wilk, Kolmogorov-Smirnov, Lilliefors and Anderson-Darling tests." In: *Journal of Statistical Modeling and Analytics* 2.1 (2011), pp. 21–33.

[205] Sasank Reddy, Min Y Mun, Jeff Burke, Deborah Estrin, Mark Hansen, and Mani Srivastava. "Using Mobile Phones to Determine Transportation Modes." In: *ACM Transactions on Sensor Networks (TOSN)* 6.2 (2010), pp. 1–27. DOI: 10.1145/1689239.1689243.

[206] Christian Reuter. "Authoring Collaborative Multiplayer Games - Game Design Patterns, Structural Verification, Collaborative Balancing and Rapid Prototyping." PhD thesis. Darmstadt, DE: Technische Universität Darmstadt, 2016.

[207] Björn Richerzhagen. "Mechanism Transitions in Publish/Subscribe Systems: Adaptive Event Brokering for Location-based Mobile Social Applications." PhD thesis. Darmstadt, DE: Technische Universität Darmstadt, 2017.

[208] Björn Richerzhagen, Dominik Stingl, Ronny Hans, Christian Gross, and Ralf Steinmetz. "Bypassing the cloud: Peer-assisted event dissemination for augmented reality games." In: *Proc. 14th IEEE International Conference on Peer-to-Peer Computing*. IEEE. 2014, pp. 1–10.

[209] Giovanni Righini and Matteo Salani. "Decremental state space relaxation strategies and initialization heuristics for solving the Orienteering Problem with Time Windows with dynamic programming." In: *Computers & Operations Research* 36.4 (2009), pp. 1191–1203. DOI: 10.1016/j.cor.2008.01.003.

[210] *Ring Fit Adventure*. Nintendo. Nintendo Switch. 2019.

[211] Brian D Ripley. "Modelling Spatial Patterns." In: *Journal of the Royal Statistical Society: Series B (Methodological)* 39.2 (1977), pp. 172–192.

[212] Brian D Ripley, ed. *Spatial Statistics*. Hoboken, NJ, USA: John Wiley & Sons, 2005. DOI: 10.1002/0471725218.

[213] C. Carl Robusto. "The cosine-haversine formula." In: *The American Mathematical Monthly* 64.1 (1957), pp. 38–40. DOI: 10.2307/2309088.

[214] Jörg Roth. "Efficient many-to-many path planning and the Traveling Salesman Problem on road networks." In: *International Journal of Knowledge-based and Intelligent Engineering Systems* 20.3 (2016), pp. 135–148. DOI: 10.3233/KES-160339.

[215] Kevin Sahr, Denis White, and A Jon Kimerling. "Geodesic Discrete Global Grid Systems." In: *Cartography and Geographic Information Science* 30.2 (2003), pp. 121–134.

[216] Martin WP Savelsbergh. "Local search in routing problems with time windows." In: *Annals of Operations Research* 4.1 (1985), pp. 285–305.

[217] Simon Scheider and Peter Kiefer. "(Re-) Localization of Location-Based Games." In: *Geogames and Geoplay*. Ed. by Ola Ahlqvist and Christoph Schlieder. Springer, 2018, pp. 131–159. DOI: 10.1007/978-3-319-22774-0_7.

[218] Christian Schiffer. *Wenn digital und analog verschmelzen*. Available: https://www.deutschlandfunk.de/pokemon-go-wenn-digital-und-analog-verschmelzen.691.de.html?dram:article_id=361679. [Accessed Sep. 9, 2020]. July 2016.

[219] Christoph Schlieder, Peter Kiefer, and Sebastian Matyas. "Geogames: Designing Location-Based Games from Classic Board Games." In: *IEEE Intelligent Systems* 21.5 (2006), pp. 40–46.

[220] Muhammad Awais Shafique and Eiji Hato. "Travel Mode Detection with Varying Smartphone Data Collection Frequencies." In: *Sensors* 16.5 (2016), pp. 716–739. DOI: 10.3390/s1605071.

[221] Noor Shaker, Georgios N Yannakakis, and Julian Togelius. "Towards Automatic Personalized Content Generation for Platform Games." In: *Proc. Artificial Intelligence and Interactive Digital Entertainment*. 2010, pp. 63–68.

[222] Fei Shao, Songmei Cai, and Junzhong Gu. "A Modified Hausdorff Distance based Algorithm for 2-Dimensional Spatial Trajectory Matching." In: *Proc. 5th International Conference on Computer Science & Education*. 2010, pp. 166–172.

[223] Erik B Sherman, ed. *Geocaching: Hike and Seek with Your GPS*. Berkeley, CA, USA: Apress, 2004.

[224] Cynthia M Sifonis. "Attributes of Ingress Gaming Locations Contributing to Players' Place Attachment." In: *Proc. Annual Symposium on Computer-Human Interaction in Play*. 2017, pp. 569–575. DOI: 10.1145/3130859.3131338.

[225] Julius Orion Smith, ed. *Mathematics of the Discrete Fourier Transform (DFT): With Audio Applications*. W3K Publishing, 2007.

[226] Heinrich Söbke, Jannicke Baalsrud Hauge, and Ioana A Stefan. "Long-Term Engagement in Mobile Location-Based Augmented Reality Games." In: *Augmented Reality Games I*. Ed. by Vladimir Geroimenko. Springer, 2019. Chap. 9, pp. 129–147. DOI: 10.1007/978-3-030-15616-9_9.

[227] Timothy Sohn, Alex Varshavsky, Anthony LaMarca, Mike Y Chen, Tanzeem Choudhury, Ian Smith, Sunny Consolvo, Jeffrey Hightower, William G Griswold, and Eyal De Lara. "Mobility Detection Using Everyday GSM Traces." In: *Proc. International Conference on Ubiquitous Computing*. Springer. 2006, pp. 212–224.

[228] Ralf Steinmetz, Melanie Holloway, Boris Koldehofe, Björn Richerzhagen, and Nils Richerzhagen. "Towards Future Internet Communications - Role of Scalable Adaptive Mechanisms." In: *Proc. 27th Annual Conference Symbiosis – Synergy of Humans & Technology*. 2015, pp. 59–61.

[229] Leon Stenneth, Ouri Wolfson, Philip S Yu, and Bo Xu. "Transportation Mode Detection using Mobile Phones and GIS Information." In: *Proc. 19th ACM SIGSPATIAL International Conference on Advances in Geographic Information Systems*. ACM. 2011, pp. 54–63.

[230] Lu Sun, Wei Zhou, Jian Guan, and You He. "Mining spatial–temporal motion pattern for vessel recognition." In: *International Journal of Distributed Sensor Networks* 14.5 (2018), pp. 1–11. DOI: 10.1177/1550147718779563.

[231] Lu Sun, Wei Zhou, Baichen Jiang, and Jian Guan. "A Real-time Similarity Measure Model for Multi-source Trajectories." In: *Proc. International Conference on Computing Intelligence and Information System*. 2017, pp. 257–262. DOI: 10.1109/CIIS.2017.60.

[232] *The Walking Dead: Our World*. Next Games. Android, iOS. 2018.

[233] Arvind Thiagarajan, James Biagioni, Tomas Gerlich, and Jakob Eriksson. "Cooperative Transit Tracking using Smart-phones." In: *Proc. 8th ACM Conference on Embedded Networked Sensor Systems (SenSys)*. ACM. 2010, pp. 85–98.

[234] Julian Togelius, Georgios N Yannakakis, Kenneth O Stanley, and Cameron Browne. "Search-based Procedural Content Generation." In: *Proc. European Conference on the Applications of Evolutionary Computation*. 2010, pp. 141–150.

[235] Julian Togelius, Georgios N Yannakakis, Kenneth O Stanley, and Cameron Browne. "Search-Based Procedural Content Generation: A Taxonomy and Survey." In: *IEEE Transactions on Computational Intelligence and AI in Games* 3.3 (2011), pp. 172–186. DOI: 10.1109/TCIAIG.2011.2148116.

[236] Thomas Tregel, Tim Dutz, Patrick Hock, Philipp N Müller, Philipp Achenbach, and Stefan Göbel. "StreetConqAR: Augmented Reality Anchoring in Pervasive Games." In: *Proc. 5th Joint International Conference on Serious Games (JCSG)*. Springer. 2020, pp. 3–16. DOI: 10.1007/978-3-030-61814-8_1.

[237] Thomas Tregel, Andreas Gilbert, Robert Konrad, Petra Schäfer, and Stefan Göbel. "Examining Approaches for Mobility Detection Through Smartphone Sensors." In: *Proc. 4th Joint International Conference on Serious Games (JCSG)*. Springer. 2018, pp. 217–228. DOI: 10.1007/978-3-030-02762-9_22.

[238] Thomas Tregel, Felix Leber, and Stefan Göbel. "Incentivise Me: Smartphone-Based Mobility Detection for Pervasive Games." In: *Proc. 1st Joint International Conference on Entertainment Computing and Serious Games (ICEC-JCSG)*. Springer. 2019, pp. 470–476. DOI: 10.1007/978-3-030-34644-7_48.

[239] Thomas Tregel, Philipp N Müller, Stefan Göbel, and Ralf Steinmetz. "Where's Pikachu: Route Optimization in Location-Based Games." In: *Proc. 10th International Conference on Virtual Worlds and Games for Serious Applications (VS-Games)*. IEEE. 2018, pp. 81–88. DOI: 10.1109/VS-Games.2018.8493448.

[240] Thomas Tregel, Philipp N Müller, Stefan Göbel, and Ralf Steinmetz. "Looking for Charizard: applying the orienteering problem to location-based games." In: *The Visual Computer* (2019), pp. 1–15. DOI: 10.1007/s00371-019-01737-z.

[241] Thomas Tregel, Lukas Raymann, and Stefan Göbel. "Match Our Cities: Cross-Location-Based Games to Enable Simultaneous Multiplayer". Submitted for publication.

[242] Thomas Tregel, Lukas Raymann, Stefan Göbel, and Ralf Steinmetz. "Geodata Classification for Automatic Content Creation in Location-Based Games." In: *Proc. 3rd Joint International Conference on Serious Games (JCSG)*. Springer. 2017, pp. 212–223. DOI: 10.1007/978-3-319-70111-0_20.

[243] Huai-Kuang Tsai, Jinn-Moon Yang, Yuan-Fang Tsai, and Cheng-Yan Kao. "An Evolutionary Algorithm for Large Traveling Salesman Problems." In: *IEEE Transactions on Systems, Man, and Cybernetics, Part B (Cybernetics)* 34.4 (2004), pp. 1718–1729. DOI: 10.1109/TSMCB.2004.828283.

[244] United States Bureau of the Census. "Urban Area Criteria for the 2010 Census." In: *Federal Register* 76.164 (Aug. 2011), pp. 53029–53043.

[245] University of Art and Design Offenbach am Main. *project-mo.de – the mobility design project*. Available: https://project-mo.de. [Accessed Sep. 15, 2020]. 2020.

[246] Vincent Van Asch. *Macro-and micro-averaged evaluation measures*. Tech. rep. Computational Linguistics & Psycholinguistics University of Antwerp, 2013.

[247] Pieter Vansteenwegen, Wouter Souffriau, and Dirk Van Oudheusden. "The orienteering problem: A survey." In: *European Journal of Operational Research* 209.1 (2011), pp. 1–10. DOI: 10.1016/j.ejor.2010.03.045.

[248] Peter Vorderer, Tilo Hartmann, and Christoph Klimmt. "Explaining the enjoyment of playing video games: the role of competition." In: *Proc. 2nd International Conference on Entertainment Computing (ICEC)*. 2003, pp. 1–9.

[249] Johan Wahlström, Isaac Skog, and Peter Händel. "Smartphone-Based Vehicle Telematics: A Ten-Year Anniversary." In: *IEEE Transactions on Intelligent Transportation Systems* 18.10 (2017), pp. 2802–2825. DOI: 10.1109/TITS.2017.2680468.

[250] Bao Wang, Linjie Gao, and Zhicai Juan. "Travel Mode Detection Using GPS Data and Socioeconomic Attributes Based on a Random Forest Classifier." In: *IEEE Transactions on Intelligent Transportation Systems* 19.5 (2017), pp. 1547–1558. DOI: 10.1109/TITS.2017.2723523.

[251] Lin Wang and Daniel Roggen. "Sound-based Transportation Mode Recognition with Smartphones." In: *Proc. International Conference on Acoustics, Speech and Signal Processing (ICASSP)*. IEEE. 2019, pp. 930–934.

[252] Shuangquan Wang, Canfeng Chen, and Jian Ma. "Accelerometer based transportation mode recognition on mobile phones." In: *Proc. 2010 Asia-Pacific Conference on Wearable Computing Systems*. IEEE. 2010, pp. 44–46. DOI: 10.1109/APWCS.2010.18.

[253] Yilun Wang, Yu Zheng, and Yexiang Xue. "Travel Time Estimation of a Path using Sparse Trajectories." In: *Proc. 20th International Conference on Knowledge Discovery and Data Mining (SIGKDD)*. 2014, pp. 25–34. DOI: 10.1145/2623330.2623656.

[254] Kazuhiro Watanabe, Norito Kawakami, Kotaro Imamura, Akiomi Inoue, Akihito Shimazu, Toru Yoshikawa, Hisanori Hiro, Yumi Asai, Yuko Odagiri, Etsuko Yoshikawa, and Akizumi Tsutsumi. "Pokémon GO and psychological distress, physical complaints, and work performance among adult workers: a retrospective cohort study." In: *Scientific Reports* 7.1 (2017), pp. 1–7. DOI: 10.1038/s41598-017-11176-2.

[255] Li Wei and Eamonn Keogh. "Semi-supervised time series classification." In: *Proc. 12th International Conference on Knowledge Discovery and Data Mining (SIGKDD)*. 2006, pp. 748–753.

[256] Thomas Weise. *Global Optimization Algorithm: Theory and Application*. Available: http://www.it-weise.de/projects/book.pdf. June 2009.

[257] Tobias Welther. "Complex Three-Dimensional Gesture Detection using IMUs and Wearables for Sensorfusion with Machine Learning." Master Thesis. TU Darmstadt, 2018.

[258] Viktor Wendel. "Collaborative Game-based Learning - Automatized Adaptation Mechanics for Game-based Collaborative Learning using Game Mastering Concepts." PhD thesis. Darmstadt, DE: Technische Universität Darmstadt, 2015.

[259] Tom Wijman. *Mobile Revenues Account for More Than 50% of the Global Games Market as It Reaches $137.9 Billion in 2018*. Available: https://newzoo.com/insights/articles/global-games-market-reaches-137-9-billion-in-2018-mobile-games-take-half. [Accessed August. 28, 2020]. Apr. 2018.

[260] World Health Organization. "Global recommendations on physical activity for health." In: (2010), pp. 1–60.

[261] World Health Organization. *Global Health Observatory data repository*. Available: https://apps.who.int/gho/data/node.main.A893?lang=en. [Accessed Sep. 09, 2020]. Nov. 2018.

[262] Linlin Wu, Biao Yang, and Peng Jing. "Travel mode detection based on GPS raw data collected by smartphones: a systematic review of the existing methodologies." In: *Information* 7.4 (2016), pp. 67–85. DOI: 10.3390/info7040067.

[263] Ying Xian, Hanzhang Xu, Haolin Xu, Li Liang, Adrian F Hernandez, Tracy Y Wang, and Eric D Peterson. "An Initial Evaluation of the Impact of Pokémon GO on Physical Activity." In: *Journal of the American Heart Association* 6.5 (2017), pp. 1–7. DOI: 10.1161/JAHA.116.005341.

[264] Feifei Xu, Dimitrios Buhalis, and Jessika Weber. "Serious games and the gamification of tourism." In: *Tourism Management* 60.1 (2017), pp. 244–256. DOI: 10.1016/j.tourman.2016.11.020.

[265] Xue Yang, Kathleen Stewart, Luliang Tang, Zhong Xie, and Qingquan Li. "A Review of GPS Trajectories Classification Based on Transportation Mode." In: *Sensors* 18.11 (2018), pp. 3741–3760. DOI: 10.3390/s18113741.

[266] Georgios N Yannakakis and Julian Togelius. "Experience-Driven Procedural Content Generation." In: *IEEE Transactions on Affective Computing* 2.3 (2011), pp. 147–161. DOI: 10.1109/T-AFFC.2011.6.

[267] Nick Yee. "Motivations for Play in Online Games." In: *CyberPsychology & behavior* 9.6 (2006), pp. 772–775.

[268] Meng-Chieh Yu, Tong Yu, Shao-Chen Wang, Chih-Jen Lin, and Edward Y Chang. "Big Data Small Footprint: The Design of A Low-Power Classifier for Detecting Transportation Modes." In: *Proc. International Conference on Very Large Data Bases (VLDB)*. 2014, pp. 1429–1440.

[269] Haozhe Zhang, Joshua Zimmerman, Dan Nettleton, and Daniel J Nordman. "Random forest prediction intervals." In: *The American Statistician* (2019), pp. 1–49. DOI: 10.1080/00031305.2019.1585288.

[270] Xinyue Zhang, Jingyi Wang, Yong Li, Riku Jäntti, Miao Pan, and Zhu Han. "Catching All Pokémon: Virtual Reward Optimization With Tensor Voting Based Trajectory Privacy." In: *IEEE Transactions on Vehicular Technology* 68.1 (2018), pp. 883–892. DOI: 10.1109/TVT.2018.2882733.

[271] Alice Zheng and Amanda Casari, eds. *Feature Engineering for Machine Learning: Principles and Techniques for Data Scientists*. Sebastopol, CA, USA: O'Reilly Media, Inc., 2018.

[272] Yu Zheng, Yukun Chen, Quannan Li, Xing Xie, and Wei-Ying Ma. "Understanding Transportation Modes Based on GPS Data for Web Applications." In: *ACM Transactions on the Web (TWEB)* 4.1 (2010), pp. 1–36. DOI: 10.1145/1658373.1658374.

[273] Yu Zheng, Quannan Li, Yukun Chen, Xing Xie, and Wei-Ying Ma. "Understanding Mobility Based on GPS Data." In: *Proc. 10th Conference on Ubiquitous Computing (UbiComp)*. ACM. 2008, pp. 312–321.

[274] Mingyang Zhong, Jiahui Wen, Peizhao Hu, and Jadwiga Indulska. "Advancing Android Activity Recognition Service with Markov Smoother." In: *Proc. IEEE International Conference on Pervasive Computing and Communications Workshops (PerCom Workshops)*. 2015, pp. 38–43.

[275] Chaoran Zhou, Hongfei Jia, Jingxin Gao, Lili Yang, Yixiong Feng, and Guangdong Tian. "Travel mode detection method based on big smartphone global positioning system tracking data." In: *Advances in Mechanical Engineering* 9.6 (2017), pp. 1–10. DOI: 10.1177/1687814017708134.

[276] *Zombies, Run!* Six to Start. Android, iOS, Windows Phone. 2012.

A

APPENDIX

A.1 ADDITIONAL INSIGHTS ON GAME AREA GENERATION

Geodata filters are designed to group location-based OpenStreetMap (OSM) data according to their similar cultural representation. Each filter contains a set of unique tags utilized to identify the particular location feature, shown in Table 19. Priority values represent the expected cultural relevance for that location, with higher values being more relevant.

Table 19: Developed geodata filter and associated OSM tags. Prioritiy values are only noted on a category basis instead of on a tag basis.

priority	category	content		
1	street and footway crossings			
2	trees, stones and springs	natural =	spring	
			rock, stone	
			tree	
3	wells, towers and survey points	man_made =	communications_tower	
			water_tower	
			water_well	
			survey_point, tower	
4	waste disposal and toilets	amenity =	waste_basket, waste_disposal, recycling	
			toilets	
		building =	toilets	
5	public communication	amenity =	post_box, post_office	
			telephone	
6	benches	amenity =	bench	
7	pedestrian walkways	highway =	pedestrian	
8	parks	leisure =	park	
9	stations and stops for means of transport	amenity =	bicycle_parking, bicycle_rental	
			charging_station, fuel	
		highway =	rest_area, services	

priority	category		content	
			car_rental, car_wash	
		amenity =	bus_station	
		railway =	halt, station, tram_stop	
		public_transport =	station, stop_position	
		building =	train_station, transportation	
		highway =	bus_stop	
10	product shops and services	craft =	*	
		shop =	*	
		vending	*	
		amenity =	atm, bank, bureau_de_change, marketplace, internet_cafe, vending_machine	
		building =	kiosk, retail, supermarket	
11	healthcare and social facilities	amenity =	dentist	
			veterinary, animal_shelter	
			pharmacy	
			social_facility	
		social_facility =	*	
		amenity =	clinics, community_center, doctors, kneipp_water_cure	
		healthcare =	*	
12	places for food or drinks	amenity =	drinking_water	
			fast_food	
			cafe, food_court, ice_cream, restaurant, pub, bar, biergarten	
13	places for doing sport	leisure =	beach_resort, sauna, swimming_pool, water_park	
		amenity =	public_bath	
		leisure =	fitness_centre, fitness_station, pitch, stadium, bowling_alley	
		amenity =	dojo	
		sport =	*	
14	educational establishments	amenity =	college, dancing_school, kindergarten, language_school, music_school, school, university	
		building =	college, kindergarten, school, university	
15	playgrounds	leisure =	playground	

priority	category	content		
16	mountain peaks	natural =	peak	
17	huts and other shelters	leisure =	bird_hide	
		amenity =	hunting_stand	
			shelter	
		building =	hut	
		tourism =	alpine_hut	
18	places for picnic or barbecue	amenity =	bbq	
		leisure =	firepit, picnic_table	
		shelter_type =	picnic_shelter	
		tourism =	picnic_site	
19	libraries and public bookcases	amenity =	library, public_bookcase	
20	town halls	amenity =	townhall	
21	places of entertainment, arts, culture and tourism	amenity =	fountain	
			cinema	
		man_made =	windwill	
		tourism =	museum	
			information	
			attraction, viewpoint	
			artwork, gallery, theme_park, zoo	
		amenity =	arts_center, conference_centre, events_venue, exhibition_centre, nightclub, planetarium, ranger_station, studio, theatre	
22	places of worship	amenity =	place_of_worship	
		building =	cathedral, chapel, church, religious, shrine, synagogue, temple	
		man_made =	cross, torii	
23	historic places	building =	ruins	
		man_made =	obelisk	
		historic =	*	

Distance Calculation Example

The relative distance between a tuple of PoIs utilizes each PoI's relative position within its game area to determine their similarity in positioning. Figure 40 shows a simplified example for one PoI tuple of three equal-sized game areas according to Equation 3.

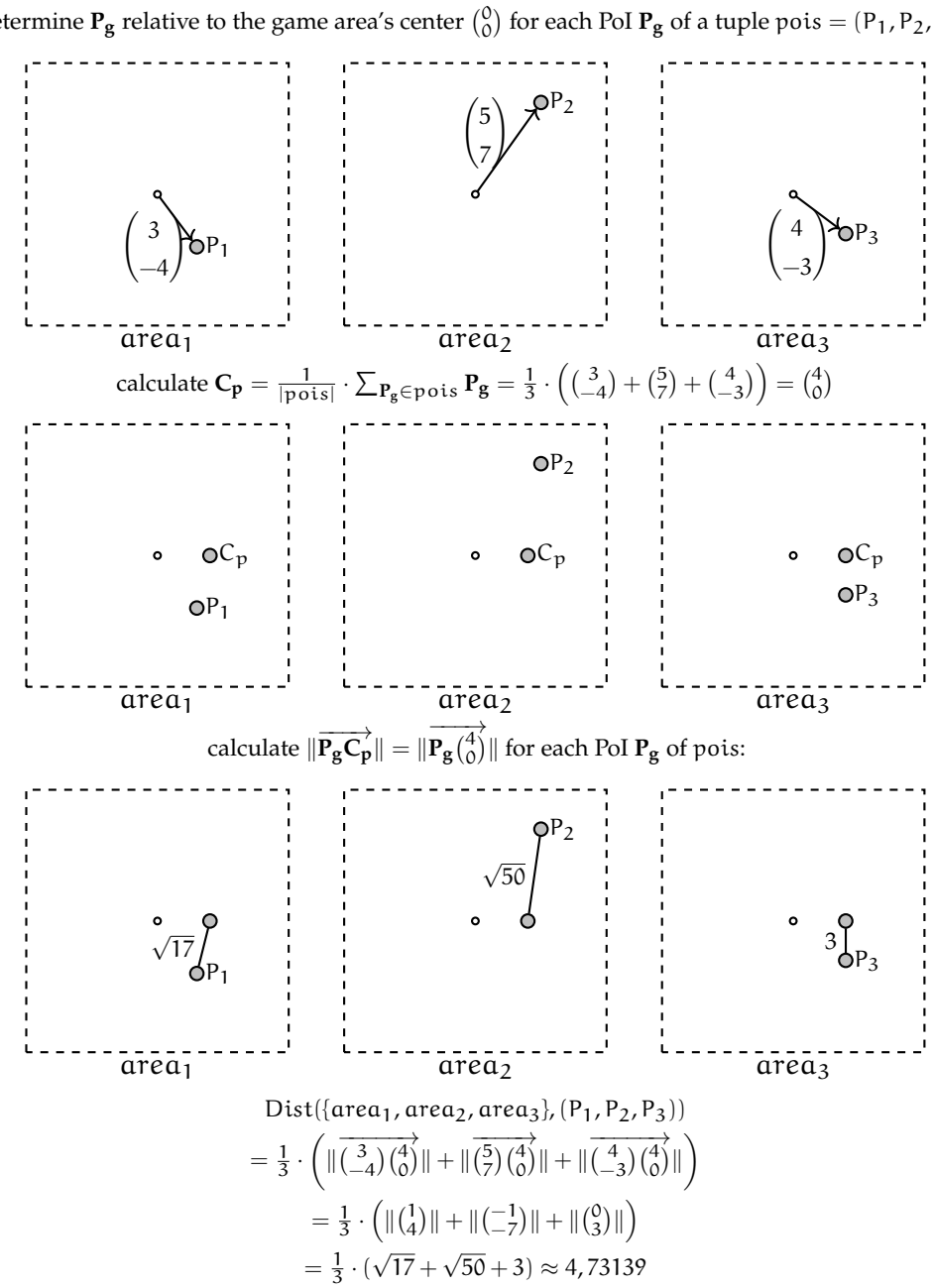

Figure 40: A simplified example calculating $\mathtt{Dist}_{\mathtt{Match}}(\{\mathtt{Area}_1, \mathtt{Area}_2, \mathtt{Area}_3\}, (P_1, P_2, P_3))$ for three game areas $\{\mathtt{Area}_1, \mathtt{Area}_2, \mathtt{Area}_3\}$ without normalization since the game areas have equal sizes.

Relative Coordinate Calculation

As a result of geographic projections, game areas and their underlying cells are distorted. For the same reason, cells can already be rotated. To compare the PoIs' relative position of one game area to PoIs in other game areas, each PoI's relative position within its area is required. With a game area's center being $(0, 0)$, the relative position $\mathbf{P} = (x_p, y_p)$ of a geographic point $\mathbf{P_g}$ is calculated. We assign the following relative coordinates to the corner locations: $\mathbf{A} = (-1, -1)$, $\mathbf{B} = (-1, 1)$, $\mathbf{C} = (1, 1)$, and $\mathbf{D} = (1, -1)$. Because we know the game area's geographic location, its corner location coordinates $\mathbf{A_g}$, $\mathbf{B_g}$, $\mathbf{C_g}$, and $\mathbf{D_g}$ are also known.

Because, for these relative coordinates, the distance between adjacent corner locations is 2, the distance of $\mathbf{P}$ to the corner locations $\mathbf{A}$ and $\mathbf{B}$ can be calculated as follows:

$$d_A = \frac{\|\overrightarrow{\mathbf{A_g}\mathbf{P_g}}\|}{\frac{1}{2}\|\overrightarrow{\mathbf{A_g}\mathbf{B_g}}\|} \qquad d_B = \frac{\|\overrightarrow{\mathbf{B_g}\mathbf{P_g}}\|}{\frac{1}{2}\|\overrightarrow{\mathbf{A_g}\mathbf{B_g}}\|}$$

As shown in Figure 42, we can now create circles at both corner locations with the determined distances as their radius. The intersection point within the game area is the relative position $\mathbf{P}$. It is calculated based on the Pythagorean theorem: $d_A^2 = g_A^2 + h_A^2$ and $d_B^2 = (2 - g_A)^2 + h_A^2$, with g_A and h_A being the right-angled triangle's legs. By substituting h_A^2 and the subsequent transformation, we get $g_A = \frac{d_A^2 - d_B^2 + 4}{4}$, and therefore $h_A = \sqrt{d_A^2 - g_A^2}$. Thus, based on $\mathbf{A} = (-1, -1)$, the relative position is $\mathbf{P} = (x_p, y_p) = (-1 + h_A, -1 + g_A)$.

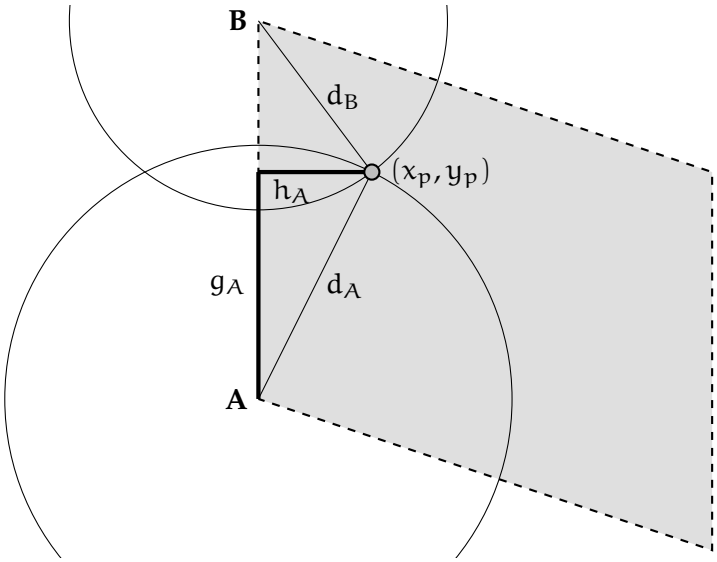

Figure 41: Finding the relative position $\mathbf{P_r} = (x_p, y_p)$ of a PoI with coordinates $\mathbf{P}$ in a game area it is located in. It is calculated as the intersection point of circles within the area around $\mathbf{A} = (-1, -1)$ and $\mathbf{B} = (-1, 1)$ with radii d_A and d_B. g_A and h_A are determined according to the Pythagorean theorem.

The calculated values x_p and y_p are now relative to the corner locations **A** and **B**. Because the game areas are usually not quadratic, these values have to be normalized according to the area's stretching and obliqueness. Thus, we determine the adjusted relative position $\mathbf{P}' = (x'_p, y'_p)$.

$\mathbf{D}' = (x'_D, y'_D)$ is the position of **D** relative to **A**, and **B**, which we determine similar to our previous approach. The obliqueness is thereby described by the resulting values of $g_{D'}$ and $h_{D'}$. In a quadratic game area, $\mathbf{D}'$ and **D** would be equal. All utilized measurements are visualized in Figure 42.

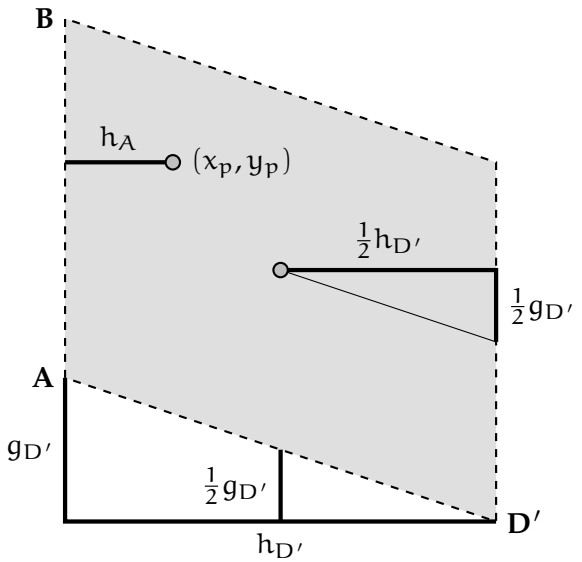

Figure 42: Calculation of $\mathbf{D}'$ analog to Figure 41, for the values of $g_{D'}$ and $h_{D'}$. They are used to normalize the position (x_P, y_P) for the area's stretching and obliqueness.

First, we determine x'_p according to the x-axis's stretching or compression. Since $h_{D'}$ would be 2 in a normalized game area, $\frac{1}{2}h_{D'}$ can be used to normalize h_A:

$$x'_p = -1 + \frac{h_A}{\frac{1}{2}h_{D'}} = \frac{2h_A}{h_{D'}} - 1$$

Second, we determine y'_p according to the y-axis's obliqueness. The proportional shift along the x-axis according to $h_{D'}$ causes a similar proportional shift along the y-axis according to $g_{D'}$. Therefore, the shift is $s_y = \frac{1}{2}g_{D'}\left(\frac{h_A}{\frac{1}{2}h_{D'}}\right)$. Applying the shift of y_p alongside the y-axis results in:

$$y'_p = y_p - s_y = -1 + g_A - \frac{1}{2}g_{D'}\left(\frac{h_A}{\frac{1}{2}h_{D'}}\right) = g_A - 1 - \frac{g_{D'}h_A}{h_{D'}}$$

In conclusion, the relative normalized position of $\mathbf{P}'$ is:

$$\mathbf{P}' = \left(\frac{2h_A}{h_{D'}} - 1\,,\; g_A - 1 - \frac{g_{D'}h_A}{h_{D'}}\right)$$

A.2 EXTENDED STUDY OF GAME AREA QUALITY

Game Area Evaluation Data

Figure 43 shows the distribution of our collected *Pokémon GO* dataset. Since we have no information on whether a cell contains no data or has not been scanned, we filtered all cells that contain no fully occupied cell neighborhood. This allows us to assess the Voronoi areas within each cell reliably. One effect is that this leads to cells at the dataset's border are ignored, which characteristically have less content. Thus, the results will instead be an overestimation regarding content density. The cells highlighted in blue contain only reliable spawn point data, as the cell either contains no Gym or PokéStop data, or the neighboring cells are missing this data. Because Gym and PokéStop data can be accessed more reliably, this indicated that the corresponding areas contain no reliable coverage of this content.

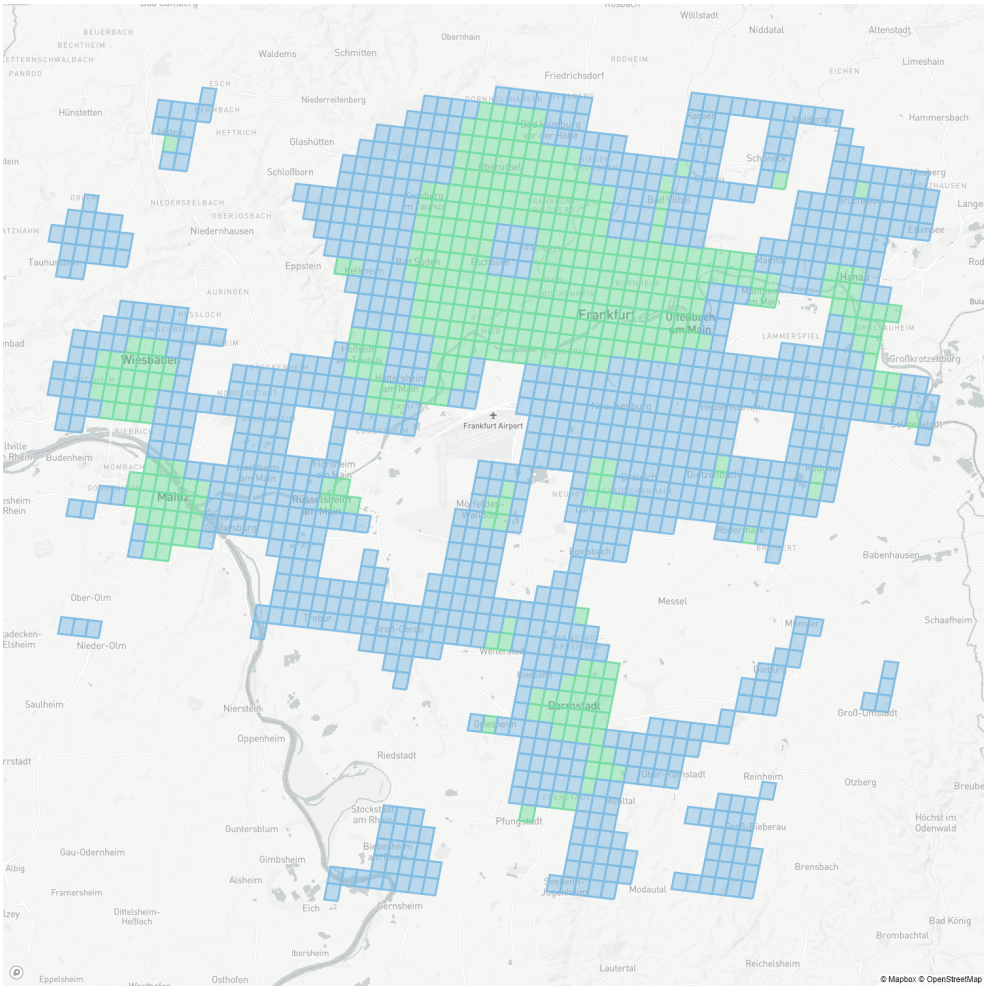

Figure 43: Overview map over *Pokémon GO* locations after cell filtering. Green cells contain a full content coverage, containing Gyms, PokéStops and spawn points. The blue cells contain only reliable spawn point data.

Table 20: All evaluated regions based on their urban categories and a continent-based location selections. Each entry belongs to a different country, increasing the coverage for each continent.

	Metropolitan area / region	Selected area in metropolitan area's vicinity		
		Urban	Suburban	Rural
Africa	Johannesburg	Vanderbijlpark	Heidelberg	Mooinooi
	Kairo	Beni Suef	Al Ayyat	Damalliij
	Lagos	Ikorodu	Igbo Ora	Lemode
	Abidjan	Anyama	Akoupé	Lopou
	Nairobi	Naivasha	Kenol	Isinya
Asia	Tokyo	Chigasaka	Samukawa	Manazuru
	Shanghai	Chongming	Zhangyan Zhen	Tongjiang Jiedao
	Delhi	Bulandshahr	Tigri	Khera Khurd
	Seoul	Guri	Sohol-eup	Yeoncheon
	Abu Dhabi	Ajman	Al Dhaid	Al Madam
Australia	Brisbane	Sunshine Coast	Southport	Byron Bay
	Sydney	Wollongong City	Nowra-Bomaderry	Moss Vale
	Auckland	Hamilton	New Lynn	Silverdale
	Wellington	Lower Hutt	Blenheim	Khandallah
	Perth	Mandurah	Rockingham	Northam
Europe	London	Oxford	Bletchley	Towcester
	Paris	Amiens	Ozoir-la-Ferrière	Montididier
	Madrid	Guadalajara	Tarancón	Villarejo de Salvanés
	Athen	Chalkida	Korinth	Aliveri
	Helsinki	Vantaa	Kerava	Sundsberg
North America	Los Angeles	Victorville	California City	Helendale
	Montreal	Saint-Jean-sur-Richelieu	Sorel-Tracy	Napierville
	Calgary	Red Deer	Okotoks	Rocky Mountain House
	Kansas City	Saint Joseph	Blue Springs	Cameron
	New York City	Paterson	Morristown	Armonk
South America	Rio de Janeiro	Magé	Vassouras	Simão Pereira
	Lima	Lurigancho-Chosica	Chilca	Cocachacra
	Santiago de Chile	Melipilla	Peumo	Lo Miranda
	Buenos Aires	Luján	Cañuelas	Sulpacha
	Bogotá	Fusagasugá	Cota	Restrepo

Game Area Availability with Varying Problem Parameters

In the following, we analyze the number of game areas meeting the requirements of increasing p_n values, i. e., the targeted amount of PoIs and varying p_{c2t} thresholds between 0.5 and 0.9. For the laxest criteria ($p_n = 8$, $p_{c2t} \geqslant 0.5$), the approach can be utilized in most regions. It is notable that the parameter sets of ($p_{c2t} \geqslant 0.5$; $p_n = 32$) and ($p_{c2t} \geqslant 0.9$; $p_n = 8$) have an almost identical coverage, with most contributing cells being identical. This introduces an interesting trade-off, where by reducing the p_{c2t} criterion, an increasing PoI amount p_n can be requested. Thus, more PoIs get selected, though allowing for more clustered game areas. Especially for game areas with larger excluded areas like rivers or highways crossing the area, accepting a locally more clustered game area is inevitable, when p_n still need to be met. The same applies for areas with a non-uniform distribution of PoI candidates, where it becomes a feasible content generation option to weigh between reduced expected content quality and an increase in availability. This effect is observable for the parameter sets of ($p_{c2t} \geqslant 0.5$; $p_n = 16$) and ($p_{c2t} \geqslant 0.9$; $p_n = 8$).

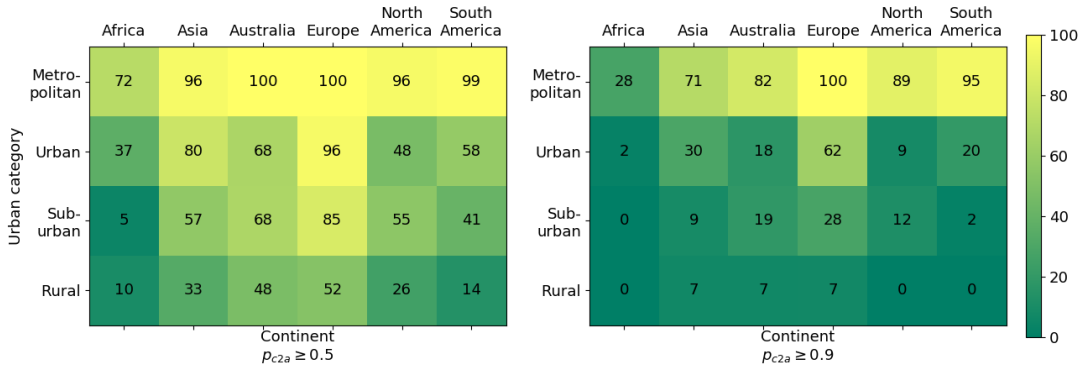

Figure 44: Percentual amount of fully generated game areas for given p_{c2t} and $p_n = 8$ with geodata filter group 3.

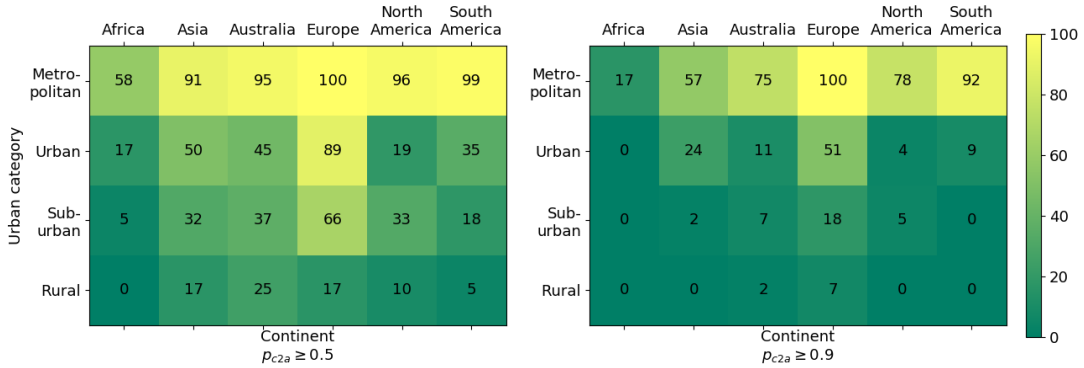

Figure 45: Percentual amount of fully generated game areas for given p_{c2t} and $p_n = 16$ with geodata filter group 3.

Figure 46: Percentual amount of fully generated game areas for given p_{c2t} and $p_n = 32$ with geodata filter group 3.

Extended Game Area Quality Evaluation

In addition to our analysis with the p_{c2t} threshold of 0.5, we assess the effect of a strict threshold of 0.9 and a threshold-less approach. Similar to our evaluation in Section 6.2.1, we choose $p_n = 32$ on the level 14 S2 cells, presenting an intentionally challenging target for most game areas. The results are depicted in Figure 47. Subsequently, we assess the generation quality for groups of level 14 cells, merged to level 13, respectively level 12 cells, each for a total of 64 PoIs.

Since the p_{c2t} threshold is highly restrictive, there are notably fewer game areas meeting the required amount of PoIs. For geofilter groups 1, nearly solely European game areas can be generated with the exception of Lima in South America, also providing reliable results. We achieve a mean priority value of 20.2, which is more than our previous evaluation, indicating a high availability of places of worship and historical places in these areas. The difference in mean priority values between groups 2 and 3 is below 1.0 for all non-rural areas. The amount of game areas is 15.5% higher for group 3 compared to group 2. This shows a good effect of group 3 filters for sparse areas, increasing the game area availability without a harsh impact on priority values. For the Nearest Neighbor Index (NNI), a mean value of 1.2 with a standard deviation of 0.18 can be achieved, showing a good PoI distribution in most game areas.

$p_n = 32$ in level 14 S2 cells

For the four cells merged into level 13 cells with $p_n = 16$, shown in Figure 48, the scenario results in at most 64 selected PoIs. With regard to the mean priority values, similar observations can be made like before. However, the NNI significantly increases to 1.3 with a lower standard deviation of 0.12. Thus, the merging process in this scenario allows for well-distributed game areas. Additionally, 9.7% more game areas are generated with geofilter group 3 compared to group 2.

Merged level 13 cells

For the 16 cells merged into level 12 cells with $p_n = 4$, shown in Figure 49, the scenario again results in at most 64 selected PoIs. The mean priority value for groups 2 and 3 rises to 17.6 and 16.8, respectively, which is an increase of five compared to the level 14 cells. However, no suburban or rural area was able to meet the generation requirements, indicating that the threshold of $p_{c2t} \geqslant 0.9$ is too high for those areas. For the areas meeting the requirements, particularly high NNI values are achieved with a mean of 1.45 and a low standard deviation of 0.07.

Merged level 12 cells

For the scenario with a p_{c2t} criterion, i. e., all game areas are evaluated. The results, shown in Figure 50, match the number of game areas that can provide a game locations (Figure 21) with one deduction. Since NNI values are only calculatable for at least two locations, areas with only one selected PoI are not visualized. To measure the quality of those game areas, an alternate metric would be required to describe an area's location quality.

NNI restrictions for small number of PoIs

For the priority value, geofilter group 1 areas achieve mean values of 19.1, while groups 2 and 3 have mean values of 12.8, respectively 11.9, further confirming the small difference between the two latter groups. In contrast to our previous scenarios, only 1% more game areas were generated when comparing geofilter group 3 to group 2, and 16.7% compared to group 1. This shows that most game areas contain at least one PoI of high cultural relevance, and almost all areas with OSM data contain at least one PoI of geofilter group 2. The mean NNI value of 1.16 is similar to the previous scenarios

$p_n = 32$ in level 14 S2 cells

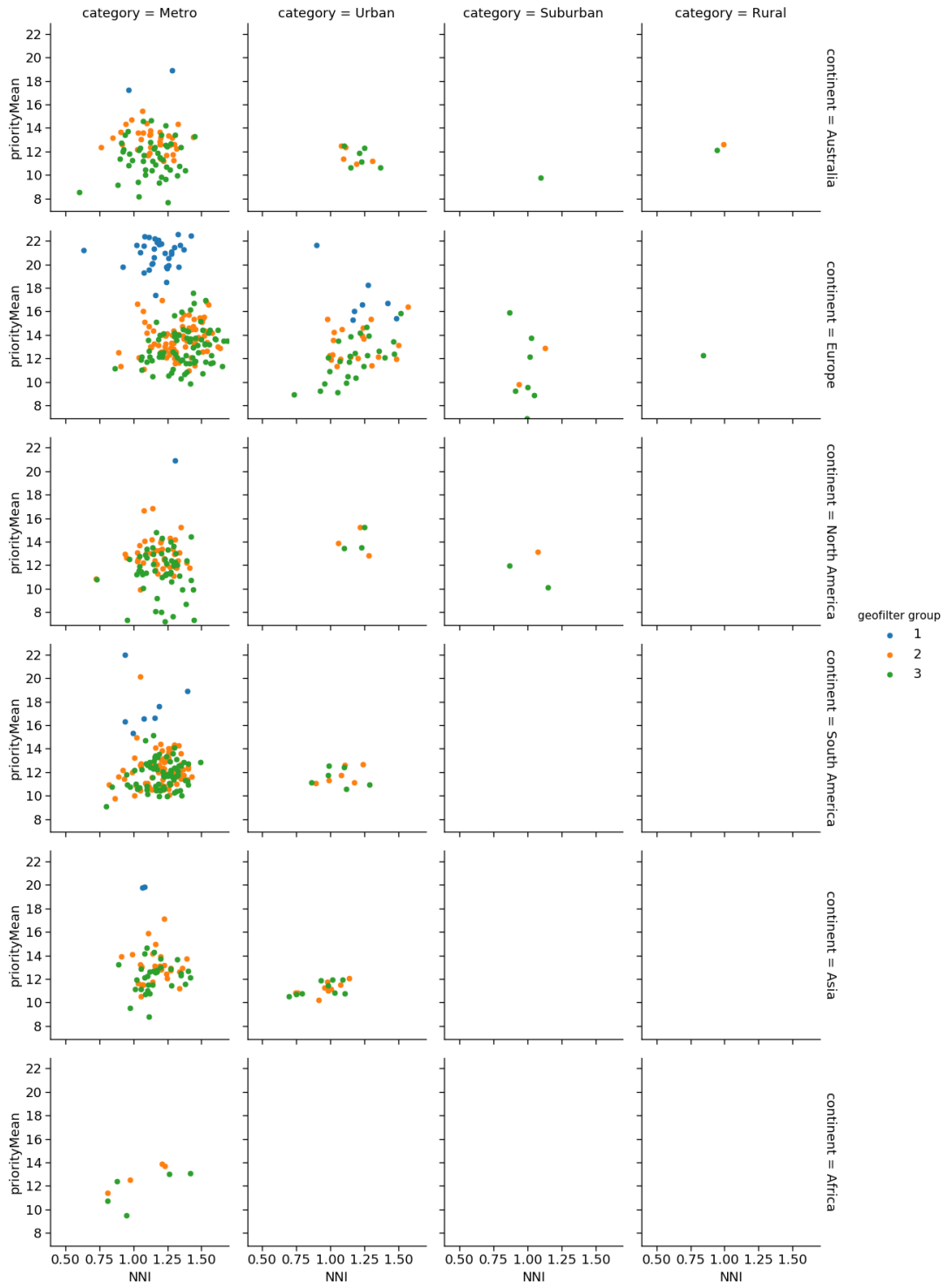

Figure 47: Game area generation quality, split by continent and urban category. Each plot shows the results for all three geofilter groups. Parameters: $p_n = 32$, $p_{c2t} \geqslant 0.9$.

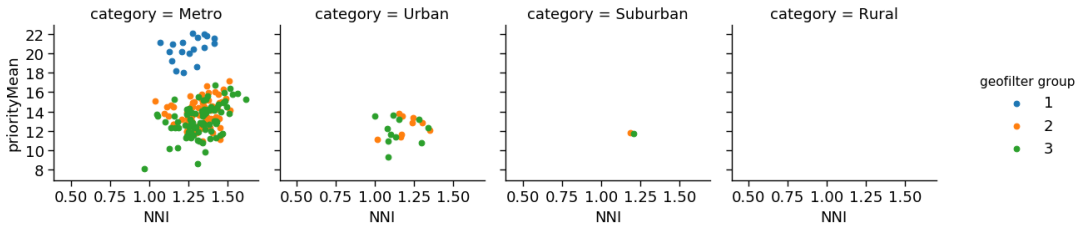

Figure 48: Game area generation quality for merged cells by urban category. Parameters: $p_n = 16$ for 4 cells, $p_{c2t} \geqslant 0.9$, $level = 13$.

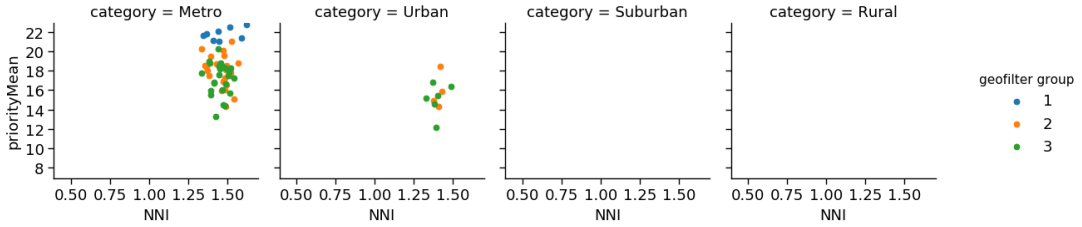

Figure 49: Game area generation quality for merged cells by urban category. Parameters: $p_n = 4$ for 16 cells, $p_{c2t} \geqslant 0.9$, $level = 12$.

with a much higher standard deviation of 0.41. Besides the common interpretation of having a high variance in this metric, it also indicates the metrics instability for small numbers of locations, discussed in Section 3.2.

Merged level 13 cells

For the four cells merged into level 13 cells with $p_n = 16$, shown in Figure 51, the scenario results in at most 64 selected PoIs. The reduced priority values for this scenario are also visible for these merged cells. However, the NNI behaves differently, as it is reduced to a mean value of 1.06. This is a good example of the effects when no p_n threshold is utilized. For the example of one well-distributed area and three areas with low PoI numbers being merged, the process results in a game area with one cluster and three almost unoccupied subareas.

Merged level 12 cells

Only slight improvements are notable for the 16 cells merged into level 12 cells with $p_n = 4$, shown in Figure 52. It results in an NNI value of 1.12, with a standard deviation of 0.32. Since merging 16 game areas together has a higher probability of containing more than one well-distributed area than when merging groups of four areas, the average NNI was expected to be slightly higher. Regardless of this increase, the values show that the generation process should not be utilized without setting a p_{c2t} threshold when quality requirements need to be met.

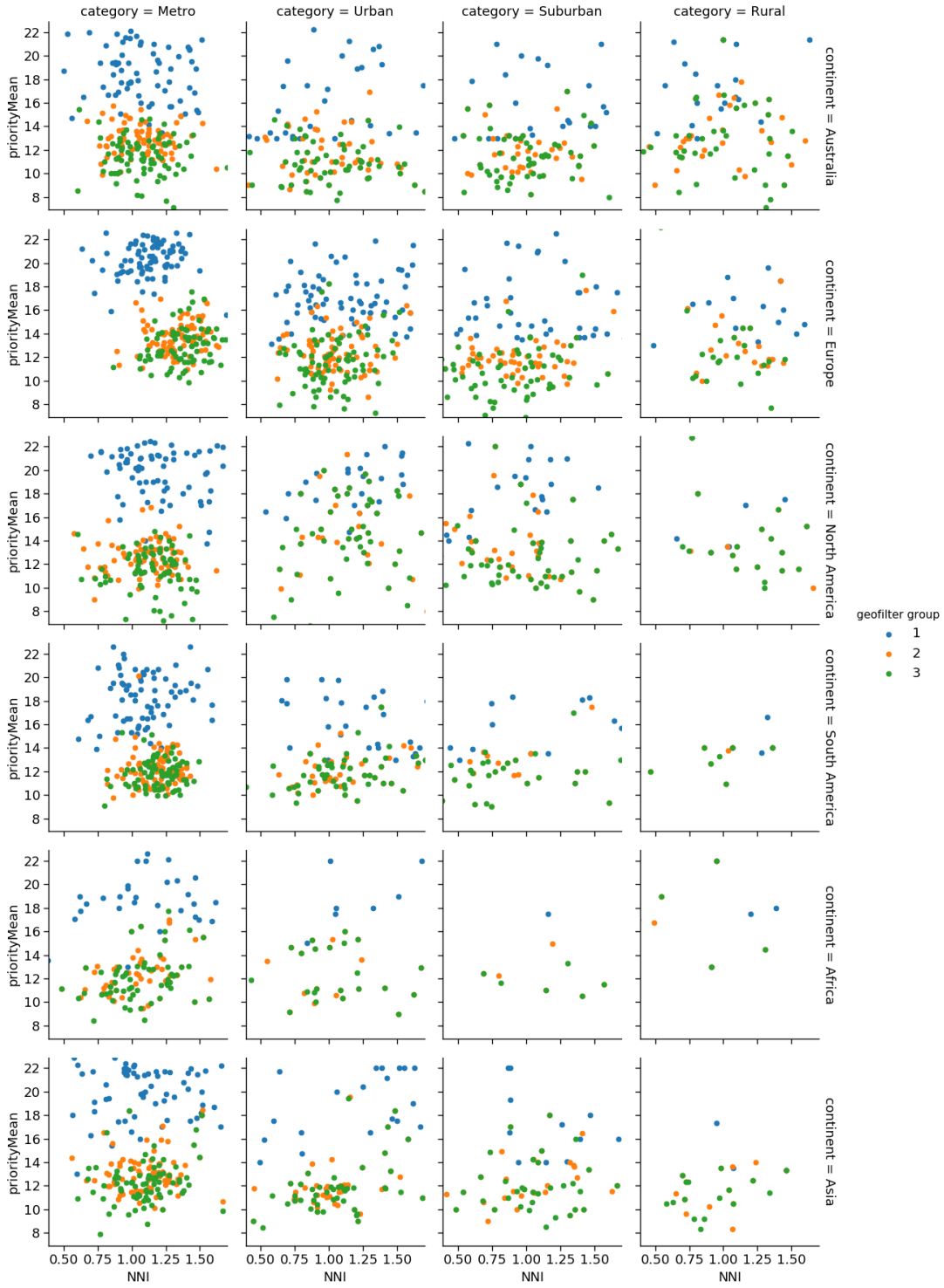

Figure 50: Game area generation quality, split by continent and urban category. Each plot shows the results for all three geofilter groups. Parameters: $p_n = 32$, $p_{c2t} > 0$.

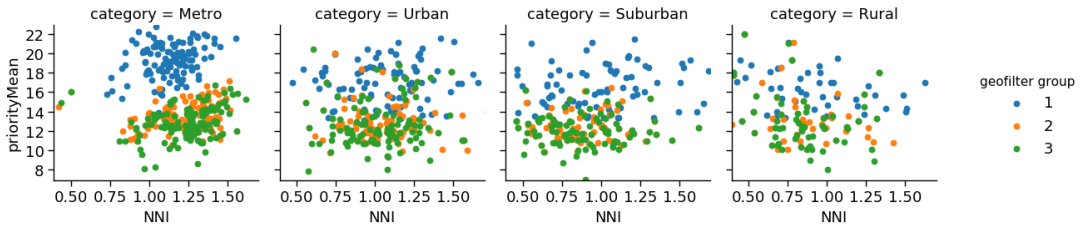

Figure 51: Game area generation quality for merged cells by urban category. Parameters: $p_n = 16$ for 4 cells, $p_{c2t} > 0$, $level = 13$.

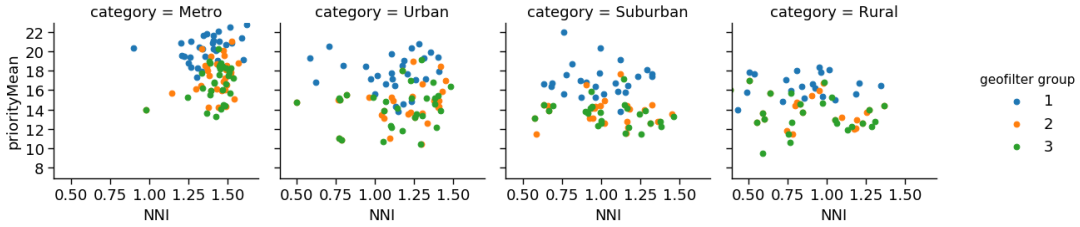

Figure 52: Game area generation quality for merged cells by urban category. Parameters: $p_n = 4$ for 16 cells, $p_{c2t} > 0$, $level = 12$.

A.3 ADDITIONAL INSIGHTS ON COUPLING QUALITY

Our coupling objective function consists of the weighted sum of four individual metrics. In Section 6.2.2, we analyze the individual impact of each metric based on each chosen weighting. Here, we present the detailed data in our evaluation scenario. Since an interdependence of these metrics cannot be ruled out, we analyze each metric within this evaluation scenario with a minimum and a maximum weighting. I. e., we observe each metric's values when it is either ignored during generation or when it is the only relevant metric. The former case depicts the case in which metric values are achieved by chance. Additionally, empirical lower and upper boundaries for each metric can be derived. Each of these plots shows the data for a full focus on the respective metric on the left side, and the ignored metric weighting on the right side.

Individual metric analysis

In the following, we visualize each metric's values with default, minimum, and maximum weighting. These are: distance (Figure 53, 54), distribution (Figure 55, 56), similarity (Figure 57, 58), and relevance (Figure 59, 60).

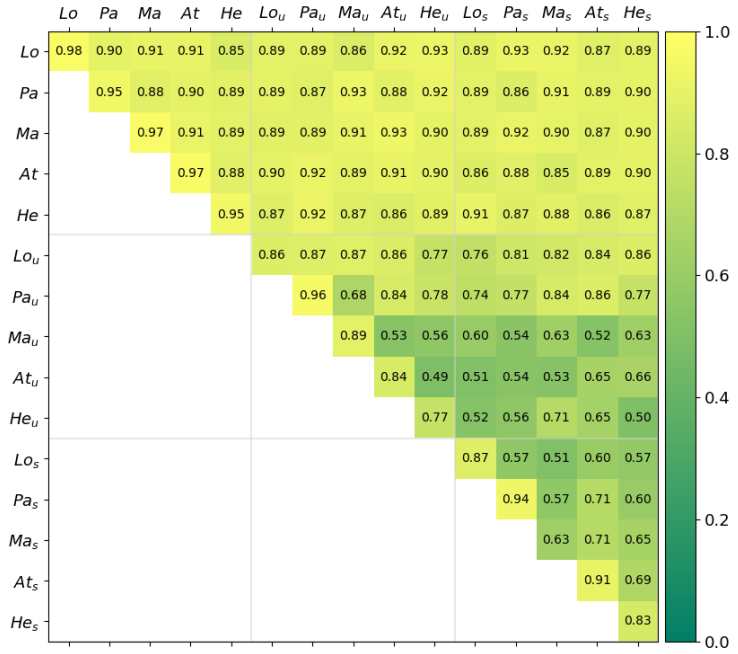

Figure 53: Distance metric values (Dist) with default weighting ($\omega_{\text{Dist}} = 0.35$) for coupled European game areas.

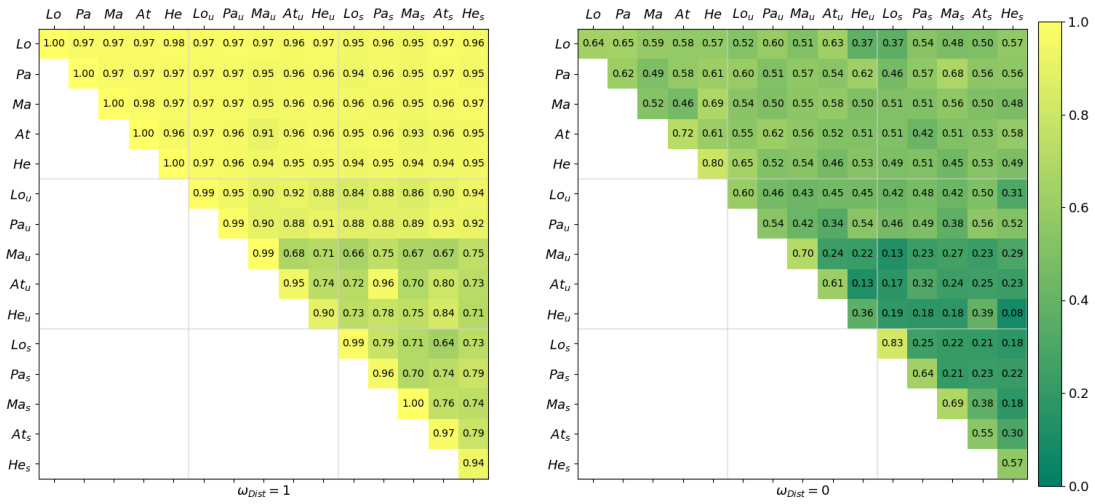

Figure 54: Distance metric value analysis for coupled European game areas.
Left weights: $\omega_{\text{Dist}} = 1$, $\omega_{\text{NNI}} = 0$, $\omega_{\text{Sim}} = 0$, $\omega_{\text{Rel}} = 0$.
Right weights: $\omega_{\text{Dist}} = 0$, $\omega_{\text{NNI}} = \frac{1}{3}$, $\omega_{\text{Sim}} = \frac{1}{3}$, $\omega_{\text{Rel}} = \frac{1}{3}$.

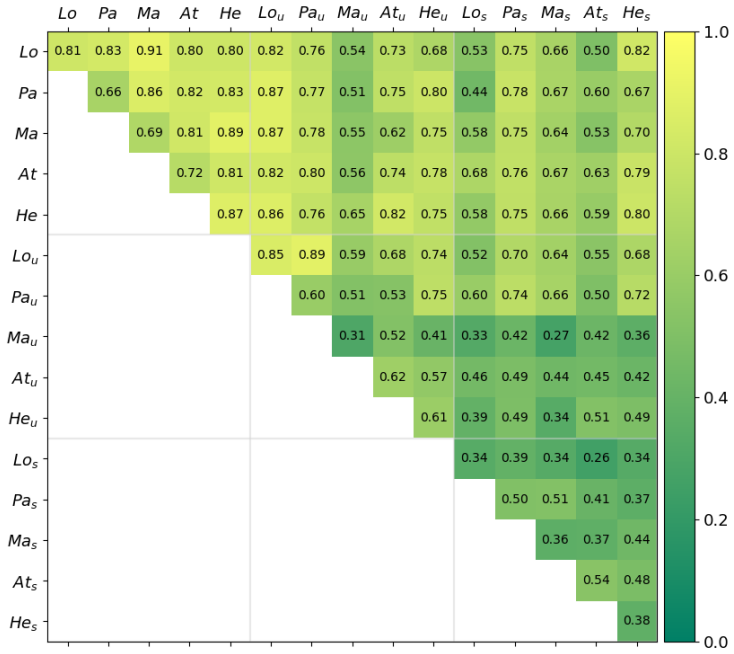

Figure 55: Distribution metric values (NNI) with default weighting ($\omega_{\mathrm{NNI}} = 0.25$) for coupled European game areas.

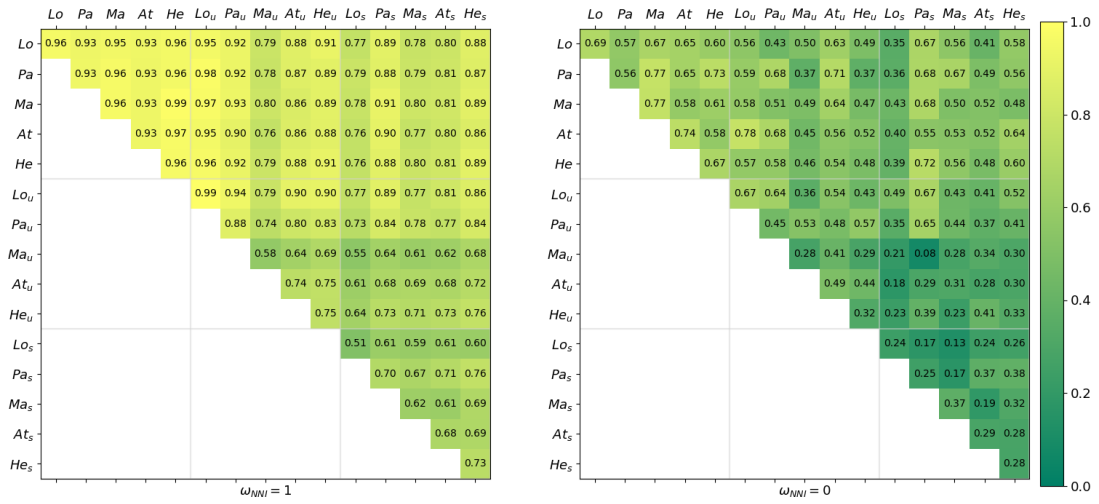

Figure 56: Distribution metric value analysis for coupled European game areas.
Left weights: $\omega_{\mathrm{Dist}} = 0$, $\omega_{\mathrm{NNI}} = 1$, $\omega_{\mathrm{Sim}} = 0$, $\omega_{\mathrm{Rel}} = 0$.
Right weights: $\omega_{\mathrm{Dist}} = \frac{1}{3}$, $\omega_{\mathrm{NNI}} = 0$, $\omega_{\mathrm{Sim}} = \frac{1}{3}$, $\omega_{\mathrm{Rel}} = \frac{1}{3}$.

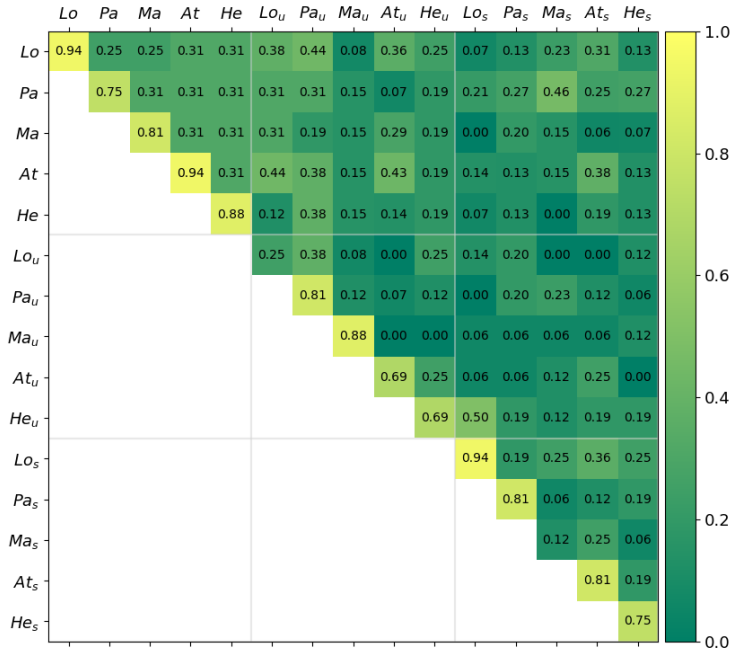

Figure 57: Similarity metric values (Sim) with default weighting ($\omega_{\mathrm{Sim}} = 0.05$) for coupled European game areas.

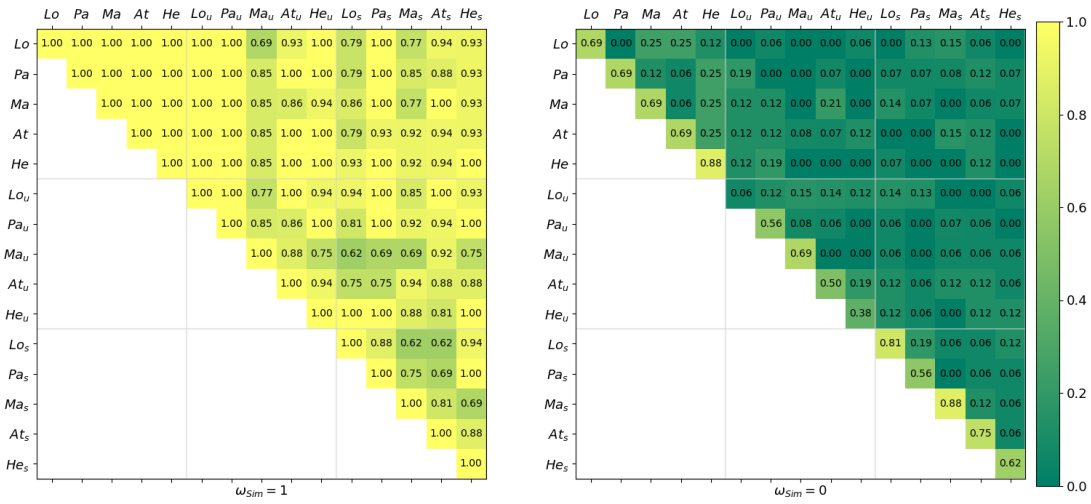

Figure 58: Similarity metric value analysis for coupled European game areas.
Left weights: $\omega_{\mathrm{Dist}} = 0$, $\omega_{\mathrm{NNI}} = 0$, $\omega_{\mathrm{Sim}} = 1$, $\omega_{\mathrm{Rel}} = 0$.
Right weights: $\omega_{\mathrm{Dist}} = \frac{1}{3}$, $\omega_{\mathrm{NNI}} = \frac{1}{3}$, $\omega_{\mathrm{Sim}} = 0$, $\omega_{\mathrm{Rel}} = \frac{1}{3}$.

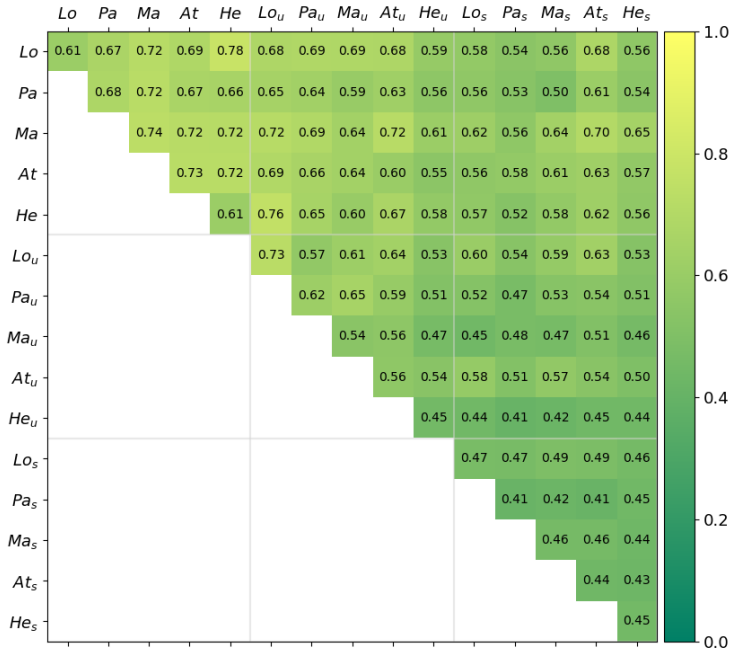

Figure 59: Relevance metric values (Rel) with default weighting ($\omega_{\mathrm{Rel}} = 0.35$) for coupled European game areas.

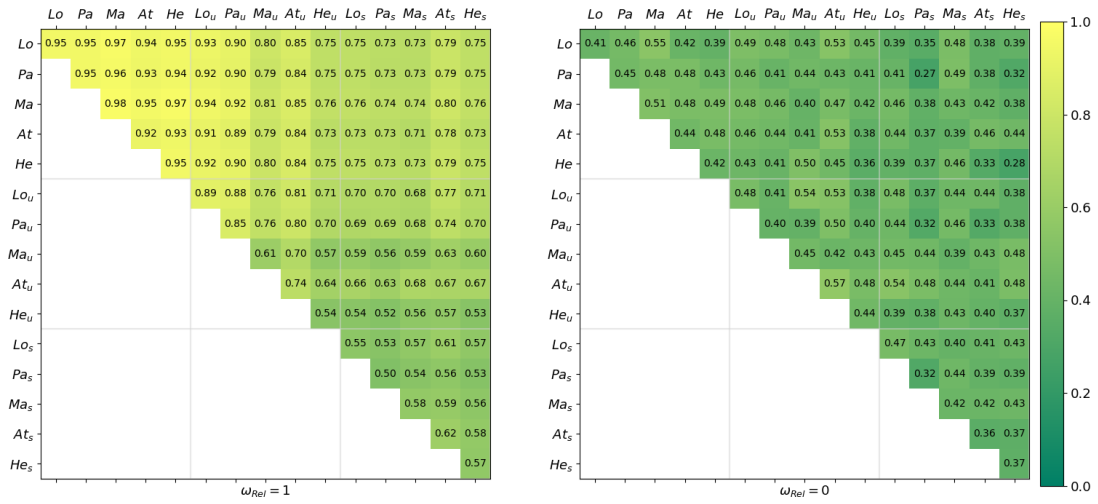

Figure 60: Relevance metric value analysis for coupled European game areas.
Left weights: $\omega_{\mathrm{Dist}} = 0$, $\omega_{\mathrm{NNI}} = 0$, $\omega_{\mathrm{Sim}} = 0$, $\omega_{\mathrm{Rel}} = 1$.
Right weights: $\omega_{\mathrm{Dist}} = \frac{1}{3}$, $\omega_{\mathrm{NNI}} = \frac{1}{3}$, $\omega_{\mathrm{Sim}} = \frac{1}{3}$, $\omega_{\mathrm{Rel}} = 0$.

A.4 EXTENDED STUDY OF ROUTE QUALITY

For a personalized route, besides the start and target location, the player's speed and his route duration can be varied. Since both problem parameters depend on the player's choice during run-time, we vary them based on various expected application scenarios. For the player's speed, shown in Figure 61, these are typical speeds for different activities: slow gait (3km/h), regular gait (5km/h), jogging (10km/h), and biking (20km/h). For the route duration, shown in Figure 62, we select short play sessions of 30 minutes up to extended routes with 4 hours.

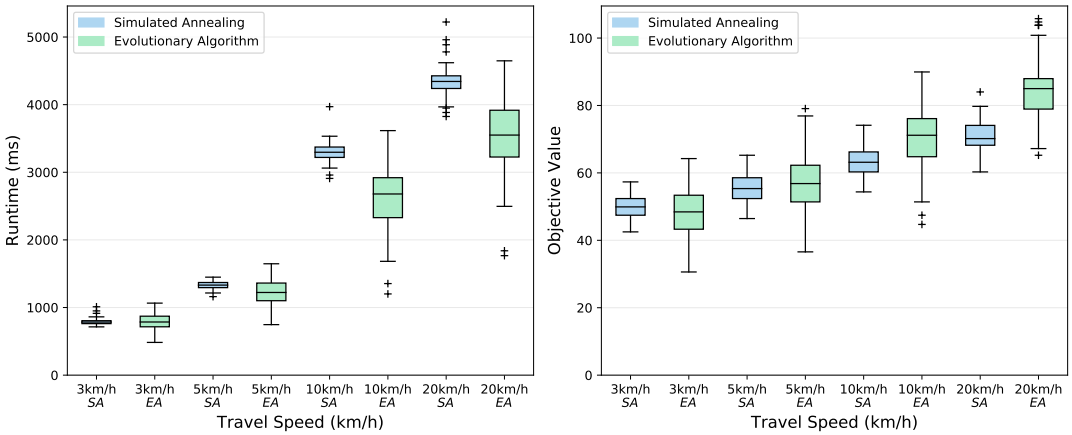

Figure 61: Route performance for different player travel speeds.

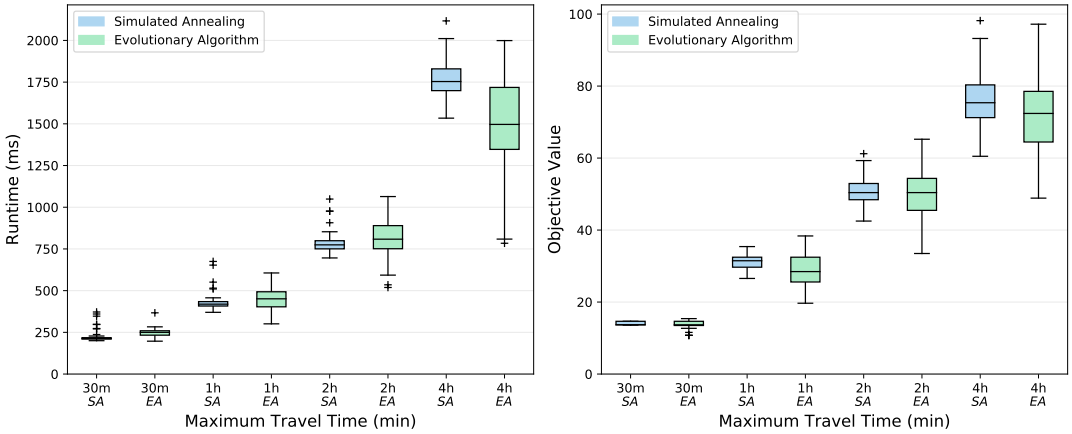

Figure 62: Route performance for different amounts of maximum travel time.

A.4.1 *Route Algorithm Performance*

Both routing algorithms have multiple optimization parameters specific to each algorithm. They are associated with the time, space, or the number of tries an algorithm

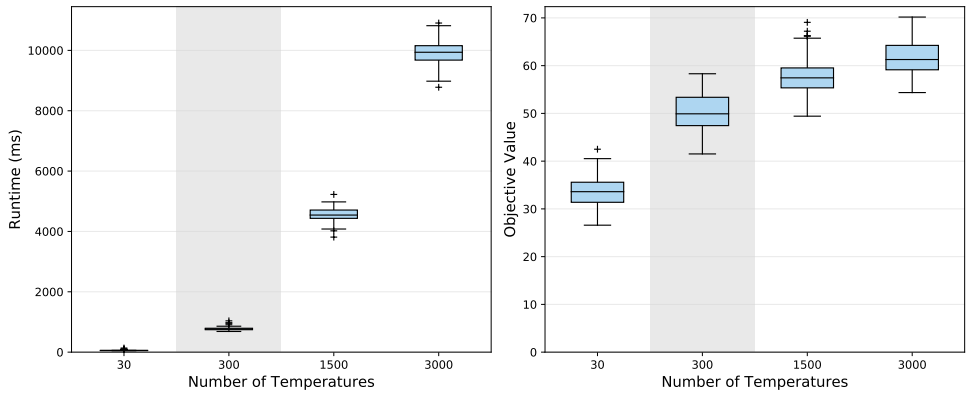

Figure 63: Simulated annealing parameter evaluation for varying the numbers of temperatures. The number of iterations is directly tied to the number of temperatures.

has to optimize its result. They thereby present a trade-off between route quality and the expected route calculation time.

Simulated annealing parameters

For the simulated annealing algorithm, we examine how the route quality correlates with its generation run time when modifying the number of iterations by either changing how often the algorithm is restarted or the number of runs between restarts.

Number of temperatures

Figure 63 shows the algorithm's performance for different numbers of temperatures used. The number of temperatures combined with the number of runs per temperature results in the total number of runs. Thus, the run time scales proportionally to the number of runs. The number of runs per temperature is another potential optimization parameter. We choose to keep it at a constant 120 runs since we observed in early empirical studies that the determining aspect in our scenario is the total number of runs.

With an increasing number of temperatures the run time increases more than linearly. We believe that this is due to longer routes being more likely to be created after more runs. These longer routes have a more expensive neighborhood generation and objective value calculation.

The median route quality increases from 33.6 to 49.9, when going up to 300 temperatures. Further increases for 1,500 temperatures are only 15% and another 7% for 3,000 temperatures. This is expected since an optimal objective value is approached with an increasing number of runs. Given the large increase in median run time for a higher number of temperatures, we select 300 temperatures as our default parameter, generating reasonably close to optimal routes under 1 second.

Number of restarts

Figure 64 shows the algorithm's performance for different numbers of restarts used. Each restart utilized the best previously generated route as a starting point.

The run time scales linearly with the total number of runs with a median run time of 131ms per run. The increase in route quality is visible for a higher number of restarts. The median objective value reaches 52.4 for 9 restarts increasing the objective value by 18% compared to runs without a restart.

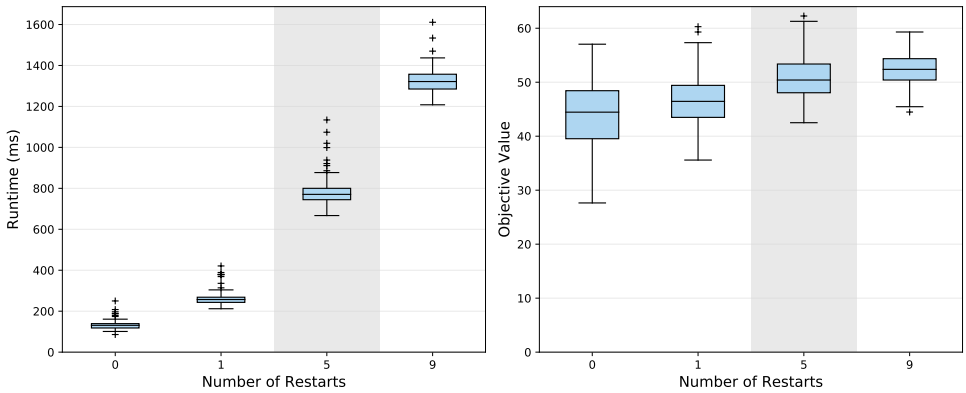

Figure 64: Simulated annealing parameter evaluation for varying the numbers of restarts.

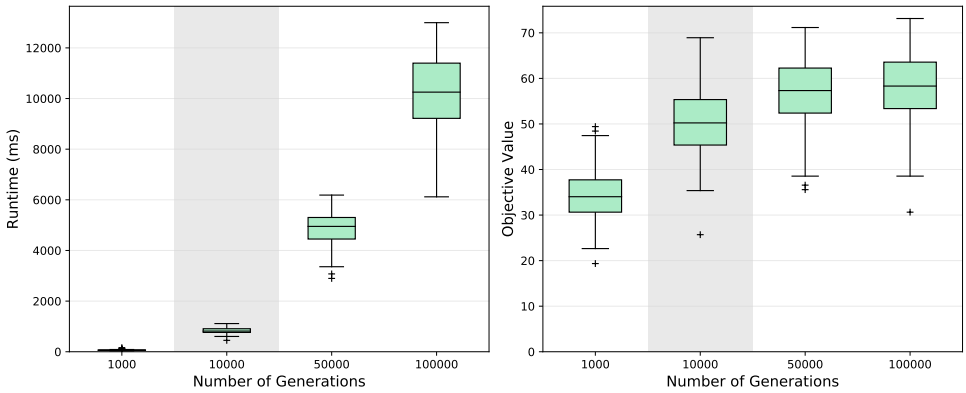

Figure 65: Evolutionary algorithm parameter evaluation for varying numbers of generations. The number of iterations is directly tied to the number of generations.

We select a default value of 5 restarts to still generate routes under 1 second and having a notable increase in objective value compared to 0 or 1 restart. We expect that for each route problem and its associated problem size, an optimal parameter set exists, maximizing the increase in objective value per increasing run time.

Evolutionary algorithm parameters

For the evolutionary algorithm, we examine how the route quality correlates with its generation run time when varying the population parameters of the number of generations, the population size, and the survival rate of each individual.

Figure 65 shows the evolutionary algorithm's performance for varying numbers of generations. This parameter behaves similarly to the number of temperatures in simulated annealing when increasing the parameter by the same factor. Analog to simulated annealing, we choose 10,000 generations, which have a median objective value of 50.2. For the longest run times with 100,000 generations, the evolutionary algorithm performs worse than simulated annealing, while being slightly better for short run times.

Number of generations

Population size

Figure 66 shows the evolutionary algorithm's performance for varying population sizes. The run time increases slightly more than linearly. However, the objective value

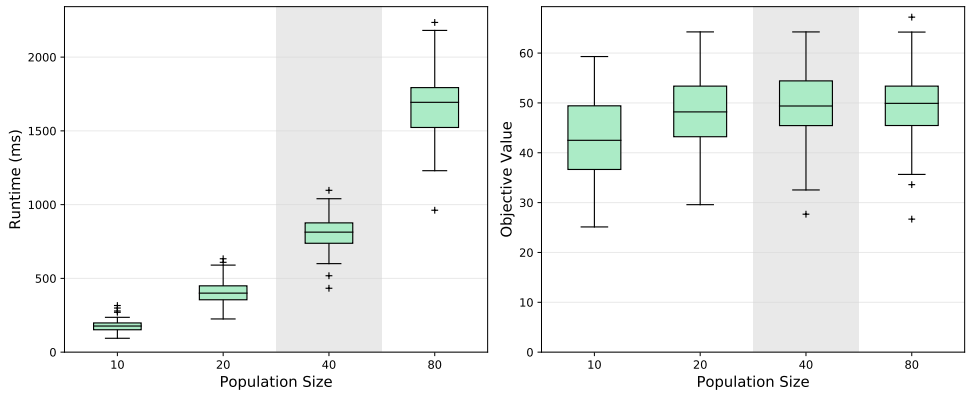

Figure 66: Evolutionary algorithm parameter evaluation for varying population sizes.

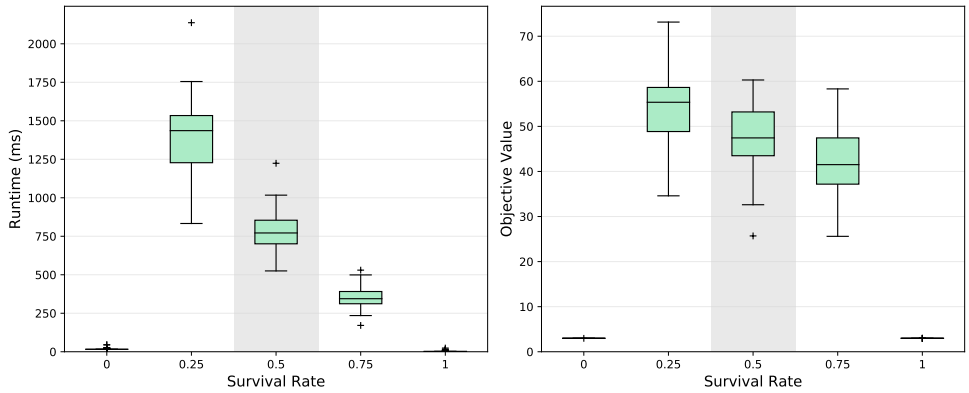

Figure 67: Evolutionary algorithm parameter evaluation for varying survival rates.

does not increase much further beyond a population size of 40, with a median value of 49.4. Therefore, we select the population size of 40 as a default value.

The population size follows a similar trend, like the number of restarts for simulated annealing. Therefore, we expect that there is also an optimal problem-specific parameter set of the number of generations and population size.

Figure 67 shows the evolutionary algorithm's performance for varying survival rates. The survival rate is used to determine the number of individuals surviving a generation, where all dying individuals are replaced by survivors' mutations.

Survival rate

For the survival rates of 0 and 1, respectively, a median objective value of 2.98 is achieved. This is expected behavior because these survival rates mean that routes either do not survive the first generation or routes are never mutated, thus no improvement after the initial random population. For lower survival rates, the neighborhood generation's costs are notable. Between the survival rates of 0.75 to 0.5, we have an increase in median run time by a factor of 2.2 with an increase in median objective value of 14.3%. When going from 0.5 to 0.25, the median run time increase by a factor of 1.9 with an increase in median objective value of 16.7%.

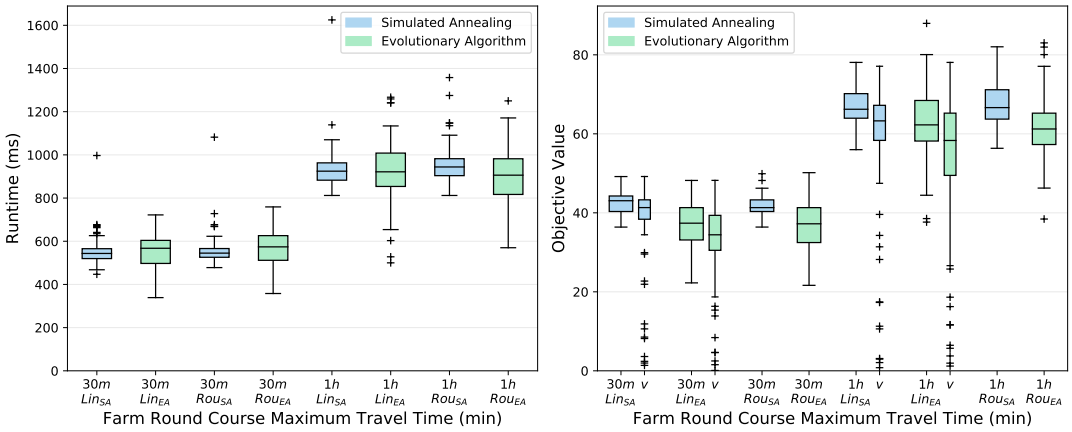

Figure 68: Route performance evaluation for experience players, with a significantly reduced retention time to 5s, leading to less time spent with the game at each spawn point.

A low survival rate yielding the best objective values can be explained by the approach of mutations. Because individuals are not randomly discarded after each generation, but the better routes survive, those routes are also the ones utilized for mutation.

Eventually, we choose a default survival rate of 0.5 as it provides a good trade-off between run time and objective value. However, this parameter could also be optimized according to each individual problem. This results in the evolutionary algorithm having three optimization parameters that could be further optimized depending on the individual problem or the problem size.

A.4.2 *Further Round Course Scenario Evaluation*

Reduced retention time for experienced players

Experienced players in most games tend to optimize their playstyle, achieving goals faster or getting higher scores. In LBGs, primarily affects the retention time at a spawn point, as players require less time to, e. g., catch a Pokémon, continue walking while interacting with the spawn point, or utilize techniques to skip recurring game animations[1].

30% gain in route quality for experienced players

By significantly reducing the retention time to five seconds, we try to model this behavior, leading to more available time traveling to different spawn points. The results in Figure 68 show the round course routes for routes of 30 and 60 minutes. Compared to our basic round course scenario, an expected increase in mean objective value can be observed, with an average median increase of 29% for 30 minutes and 31% for 60 minutes for all approaches.

The highest achieved median objective value for 60-minute routes is 66.63. When assuming an upper bound guess of 70 visited locations, this results in 5 minutes and 50 seconds of retention time, being less than 10% of the total route time.

1 `https://www.reddit.com/r/TheSilphRoad/comments/9f3hcy/a_collection_of_known_fast_catch_methods_and/` (last accessed: August 14, 2020)

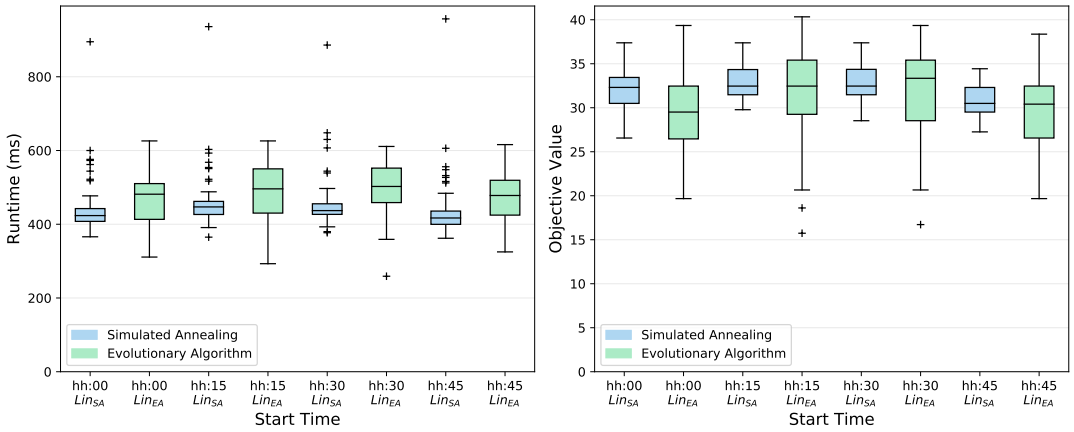

Figure 69: Route performance evaluation varying the start time in 15 minute intervals.

Due to the nature of spawn time windows, the availability of spawn points at a given time varies. In Figure 69 we investigate the impact a start at a different time in an hour has on the generated route. We vary the starting time in quarter-hourly steps with a maximum travel time of one hour, where longer routes would blur the impact this variation might have. The chosen notation of *hh:15* represents all routes starting at an arbitrary hour with 15 minutes in. Since spawn points are active for 30 minutes, we do not expect large variances in route quality.

Analysis of quarter-hourly varied starting times

Interestingly enough, the median objective values of routes starting at *hh:00*, *hh:15*, and *hh:30* are almost identical. For routes starting at *hh:45*, we observed a drop in objective value by up to 6%, indicating that generated routes are worse because narrowly located spawn points are inactive during that time, or profitable clustered locations cannot be reached for that starting time within one hour.

Worse generated routes when starting 45 minutes into an hour

A.5 ADDITIONAL INSIGHTS ON AUTOMATIC MOBILITY DETECTION

A.5.1 *Extended Related Work Overview*

Table 21: Overview of related work of the last decade distinguishing at least two different motorized transportation vehicles. When multiple algorithms were used the selected algorithm is emphasized. Common abbreviations used in this Table are DT (decision trees), RF (random forest), and CV (cross-validation).

work	mobility types	description (**S**ensors, **F**eatures, **M**ethods, **A**lgorithms, **R**emarks)	**F**eature **S**election **A**pproach (-based) **R**un-**T**ime	dataset size (locations)	macro-averaged accuracy (test approach)
Zheng et al. [272, 273] (2008, 2010)	walk, bike, car, bus	**S:** GPS (standalone) **A:** DT & post-processing **R:** no resampling or class balancing	**FS:** ✓ **A:** trip **RT:** ✗	2,000h (different cities)	75% (test dataset)
Wang et al. [252] (2010)	stand, walk, bike, car, bus, subway	**S:** accelerometer (35 Hz) **F:** 23 features (statistical features, frequency feature in [0 Hz, 4 Hz], peak-detection **M:** 8s sliding window, no overlap **A:** **J48 DT**, k-NN, SVM **R:** no resampling or class balancing with high ratio of walk data	**FS:** ✓ **A:** window **RT:** ✗	12h (Peking, CHN)	71% (10-fold CV)
Stenneth et al. [229] (2011)	stand, walk, bike, car, bus, train	**S:** GPS + external GIS data **F:** 8 features (GPS accuracy, speed, heading, acceleration; distance to nearest bus or train) **M:** 30s sliding window **A:** RF	**FS:** ✓ **A:** window **RT:** ✓ (server)	6h (Chicago, USA)	93% (10-fold CV)
Bolbol et al. [28] (2012)	walk, bike, car, bus, train, subway	**S:** GPS (0.016 Hz) **F:** speed & acceleration **A:** SVM	**FS:** ✓ **A:** trip **RT:** ✗	k.A. (London, GBR)	74% (n/a)
Hemminki et al. [108] (2013)	stand, walk, car, bus, tram, metro, train	**S:** accelerometer (60 Hz to 100 Hz) **F:** 78 features of time- and frequency-domain (FFT-coefficients with 2, 3, and 5 Hz) **M:** 3 classifiers (stationary, kinematic motion, motorized) 1.2s sliding window von 1.2s, 50% overlap **A:** AdaBoosted DT **R:** no resampling or class balancing	**FS:** ✗ **A:** mixed **RT:** n/a	150h (multiple)	82% (leave-one-out CV)
Brunauer et al. [32] (2013)	walk, bike, car, bus, train	**S:** GPS **F:** 54 Features **A:** multilayer perceptron, logistic Model Trees, C4.5	**FS:** ✓ **A:** trip **RT:** ✗	322h (DEU, AUT, CHE)	93% (5-fold CV)
Jahangiri and Rakha [126] (2015)	walk, run, bike, car, bus	**S:** accelerometer, gyroscope (both 25 Hz) **F:** 165 features of time- and frequency-domain, 80 selected **M:** 1s sliding window **A:** k-NN, SVM, SVM ensemble, DT, Bagging, **RF**	**FS:** ✓ **A:** window **RT:** ✗	25h (Virginia, USA)	94% (5-fold CV)
Lari and Golroo [153] (2015)	walk, car, bus	**S:** GPS **F:** 6 features (with GPS-accuracy) **A:** RF **R:** no resampling or class balancing	**FS:** ✗ **A:** trip **RT:** ✗	n/a (Teheran, IRN)	91% (test dataset)
Montoya et al. [183] (2015)	stand, walk, bike, car, bus, tram, train	**S:** GPS (1 Hz), accelerometer (20 Hz), Wi-Fi, Bluetooth, OSM data & public transport schedule **A:** bayesian net **R:** evaluation on training data	**FS:** ✗ **A:** trip **RT:** ✗	43h (Paris, FRA)	86% (training dataset)
Fang et al. [68] (2016)	stand, walk, run, bike, motorbike, car, bus, metro, train, high-speed rail	**S:** accelerometer, gyroscope, magenetometer **F**: 14 features (1 in time- and 13 in frequency-domain) **M:** 17.06s sliding window, 75% overlap two-step approach (non-motorized vs. motorized; then detailed motorized distinction) **A:** **SVM** (first step), **k-NN** (second step), DT	**FS:** ✗ **A:** window **RT:** ✗	20% of HTC-dataset [268] ≈ 1,600h	93% (first step) 81% (second step) (test dataset)

work	mobility types	description (**S**ensors, **F**eatures, **M**ethods, **A**lgorithms, **R**emarks)	**F**eature **S**election **A**pproach (-based) **R**un-**T**ime	dataset size (locations)	macro-averaged accuracy (test approach)
Shafique and Hato [220] (2016)	walk, bike, car, bus, train, subway	**S:** accelerometer, gyroscope (both 10 Hz) **F:** 9 features in time-domain (i. a.: pitch, roll, skewness, kurtosis) **M:** 10min sliding window **A:** RF (100 trees) **R:** no resampling or class balancing with high ratio (71%) of walk data	**FS:** ✗ **A:** trip **RT:** ✗	203h (Kobe, JPN)	99.89% (test dataset)
Zhou et al. [275] (2017)	walk, bike, e-bike, car, bus, subway	**S:** GPS **F:** 24 features (speed, acceleration, heading) **A:** RF **R:** skip closest 10 data points to activity transitions	**FS:** ✗ **A:** trip **RT:** ✗	3593 segments (Shanghai, CHN)	92% (test dataset)
Wang et al. [250] (2017)	walk, bike, e-bike, car, bus	**S:** GPS & socio-economic data (possession of ticket, bikes, or cars in household) **A:** **RF**, SVM, artifical neural network	**FS:** ✓ **A:** trip **RT:** ✗	2740 segments (Shanghai, CHN)	81% (test dataset)
Güvensan et al. [96] (2018)	stand, walk, car, bus, tram, train, metro, ferry	**S:** accelerometer, gyroscope, magnetometer (all 100 Hz) **F:** 348 features: 29 features in time-domain for each of 12 sensor axes **M:** 60s sliding window, 40% Overlap post-processing with "healing" algorithm for correction **A:** **RF**, J48, k-NN, Naïve Bayes **R:** no resampling or class balancing, feature selection discarded due to bad results	**FS:** ✗ **A:** mixed **RT:** ✓	49h (Istanbul, TUR)	79% (window) 94% (trip-based) (test dataset)
Lu et al. [168] (2018)	walk, bike, motorbike, car, bus	**S:** accelerometer (50 Hz) **M:** 5s / 6s sliding window, 75% overlap **F:** 27 features (23 in time- and 4 in frequency-domain) **A:** **RF**, Naïve Bayes, J48, SVM, k-NN **R:** no resampling or class balancing	**FS:** ✓ **A:** window **RT:** ✗	32h one city	98% (10-fold CV)
Coroamă et al. [47] (2019)	walk, bike, car, bus, tram, train	**S:** GPS, accelerometer, Bluetooth, Wi-Fi **F:** 28 GPS features, 16 accelerometer features, 28 vicinity Bluetooth features, 15 vicinity Wi-Fi features **M:** 10s and 120s sliding windows **A:** RF **R:** low accuracy of *bus* (67.5%)	**FS:** ✗ **A:** trip **RT:** ✗	153h (Zürich, CHE)	87% (test dataset)
Aşçı and Güvensan [13] (2019)	stand, walk, run, bike, motorbike, car, bus, metro, train, high-speed rail	**S:** accelerometer, gyroscope, magnetometer (all 100 Hz) **F:** 252 features: 15 features in time- and 6 features in frequency-domain (i. a.: spectral roll-off, spectral flatness, kurtosis, skewness) for each of 12 sensor axes **M:** 12s window, no overlap **A:** long short-term memory (LSTM)	**FS:** ✗ **A:** window **RT:** ✗	HTC-dataset [268]	97% (training or test dataset)

A.5.2 *Mobility Detection Features*

In the following we provide an overview over all employed features for mobility detection. The features are divided as follows: statistical features in Table 22, time- and frequency-domain acceleration features in Table 23, location features in Table 24, OSM-based features in Table 25, and meta-classifier features in Table 26.

Table 22: Developed statistical features based on `acceleration`, `speed`, and `accuracy`.

feature	feature name		
	acceleration	speed	accuracy
minimum	`acceMin`	`speedMin`	`accuMin`
maximum	`acceMax`	`speedMax`	`accuMax`
arithmetic mean	`acceMean`	`speedMean`	`accuMean`
25% quantile (1st quartile)	`acce25`	`speed25`	`accu25`
50% quantile (2nd quartile / median)	`acce50`	`speed50`	`accu50`
75% quantile (3rd quartile)	`acce75`	`speed75`	`accu75`
95% quantile	`acce95`	`speed95`	`accu95`
measures of dispersion			
variance	`acceVar`	`speedVar`	`accuVar`
range (difference between min and max)	`acceRange`	`speedRange`	`accuRange`
difference between min and 95% quantile	`acceRangeTo95`	`speedRangeTo95`	`accuRangeTo95`
interquartile range	`acceRange25To75`	`speedRange25To75`	`accuRange25To75`

Table 23: Developed `acceleration` features in the time- and frequency-domain.

feature name	feature description
time-domain features	
`acceRMS`	root mean squared
`acceNormEnergy`	squared quadratic mean
`acceMCR`	mean-crossing rate
`acceZCR`	zero-crossing rate
`acceSlopeSignChangeRate`	derivation of zero-crossing rate
`acceSkewness`	skewness
`acceKurtosis`	kurtosis
frequency-domain features	
`acce1To3Hz`	frequency band with $1\text{Hz} < f \leqslant 3\text{Hz}$
`acce3To8Hz`	frequency band with $3\text{Hz} < f \leqslant 8\text{Hz}$
`acce5To8Hz`	frequency band with $5\text{Hz} < f \leqslant 8\text{Hz}$
`acce8To10Hz`	frequency band with $8\text{Hz} < f \leqslant 10\text{Hz}$
`acce10To14Hz`	frequency band with $10\text{Hz} < f \leqslant 14\text{Hz}$
`acce14To20Hz`	frequency band with $14\text{Hz} < f \leqslant 20\text{Hz}$
`acce20To22Hz`	frequency band with $20\text{Hz} < f \leqslant 22\text{Hz}$
`acce22To25Hz`	frequency band with $22\text{Hz} < f \leqslant 25\text{Hz}$
`acce25To30Hz`	frequency band with $25\text{Hz} < f \leqslant 30\text{Hz}$
`spectralNormEnergy`	normalized spectral energy
`spectralCentroidHz`	centroid of frequency spectrum
`spectralSpreadHz`	width of frequency spectrum
`spectralFlatness`	noisiness of frequency spectrum
`spectralCrest`	spectral crest factor
`spectralRollOffHz`	cut-off frequency between high and low frequency bands
`spectralKurtosis`	spectral kurtosis
`spectralSkewness`	spectral skewness

Table 24: Developed location sensor-based distance and `speed` features.

feature name	feature
`travelDistance`	distance between a frame's first and last position
`travelDistanceAcc`	accumulated distance between consecutive positions
`travelDistanceMax`	maximum distance of consecutive positions
`speedPointRatioStationary`	ratio of `speed` values $< 0.1\text{m/s}$
`speedPointRatioLow`	ratio of `speed` values $< 3\text{m/s}$
`speedPointRatioMedium`	ratio of `speed` values $\geqslant 4\text{m/s}$
`speedPointRatioHigh`	ratio of `speed` values $\geqslant 10\text{m/s}$
`headingVar`	accumulated change in heading

Table 25: Developed external data features based on OSM data.

feature name	feature
`stopsTrafficSig` `stopsTrafficSigLong`	number of stops at OSM nodes with tag `'highway' = 'traffic_signals'`
`stopsPubTransportStop` `stopsPubTransportStopLong`	number of stops at OSM nodes with tag `'public_transport' = 'stop_position'`
`stopsBusStop`, `stopsBusStopLong`, `stopsTramStop`, `stopsTramStopLong`, `stopsTrainStop`, `stopsTrainStopLong`	similar `stopsPubTransportStop` with the additional tag of either `'bus' = 'yes'`, `'tram' = 'yes'`, or `'train' = 'yes'`
`stopsExclBusStop`, `stopsExclBusStopLong`, `stopsExclTramStop`, `stopsExclTramStopLong`, `stopsExclTrainStop`, `stopsExclTrainStopLong`	similar to the respective stop features, with the additional restriction of the OSM node being an exclusive station for the respective movement type
`distanceBus`, `distanceTram`, `distanceTrain`	smallest one-sided Hausdorff distance for the respective movement type for all nearby public transport routes

Table 26: Overview of meta-classifier features.

feature name	feature
`predS`, `predM`, `predL`	frame classifier prediction for `short`, `medium` and `long`
`prevPredS`, `prevPredM`, `prevPredL`	previous frame classifier's prediction
`scoreS`, `scoreM`, `scoreL`	measure of reliability of each frame classifier's prediction
`prevScoreS`, `prevScoreM`, `prevScoreL`	previous frame classifier's score

A.5.3 *Extended Study of Mobility Detection Quality*

S2 level parameter

The S2 level parameter variation shows no substantial impact on the overall result, as shown in Table 27. We believe this is because we use the information of all eight neighboring S2 cells. Thus, the covered area is large enough for all features.

Looking at the results in Table 27, for the setup with the shorter frame durations in detail, the only difference is the detection of *bus*. For this type of transport, an S2 level of 13, i. e., a larger cell size containing more information, seems better. For the evaluation setup with larger frame durations , the only substantial difference exists for *tram*, where larger cells perform slightly better.

The differences in accuracy between the two cell sizes are hardly measureable and can also be cause by the random component of the random forest application. In terms of OSM data requirement, however, a detrimental difference between the two cell sizes can be found. For larger cells (`s2Level = 13`) the processing time required for pre-processing and meta-pre-processing increases by 50% compared to the smaller cells (`s2Level = 14`) in our evaluation setup.

Table 27: Evaluation results for `s2Level`. Parameters: T_S, T_M, and T_L defined in Table, `cutoffDistance = 1000m`, `maxStopSpeed = 0.5 m/s`, `minDurationLongStop = 8s`, and `stopRadius = 20m`.

`s2Level`	accuracy			F1 scores of meta-classifier						
	meta	`medium`	`long`	stand	walk	bike	car	bus	tram	train
$T_S = 5s$, $T_M = 20s$, $T_L = 90s$										
13 (large cells)	98.8%	99.0%	99.7%	97.9%	99.5%	99.5%	97.9%	97.8%	99.4%	99.1%
14 (small cells)	98.9%	99.0 %	99.7%	98.0%	99.5%	99.6%	98.1%	**98.3%**	99.5%	99.2%
$T_S = 5s$, $T_M = 45s$, $T_L = 300s$										
13 (large cells)	98.7%	99.6%	99.9%	97.8%	99.6%	99.5%	97.8%	97.8%	**99.2%**	98.9%
14 (small cells)	98.6%	99.6%	99.9%	97.9%	99.5%	99.5%	97.6%	97.7%	98.8%	98.9%

Cutoff distance parameter

The `cutoffDistance` parameter also shows no substantial impact on the overall system during variation. A small value risks ignoring routes that are considered to be too far away only due to location sensor inaccuracies mostly prevalent in trains. A large value, on the other hand, has the disadvantage of longer processing times. According to our

evaluation results shown in Table 28, for the shorter frame lengths an initial distance of `600m` provides the highest accuracy of the entire system. For the longer frames a trajectory distance of `800m` performs better, although the differences between the individual distances are slightly larger than for the shorter frame lengths. Especially public transport benefits from the shorter initial distance. Since very good results are achieved for both scenarios with `cutoffDistance = 800m`, we choose this value.

Table 28: Evaluation results for `cutoffDistance`. Parameters: T_S, T_M, and T_L defined in Table, `s2Level = 14`, `maxStopSpeed = 0.5 m/s`, `minDurationLongStop = 8s`, and `stopRadius = 20m`.

`cutoff Distance`	accuracy			F1 scores of meta-classifier						
	meta	`medium`	`long`	stand	walk	bike	car	bus	tram	train
$T_S = 5s$, $T_M = 20s$, $T_L = 90s$										
600m	98.90%	98.9%	99.8%	98.0%	99.6%	99.6%	98.3%	98.3%	99.2%	99.4%
800m	98.88%	99.0%	99.7%	98.0%	99.6%	99.6%	98.1%	98.2%	99.4%	99.3%
1000m	98.88%	99.0%	99.7%	98.0%	99.5%	99.6%	98.1%	98.3%	99.5%	99.2%
1200m	98.89%	99.0%	99.7%	98.0%	99.6%	99.5%	98.2%	98.3%	99.4%	99.3%
$T_S = 5s$, $T_M = 45s$, $T_L = 300s$										
600m	98.58%	99,5%	99.5%	97.9%	99.5%	99.5%	97.6%	97.7%	98.9%	99.0%
800m	98.69%	99.6%	99.9%	98.0%	99.6%	99.5%	97.7%	98.1%	99.0%	99.0%
1000m	98.55%	99.6%	99.9%	97.9%	99.5%	99.5%	97.6%	97.7%	98.8%	98.9%
1200m	98.56%	99.7%	99.9%	97.9%	99.5%	99.5%	97.8%	97.7%	98.8%	98.7%

Stop speed parameter

The stop-based features are calculated exclusively in the `long` frame. The `maxStopSpeed` parameter determines the maximum location sensor `speed` value that is treated as a stop. This is required to compensate for potential location sensor inaccuracies and sensor drift. According to our evaluation results shown in Table 29 for both evaluated scenarios a speed threshold of $0.5m/s$ achieves the best results. Similar to the previous parameter, the differences are small but consistent.

Stop radius parameter

The `stopRadius` parameter determines the range up to which nearby public transport stations, lines, or traffic signals are assigned to a stop event. In our evaluation scenario shown in Table 30, 20 meters turned out to be an optimal value by a small margin. Thereby, recorded stops can have a distance of 20 meters to a station or traffic signal, and still be allocated to it. This parameter can compensate for a public transport station's length, vehicle length (especially crucial for trains), and location sensor inaccuracies.

Table 29: Evaluation results for `maxStopSpeed` highlighting the selected parameter value. Parameters: T_S, T_M, and T_L defined in Table, `s2Level = 14`, `cutoffDistance = 800m`, `minDurationLongStop = 8s` and `stopRadius = 20m`.

`maxStopSpeed`	accuracy		F1 scores of meta-classifier						
	meta	`long`	stand	walk	bike	car	bus	tram	train
$T_S = 5s$, $T_M = 20s$, $T_L = 90s$									
0.3 m/s	98.72%	99.7%	97.7%	99.3%	99.4%	98.0%	97.9%	99.3%	99.3%
0.5 m/s	98.88%	99.7%	98.0%	99.6%	99.6%	98.1%	98.2%	99.4%	99.3%
0.7 m/s	98.75%	99.7%	97.8%	99.5%	99.5%	98.0%	98.0%	99.2%	99.1%
0.9 m/s	98.82%	99.8%	97.7%	99.5%	99.5%	98.2%	98.1%	99.3%	99.3%
$T_S = 5s$, $T_M = 45s$, $T_L = 300s$									
0.3 m/s	98.67%	99.9%	97.9%	99.5%	99.4%	97.8%	98.0%	99.1%	98.9%
0.5 m/s	98.69%	99.9%	98.0%	99.6%	99.5%	97.7%	98.1%	99.0%	99.0%
0.7 m/s	98.53%	99.9%	97.6%	99.5%	99.5%	97.9%	97.6%	98.9%	98.7%
0.9 m/s	98.59%	99.9%	97.7%	99.6%	99.5%	98.0%	97.8%	98.9%	98.7%

Table 30: Evaluation results for `stopRadius`. Parameters: T_S, T_M, and T_L defined in Table, `s2Level = 14`, `cutoffDistance = 800m`, `maxStopSpeed = 0.5 m/s`, and `minDurationLongStop = 8s`.

`stopRadius`	accuracy		F1 scores of meta-classifier						
	meta	`long`	stand	walk	bike	car	bus	tram	train
$T_S = 5s$, $T_M = 20s$, $T_L = 90s$									
15m	98.12%	99.78%	97.4%	99.6%	99.2%	96.8%	97.1%	98.6%	98.2%
20m	98.12%	99.77%	97.4%	99.6%	99.2%	96.7%	97.0%	98.8%	98.2%
25m	98.08%	99.77%	97.3%	99.5%	99.2%	96.6%	96.9%	98.8%	98.1%
30m	98.08%	99.76%	97.1%	99.6%	99.2%	96.7%	97.1%	98.8%	98.1%
40m	98.04%	99.76%	97.3%	99.5%	99.2%	96.6%	96.3%	98.7%	98.0%
$T_S = 5s$, $T_M = 45s$, $T_L = 300s$									
15m	97.71%	99.92%	97.0%	99.4%	99.0%	96.3%	96.3%	98.0%	97.8%
20m	97.73%	99.95%	97.0%	99.4%	99.0%	96.4%	96.3%	98.2%	97.8%
25m	97.69%	99.87%	96.9%	99.5%	99.1%	96.2%	96.2%	98.1%	97.7%
30m	97.69%	99.92%	97.0%	99.5%	99.0%	96.2%	96.1%	98.1%	97.8%
40m	97.65%	99.85%	96.9%	99.4%	98.9%	96.3%	96.3%	98.0%	97.7%

Feature selection

Tables 31-33 show the detailed feature selection results for each of the three frame classifiers. We select the feature selection approach based on the trade-off between feature count and frame classifier accuracy. Since our goal is to reduce the number of features required to identify particularly important features for each mobility type and its frame length, we accept slightly lower accuracies for largely reduced feature counts.

Table 31: Evaluation results for feature selection in `short` frame classifier, indicating selected feature count and frame classifier accuracy.

`short` feature selection	feature count	accuracy `short`	F1 scores of meta-classifier						
			stand	walk	bike	car	bus	tram	train
Random Forest with I = 30									
Baseline	65	97.60%	98.6%	99.7%	98.8%	94.4%	95.1%	98.6%	97.9%
Evolutionary Search	32	97.43%	98.6%	99.6%	98.7%	94.0%	94.7%	98.3%	98.0%
Genetic Search	32	97.59%	98.6%	99.7%	98.8%	94.5%	95.1%	98.5%	98.0%
Best First	25	97.53%	98.5%	99.7%	98.7%	94.3%	95.1%	98.5%	97.9%
AdaBoostM1 with I = 15 and J48									
Genetic Search	32	97.66%	98.7%	99.7%	99.1%	94.7%	95.1%	98.4%	98.0%
Best First	25	97.55%	98.6%	99.7%	98.9%	94.4%	94.8%	98.3%	98.1%

Table 32: Evaluation results for feature selection in `medium` frame classifier, indicating selected feature count and frame classifier accuracy.

`medium` feature selection	feature count	accuracy `medium`	F1 scores of meta-classifier						
			stand	walk	bike	car	bus	tram	train
Random Forest with I = 30									
Baseline	136	98.77%	99.6%	99.9%	99.5%	96.5%	97.1%	99.8%	99.1%
Evolutionary Search	65	98.83%	99.5%	99.9%	99.4%	96.8%	97.4%	99.8%	99.0%
Genetic Search	48	98.62%	99.6%	99.9%	99.4%	96.0%	96.7%	99.8%	98.9%
Best First	29	98.77%	99.6%	99.9%	99.3%	96.5%	97.3%	99.9%	99.0%
AdaBoostM1 with I = 15 and J48									
Genetic Search	48	98.89%	99.7%	99.9%	99.5%	96.8%	97.3%	99.7%	99.3%
Best First	29	98.89%	99.6%	99.9%	99.5%	97.0%	97.5%	99.7%	99.1%

Table 33: Evaluation results for feature selection in `long` frame classifier, indicating selected feature count and frame classifier accuracy.

`long` feature selection	feature count	accuracy `long`	F1 scores of meta-classifier						
			stand	walk	bike	car	bus	tram	train
Random Forest with $I = 30$									
Baseline	180	99.79%	100%	100%	100%	99.5%	99.4%	99.9%	99.8%
Evolutionary Search	84	99.76%	100%	100%	100%	99.4%	99.4%	99.8%	99.8%
Genetic Search	53	99.67%	100%	100%	100%	99.1%	99.1%	99.8%	99.8%
Best First	29	99.73%	99.9%	100%	100%	99.3%	99.3%	99.9%	99.7%
AdaBoostM1 with $I = 15$ and J48									
Genetic Search	53	99.76%	99.9%	100%	100%	99.3%	99.2%	99.9%	99.7%
Best First	29	99.81%	99.9%	100%	100%	99.5%	99.5%	99.9%	99.7%

Algorithm selection

We evaluate classification algorithms for each frame classifier in Tables 34-36. For each of the ensemble learning algorithms Random Forest and AdaBoostM1 with J48, we vary the number of iterations I. The indicated training time is the time required for one training run on our evaluation system. Because we utilize a 10-fold stratified cross-validation, ten training runs are conducted.

Table 34: Evaluation of different classification algorithms for the `short` classifier, evaluating the number of iterations I for the ensemble learners with Genetic Search.

`short`	size in kB	accuracy meta	time	F1 scores of meta-classifier						
				stand	walk	bike	car	bus	tram	train
J48	219	95.00%	8s	96.9%	99.4%	97.9%	90.1%	90.3%	95.2%	95.0%
REP-Tree	121	92.98%	3s	96.5%	99.2%	97.5%	86.4%	86.6%	91.9%	92.8%
Random Tree[2]	807	95.24%	1s	96.1%	99.4%	97.8%	89.7%	91.5%	97.4%	94.6%
Random Forest										
I = 10	6409	97.16%	6s	98.3%	99.6%	98.6%	93.6%	94.5%	98.3%	97.2%
I = 15	9536	97.37%	8s	98.4%	99.7%	98.7%	94.1%	94.8%	98.4%	97.4%
I = 20	12701	97.47%	10s	98.5%	99.7%	98.7%	94.3%	95.0%	98.4%	97.7%
I = 25	15977	97.54%	12s	98.6%	99.7%	98.7%	94.5%	95.1%	98.5%	97.7%
AdaBoostM1 with J48										
I = 10	2555	97.55%	90s	98.5%	99.7%	99.0%	94.5%	94.9%	98.3%	97.9%
I = 15	3874	97.66%	152s	98.7%	99.7%	99.1%	94.7%	95.1%	98.4%	98.0%
I = 20	5190	97.81%	186s	98.7%	99.7%	99.1%	95.1%	95.4%	98.5%	98.2%
I = 25	6562	97.84%	203s	98.7%	99.7%	99.1%	95.0%	95.5%	98.6%	98.2%
I = 30	7882	97.88%	297s	98.7%	99.7%	99.2%	95.2%	95.5%	98.6%	98.3%
I = 35	9212	97.93%	313s	98.8%	99.7%	99.2%	95.4%	95.7%	98.6%	98.3%
I = 40	10522	97.94%	347s	98.7%	99.7%	99.2%	95.4%	95.7%	98.6%	98.2%
I = 45	11853	97.95%	364s	98.7%	99.7%	99.2%	95.5%	95.8%	98.6%	98.2%

2 With maximum tree depth of 30, as it provided slightly better results.

Table 35: Evaluation of different classification algorithms for the `medium` classifier, evaluating the number of iterations I for the ensemble learners with Genetic Search.

`medium`	size in kB	accuracy meta	time	F1 scores of meta-classifier						
				stand	walk	bike	car	bus	tram	train
J48	56	97.02%	1s	98.6%	99.6%	98.7%	92.6%	93.7%	98.9%	97.0%
REP-Tree	33	95.74%	1s	98.1%	99.5%	97.9%	90.4%	90.4%	97.8%	96.0%
Random Tree	235	96.84%	1s	98.4%	99.6%	98.6%	92.1%	93.5%	98.9%	96.7%
Random Forest										
I = 10	1863	98.50%	1s	99.4%	99.9%	99.3%	95.9%	96.7%	99.6%	98.7%
I = 15	2810	98.58%	2s	99.4%	99.9%	99.4%	96.1%	96.8%	99.8%	98.8%
I = 20	3705	98.61%	2s	99.5%	99.9%	99.3%	96.1%	96.9%	99.8%	98.8%
I = 25	4587	98.76%	3s	99.6%	99.8%	99.3%	96.5%	97.3%	99.9%	98.9%
AdaBoostM1 with J48										
I = 10	729	98.87%	21s	99.5%	99.9%	99.4%	97.0%	97.6%	99.7%	99.1%
I = 15	1102	98.89%	32s	99.6%	99.9%	99.5%	97.0%	97.5%	99.7%	99.1%
I = 20	1497	98.98%	43s	99.6%	99.9%	99.5%	97.2%	97.7%	99.7%	99.2%
I = 25	1839	99.01%	53s	99.6%	99.9%	99.5%	97.2%	97.8%	99.7%	99.2%
I = 30	2199	99.06%	56s	99.6%	99.9%	99.6%	97.4%	97.9%	99.8%	99.2%
I = 35	2585	99.09%	75s	99.7%	99.9%	99.5%	97.5%	98.0%	99.8%	99.3%
I = 40	2958	99.07%	96s	99.7%	99.9%	99.5%	97.5%	97.9%	99.8%	99.2%

Table 36: Evaluation of different classification algorithms for the `long` classifier, evaluating the number of iterations I for the ensemble learners with Genetic Search.

`long`	size in kB	accuracy meta	time	F1 scores of meta-classifier						
				stand	walk	bike	car	bus	tram	train
J48	36	98.63%	1s	99.8%	99.9%	99.7%	96.8%	96.7%	98.8%	98.7%
REP-Tree	26	98.12%	1s	99.3%	99.6%	99.4%	96.3%	95.8%	98.6%	97.7%
Random Tree	71	98.91%	1s	99.8%	99.8%	99.6%	97.3%	97.4%	99.4%	99.0%
Random Forest										
I = 10	714	99.65%	1s	99.9%	100%	99.9%	99.0%	99.1%	99.9%	99.7%
I = 15	1101	99.67%	1s	99.9%	100%	100%	99.1%	99.1%	99.9%	99.7%
I = 20	1485	99.73%	1s	99.9%	100%	100%	99.3%	99.3%	99.9%	99.7%
I = 25	1825	99.71%	2s	99.9%	100%	100%	99.3%	99.3%	99.9%	99.6%
AdaBoostM1 with J48										
I = 10	312	99.80%	15s	100%	100%	100%	99.4%	99.5%	100%	99.8%
I = 15	461	99.81%	19s	99.9%	100%	100%	99.5%	99.5%	99.9%	99.7%
I = 20	611	99.83%	26s	100%	100%	100%	99.6%	99.6%	99.9%	99.7%
I = 25	764	99.83%	36s	99.9%	100%	100%	99.5%	99.6%	99.9%	99.8%
I = 30	894	99.84%	40s	99.9%	100%	100%	99.6%	99.6%	99.9%	99.8%
I = 35	1057	99.84%	47s	99.9%	100%	100%	99.6%	99.6%	99.9%	99.8%

Feature set importance

In Table 14, we defined different feature sets, each having a distinct feature composition of sensor and external data sources. In Table 37, we provide an overview of each feature set's performance, including the F1 scores for each mobility type.

Table 37: Evaluation results for different feature sets. Each feature set is defined in Table 37 and investigated with and without the inclusion of delta features (+δ).

feature sets	accuracy	F1 scores of meta-classifier						
	meta	stand	walk	bike	car	bus	tram	train
$A_F L_E$	98.91%	97.7%	99.6%	99.4%	98.3%	98.5%	99.5%	99.3%
+δ	-0.07%	-0.2%	0.0%	-0.1%	0.0%	-0.1%	+0.1%	0.0%
$A_F L$	98.87%	97.6%	99.7%	99.4%	98.3%	98.5%	99.4%	99.2%
+δ	-0.03%	-0.1%	-0.1%	-0.2%	0.0%	0.0%	+0.1%	+0.1%
$A L_E$	98.41%	97.4%	99.7%	99.2%	96.9%	97.1%	99.3%	99.2%
+δ	+0.03%	0.0%	-0.1%	0.0%	0.0%	+0.3%	+0.2%	-0.1%
$A L$	98.35%	97.4%	99.6%	99.3%	96.9%	97.1%	99.1%	99.0%
+δ	-0.22%	0.0%	0.0%	-0.1%	-0.8%	-0.5%	+0.1%	-0.2%
L_E	97.81%	97.1%	98.9%	98.6%	95.5%	96.9%	99.4%	98.3%
+δ	+0.22%	+0.1%	+0.1%	+0.3%	+0.6%	+0.2%	0.0%	+0.2%
L	97.60%	97.0%	98.8%	98.4%	95.2%	96.5%	98.9%	98.4%
+δ	-0.18%	0.0%	+0.1%	0.0%	-0.4%	-0.7%	-0.2%	-0.1%
A_F	97.62%	94.2%	99.4%	99.1%	97.6%	97.1%	98.7%	97.2%
+δ	-0.13%	-0.1%	+0.1%	-0.1%	-0.4%	-0.4%	+0.1%	-0.1%
A	96.70%	93.9%	99.4%	99.0%	95.1%	95.0%	98.8%	95.6%
+δ	-0.31%	0.0%	0.0%	-0.3%	-0.5%	-0.6%	-0.2%	-0.5%

Final model details

In Table 38, we show the confusion matrix of our final $A_F L_E$ model, with a macro-averaged accuracy of 98.91%.

Table 39 shows the information gain of each meta-classifier feature. Since no feature selection was applied, all twelve features are utilized. The predictions of each frame classifier, and their previous prediction achieved the highest information gain. Our score features, describing the ratio of individual trees predicting the given class, are included in the classifier but have less information gain.

Table 40 shows the selected features for each frame classifier, sorted by and their respective information gain. Especially acceleration-based features in the time- and frequency-domain are assigned high information gain values. `Speed` features are also commonly integrated. Only a few features are selected for external data features, with two distinct distance-based features and two stop-based features.

Table 38: Meta-classifier confusion matrix in a stratified 10-fold cross-validation for the final $A_F L_E$ model.

	predicted as						
actual class	stand	walk	bike	car	bus	tram	train
stand	3496	5	12	20	19	10	18
walk	12	3562	0	2	2	0	2
bike	8	1	3564	7	0	0	0
car	26	3	13	3507	22	4	5
bus	20	2	2	15	3523	12	6
tram	4	0	0	2	1	3571	2
train	7	0	0	3	6	1	3563

Table 39: $A_F L_E$ model: information gain of meta-features.

information gain	and feature
2.26	predM
2.18	predS
2.10	prevPredM
1.99	prevPredS
1.74	predL
1.70	prevPredL
0.58	prevScoreL
0.58	scoreL
0.53	scoreM
0.52	prevScoreM
0.46	scoreS
0.40	prevScoreS

Table 40: $A_F L_E$ model: information gain of selected features.

`short` (32 out of 65)		`medium` (26 out of 68)		`long` (25 out of 90)	
1.44	acce25	1.60	acce25	1.80	acce75
1.43	acce50	1.57	acce50	1.80	acce50
1.37	acce5To8Hz	1.52	acce5To8Hz	1.76	acce25
1.35	acce8To10Hz	1.51	acceMean	1.75	acceMean
1.35	acceNormEnergy	1.49	acce8To10Hz	1.70	acce5To8Hz
1.33	acce10To14Hz	1.48	acce10To14Hz	1.70	acce95
1.28	acceRangeTo95	1.40	acceRange25To75	1.69	acce10To14Hz
1.26	acceRange25To75	1.33	acce14To20Hz	1.69	acce8To10Hz
1.22	acce14To20Hz	1.24	acceRange	1.63	acceRange25To75
1.19	acceVar	1.19	acce1To3Hz	1.55	acceVar
1.16	acceRange	1.18	acce22To25Hz	1.40	acce25To30Hz
1.13	acce3To8Hz	1.13	speedMean	1.40	acce1To3Hz
1.11	speedMax	1.10	travelDistance	1.38	acce22To25Hz
1.09	speed95	1.08	acceMin	1.03	spectralSpreadHz
1.04	acce20To22Hz	0.79	spectralSpreadHz	0.97	spectralRollOffHz
1.04	speed25	0.76	spectralRollOffHz	0.88	acceMin
1.04	acceMin	0.61	speedPointRatioLow	0.84	speedMean
1.03	acce1To3Hz	0.57	accu25	0.66	spectralCrest
1.00	travelDistance	0.56	speedPointRatioMedium	0.65	speedPointRatioMedium
0.95	travelDistanceAcc	0.51	distanceTram	0.57	acceSkewness
0.91	acceSlopeSignChangeRate	0.49	speedVar	0.51	speedPointRatioHigh
0.69	spectralSpreadHz	0.48	spectralCrest	0.43	distanceTram
0.67	spectralRollOffHz	0.45	speedPointRatioHigh	0.40	acceZCR
0.58	accu75	0.29	distanceTrain	0.20	stopsTramStop
0.54	speedPointRatioLow	0.27	speedPointRatioStationary	0.14	stopsBusStop
0.49	speedPointRatioMedium	0.23	acceZCR		
0.49	speedRangeTo95				
0.33	spectralCrest				
0.32	spectralSkewness				
0.24	speedPointRatioStationary				
0.16	acceZCR				
0.12	acceSkewness				

A.6 LIST OF ACRONYMS

API	Application Programming Interface
FFT	Fast Fourier Transform
GIS	Geographic Information System
LBG	Location-based Game
NNI	Nearest Neighbor Index
OSM	OpenStreetMap
PCG	Procedural Content Generation
PoI	Point Of Interest

Master theses

[1] Johannes Alef. "Design and Implementation of a Content Adaption Algorithm for Cooperative Role-based Multiplayer Games." Master Thesis. TU Darmstadt, 2016.

[2] Sanja Huhle. "Live Modalitydetection with Smartphone Sensors using Machine Learning." Master Thesis. TU Darmstadt, 2020.

[3] Aurel Killian. "Skalierung und Anwendung des Orientierungslaufproblems auf stadtweite Standorte unter Verwendung realer Straßennetze." Master Thesis. TU Darmstadt, 2020.

[4] Sebastian Linsner. "Multifaktorielle Validierung von Sensordaten zur Detektion von Spoofing Angriffen." Master Thesis. TU Darmstadt, 2017.

[5] Chris Michel. "Automatische Inhaltsadaption durch Nutzerprofilierung für Ortsbezogene Spiele mit Hilfe von Kontextinformationen." Master Thesis. TU Darmstadt, 2017.

[6] Philipp Niklas Müller. "Design and Implementation of an Algorithm for the Traveling Salesman Problem with Time Windows for Movement Optimization in Location-based Games." Master Thesis. TU Darmstadt, 2017.

[7] Adrian Petschenka. "Concept and Implementation of Adaptationservices for Cross-Location-based Multiplayer Games." Master Thesis. TU Darmstadt, 2019.

[8] Lukas Raymann. "Concepts and Implementation for Cross-Location-based Games to enable simultaneous Multiplayer." Master Thesis. TU Darmstadt, 2019.

[9] Jannis Weil. "Cooperative Multi-Agent Reinforcement Learning für Role-Based Games mit Unity." Master Thesis. TU Darmstadt, 2019.

[10] Tobias Welther. "Complex Three-Dimensional Gesture Detection using IMUs and Wearables for Sensorfusion with Machine Learning." Master Thesis. TU Darmstadt, 2018.

Bachelor theses

[11] Sören Albrecht. "Konzept und Implementierung eines Analyse und Feedback Moduls zur Laufzeit für rollenbasierte Multiplayer Spiele." Bachelor Thesis. TU Darmstadt, 2018.

[12] Florian Baptistella. "Anwendung von Machine Learning auf Musik-basierte Exergames - Automatisierte Inhaltsgenerierung am Beispiel von Beat Saber." Bachelor Thesis. TU Darmstadt, 2019.

[13] Wolfgang Brabänder. "Cooperative Multi-Agent Learning for Role-based Multiplayer Games using Unity." Bachelor Thesis. TU Darmstadt, 2018.

[14] Sanja Huhle. “Development of adaptable Cooperation Mechanisms for Role-based Multiplayer Games.” Bachelor Thesis. TU Darmstadt, 2016.

[15] Felix Leber. “Entwicklung und Umsetzung von Adaptionsansätzen durch Smartphone-basierte Kontexterkennung für pervasive Spiele.” Bachelor Thesis. TU Darmstadt, 2018.

[16] Tamara Liebich. “Regulieren der Anstrengung beim Sport mit Hilfe eines mobilen Spiels und des ambiotex-Fitnessshirts.” Bachelor Thesis. TU Darmstadt, 2018.

[17] Iryna Makovetska. “Analyse und Entwicklung von Spiel- und Aktivierungskonzepten zur spielerischen Bewegungsförderung für Adipositaspatienten.” Bachelor Thesis. TU Darmstadt, 2018.

[18] Maja Nöll. “Erkennung multimodaler Bewegungsmuster anhand von Smartphonesensoren.” Bachelor Thesis. TU Darmstadt, 2017.

[19] Thilo Petry. “Konzeption und Umsetzung personalisierte Adaptionskomponenten für rollenbasierte Multiplayerspiele.” Bachelor Thesis. TU Darmstadt, 2019.

[20] Lukas Raymann. “Design and Implementation of a Geodata Classification Algorithm for Automatic Content Generation in Location-based Games.” Bachelor Thesis. TU Darmstadt, 2016.

[21] Tim Rieber. “Player and Team Performance Prediction in Competitive Multiplayer Games using League of Legends.” Bachelor Thesis. TU Darmstadt, 2019.

[22] Kai Riemann. “Creation and Verification of Incentives to Increase Interaction in Location-Based Games.” Bachelor Thesis. TU Darmstadt, 2017.

Student research projects

[23] Yannik Klein. “Concept and Evaluation of a Live Modality Detection Algorithm for Mobile Devices.” Studienarbeit. TU Darmstadt, 2019.

[24] Yannik Klein, Felix Klose, Sarah Lettmann, and Maximilian Ratzke. “TrainyMcTrainface: Wie heißt mein Zug?” Serious Games Lab Course Report. TU Darmstadt, 2018.

[25] Maximillian Ratzke. “Concept and Evaluation of Live Modality Detection Algorithms with a Simulation Component for Mobile Devices.” Studienarbeit. TU Darmstadt, 2020.

B

AUTHOR'S PUBLICATIONS

MAIN PUBLICATIONS

[1] Thomas Tregel, Johannes Alef, Stefan Göbel, and Ralf Steinmetz. "Towards Multiplayer Content Online Adaptation using Player Roles and their Interactions." In: *Proc. 11th European Conference on Games Based Learning (ECGBL)*. Academic Conferences International Limited. 2017, pp. 677–686.

[2] Thomas Tregel, Tim Dutz, Patrick Hock, Philipp N Müller, Philipp Achenbach, and Stefan Göbel. "StreetConqAR: Augmented Reality Anchoring in Pervasive Games." In: *Proc. 5th Joint International Conference on Serious Games (JCSG)*. Springer. 2020, pp. 3–16. DOI: 10.1007/978-3-030-61814-8_1.

[3] Thomas Tregel, Andreas Gilbert, Robert Konrad, Petra Schäfer, and Stefan Göbel. "Examining Approaches for Mobility Detection Through Smartphone Sensors." In: *Proc. 4th Joint International Conference on Serious Games (JCSG)*. Springer. 2018, pp. 217–228. DOI: 10.1007/978-3-030-02762-9_22.

[4] Thomas Tregel, Stefan Göbel, and Ralf Steinmetz. "Role-Based Multiplayer Content Online Adaptation in Large-Scale Scenarios." In: *Proc. 12th European Conference on Games Based Learning (ECGBL)*. Academic Conferences International Limited. 2018, pp. 720–729.

[5] Thomas Tregel, Felix Leber, and Stefan Göbel. "Incentivise Me: Smartphone-Based Mobility Detection for Pervasive Games." In: *Proc. 1st Joint International Conference on Entertainment Computing and Serious Games (ICEC-JCSG)*. Springer. 2019, pp. 470–476. DOI: 10.1007/978-3-030-34644-7_48.

[6] Thomas Tregel, Philipp N Müller, Stefan Göbel, and Ralf Steinmetz. "Where's Pikachu: Route Optimization in Location-Based Games." In: *Proc. 10th International Conference on Virtual Worlds and Games for Serious Applications (VS-Games)*. IEEE. 2018, pp. 81–88. DOI: 10.1109/VS-Games.2018.8493448.

[7] Thomas Tregel, Philipp N Müller, Stefan Göbel, and Ralf Steinmetz. "Looking for Charizard: applying the orienteering problem to location-based games." In: *The Visual Computer* (2019), pp. 1–15. DOI: 10.1007/s00371-019-01737-z.

[8] Thomas Tregel, Lukas Raymann, and Stefan Göbel. "Match Our Cities: Cross-Location-Based Games to Enable Simultaneous Multiplayer". Submitted for publication.

[9] Thomas Tregel, Lukas Raymann, Stefan Göbel, and Ralf Steinmetz. "Geodata Classification for Automatic Content Creation in Location-Based Games." In: *Proc. 3rd Joint International Conference on Serious Games (JCSG)*. Springer. 2017, pp. 212–223. DOI: 10.1007/978-3-319-70111-0_20.

[10] Thomas Tregel, Christian Reuter, Stefan Göbel, and Ralf Steinmetz. "Generating Multiplayer Games for Interaction Learning using Game Design Patterns." In: *Proc. 10th European Conference on Games Based Learning (ECGBL)*. Academic Conferences International Limited. 2016, pp. 686–695.

[11] Thomas Tregel, Miriam C Schwab, Thanh Tung Linh Nguyen, Philipp N Müller, and Stefan Göbel. "Costs to Compete – Analyzing Pay to Win Aspects in Current Games." In: *Proc. 5th Joint International Conference on Serious Games (JCSG)*. Springer. 2020, pp. 177–192. DOI: 10.1007/978-3-030-61814-8_14.

CO-AUTHORED PUBLICATIONS

[12] Hagen Becker, Augusto Garcia-Agundez, Philipp N Müller, Thomas Tregel, André Miede, and Stefan Göbel. "Predicting functional performance via classification of lower extremity strength in older adults with exergame-collected data." In: *Journal of NeuroEngineering and Rehabilitation* 17.1 (2020), pp. 1–8. DOI: 10.1186/s12984-020-00778-z.

[13] Polona Caserman, Thomas Tregel, Marco Fendrich, Moritz Kolvenbach, Markus Stabel, and Stefan Göbel. "Recognition of Full-Body Movements in VR-Based Exergames Using Hidden Markov Models." In: *Proc. 4th Joint International Conference on Serious Games (JCSG)*. Springer. 2018, pp. 191–203. DOI: 10.1007/978-3-030-02762-9_20.

[14] Augusto Garcia-Agundez, Ann-Kristin Folkerts, Robert Konrad, Polona Caserman, Thomas Tregel, Mareike Goosses, Stefan Göbel, and Elke Kalbe. "Recent advances in rehabilitation for Parkinson's Disease with Exergames: A Systematic Review." In: *Journal of NeuroEngineering and Rehabilitation* 16.1 (2019), p. 16. DOI: 10.1186/s12984-019-0492-1.

[15] Andreas Gibert, Petra K Schäfer, Thomas Tregel, and Stefan Göbel. "Förderung von umweltfreundlichen Verkehrsmitteln durch Gamification und Serious Games." In: *Neue Dimensionen der Mobilität*. Ed. by Heike Proff. Wiesbaden, DE: Springer, 2020, pp. 745–753. DOI: 10.1007/978-3-658-29746-6_58.

[16] Stefan Göbel, Alvar Gámez-Zerban, Philipp Müller, Thomas Tregel, Andreas Gilbert, Jason Christian, and David Schmoldt. "SG4Mobility: Educational Game for Environment-Friendly Mobility Behaviour." In: *Proc. 13th European Conference on Games Based Learning (ECGBL)*. Academic Conferences International Limited. 2019, pp. 261–276. DOI: 10.34190/GBL.19.092.

[17] Robert Konrad, Thomas Tregel, and Stefan Göbel. "Game Design Principles in a Game Programming Framework." In: *Proc. 4th Joint International Conference on Serious Games (JCSG)*. Springer. 2018, pp. 248–252. DOI: 10.1007/978-3-030-02762-9_26.

[18] Marianne Halblaub Miranda, Maria Ustinova, Thomas Tregel, and Martin Knöll. "MoMe@school – A pilot study on a analytical and participatory tool for active learning spaces design." In: *Journal of Urban Design and Mental Health* 3.10 (2017), p. 14. URL: https://www.urbandesignmentalhealth.com/journal-3---mome.html.

[19] Marianne Halblaub Miranda, Maria Ustinova, Thomas Tregel, and Martin Knöll. ""I spy with my little eye" A child-led Assessment of the School Built Environment." In: *Proc. ANFA Conference*. Academy of Neuroscience for Architecture. 2018, pp. 1–2.

[20] Marianne Halblaub Miranda, Maria Ustinova, Thomas Tregel, and Martin Knöll. "Growing up in urban school environments." In: *City at eye level for kids*. Ed. by Rosa Danenberg, Vivian Doumpa, and Hans Karssenberg. Rotterdam, NL: STIPO Publishing, 2018, pp. 281–285.

[21] Philipp N Müller, Philipp Achenbach, André Mihca Kleebe, Jan Ulrich Schmitt, Ute Lehmann, Thomas Tregel, and Stefan Göbel. "Flex your muscles: EMG-based serious game controls." In: *Proc. 5th Joint International Conference on Serious Games (JCSG)*. Springer. 2020, pp. 230–242. DOI: 10.1007/978-3-030-61814-8_18.

[22] Christian Reuter, Thomas Tregel, Florian Mehm, Stefan Göbel, and Ralf Steinmetz. "Rapid prototyping for multiplayer serious games." In: *Proc. 8th European Conference on Games Based Learning (ECGBL)*. Academic Conferences International Limited. 2014, pp. 478–486.

EDITED BOOKS

[23] Stefan Göbel, Augusto Garcia-Agundez, Thomas Tregel, Minhua Ma, Jannicke Baalsrud Hauge, Manuel Oliveira, Tim Marsh, and Polona Caserman, eds. *Proceedings of the 4th Joint International Conference on Serious Games (JCSG)*. Darmstadt, DE: Springer, 2018. DOI: 10.1007/978-3-030-02762-9.

[24] Stefan Göbel, Robert Konrad, Florian Mehm, Polona Caserman, Thomas Tregel, and Augusto Garcia-Agundez. "Serious-Games-Forschung und -Lehre in der Informatik." In: *Games studieren – was, wie, wo?* Ed. by Björn Bartholdy, Linda Breitlauch, André Czauderna, and Gundolf S Freyermuth. Bielefeld, DE: Transcript, 2019. Chap. 3, pp. 613–656. DOI: 10.14361/9783839440322.

C

ERKLÄRUNG LAUT PROMOTIONSORDNUNG

§8 Abs. 1 lit. c PromO

Ich versichere hiermit, dass die elektronische Version meiner Dissertation mit der schriftlichen Version übereinstimmt.

§8 Abs. 1 lit. d PromO

Ich versichere hiermit, dass zu einem vorherigen Zeitpunkt noch keine Promotion versucht wurde. In diesem Fall sind nähere Angaben über Zeitpunkt, Hochschule, Dissertationsthema und Ergebnis dieses Versuchs mitzuteilen.

§9 Abs. 1 PromO

Ich versichere hiermit, dass die vorliegende Dissertation selbstständig und nur unter Verwendung der angegebenen Quellen verfasst wurde.

§9 Abs. 2 PromO

Die Arbeit hat bisher noch nicht zu Prüfungszwecken gedient.

Darmstadt, 20. Oktober 2020

Thomas Tregel